الجمهوريــة الجزائريــة الديمقراطيــة الشعبيــة
République Algérienne Démocratique et Populaire
و البـحـث الـعـلـمـي وزارة الـتـعـلـيـم الـعـالي
Ministère de l'Enseignement Supérieur et de la Recherche Scientifique

Université MUSTAPHA Stambouli
Mascara

جامعة مصطفى اسطمبولي
معسكر

Faculté des sciences exactes
Département de physique
Laboratoire de physique quantique de la matière et modélisation mathématique

THESE de DOCTORAT

Spécialité matériaux pour les énergies nouvelles

Intitulée

Optimisation des performances thermoélectriques des composées Skutterudites

Présentée par : **Mme. BENHALIMA Zoulikha**

Le 08 /04/2021

Devant le jury :

Président	**H. BALTACH**	**Professeur**	**Université de Mascara**
Examinateur	**S. FASLA**	**Professeur**	**L'ENPO-MA**
Examinateur	**A . SOUIDINI**	**Professeur**	**Université de SIDI BELABBES**
Examinateur	**O. SAHNOUN**	**MCA**	**Université de Mascara**
Rapporteur	**M. SAHNOUN**	**Professeur**	**Université de Mascara**
Corapporteur	**A. SIAD-BEKHTI**	**MCA**	**Université de Mascara**

Année Universitaire : 2020 - 2021

Table of contents

List of figures

List of tables

ملخص

بفضل طريقة ab initio المتقدمة ، أصبح من الممكن الآن الوصول إلى قاعدة بيانات حول بنية البلورات واستخدام برامج الكمبيوتر للحصول على خصائص مثيرة للاهتمام في حالة فقدان القياسات التجريبية. لهذا السبب ، حاولنا تحديد تأثير تعبئة العناصر و / أو الاستبدال على الخصائص الهيكلية والإلكترونية والكهروحرارية لمواد Skutterudites القائمة على CoSb3 باستخدام الحسابات كجزء من الطريقة. LAPW) في نظرية الكثافة الوظيفية (DFT) ونظرية النقل شبه الكلاسيكية Boltzmann والتي يتم تنفيذها في كل من رموز Wien 2K و Boltztrap ، على التوالي.

أولاً ، نقدم دراسة نظرية للخصائص الهيكلية والإلكترونية والكهروحرارية لمركبات MX_3 skutterudite الثنائية .(M= Co, Fe, Rh et Ir ; X=Sb, P et As) سمح لنا حساب الخصائص الإنشائية بملاحظة أن المعلمات الهيكلية المحسوبة في توافق ممتاز مع البيانات النظرية والتجريبية. تُظهر هياكل النطاق الإلكتروني لهذه المركبات أن : $CoSb_3$و $IrSb_3$ و $CoAs_3$ و $IrAs_3$ و $RhAs_3$ عبارة عن مواد شبه موصلة ذات فجوات مباشرة ضيقة ، بينما تُظهر المركبات CoP_3 و IrP_3 و $RhSb_3$ نطاقات ممنوعة غير مباشرة. من ناحية أخرى ، تُظهر هياكل النطاق الإلكترونية لمركب RhP_3 سلوكًا معدنيًا. من ناحية أخرى ، يقدم هيكل النطاق الخاص بأغلبية دوران $FeSb_3$ سلوكًا شبه موصل به فجوة مباشرة بينما في حالة دوران الأقلية ، فإنه يقدم طابعًا معدنيًا يؤكد النصف المعدني للمركب. تكشف دراستهم للخصائص الكهروحرارية أن مركب $CoSb_3$ له coefficient seebeck عالي ، جنبًا إلى جنب مع الموصلية الكهربائية العالية ، مما ينتج عنه قيمة ZTe أعلى من المركبات الثنائية الأخرى ، ولكن أيضًا توصيلها الحراري مرتفع نسبيًا ، مما يجعله على ما يبدو يجعله أقل جاذبية كمادة حرارية مطبقة.

درسنا أيضًا دور ملء الفراغات الهيكلية في skutterudites القائمة على $CoSb_3$ حسب الأنواع (AM = K و Na و Rb و Cs ؛ EM = Ba و RE = Yb) أو عن طريق المنشطات في مواقع Co / Sb مع ذرات (Te ،Fe / Ge) على الخصائص الإلكترونية والأداء الكهروحراري. سمح لنا التحليل النظري للخصائص الإلكترونية بملاحظة أن سلوك أشباه الموصلات للمركبات يتضرر بسبب ملء أو تعاطي المنشطات من skutterudites المستندة إلى $CoSb_3$ بسبب نقل الشحنة من هذه العناصر ؛ بينما تم تحسين coefficient seebeck والتوصيل الكهربائي في skutterudites المملوءة جزئيًا مقارنةً بتلك المملوءة بالكامل أو المسننة وبالتالي يزداد PF.

أخيرًا ، في هذه الأطروحة ، نقوم بتحليل تأثير تعويض الشحنة على الخصائص الهيكلية والإلكترونية والكهروحرارية skutterudite المملوءة جزئيًا بناءً على$CoSb_3$ ($Ba_{0.25}Co_8Sb_{24-x}Sn_x$) حيث (x = 0 ، 1 ، 2 ، 3 و 4) و $Co_{4-x}Fe_xSb_{24-y}Te_y$ شارك في المنشطات Te. تظهر النتائج النظرية أن توازن الشحن في هذين المركبين يعتمد بشدة على تكوين الاستبدال، حيث تبين أن تكوين $Ba_{0.25}Co_8Sb_{24-x}Sn_x$ أكثر استقرارًا للطاقة من غيره. من خلال فحص تأثير استبدال Sn / Te-Fe على الخواص الإلكترونية والكهروحرارية ، نؤكد أن الخصائص الإلكترونية معتدلة وأن أداء TE قد تم تحسينه مع تقدير الجدارة الإلكترونية عديم الأبعاد (ZTe) بحوالي 0.67 و 0.72 و 0.78 عند T = 500K للتركيبات $Ba_{0.25}Co_8Sb_{23}Sn$ و $FeCo_7Sb_{23}Te$ و $Fe_2Co_7Sb_{23}Te_2$ على التوالي ، مما يجعل هذه المركبات مرشحة واعدة للتطبيقات الكهروحرارية.

Résumé

Grâce à la méthode ab initio avancée, il est maintenant possible d'accéder à une base de données sur la structure des cristaux et d'utiliser un logiciel informatique pour obtenir des propriétés intéressantes dans le cas où des mesures expérimentales sont absentes. Pour cette raison, nous avons tenté de déterminer l'effet du remplissage et/ou de la substitution d'éléments sur les propriétés structurelles, électroniques et les performances thermoélectriques des matériaux Skutterudite à base de $CoSb_3$ en utilisant des calculs dans le cadre de la méthode des ondes planes augmentées linéarisées à plein potentiel (FP-LAPW) implémentée dans la théorie fonctionnelle de la densité (DFT) et de la théorie de transport Boltzmann semi classique qui sont mises en œuvre dans les deux codes Wien 2K et Boltztrap, respectivement.

Tout d'abord, nous présentons une étude théorique des propriétés structurelles, électroniques et thermoélectriques des composés binaires de skutterudite MX_3 (M= Co, Fe, Rh et Ir ; X=Sb, P et As). Le calcul des propriétés structurelles nous a permis de constater que les paramètres structurels calculés sont en excellent accord avec les données théoriques et expérimentales. Les structures de bandes électroniques de ces composés montrent que: $CoSb_3$, $IrSb_3$, $CoAs_3$, $IrAs_3$ et $RhAs_3$ sont des matériaux semi-conducteurs avec des gaps directs étroites, alors que les composés CoP_3, IrP_3 et $RhSb_3$ présentent des bandes interdites indirectes. D'autre part les structures de bande électronique pour du le RhP_3 composé montrent un comportement métallique. En revanche, la structure de bande pour le spin majoritaire du $FeSb_3$ présente un comportement semi-conducteur avec un gap direct alors que dans le cas de spin minoritaires, elle présente un caractère métallique qui confirme la demi-métallicité du composé. Leur étude de propriétés thermoélectriques révèle que le composé $CoSb_3$ possède un coefficient Seebeck élevé, combiné à une conductivité électrique élevée, ce qui lui résulte une valeur ZTe plus élevée que les autres composés binaires, mais aussi leur conductivité thermique est relativement élevée, ce qui le rend apparemment moins attrayant comme un matériau thermoélectrique appliqué.

Nous avons également étudié le rôle du remplissage des vides structurels des skutterudites à base de $CoSb_3$ par espèce (AM= K, Na, Rb et Cs ; EM= Ba et RE= Yb) ou par dopage dans les sites Co/Sb avec des atomes Fe/(Ge, Te) sur les propriétés électroniques et les performances thermoélectriques. L'analyse théorique des propriétés électroniques nous a permis de constater que le comportement des semi-conducteurs des composés est endommagé par le remplissage ou le dopage des skutterudites à base de $CoSb_3$ en raison du transfert de charge à partir de ces éléments; tandis que le coefficient de Seebeck et la conductivité

électrique sont améliorés dans les skutterudites partiellement remplis par rapport à ceux entièrement remplis ou dopés et, par conséquent, le facteur de puissance (PF) est augmenté.

Enfin, dans cette thèse, nous analysons l'effet de la compensation de charge sur les propriétés structurelles, électroniques et thermoélectriques de skutterudites partiellement remplis à base de $CoSb_3$ ($Ba_{0.25}Co_8Sb_{24-x}Sn_x$) où (x= 0, 1, 2, 3 et 4) et de Te co-dopé $Co_{4-x}Fe_xSb_{24-y}Te_y$. Les résultats théoriques montrent que la balance des charges dans ces deux composés dépend fortement à la configuration de substitution, ou la composition $Ba_{0.25}Co_8Sb_{24-x}Sn_x$ s'avérant être la plus stable énergétiquement que les autres. En examinant l'effet de substitution Sn /Te-Fe sur les propriétés électroniques et thermoélectriques, nous soulignons que les propriétés électroniques sont modérées et que la performance TE est améliorée avec la valeur estimée du facteur de mérite électronique sans dimension (ZTe) d'environ 0,67, 0,72 et 0,78 à T= 500K pour les compositions $Ba_{0,25}Co_8Sb_{23}Sn$ et $FeCo_7Sb_{23}Te$ et $Fe_2Co_7Sb_{23}Te_2$, faisant respectivement de ces composés des candidats prometteurs pour les applications thermoélectriques.

ملخص

بفضل طريقة ab initio المتقدمة ، أصبح من الممكن الآن الوصول إلى قاعدة بيانات حول بنية البلورات واستخدام برامج الكمبيوتر للحصول على خصائص مثيرة للاهتمام في حالة فقدان القياسات التجريبية. لهذا السبب ، حاولنا تحديد تأثير تعبئة العناصر و / أو الاستبدال على الخصائص الهيكلية والإلكترونية والكهروحرارية لمواد Skutterudites القائمة على CoSb3 باستخدام الحسابات كجزء من الطريقة. LAPW) في نظرية الكثافة الوظيفية (DFT) ونظرية النقل شبه الكلاسيكية Boltzmann والتي يتم تنفيذها في كل من رموز Wien 2K و Boltztrap ، على التوالي.

أولاً ، نقدم دراسة نظرية للخصائص الهيكلية والإلكترونية والكهروحرارية لمركبات MX_3 skutterudite الثنائية (M = Co و Fe و Rh و Ir ؛ X = Sb و P و .(As سمح لنا حساب الخصائص الإنشائية بملاحظة أن المعلمات الهيكلية المحسوبة في توافق ممتاز مع البيانات النظرية والتجريبية. تُظهر هياكل النطاق الإلكتروني لهذه المركبات أن : $CoSb_3$و $IrSb_3$ و $CoAs_3$ و $IrAs_3$ و $RhAs_3$ عبارة عن مواد شبه موصلة ذات فجوات مباشرة ضيقة ، بينما تُظهر المركبات CoP_3 و IrP_3 و $RhSb_3$ نطاقات ممنوعة غير مباشرة. من ناحية أخرى ، تُظهر هياكل النطاق الإلكترونية لمركب RhP_3 سلوكًا معدنيًا. من ناحية أخرى ، يقدم هيكل النطاق الخاص بأغلبية دوران $FeSb_3$ سلوكًا شبه موصل به فجوة مباشرة بينما في حالة دوران الأقلية ، فإنه يقدم طابعًا معدنيًا يؤكد النصف المعدني للمركب. تكشف دراستهم للخصائص الكهروحرارية أن مركب $CoSb_3$ له coefficient seebeck عالي ، جنبًا إلى جنب مع الموصلية الكهربائية العالية ، مما ينتج عنه قيمة ZTe أعلى من المركبات الثنائية الأخرى ، ولكن أيضًا توصيلها الحراري مرتفع نسبيًا ، مما يجعله على ما يبدو يجعله أقل جاذبية كمادة حرارية مطبقة.

درسنا أيضًا دور ملء الفراغات الهيكلية في skutterudites القائمة على $CoSb_3$ حسب الأنواع (AM = K و Na و Rb و Cs ؛ EM = Ba و RE = Yb) أو عن طريق المنشطات في مواقع Co / Sb مع ذرات (Te ،Fe / Ge) على الخصائص الإلكترونية والأداء الكهروحراري. سمح لنا التحليل النظري للخصائص الإلكترونية بملاحظة أن سلوك أشباه الموصلات للمركبات يتضرر بسبب ملء أو تعاطي المنشطات من skutterudites المستندة إلى $CoSb_3$ بسبب نقل الشحنة من هذه العناصر ؛ بينما تم تحسين coefficient seebeck والتوصيل الكهربائي في skutterudites المملوءة جزئيًا مقارنةً بتلك المملوءة بالكامل أو المسننة وبالتالي يزداد PF.

أخيرًا ، في هذه الأطروحة ، نقوم بتحليل تأثير تعويض الشحنة على الخصائص الهيكلية والإلكترونية والكهروحرارية skutterudite المملوءة جزئيًا بناءً على $CoSb_3$ ($Ba_{0.25}Co_8Sb_{24-x}Sn_x$) حيث (x = 0 ، 1 ، 2 ، 3 و 4) و $Co_{4-x}Fe_xSb_{24-y}Te_y$ شارك في المنشطات Te. تظهر النتائج النظرية أن توازن الشحن في هذين المركبين يعتمد بشدة على تكوين الاستبدال، حيث تبين أن تكوين $Ba_{0.25}Co_8Sb_{24-x}Sn_x$ أكثر استقرارًا للطاقة من غيره. من خلال فحص تأثير استبدال Sn / Te-Fe على الخواص الإلكترونية والكهروحرارية ، نؤكد أن الخصائص الإلكترونية معتدلة وأن أداء TE قد تم تحسينه مع تقدير الجدارة الإلكترونية عديم الأبعاد (ZTe) بحوالي 0.67 و 0.72 و 0.78 عند T = 500K للتركيبات $Ba_{0.25}Co_8Sb_{23}Sn$ و $FeCo_7Sb_{23}Te$ و $Fe_2Co_7Sb_{23}Te_2$ على التوالي ، مما يجعل هذه المركبات مرشحة واعدة للتطبيقات الكهروحرارية.

Abstract

The theoretical studies have been fundamental in the development of new materials and new devices for diverse industrial applications. With advanced ab initio method, it is now feasible to access a database of crystal structure and use computer software to obtain interesting properties in the case in which experimental measurements are missing. For this raison we have attempt to determine the effect of filling or/and substituting elements on the structural, electronic properties and thermoelectric performance for $CoSb_3$-based Skutterudite materials using calculations within the full-potential linearized augmented plane wave method (FP-LAPW) inside of the density functional theory (DFT) and semi classical Boltzmann transport theory which are implemented in the Wien 2K and Boltztrap codes.

Firstly, we present theoretical study of structural, electronic and thermoelectric properties of binary skutterudite compounds MX_3 (M= Co, Fe, Rh and Ir; X=Sb). The calculated structural parameters are in excellent agreement with the theoretical and experimental data. From the calculation of structural properties, we have found that our calculated structural parameters are in excellent agreement with the theoretical and experimental data. The calculated electronic band structures of the challenging compounds show that the $CoSb_3$, $IrSb_3$, $CoAs_3$, $IrAs_3$ and $RhAs_3$ compounds are semiconductors materials with fundamentals narrowing directs band gaps, however, the CoP_3, IrP_3 and $RhSb_3$ compounds exhibit indirects band gaps. Whereas the electronic band structures for the binary skutterudite RhP_3 compound shows a metallic behavior. In the other hand, the spin up band structure in $FeSb_3$ show a direct band gap semiconductor behavior while in the opposite case, it show metallic character and thus confirm the half metallicity of compound.

From the investigation of the their thermoelectric properties, the $CoSb_3$ compound has been found to have a large Seebeck coefficient, combined with high electrical conductivity and consequently resulting in high ZTe value than the other compounds, although it has a comparatively high thermal conductivity, which apparently makes it less attractive as an applied thermoelectric material.

Also, we have study the role of filling in the structural voids of $CoSb_3$ based skutterudites by species (AM= K, Na, Rb and Cs; EM= Ba and RE= Yb) or by doping at Co/Sb sites with Fe/(Ge, Te) atoms on the electronic properties and thermoelectric performance. From the theoretical analysis of the electronic properties we found that semiconductor behavior of compound is damaged by filling or doping $CoSb_3$ due to the charge transfer from these elements; whereas the both seebeck coefficient and the electrical

conductivity are improved in partially filled skutterudite compounds than the fully or doped and consequently, the power factor is enhanced.

Finally, in this thesis, we analyze the effect of charge balance on the structural, electronic, and thermoelectric properties on partially filled $CoSb_3$ ($Ba_{0.25}Co_8Sb_{24-x}Sn_x$) where (x= 0, 1, 2, 3 and 4) and Fe/Te co-doped $CoSb_3$ ($Co_{4-x}Fe_xSb_{24-y}Te_y$). The theoretical analyses show that the charge balance in $Ba_{0.25}Co_8Sb_{24-x}Sn_x$ and $Co_{4-x}Fe_xSb_{24-y}Te_y$ compounds is found to be strongly dependent on the substitution configuration, where the $Ba_{0.25}Co_8Sb_{23}Sn$ composition found to be the most stable energetically than the other ones. Examining the Sn-Fe/Te substitution effect on the electronic and thermoelectric properties, we point out that the electronic properties are moderate and the TE performance is enhanced with the estimated dimensionless electronic figure of merit (ZT_e) value of about 0.67, 0.72 and 0.78 at T= 500K for $Ba_{0.25}Co_8Sb_{23}Sn$ and $FeCo_7Sb_{23}Te$ and $Fe_2Co_7Sb_{23}Te_2$ compositions, respectively making these compounds as promising candidates for thermoelectric applications.

.

General Introduction

General introduction

Through the use of so-called first principles "ab-initio" methods (meaning from the very beginning) [1,2], physicists can predict new materials or alloys with important properties. These numerical simulation methods are means of accessing the understanding of physical systems. The advantage of these methods lies in the fact that they do not require any experimental knowledge to perform such calculations and most of these methods undergo continual updates, which adapt to speed and memory capacity for calculators. These calculation methods are a very powerful tool for the prediction and study of new materials. They are based on the density functional theory (DFT), the main idea of which is to show that the total energy of a system of N interacting electrons, subjected to an external potential, can be written as a functional F [n] of the density [3]. The density of the ground state can be obtained by minimizing the energy for any external potential. DFT is generally used to calculate the electronic structure of complex systems containing several atoms such as molecules or solids. It is based on electron density rather than wave function.

Demographic growth and climate change open up many debates and lead to important questions. By 2030, the increase in global energy demand is estimated at 50%, with energy production alone responsible for 2/3 of total green house gas (GHG) emissions. Associated with an energy production based at 80% on fossil resources, this generated CO_2 emissions by 50% higher and a maximum global warming of$6^{\circ}C$ which is not viable in the current context, even at short term. Reducing fossil fuel consumption is therefore becoming the primary concern of energy policy.This is why the energy concerns of the planet have generated a new interest in thermoelectricity as part of the development of renewable energies. Indeed, thermoelectricity could make it possible to recycle the waste heat by many systems. For example, recycling the heat accumulated in car exhaust pipes or industrial chimneys could enable the production of clean and inexpensive electricity. In the case of motor vehicles, it would simply be enough to double the efficiency of the thermoelectric modules to produce enough power to replace the alternator, thereby increasing the life of the vehicle. Therefore thermoelectric conversion is one of the pillars for modern times; it requires the use of specific materials with thermoelectric properties.

Thermoelectric generators (TEGs) offer the possibility of exploiting the energy dissipated under form of heat and therefore lost. It is estimated at 520 Mtep (million tones

equivalent petroleum) for heavy industry and transport in Europe. Therefore, the systems recovery of energy losses by means of thermoelectric converters can represent a source of green energy in the energy mix of tomorrow. TEGs are compact, static and self-contained devices which convert thermal energy into electrical energy. They are made up of the assembly of several pairs of semiconductors of type -n and -p, connected electrically in series and thermally in parallel. The heat applied to one side of the thermoelectric generator (TEG) forces electrons (in -n type material) and holes (-p type) to migrate to the opposite (cold) side, which generates an electrical voltage due to the Seebeck effect and an electric current driven by the heat flow. The low conversion efficiency of thermoelectric (TE) systems has long confined them to niche applications in space (radio isotopic generators for space probes and planetary rovers) and electronics (production of cold by Peltier effect modules). However, since the late 1990s, the emergence of new concepts has made it possible to realize significant progress that has helped improve the competitiveness of this technology.

The conversion efficiency of TEGs depends on a combination of antagonistic properties, called the merit factor (ZT), which expresses the performance of thermoelectric materials (TEM). This merit factor reflects the fact that the conversion efficiency of a TEG depends on the capacity of the constituent material (semiconductor pairs) to: generate a potential difference by Seebeck effect, conduct the current, and maintain the thermal gradient between the hot spring and the well cold. Increasing the conversion efficiency of a TEG therefore implies optimizing the transport properties of materials so as to maximize ZT.

Since to be effective, a thermoelectric material must behave at both as an electrical conductor (with a high Seebeck coefficient) and as an insulator one of the main strategies developed in the literature is to minimize the thermal conductivity of semiconductors without affecting electronic transport. The total thermal conductivity of semiconductors is the sum of different contributions of electrons and phonons. So the goal of lowering the conductivity thermal without reduction of electrical conductivity can be achieved by disturbing only phononic transport. This can be achieved by multiplying the sources of diffusion phonons to decrease their average free path.

Doped and Partial filled Skutterudite based thermoelectric (TE) devices have high potential for engineering and power generation applications because both n- and p-type Skutterudites demonstrate excellent TE performance [4-5].

The work presented in this thesis aims to contribute; on the one hand, to a theoretical analysis of doped and partially filled $CoSb_3$ skutterudites using the linearized augmented plane wave and total potential (FP-LAPW) method implemented in Wien2k code. On the other hand, we study the effect of charge balance on structural, electronic and thermoelectric performance $CoSb_3$ based skutterudite compounds herein the Co and Sb atoms have been partially replaced with Fe and Te elements, respectively, by using the two approximations of the exchange and correlation potential: the generalized gradient (GGA-PBE) and TB-mBJ [6]. The rest of this thesis is organized as follows:

The first chapter will be devoted to brief reminders of thermoelectricity. After a brief description of the thermoelectric effects, we will introduce the notion of dimensionless figure of merit ZT, an essential parameter which should be optimized to obtain high conversion performance and to make a comparison between the different studied compounds. We will end this chapter by explaining the criteria that have been established to guide researchers in their selection of materials.

The description of the main ab-initio methods and the theoretical bases of density functional will be the subject of the second chapter. We will finish this part with a little overview of the electronic Boltzmann transport equations (for electrons).

The last chapter concerns the presentation of the theoretical results. It comes in fourth parts:

The first presents the most important investigation of binary skutterudites compounds MX_3 (M= Co, Ir and Rh and X= As, P and Sb), starting with study of structural and electronic properties, then we spotlight on the investigation of their thermoelectric performances.

The most relevant results obtained for the role of filling in the structural voids of $CoSb_3$ by species on the structural, electronic properties and thermoelectric performance of $CoSb_3$based skutterudites compounds are presented and discussed in Chapter IV.

The first section includes the study of structural, electronic properties and thermoelectric performance of *n*-type filled $CoSb_3$based skutterudites with alkali metals (AM= K, Na, Rb and Cs); alkali earth metals (EM= Ba) and rare earth metal (RE= Yb). In last section the effect of *p*-type boron filled $CoSb_3$based skutterudites ($BrCoSb_3$) on the structural, electronic properties and thermoelectric performance is analyzed.

Next the structural, electronic and thermoelectric properties of substituted Cobalt or antimony (Co/Sb) sites with (Fe/(Ge-Te)) atoms compound are presented and discussed in chapter V.

Chapter VI will be devoted to the analysis of charge balance on the structural, electronic properties and thermoelectric performance of $CoSb_3$based skutterudites skutterudite materials in the both cases with and without filling. First, we will analyzed and discussed the thermoelectric performance of Sn compensated Ba partially filled *p*-type $CoSb_3$ based skutterudites ($Ba_{0.5}Co_8Sb_{24-x}Sn_x$), starting from the structural and total energies, following by the electronic properties to the thermoelectric performance of $Ba_{0.5}Co_8Sb_{24-x}Sn_x$ compositions. Then, we will discuss the most representative results obtained for Te compensated Fe doped $CoSb_3$ based skutterudite ($Fe_xCo_{8-x}Sb_{24-y}Te_y$) compounds.

Finally, this study ends with a general conclusion which regroups the main conclusions and foundations.

Bibliography

[1] C. Fiolhais, F. Nogeuira, M.A.L. Marques, A Primer in Density-Functional Theory, lecture notes in Physics, Vol. 620, Springer, Berlin, 2003, chapitres 1 et 6.

[2] K.Burke and friends, The ABC of FT,http://dft.ucII.edu/materials/bookABCDFT/gamma /g1.pdf

[3] P. Chaquin (LCT-UPMC) Pratique de la Chimie Théorique.

[4] Y.Z. Pei, L.D. Chen, W. Zhang, X. Shi, S.Q. Bai, X.Y. Zhao, Z.G. Mei, and X.Y. Li, Appl. Phys. Lett. 89, 221107 (2006).

[5] X. Shi, H. Kong, C.-P. Li, C. Uher, J. Yang, J.R. Salvador, H. Wang, L. Chen, and W. Zhang, Appl. Phys. Lett. 92, 182101 (2008).

[6] F. Tran and P. Blaha : Accurate Band Gaps of Semiconductors and Insulators with a Semilocal Exchange-Correlation Potential , Phys. Rev. Lett. 102, 226401 (2009).

Chapter I

I.1. Introduction

Thermoelectricity was discovered and developed in Western Europe by academic scientists in the 100 years between 1820 and 1920 (at the beginning of the 19th century). The thermoelectric effect describes the processes which link a flow of electric charges to a heat transfer within a material. This reversible phenomenon allows the direct conversion of thermal energy into electrical energy or vice versa. These two quantities are therefore directly linked to the thermoelectric material involved and more particularly to its thermal and electronic properties. Since 1970, the need for reliable and remote energy sources has allowed niche applications for thermoelectric materials such as space exploration missions (Voyager, Curiosity, etc.) even if conventional processes are more efficient. Interest in thermoelectricity was renewed in the 1990s with the influx of new ideas such as engineering structures at the nanoscale. The global need for alternative energy sources has rekindled interest in commercial applications and the development of inexpensive and environmentally friendly thermoelectric materials.

I.2. Thermoelectric effects

There are three separately identified thermoelectric effects: the Seebeck effect, the Peltier effect, and the Thompson effect. In 1794, **Alessandro Volta** highlighted the appearance of forces under the influence of the temperature difference [1]. Fig. I. 1 presents a diagram of his experience.

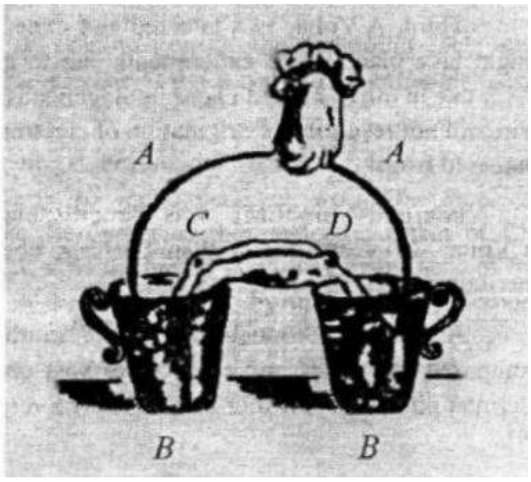

Fig. I.1: Diagram of the Volta experience. A - Metal (iron) bow, B - glasses filled with water, C and D - parts of frogs dipped in glasses of water.

In 1821, a German physicist **Thomas Johann Seebeck** noticed that a circuit formed by two different metallic conductors whose two junctions are subjected to a different temperature deflects a metallic needle (Fig. 1.2) [2].

Seebeck mistakenly thinks that this effect is due to the magnetic field induced by the temperature difference and that it must be related to the earth's magnetic field. Shortly after, in 1825, **Oersted** gave the correct explanation. He realizes that in reality, the temperature difference creates a potential difference, if the circuit is closed allows current to flow and therefore induces a magnetic field. It was the first thermoelectric effect.

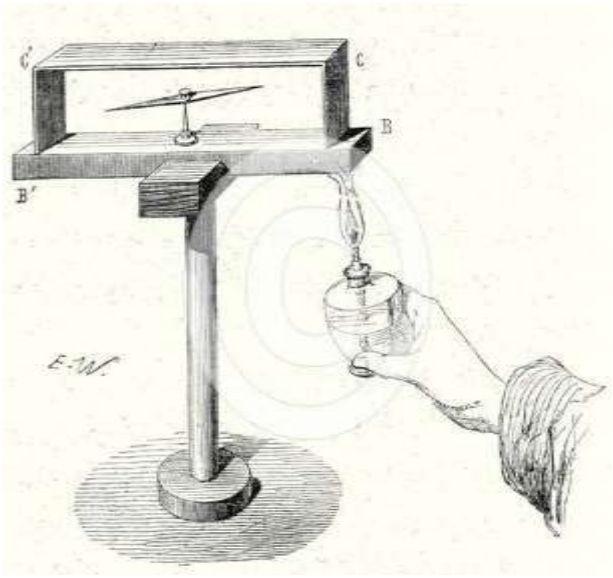

Fig. I.2 : Original experience by Thomas Johann Seebeck.

A few years later, **Jean Charles Athanase Peltier** (1785-1845), the French watchmaker and physicist discovered the reciprocal effect which constitutes the second thermoelectric effect; he demonstrated a release or absorption of heat at the junctions of two materials with different nature traversed by an electric current [3].

It was not until the **Lens** experience in 1838 that this effect, the foundation of refrigeration applications, was properly understood. This effect is illustrated in Fig. I.3.

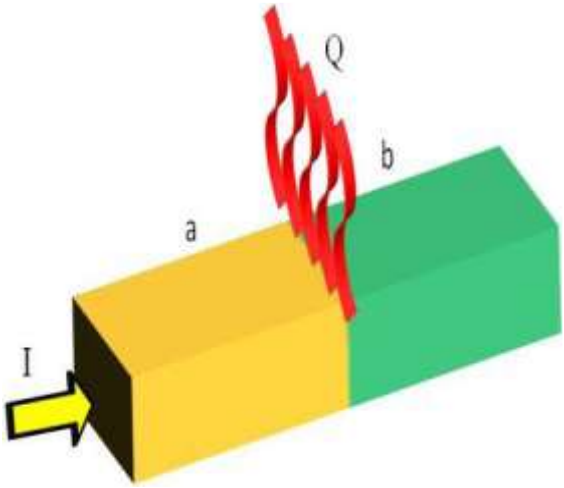

Fig. I. 3: Peltier effect illustration

With Q the heat flow, I the electric current, *a* and *b* the materials a and b respectively.

In 1854; **Thomson** (who became Lord Kelvin in 1892) postulated that there should be a thermodynamic relationship between the Seebeck and Peltier effects, Thomson came to the remarkable conclusion that a third thermoelectric effect must necessarily occur. This effect, known today as the Thomson effect; which does not require the existence of two materials and a junction [4,5].

Fig. I.4 presents a chronology of the pioneers of thermoelectricity.

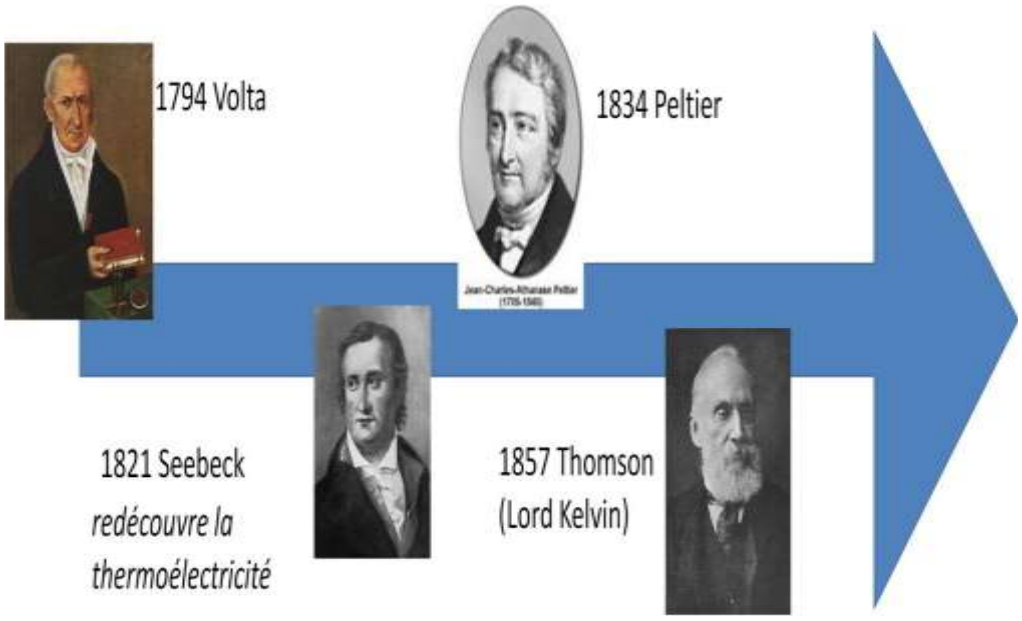

Fig. I.4: Chronology of important figures in thermoelectricity

I.3. Dimensionless Merit Factor

Fig. I.5 shows the basic structure of a thermoelectric device (also called thermocouple) made up of two branches of semiconductor materials, one of p-type and the other of n-type [6]. If the Peltier effect makes it possible to consider the use of this type of device as a heat pump or refrigerator, the Seebeck effect offers the possibility of converting thermal energy into electrical energy that can be exploited for example; by supplying an external load.

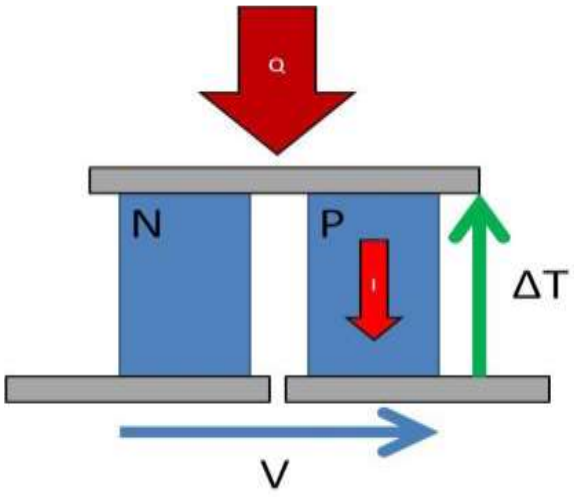

Fig. I.5: Thermocouple

The performance of a thermoelectric device is defined identically to that of diatherm machines. It is possible to define a coefficient of performance (C.O.P.) and an efficiency η when the thermocouple is configured for refrigeration and generation, respectively. The C.O.P. is defined by the ratio between the quantity of heat absorbed on the cold side over the quantity of work supplied by the external electrical source while the efficiency is equal to the ratio of the electrical work that can be generated in the external load over the quantity of heat that must be supplied on the hot side. We can show that the C.O.P. and the maximum yield can be written [7]:

$$C.O.P_{max} = \frac{T_c}{T_c - T_f} \frac{\sqrt{1 + Z_{np}T_m} - \frac{T_c}{T_f}}{\sqrt{1 + Z_{np}T_m} + 1} \quad \text{I.1}$$

$$\eta = \frac{T_c - T_f}{T_c} \frac{\sqrt{1 + Z_{np}T_m} - 1}{\sqrt{1 - Z_{np}T_m} + \frac{T_f}{T_c}} \quad \text{I.2}$$

Where T_f is the temperature of the cold source, T_C the temperature of the hot source, T_m the average operating temperature defined by:

$$T_m = \frac{(T_c + T_f)}{2} \quad \text{I.3}$$

and Z_{np} is the figure of merit of the pair (n, p) expressed in K^{-1}. This factor is only a function of the transport properties of the materials constituting the two branches n and p:

$$Z_{np} = \frac{(\alpha_p - \alpha_n)^2}{[\sqrt[2]{(\rho_n \lambda_n) + (\rho_p \lambda_p)}]^2} \quad \text{I.4}$$

With $\lambda_n$and λ_p the thermal conductivities of n and p doped thermoelectric materials respectively, and ρ_n, ρ_p the electrical resistivities of n and p doped thermoelectric materials.

The expressions of the C.O.P. and maximum efficiency show that the performance of a thermoelectric device is limited by that of a Carnot machine (ideal reversible machine) and this regardless of the configuration used (refrigerator or generator). Moreover, these two coefficients only depend on the materials used through the figure of meritZ_{np}.

However, in practice, we only have to work on a single branch, we seek to optimize the dimensionless figure of merit ZT, by analogy to the relation ofZ_{np}, and it is possible to introduce the ZT according to the relation:

$$ZT = \frac{\alpha^2}{\rho\lambda} T = \frac{P}{\lambda} T \quad \text{I.5}$$

Where $P = \alpha^2 / \rho$ is called the power factor.

Fig. I.6 shows the efficiency for different values of factor ZT.

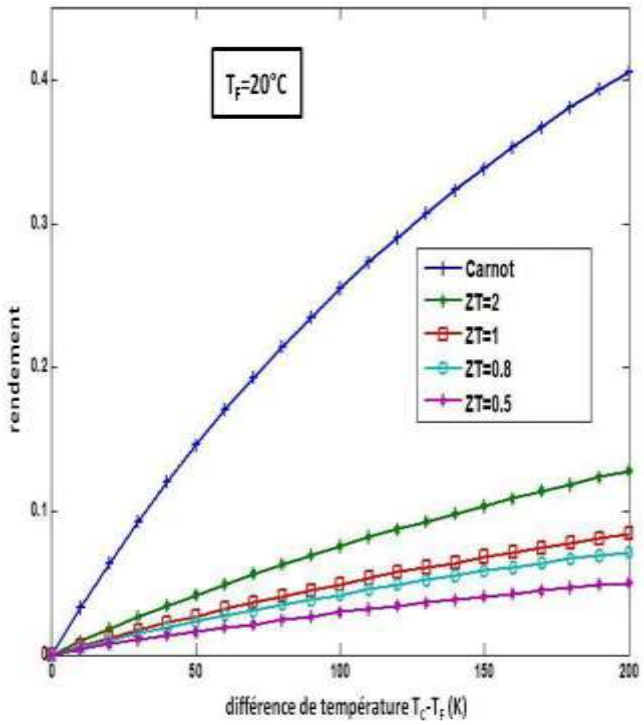

Fig. I.6: Thermoelectric efficiency as a function of the temperature difference set by the figure of merit.

We have just seen that high performance thermoelectric materials must have a high ZT factor, hence a high Z figure of merit. Returning to the termZ_{np}, we can establish the properties of a good thermoelectric material.

The selection of the best thermoelectric materials goes through the search for materials with a high ZT and this, in the widest possible temperature range to increase its operating range. Thus, it is highly desirable to have a material which has high thermoelectric power but also low electrical resistivities and thermal conductivities. Unfortunately, these two characteristics are strongly correlated and good thermal conductors are also good electrical conductors. It should be added that good mechanical strength and good thermal stability are also necessary so that no degradation occurs in service. For the torque, it is also recommended to combine n and p branches with similar transport properties so that the geometry of the parts is similar and thus limits the problems of thermal stresses [8,9].

Fig. I.7 gives an overview of the evolution of the physical characteristics as a function of the concentration of charges.

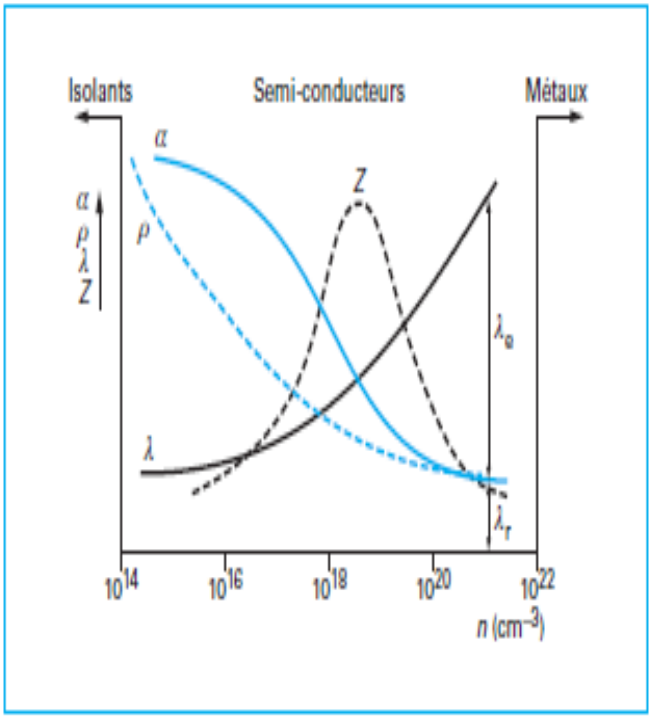

Fig. I.7: Coefficients α, ρ, λ and Z as a function of the concentration of carriers at room temperature [10].

From Figure (1.8); we can see that there is an optimal charge density at the maximization of Z, and that this corresponds to the domain of semiconductors [11].

I.4. Concepts for Novel Thermoelectric Materials

One of the interest concepts for novel thermoelectric materials was formulated by Slack, who successfully initiated a new research on novel thermoelectric materials [6]. In his work he highlighted five major points, which are important for efficient thermoelectric materials:

1. Reduction of the lattice thermal conductivity κ_l.

This Point refers to the fact that the electronic thermal conductivity κ_e is strongly correlated to the electrical conductivity of the material. This is described in the Wiedemann-Franz law, where the electronic thermal conductivity is related to the electrical conductivity:

$$\kappa_e = L \cdot \sigma \cdot T \qquad \text{I.6}$$

$L$is the Lorenz number, which is in the range of $10^{-8}\ V^2K^{-2}$. In consideration of an enhanced ZT, the electronic part is an inevitable contribution to the overall thermal conductivity. Consequently the reduction of the lattice thermal conductivity is the only possible way to

optimize the thermal conductivity without deteriorating the electrical conductivity. Thus it is of interest, what is the possibly lowest lattice thermal conductivity. Slack calculated the minimum thermal conductivity for several compounds [12]. These values are comprehensibly very close to that of amorphous materials, e.g. the minimum thermal conductivity κ_{min} of $CoSb_3$ is κ_{min} = 0.37 Wm^{-1} K^{-1} [13].

2. High carrier mobility μ (for both *n*- and *p*-type materials)

Point (2) considers the charge carrier mobility μ, which is proportional to the electrical conductivity σ and inversely proportional to the charge carrier density n. This can be expressed as follows:

$$\sigma = n\ e\ \mu \qquad \text{I.7}$$

where n is the charge carrier density, e the electron charge and μ the charge carrier mobility. It has to be noted that this equation accounts for one type of charge carriers, i.e. *n*- or *p*-type. In total it is assumed that high charge carrier mobility is most desirable and can be expressed in terms of a good thermoelectric material as the weighed mobility U [11, 14, 15].

Accordingly the weighed mobility U is defined as:

$$U = \mu \left(\frac{m^*}{m_0}\right)^{3/2} \qquad \text{I.8}$$

3. The density of states effective mass m^* should be equal to the free electron massm_0.

The equation of the weighed mobility U already explains point (3), which proclaims a balanced ratio of the density of states effective mass m^* and the free electron massm_0.

4. The bandgap energy E_g should be equal or higher than 0.25 eV.

This is mainly based on calculations, which were carried out by Mahan [14]. He found that the best semiconductor for large figure of merit should be 10 k_BT, where k_B is the Boltzmann constant. At room temperature it gives a value of 0.25 eV. Lower values tend to a decrease of the absolute Seebeck coefficient and a rise of the thermal conductivity at higher temperatures due to bipolar thermo diffusion.

5. **μ, κ_l and m^* are independent of the charge carrier concentration n, and κ_l and m^* are independent of temperature T.**

Point (5) denotes that the parameters of the figure of merit are interdependent and of different weight. For this reason decoupling of parameters and optimization processes would be desirable.

Optimization is needed e.g. for the doping concentration and as a consequence for the charge carrier density. Latter increases indeed the electrical conductivity; however it deteriorates the absolute Seebeck coefficient value and the carrier mobility. Slack furthermore pointed out those metals, even semi-metals do not tend to have large Seebeck coefficients. Therefore small bandgap semiconductors seem to be ideal, because those comprise a reasonable Seebeck coefficient and at the same time a good carrier mobility and low thermal resistivity. The bandgap can be also regarded as a result of the "character" of the bonding which also provides further information of the material, e.g. for large bandgaps ionic bonding can be assumed (and therefore high(κ_l), whereas for smaller bandgaps of semiconductors more covalent bonding is expected.

Slack formulated his concept in form of a key term ("Phonon Glass Electron Crystal") [7], which concisely encompasses the five assumptions. This concept pushed forward the discovery of new thermoelectric materials, such like cage compounds, where a decoupling of thermal and electrical properties is possible to a certain extent. Nevertheless recent publications also tend to deviate from this path and e.g. search for strong dependencies between the density of states effective mass and the charge carrier density at different temperatures [16] or attenuate the concept, like in the case of rattling in skutterudites [17].

Bibliography

[1] A. Volta, "Nuova memoria Sull' elettricita a animale. Divisa in tre lettere diretta al signor Abate Anton Maria Vassali, proffessore di fisica nella R. Université Torino. 1794-1795." Institute for experimental medicine of Russia — «A.Galvani and A.Volta, selected papers on animal e1ectricity», OGIZ Publ., M.— L., 1795-1794 (1937).

[2] T.J. Seebeck, Abhandlungen der Deutschen Akademic der Wissenschaften zu Berlin, 265 1822 (1821).

[3] Peltier, J. C. Annales de chimie, 56 371 (1834).

[4] W. Thomson, Mathematecal and Physical Paper, 1 175 (1851).

[5] Thomson,W. Proceeding of the Royal Society of Edinbugh, 91 (1851).

[6] D.M. Rowe, CRC Handbook of Thermoélectrics, CRC Press (1995).

[7] E. Altenkirch, Physikalishe Zeitschrift, 12 920 (1909).

[8] E. Altenkirch, Physikalishe Zeitschrift, 10 560 (1909).

[9] B. Lenoir, "Thermoélectricité: des principes aux applications," *Transport*, pp. 1–19, (1990).

[10] R.L. Cataldo and G.L. Bennett, U.S. Space Radioisotope Power Systems and Applications: Past, Present and Future, Radioisotopes - Applications in Physical Sciences. 2011.

[11] Ioffe, A. Semiconducters, Thermoelements and thermoelectric cooling ; Infosearch : London, (1957).

[12] G. A. Slack. J. Solid Stat Phys, 34 (1979).

[13] H. Kim, M. Kaviany, J.C. Thomas, A. Van der Ven, C. Uher, and B. Huang, J. Phys. Rev. Lett., 105(26) 265901 (2010).

[14] G. D. Mahan, J. Appl. Phys, 65(4) 1578 (1989).

[15] H.J. Goldsmid. Electronic refrigeration. Pion, (1986).

[16] Y. Pei, X. Shi, A. LaLonde, H. Wang, L. Chen, and G.J. Snyder. J. Nature, 473(7345) 66 (2011).

[17] M. M. Koza, M. R. Johnson, R. Viennois, H. Mutka, L. Girard, and D. Ravot, J. Nat. Mater, 7(10) 805 (2008).

Chapter II

II.1 Density Functional Theory (DFT)

Understanding the behavior of interacting electrons in a solid is of great importance for both scientific and technological applications. However, treat the interacting electronic problem via many-body wave functions is an impossible task due to the large number of degrees of freedom. Therefore we need an approximation to well define this problem.

This fact leads to the burn of two types of approaches; the first is the traditional Hartree-Fock (H-F) method [1] which is based on the wave function description. While the second approach is the powerful, Density Functional Theory (DFT) developed by Hohenberg and Khon 1964 [2], which is based on the electron density. The following chapter is a brief overview of both methods; Hartree-Fock and Density Functional Theory, and their roles for solving the quantum mechanical problems.

II.1.1 The Many-Body Problem

As far as our main aim is to understand and investigate the properties of real materials, we come to the problem of an appropriate quantum-mechanical description of these systems. However a quantum mechanical understanding of a given material system begins with a many-electron Schrödinger equation and its corresponding Hamiltonian, which in the time independent, non-relativistic, Born-Oppenheimer approximation is:

$$\hat{H}\Psi(r_1, r_2, \ldots\ldots\ldots, r_N)=E\Psi(r_1, r_2, \ldots\ldots\ldots, r_N) \quad \text{(II.1)}$$

The Hamiltonian operator, H, consists of a sum of three terms, the kinetic energy, the interaction with external potential (V_{ext}) and the electron-electron interaction ($V_{e\text{-}e}$). That is:

$$\hat{H}=\frac{1}{2}\sum_i^N \nabla_i^2 +\hat{V}_{ext}+\sum_{i<j}^N \frac{1}{|r_i-r_j|} \quad \text{(II.2)}$$

In materials simulation the external potential of interest is simply the interaction of the electrons with the atomic nuclei:

$$\hat{V}_{ext}=-\sum_\alpha^{Nat} \frac{Z_\alpha}{|r_i-R_\alpha|} \quad \text{(II.3)}$$

Here, r_i is the coordinate of electron i and the charge on the nucleus at R_α is Z_α.

We can see that from the Hamiltonian equation (II.2), the solution of the electronic Schrödinger equation is very complicated. Therefore we must simplify the quantum mechanical calculations by the reduction of the many-electron Hamiltonian to a physically equivalent/similar system which is easy to solve. For that, two famous principle ways are used; the first one is the Hartree-Fock [1] method.

II.1.2 Hartree-Fock Equation

We know that in the original Hartree solution [3] of Schrödinger equation, the wave function is not anti-symmetric, that fact is incorrect from Pauli principle (for the system consists of fermions (electrons) two particles can't be described by the same one-particle wave function). Take account of this principle Hartree-Fock have introduced a correction to the Hartree method, they have assumed that the total wave function is constructed by using the one-electron wave functions as an anti-symmetrized sum of all their products. This wave function can be represented by Slater determinant [4]:

$$\Psi(\vec{r})=\frac{1}{\sqrt{N!}}\begin{vmatrix} \phi_1(\vec{r_1})\,\phi_1(\vec{r_2})\,\cdots\cdots\,\phi_1(\vec{r_N}) \\ \phi_2(\vec{r_1})\,\phi_2(\vec{r_2})\,\cdots\cdots\,\phi_2(\vec{r_N}) \\ \vdots\vdots\vdots \\ \vdots\vdots\vdots \\ \phi_1(\vec{r_1})\phi_1(\vec{r_1})\cdots\cdots\,\phi_1(\vec{r_1}) \end{vmatrix} \tag{II.4}$$

Substitution of equation (II.4) into the equation (II.1) results in an expression for the H-F energy:

$$E_{H-F} = \int \phi_i^*(r)\left(-\frac{1}{2}\sum_i^N \nabla_i^2 + \hat{V}_{ext}\right)\phi_i + \frac{1}{2}\sum_{i,j}^N \int \frac{\phi_i^*(r_1)\phi_i(r_1)\phi_j^*(r_2)\phi_j(r_2)}{|r_i - r_j|}dr_1 dr_2 - \frac{1}{2}\sum_{i,j}^N \int \frac{\phi_i^*(r_1)\phi_j(r_1)\phi_i(r_2)\phi_j^*(r_2)}{|r_i - r_j|}dr_1 dr_2 \tag{II.5}$$

The second term is simply the classical coulomb energy written in term of the orbitals and the third term is the exchange energy. The ground state orbitals are determined by applying the variation theorem expression to this energy:

$$E[\Psi] \geq E_0 \tag{II.6}$$

And the orbital are orthonormal. This leads the H-F (or SCF) equation:

$$\left[-\frac{1}{2}\nabla^2 + V_{ext}(r) + \int \frac{\rho(\acute{r})}{|r-\acute{r}|} d\acute{r}\right]\phi_i(r) + \int V_x(r,\acute{r})\phi_i(\acute{r})d\acute{r} = \epsilon_i\phi_i(r) \quad \text{(II.7)}$$

Where the non-local exchange potential, V_x, is such that:

$$\int V_x(r,\acute{r})\phi_i(\acute{r})d\acute{r} = -\sum_j^N \int \frac{\phi_j(r)\phi_j^*(\acute{r})}{|r-\acute{r}|}\phi_i(\acute{r})d\acute{r} \quad \text{(II.8)}$$

The H-F equation described the non-interacting electrons structure where the exchange is taken in to account, while it does not include the correlation effect. Then the second way to solving the Schrödinger equation is the famous and powerful approach density functional theory (DFT).

II.1.3 Theorems for Density Functional Theory

The origin of this theory is the Thomas-Fermi approach [5]. When in this approach they try to find out an expression for the energy as a function of the charge density. In 1964 Hohenberg and Khon [2] based in this approach, focusing on the charge density of system not on the wave function like in H-F approach, have assumed that knowing the charge density of system leads us to determine all properties of this system. They have proved two remarkable theorems:

Theorem 1:

- ***The density as the basic variable uniquely determines the external potential.***

That mean for any density ρ we have unique external potential V_{ext}, when ρ is the ground charge density and because there is V_{ext} there is a many-body Schrödinger equation which their Hamiltonian is specified by this V_{ext} and the total number of electrons N, which can be computed from the density simply by integration over all space:

$$\int \rho(\vec{r})d\vec{r} = N \quad \text{(II.9)}$$

Also there is a wave function Ψ that is going to be a wave function ground state of that many-body Schrödinger equation.

- The ground state energy of many-electron system is unique functional of the density and is given by:

$$E_0 = E[\rho(\vec{r})] = T[\rho] + \hat{V}_{ext}[\rho] + V_{e-e}[\rho] \quad \text{(II.10)}$$

Where

$$V_{ext}[\rho] = \int \hat{V}_{ext}\left(\rho(\vec{r})\right)dr \quad \text{(II.11)}$$

T represents the kinetic energy and $V_{e\text{-}e}$ is the electron-electron interaction potential.

Theorem 2:

- ***The ground state density can be calculated in principle by the variational method.***

From the first theorem we know that the trial density ρ_t determines a unique trial Hamiltonian H_t and thus wave function Ψ_t: $E[\rho_t] = \langle \Psi_t | H | \Psi_t \rangle \geq E_0$ follows immediately from the variational theorem equation (II.6).

Consequently, from both theorem we can concludes that for any given $\acute{\rho}$ which determine $Vext'$ and $\acute{\Psi}$ we can define $F[\acute{\rho}]$ and write a new expression:

$$E[\acute{\rho}(\vec{r})] = F[\acute{\rho}(\vec{r})] + \int \acute{V}_{ext}\,\acute{\rho}(\vec{r})dr \geq E_0 \quad \text{(I.12)}$$

Where

$$F[\acute{\rho}(\vec{r})] = \left\langle \acute{\Psi} \middle| \hat{T} + \hat{V}_{e-e} \middle| \acute{\Psi} \right\rangle \quad \text{(I.13)}$$

The equation (II.12) is always going to be ≥ to the ground state energy E_0 that we obtained from Schrodinger equation in present of V_{ext}.

In other words, the lowest $E[\acute{\rho}(\vec{r})]$ will be the ground state energy. Then we have simply to minimize this$E[\acute{\rho}(\vec{r})]$.

Although the H-K theorem greatly simplified the many-body problem by proposing the density to be the basic quantity describing the electronic structure, however they only prove the existence of universal density functional, but do not show how to determine the exact form of $F[\acute{\rho}(\vec{r})]$ because both kinetic and electron-electron functional are unknown.

I.1.4 Khon-Sham Equation

Hohenberg and Khon have reformulated the many-electron problem and give us a new expression of energy equation (II.12).

But in this expression is very complicate to find the exact form of $F[\rho(\vec{r})]$, then we need to figure out an approximation to determine this functional. Khon and Sham proposed the following approach to approximating the kinetic and electron-electron functional [6]. They introduced a system of N non-interacting electrons to be described a single determinant wave function in N orbitals ϕ_i and live in external potential. In this system the ground state density is identical to the ground state density of interacting system and the kinetic energy and electron density are known exactly from the orbitals.

$$Ts[\rho] = -\frac{1}{2}\sum_{i}^{N}\langle\phi_i|\nabla^2|\phi_i\rangle \tag{II.14}$$

$$\rho(\vec{r}) = \sum_{i}^{N}|\phi_i|^2 \tag{II.15}$$

Now we can write the density functional by using kinetic energy as:

$$F[\rho] = T_s[\rho] + \frac{1}{2}\iint\frac{\rho(\overrightarrow{r})\rho(\overrightarrow{\dot{r}})}{|\vec{r}-\vec{\dot{r}}|}d\vec{r}d\vec{\dot{r}} + E_{xc}[\rho] \tag{II.16}$$

Where T_s the kinetic energy of the non-interacting system the second term is the Hartree energy and the third term is the exchange-correlation energy. Using the density functional, the K-S energy functional is obtained as the following:

$$E_{KS}[\rho] = T_s[\rho] + \int\rho\,(\vec{r})V_{ext}(\vec{r})d\vec{r} + \frac{1}{2}\iint\frac{\rho(\overrightarrow{r})\rho(\overrightarrow{\dot{r}})}{|\vec{r}-\vec{\dot{r}}|}d\vec{r}d\vec{\dot{r}} + E_{xc}[\rho] \tag{II.17}$$

Or

$$E_{KS}[\rho] = T_s[\rho] + \int\rho\,(\vec{r})(V_{ext}(\vec{r}) + \frac{1}{2}V_H)d\vec{r} + E_{xc}[\rho] \tag{II.18}$$

E_{xc} is simply the sum of the error made in using non-interacting kinetic energy and the error made in treating the electron-electron interaction classically.

$$E_{xc}[\rho] = (T[\rho] - T_s[\rho]) + (V_{e-e}[\rho] - V_H[\rho]) \tag{II.19}$$

Therefore, in order to find the ground state density and the energy, one has to solve the one-electron Schrödinger. This leads to the Kohn-Sham equations, an eigenvalue problem for the eigenfunctions $\phi_i(\vec{r})$ and eigenvalues ε_i.

$$\left(-\frac{1}{2}\nabla^2 + V_{KS}(\vec{r})\right)\phi_i(\vec{r}) = \varepsilon_i\phi_i(\vec{r}) \tag{II.20}$$

$$V_{KS} = V_{ext}[\rho] + V_H[\rho] + V_{xc}[\rho] \tag{II.21}$$

And$V_{xc}[\rho] = \frac{\delta E_{xc}[\rho]}{\delta\rho(\vec{r})}$ is the exchange and correlation potential which is an a priori complicated quantity and needs approximation in order to apply the K-S formalism in practice.

II.1.4.1 Exchange correlation Functional

Although density functional theory with K-S equation provides the scheme to reduce the many-body problem to a Schrödinger-like effective single-particle equation. But there are also some problematic cases. One of these problems is the exchange-correlation energy $\boldsymbol{E_{xc}}$ because there is no exact value or solution for it currently. Since there is no way of exactly accounting for $\boldsymbol{E_{xc}}$ energy we must rely on further approximation in order to provide a closed solution for the total electronic Hamiltonian. The simplest and earliest solution is known as the Local Density Approximation **(LDA)**.

II.1.4.1.a The Local Density Approximation

The simplest approximation to the exchange and correlation energy is the local density approximation (LDA). One uses the exchange and correlation energy of the homogeneous electron gas.

$$\boldsymbol{\varepsilon_{xc}^{LDA}}[\rho] = \varepsilon_{xc}^{hom}[\rho] \tag{II.22}$$

That yields the following exchange and correlation energy function:

$$E_{\boldsymbol{xc}}[\rho] = \int \rho(\vec{r})\,\varepsilon_{xc}^{hom}(\rho)d^3\vec{r} \tag{II.23}$$

We can see that the accuracy of this approximation is good only for slowly varying electronic density resembling the one of the homogeneous electron gas. However, it has proved to work rather well even for systems which have inhomogeneous electron density.

The exchange-correlation potential within LDA is expressed as:

$$V_{xc}^{LDA} = \varepsilon_{xc}^{LDA}[\rho(\vec{r})] + \rho(\vec{r})\frac{\delta\varepsilon_{xc}^{LDA}([\rho(\vec{r})])}{\delta\rho(\vec{r})} \quad \text{(II.24)}$$

The energy $\varepsilon_{xc}^{LDA}(\rho)$ can be separated into exchange and correlation contribution:

$$\varepsilon_{xc}(\rho) = \varepsilon_x(\rho) + \varepsilon_c(\rho) \quad \text{(II.25)}$$

The exchange energy of the homogeneous electron gas can be found analytically by the Dirac form [7]

$$\varepsilon_x(\rho) = -\frac{3}{4}\left(\frac{3}{\pi}\right)^{1/3}\rho^{1/3} \quad \text{(II.26)}$$

With the correlation energy is obtained by means of the QMC calculation. The most widely used approximation is the parameterization by Perdew and Zunger's [8] of the QMC results of Ceperley and Alder [9].

II.1.4.1.b The gradient Generalized Approximation

As mentioned above, the LDA neglects the inhomogeneities of the real charge density which could be very different from the homogeneous electron gaz. This leads to the development of various generalized-gradient approximations (GGAs) which include density gradient corrections and higher spatial derivatives of the electron density and give better results than LDA in many cases. Three most widely used GGAs are the forms proposed by Becke [10] (B88), Perdew et al. [11], and Perdew, Burke and Ernzerhof [12] (PBE).

This resulting exchange-correlation functional has the following form:

$$E_{xc}^{GGA} = \int f_{xc}(\rho(\vec{r}), |\nabla\rho(\vec{r})|)\rho(\vec{r})d\vec{r} \quad \text{(II.27)}$$

Where f_{xc} can be decomposed linearly into exchange contribution f_x and correlation contribution f_c as $f_{xc} = f_x + f_c$.

II.1.4.2 Self-Consistent Khon-Sham (K-S Scheme)

The solution to the KS equations can be obtained by using iterative procedure since the effective potential V_{KS} depends on the density through the exchange-correlation potential. The procedure starts with an initial guess for density and this density is used to construct the KS potential and the total energy. With this information, the equations are solved to generate

the new set of the KS orbitals, and they are used to obtain a new density, the KS potential and the total energy. This cycle is repeated until the convergence is reached. A typical Khon-Sham self-consistent scheme is defined in Fig II.1.

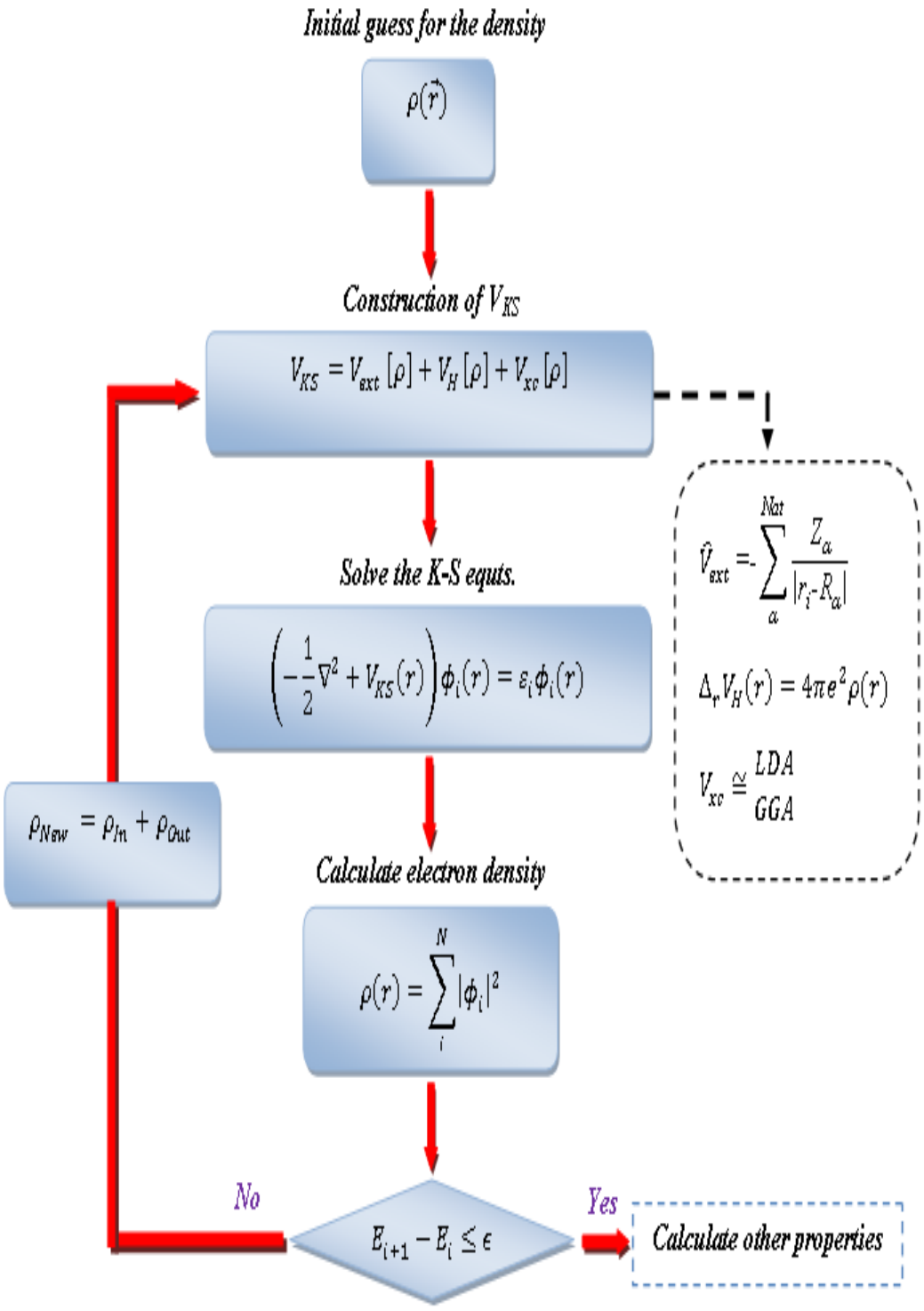

Fig. II.1: Self-consistent K-S scheme.

In these sections, we have seen that for solving the many-electron problem we can used two kinds of approach, the first is Hartree-Fock method and the second is density functional theory DFT developed by Hohenberg and Khon. This later is very powerful method it can give a new reformulation to the many-body problem based on the electron density and the only problem is the unknown of the kinetic and electron-electron functional.

For that reason, Khon and Sham have proposed a new equation which is called the K-S equation. It's Schrödinger like equation with the external potential replaced by the effective potential (potential of K-S V_{KS}) which depends on the density. This density itself depends on the single particle state ϕ_i. The K-S equation allows us to derive all the potential except the exchange and correlation potential that needs approach to determine it. There are two choices in order to treat this potential, the first is the local density approximation LDA and the second is the gradient generalized approximation GGA.

Let us assume that this V_{xc} is well define, now the last thing needed to solve the K-S equation is the appropriate wave function to describe the electron-ion interaction. Then the question is how to express the K-S orbital's? In this case we attempt to discuss this problem in the next part.

Now we are going to present a small introduction into a newly developed scheme for solving the K-S equation with the FP-(L)APW+lo formalism. We introduce a brief description of Bloch theorem, the original method of LAPW, APW and the concept of FP-(L)APW+lo method.

II.1.5 Bloch's Theorem

Bloch's theorem [13] proves that if the potential V has translation symmetry, we can write any eigenfunction $\Psi(\vec{r})$ as a product of a function ϕ_g $(\vec{r})$ that has the periodicity of the lattice, and a plane wave $e^{ig.r}$ with g any vector in reciprocal space,

$$\Psi(\vec{r}) = \phi_g(\vec{r})e^{ig.r} \tag{II.28}$$

If the reciprocal vector g is written as the sum of a vector (k) in the first Brillouin zone and a reciprocal lattice vector $\vec{K}$, $\vec{g} = \vec{k}+\vec{K}$, the Bloch theorem is rewritten as,

$$\Psi(\vec{r}) = \Psi_{k_n}(\vec{r}) = \left[\phi_g(\vec{r})e^{i\vec{K}.\vec{r}}\right] e^{i\vec{K}.\vec{r}=\phi_{k_n}(\vec{r})e^{i\vec{K}.\vec{r}}} \quad \text{(II.29)}$$

Where, *n* indicates the number of Brillouin zone where *g* is in, and is called band index.

The first term in Eq. (II.29) $\phi_{k_n}(\vec{r})$, determines the eigenfunction, $\Psi(\vec{r})$. Due to the periodicity of the lattice, the straight idea to get $\phi_{k_n}(\vec{r})$ is to sum over waves that have the same periodicity of the lattice. Then

$$\phi_{k_n}(\vec{r}) = \sum_K c_K^{n,\vec{K}}\, e^{i\vec{K}.\vec{r}} \quad \text{(II.30)}$$

The expansion of $\Psi_{k_n}(\vec{r})$ becomes

$$\Psi_{k_n}(\vec{r}) = \sum_K c_K^{n,\vec{K}}\, e^{i(\vec{g}).\vec{r}} \quad \text{(II.31)}$$

II.1.6 The Augmented Plane Wave (APW) Method

The APW method is based on the Slater [14] observation that:

- Close to the nuclei, electrons bind strongly to their nuclei. Their behavior is quite as in a free atom and they could be described more efficient by atomic functions.
- Far away from nuclei, electrons are free in space and are then suitably described by plane waves.

Therefore, space is divided into spheres centered at each atom site, the so called *Muffin_tin* (Mt), and the Interstitial (I) region Fig. II.2.a.

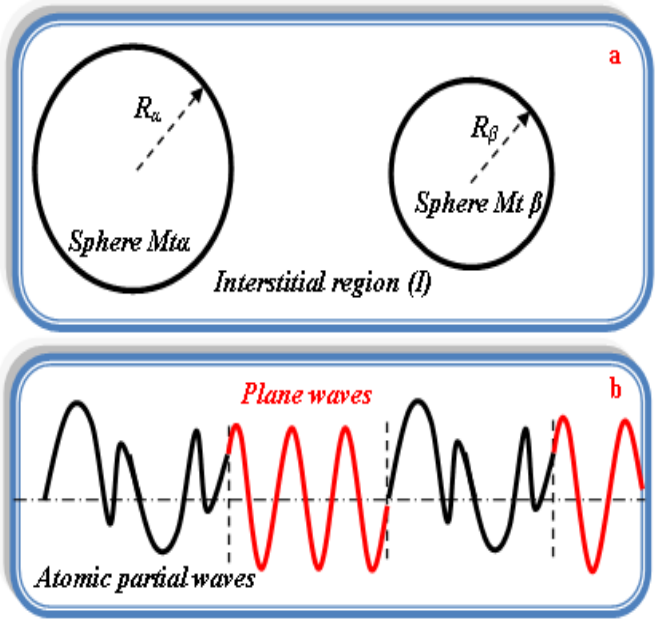

Fig. II.2: Schematic division for: a) Space into Muffin_tin sphere and interstitial region. b) Basis set, black atomic partial waves in the Mt sphere and red plane waves in I region.

Inside the muffin_tin the sphere is approximated by a spherically symmetric shape, and in interstitial region the potential is set to a constant, and two types of basis set are used in the two different regions Fig. (II.1.a):

$$\phi = \begin{cases} \frac{1}{\sqrt{\Omega}} e^{i(\vec{G}+\vec{k})\vec{r}} & (r \in I) \\ \sum_{lm} A_{lm}\, u_l^{\alpha}(r, E_l) Y_{lm}(\hat{r}) & (r \in Mt) \end{cases} \qquad \text{(II.5)}$$

Where, Ω is the cell volume, u_l radial function, Y_{lm} spherical harmonic and A_{lm} coefficients, which are determined from the requirement that the wave functions have to be continuous at the boundary of the Muffin_tin spheres.

$$A_{lm} = \frac{4\pi i^l}{\sqrt{\Omega} u_l(R_\alpha)} \sum_G J_l\left(|\vec{k}+\vec{g}|R_\alpha\right) Y_{lm}^*(\vec{k}+\vec{g}) \qquad \text{(II.6)}$$

In the interstitial region the plane waves solves de Schrödinger equation in a constant potential, while spherical harmonics times radial function are the solution of Schrödinger equation in a potential $V(\vec{r})$and energy E_l:

$$-\frac{1}{r^2}\frac{d}{d\vec{r}}\left(r^2\frac{du_l}{d\vec{r}}\right)+\left(\frac{l(l+1)}{r^2}+V(\vec{r})-E_l\right)\vec{r}u_l=0 \qquad \text{(II.7)}$$

In the APW method, the biggest disadvantage is that the parameter E_l in Eq. (II.5) which is needed to describe the eigenstate $\Psi_{k_n}(\vec{r})$ is unknown, and requiring the E_l's to be equal to the band energies.

APW method can't get this energy from a simple diagonalization of the Hamiltonian matrix. Since the radial function u_l's depend on the band energies, the secular equation becomes a nonlinear problem. One has to set trial energy for E_l, obtaining the APW basis by solving Eq. (II.7), set up the matrix elements and computes the determinant $|H-ES|$.

If the eigenenergy does not equal E_l, trial energy must be chosen until eigenenergy equal E_l Fig. (II.3). this makes the APW method extremely inefficient.

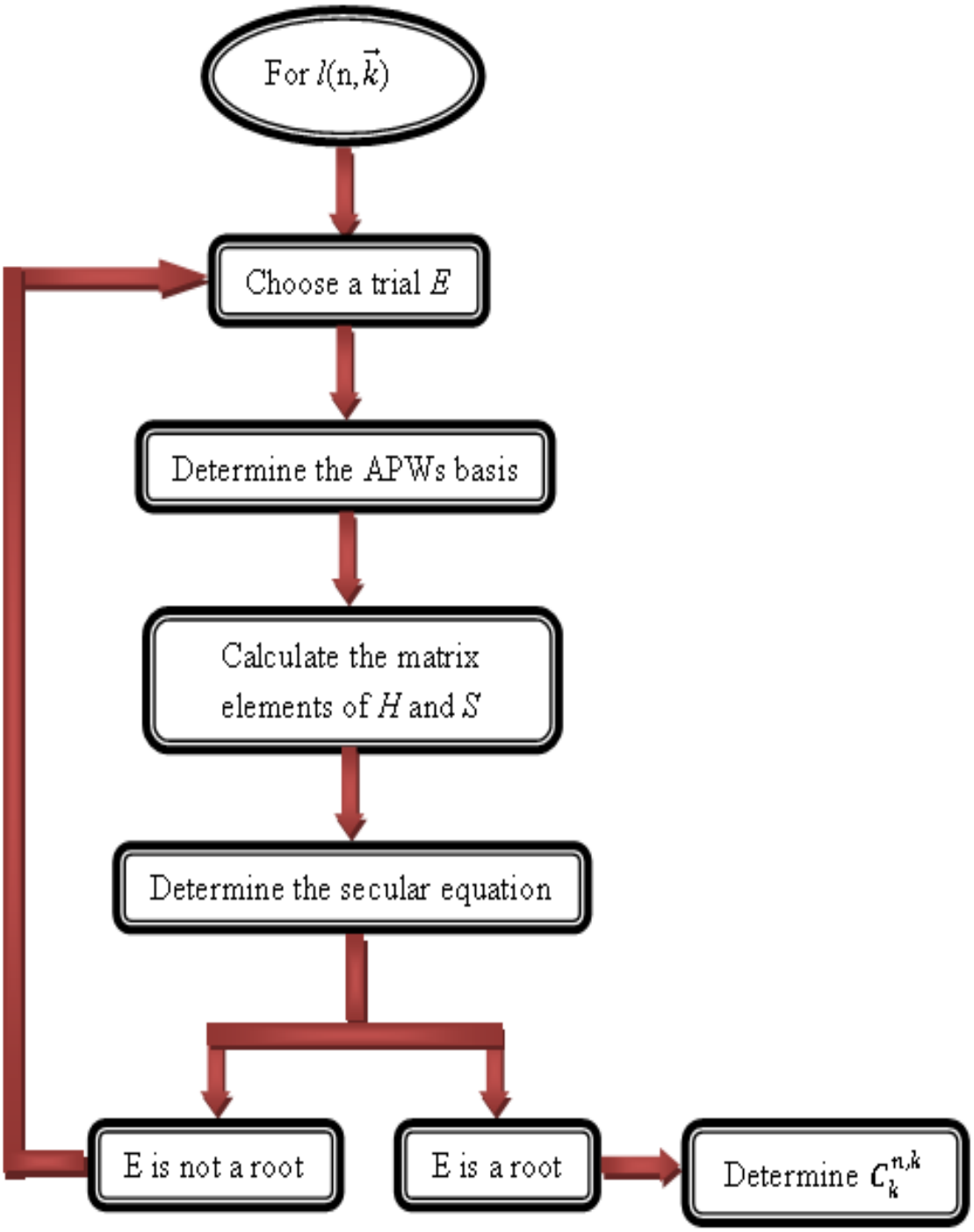

Fig. II.3: Flowchart of APW method.

Another disadvantage is that, when u_l in Eq. (II.6) becomes zero, the radial function and the plane wave becomes decoupled, known as the asymptote problem. That means there is not continuity between the radial function and the plane wave in the boundary of Mt sphere Fig. II.1.b.

II.1.7 The Concept of LAPW Method

To avoid the non-linearity problem and the continuity in the APW method, the linearized plane wave LAPW method have developed by Anderson [15] and Kolling and Arbman [16]. Based on idea proposed by Marcus [17], the radial function u_l in the Mt sphere were supplemented by their energy derivative $\dot{u}_l = \frac{\partial u_l}{\partial E_l}$, but both, u_l and $\dot{u}_l$ are now evaluated at a fixed energy E_l. then the LAPW basis function are in the interstitial region, the basis set is the same as in APW method, but in the Mt spheres, the basic functions not only depend on u_l, but also on its energy derivative $\dot{u}_l$.

$$\phi = \begin{cases} \frac{1}{\sqrt{\Omega}} e^{i(\vec{G}+\vec{k})r} & (r \in I) \\ \sum_{lm} [A_{lm}\, u_l^{\alpha}(r, E_l) + B_{lm} \dot{u}_l^{\alpha}(\vec{r}, E_l)]\, Y_{lm}(\hat{r}) & (r \in Mt) \end{cases} \quad \text{(II.8)}$$

Where A_{lm} and B_{lm} are the coefficients determined by requiring that not only the u_l, but $\dot{u}_l$ are continuous at the Mt spheres boundary. $\dot{u}_l$ is calculated from a Schrödinger-like equation, derived by taking the energy derivative of Eq. (II.7) with respect to E_l:

$$-\frac{1}{r^2}\frac{d}{d\vec{r}}\left(r^2 \frac{du_l}{d\vec{r}}\right) + \left(\frac{l(l+1)}{r^2} + V(\vec{r}) - E_l\right) r\dot{u}_l = \vec{r} u_l \quad \text{(II.9)}$$

Furthermore if u_l is zero at the sphere boundary, its radial derivative is in general non zero. Hence, the boundary conditions can always be satisfied and there is no asymptote problem. Now if E_l differs slightly from the band energy ε, a linear combination will reproduce the APW radial function constructed at the band energy by following relation:

$$u_l(\varepsilon, \vec{r}) = u_l(E_l, \vec{r}) + (\varepsilon - E_l)\dot{u}_l(E_l, \vec{r}) + O((\varepsilon - E_l)^2) \quad \text{(II.10)}$$

II.1.8 The Concept of LAPW+LO Method

Some materials contain chemical elements with states intermediate between band and core states and those are coined semi-core states. They have same angular quantum number l as the valence states but with lower principal quantum number n. when applying LAPW on these states, it is thus hard to use one $\hat{E}_l$ to determine the two same l in Eq. (II.8). This

dilemma is solved by adding another type of basis function to the LAPW basis set, called a Local Orbital (LO), which is defined as:

$$\phi_{lm}^{LO} = \begin{cases} 0 & (r \in I) \\ \sum_{lm} [A_{lm}\, u_l^{\alpha}(\vec{r}, E_l^1) + B_{lm} \dot{u}_l^{\alpha}(\vec{r}, E_l^1) + C_{lm} u_l(\vec{r}, E_l^2)]\, Y_{lm}(\hat{r}) & (r \in Mt) \end{cases} \quad \text{(II.11)}$$

This local orbital is zero in the interstitial region and in the Mt sphere of the other atoms. The three coefficients A_{lm}, B_{lm} and C_{lm} are determined by requiring the LO to have zero value at the Mt boundary.

II.1.9 The Concept of APW+lo Method

This method combines the good feature of APW and LAPW+LO which the basis set will be energy dependent and still have the same size as in the APW method and the problem of description of the eigenfunctions in the APW method is treated by adding a new local orbital (lo) which is different from the LOs.

The APW+lo basis set contains the APWs function:

$$\phi = \begin{cases} \frac{1}{\sqrt{\Omega}} e^{i(\vec{G}+\vec{k})\vec{r}} & (r \in I) \\ \sum_{lm} A_{lm}\, u_l^{\alpha}(\vec{r}, E_l) Y_{lm}(\hat{r}) & (r \in Mt) \end{cases} \quad \text{(II.12)}$$

And the local orbital's:

$$\phi = \begin{cases} 0 & (r \in I) \\ \sum_{lm} [A_{lm}\, u_l^{\alpha}(\vec{r}, E_l) + B_{lm} \dot{u}_l^{\alpha}(\vec{r}, E_l)]\, Y_{lm}(\hat{r}) & (r \in Mt) \end{cases} \quad \text{(II.13)}$$

The two coefficients A_{lm} and B_{lm} are determined by normalization, and by requiring that the local orbital has zero value at the Mt boundary. Hence, both the APW and the (lo) are continuous at the sphere boundary.

II.1.10 The Full Potential APW+lo Method

The full potential APW+lo method combines the choice of the APW+lo basis set with the treatment of the full potential and charge density without any shape approximations in both interstitial region and inside Mt sphere. The potential is defined as:

$$V(\vec{r}) = \begin{cases} \sum_{G} V_I^G e^{i\vec{G}\vec{r}} & I\ region \\ \sum_{L} V_{Mt}^L(\vec{r})\, Y_L(\hat{r}) & Mt\ sphere \end{cases} \quad \text{(II.14)}$$

And the charge density is represented in the same way as the potential:

$$\rho(\vec{r}) = \begin{cases} \sum_{G} \rho_I^G e^{i\vec{G}\vec{r}} & Iregion \\ \sum_{L} \rho_{Mt}^L(\vec{r})\, Y_L(\hat{r}) & Mt\ sphere \end{cases} \quad \text{(II.15)}$$

In these latest sections, we have seen that the FP-LAPW method is one of the methods developed to give solution of K-S equation. The origin of this method is the APW method developed by Slater, which is based on the space separation and use of suitably modified basis functions for different regions of space. The latter are modified by LAPW method in order to avoid the non-linearity problem and the continuity in the APW method.

However some materials contain chemical elements with states intermediate between band and core states and those are coined semi-core states. They have same angular quantum number *l* as the valence states but with lower principal quantum number *n.* When applying LAPW on these states, it is thus hard to use one $\hat{E}l$ to determine the two same *l.* This dilemma is solved by adding another type of basis function to the LAPW basis set, called a Local Orbital (LO) and we have a new method called LAPW+LO method.

Moreover a further method have developed which combines the good feature of APW and LAPW+LO, which the basis set will be energy dependent and still have the same size as

in the APW method and the problem of description of the eigenfunctions in the APW method is treated by adding a new local orbital (lo) which is different from the LOs. This method is called APW+lo method.

II.2 Electron Boltzmann Transport Equations (EBTE)

Solid matter is composed basically by ions and electrons. Electrons move in a metal or semiconductor through the laws of Quantum Mechanics, although for many purposes they can be treated as classical particles. In a first approximation, electrons move in a perfect lattice (Born–Oppenheimer approximation), within a periodic potential given by the crystal periodicity of the solid. Phonons are a consequence of the disorder or the lack of periodicity in real lattices. They can also be treated as quasi-particles, with quasi-momentum $\hbar q = h/\lambda_{ph}$, λ_{ph} defined the phonon wavelength. In a real lattice, electrons can interact with network defect, a phenomenon known as diffusion (scattering). The main source of lattice defect is the dependence with temperature.

At low temperature, the major basis of electron scattering is the presence of impurities or the existence of boundaries, the last factor being extremely important in nanometric dimension materials; where the diffusion of electrons caused by impurity is elastic.

At high temperatures, electron–phonon interaction is the majority important diffusion process. Diffusion by optical phonons is inelastic, whereas that by acoustic phonons is elastic, after the scattering process the electron energy is not conserved because the electrons lose the phonon energy. In the analysis of electron–phonon scattering, phonons are necessarily treated as quasi-particles. On the other side, electrons are fermions and follow the Fermi–Dirac statistics, the distribution function f_0 being:

$$f_0 = \frac{1}{e^{(\varepsilon(\vec{k})-\mu)/k_B T} + 1} \qquad \text{II.16}$$

Where $\varepsilon(k)$ is the electron energy, μ the chemical potential (the Fermi energy at T= 0 K), k_B the Boltzmann constant, and T the absolute temperature.

II.2.1 The Boltzmann Transport Equation for Electrons

The distribution function f($\vec{r}$, $\vec{k}$, t) gives the probability of occupation of a band (state) by an electron situated at $\vec{r}$ with a wave integer $\vec{k}$ at time t. the both first parameters ($\vec{r}$ and $\vec{k}$) can be assumed to be within a given interval Δr and Δk, respectively, in sequence to fulfill the Heisenberg's rule. The number of electrons occupying the volume element d^3k in r at t per unit volume of the crystal is [1]:

$$dn(r) = \frac{2}{(2\pi)^3} f(\vec{r}, \vec{k}, \mathrm{t}) d^3\vec{k} \qquad \text{II.17}$$

Where the factor 2 assumes spin degeneracy. In equilibrium, the distribution function can be written as:

$$f_0(\vec{r}, \vec{k}) = \frac{1}{e^{(\varepsilon(\vec{k}) - \mu(\vec{r}))/k_B T(\vec{r})} + 1} \qquad \text{II.18}$$

Where the dependence on k is given by the electronic band structure of the solid (the band index has been omitted for simplicity) and that on r via a possible gradient of the temperature or carrier concentration (via the chemical potential).

The distribution function can change in time due to the existence of internal or external forces. The rate of variation of the distribution function can be written, using the chain rule, as:

$$\frac{df}{dt} = \nabla_r f.\ \frac{dr}{dt} + \frac{1}{\hbar} \nabla_k f.\ \frac{dp}{dt} + \frac{\partial f}{\partial t} = v.\ \nabla_r f + \frac{1}{\hbar} \nabla_k f.\ F_a + \frac{\partial f}{\partial t} \qquad \text{II.19}$$

F_a being the set of applied forces, which can be divided into external (F) and internal forces (F_D), that last due to the existence of impurities, defects, phonons, etc. Since the total number of states is constant, $df/dt = 0$, the previous equation can be written as:

$$v.\ \nabla_r f + \frac{1}{\hbar} \mathrm{F}.\nabla_k f + \frac{1}{\hbar} \mathrm{F_D}.\nabla_k f = -\frac{\partial f}{\partial t} = -\left(\frac{\partial f}{\partial t}\right)_{drift} - \left(\frac{\partial f}{\partial t}\right)_{scatt} \qquad \text{II.20}$$

We can separate the previous equation (Equ. II.20) into:

$$\begin{cases} -\left(\frac{\partial f}{\partial t}\right)_{scatt} = \frac{1}{\hbar}\,\mathrm{F_D}.\nabla_k f & \text{II.21} \\ -\left(\frac{\partial f}{\partial t}\right)_{drift} = v.\ \nabla_r f + \frac{1}{\hbar}\,\mathrm{F}.\nabla_k f & \text{II.22} \end{cases}$$

Where equation II.21 being to the presence of external fields (drift) and equation II.22 for the presence of the internal fields (scattering).

II.2.2 Relaxation Time Approximation

At equilibrium ($t = 0$), the drift term is concealed and the system will return to due to the existence of diffusion. In that case, the scattering will produce an arbitrary movement of the electrons and the time development of f would be:

$$\left(\frac{\partial f}{\partial t}\right) = \left(\frac{\partial f}{\partial t}\right)_{scatt} \quad \text{II.23}$$

If the system is out of equilibrium, the speed of evolution of the distribution function can be assumed to be proportional to:

$$\left(\frac{\partial f}{\partial t}\right) = \left(\frac{\partial f}{\partial t}\right)_{scatt} = \frac{f(\vec{r},\vec{k},t) - f_0(\vec{r},\vec{k})}{\tau(\vec{k})} \quad \text{II.24}$$

And $1 / \tau(k)$ being the proportionality constant. The solution of equation II.24 is:

$$f(\vec{r},\vec{k},t) - f_0(\vec{r},\vec{k}) = \left[f(\vec{r},\vec{k},0) - f_0(\vec{r},\vec{k})\right] e^{-\left(\frac{t}{\tau(\vec{k})}\right)} \quad \text{II.25}$$

In terms of τ(k), the Boltzmann equation can be written as:

$$v.\ \nabla_r f + \frac{1}{\hbar}\,\mathrm{F}.\nabla_k f = -\frac{f(\vec{r},\vec{k}) - f_0(\vec{r},\vec{k})}{\tau(\vec{k})} \quad \text{II.26}$$

II.2.3 The Linearized Boltzmann Equation

The relaxation time approximation allows a critical solution of the Boltzmann equation for the stationary case. If we assumed$Fa = eE$, and believe space homogeneity, the Boltzmann equation can be written as:

$$\frac{e}{\hbar}\,\mathrm{E}.\nabla_k f = -\frac{f(\vec{k}) - f_0(\vec{k})}{\tau(\vec{k})} \quad \text{II.27}$$

in terms of $f(k)$, we can rewrite the equation as follow:

$$f(\vec{k}) = f_0(\vec{k}) - \frac{e}{\hbar}\,\tau(\vec{k})\mathrm{E}.\nabla_k f \quad \text{II.27}$$

In principle, this equation can be solved iteratively, but, if we are interested in linear phenomena on the electric field E, an approximated solution is obtained replacing the distribution function $f(\vec{k})$ by the equilibrium distribution function $f_0(\vec{k})$ in the k derivative:

$$f(\vec{k}) \approx f_0(\vec{k}) - \frac{e}{\hbar}\tau(\vec{k})\mathrm{E}.\nabla_k f_0 \qquad \text{II.28}$$

Thus, for a linear problem or weak electric fields, the Boltzmann equation can be interpreted as a linear expansion of the distribution function around $\vec{k}$. Since $f(\vec{k})$ is not far from equilibrium,

$$f(\vec{k}) \approx f_0(\vec{k} - \frac{e}{\hbar}\tau(\vec{k})E) \qquad \text{II.29}$$

II.2.3.1 The Effect of a Magnetic Field on the Boltzmann Equation

Following Ziman, a magnetic field does not produce drift on the electrons (it does not produce work), but deviates the electron path due to the Lorentz force. Thus, the time variation of the distribution function due to the presence of a magnetic field (the Lorentz force),

$$\left(\frac{\partial f}{\partial t}\right)_B = \frac{e}{\hbar} v \times B.\nabla_k f^{(1)} \qquad \text{II.30}$$

Where

$$f^{(1)}(\vec{r},\vec{k}) = \frac{\partial f_0}{\partial \varepsilon}\tau(\vec{k})V.A(\vec{r},\vec{k}) \qquad \text{II.31}$$

With

$$A(\vec{r},\vec{k}) = [\nabla(\mathrm{e}\emptyset + \mu) + (\varepsilon - \mu)\nabla \ln \mathrm{T}] \qquad \text{II.32}$$

Cannot be included in the drift, but in parallel with the scattering terms: the deviation of the electrons due to the magnetic field is equivalent to a scattering process. However, we cannot linearized the previous equation since $v.v \times B = 0$ and the effect of the magnetic field is neglected.

The Boltzmann equation, including the effect of the magnetic field, is

$$v.\ \nabla_r f + \frac{1}{\hbar}\ \mathrm{F}.\nabla_k f = -\frac{f^{(1)}(\vec{r},\vec{k})}{\tau(\vec{k})} + \frac{e}{\hbar} v \times B.\nabla_k f^{(1)} \qquad \text{II.33}$$

By generalizing the A vector to a new amount, Ξ The solution for $f^{(1)}(\vec{r},\vec{k})$ written as follow:

$$f^{(1)}(\vec{r},\vec{k}) = \frac{\partial f_0}{\partial \varepsilon}\tau(\vec{k})V.\Xi \qquad \text{II.34}$$

If there is no magnetic field, the solution must be reduced to Ξ = A. The first derivative of the distribution function can be found to be:

$$\nabla_k f^{(1)} = -\frac{\partial f_0}{\partial \varepsilon}\tau\hbar M^{*-1}\,\Xi \qquad \text{II.35}$$

M^* being the effective mass tensor and a dependence of k through the energy has been assumed for τ and Ξ. In that case, the derivative with respect to k would contain the velocity, which is perpendicular to $v \times B$. We arrive to the equation:

$$\Xi = \nabla(\mathrm{e}\emptyset + \mu) + (\varepsilon - \mu)\nabla \ln \mathrm{T} + eM^{*-1}\,\Xi \times \mathrm{B} = \mathrm{A} + eM^{*-1}\,\Xi \times \mathrm{B} \qquad \text{II.36}$$

Assuming an isotropic effective mass for simplicity, the solution is:

$$f^{(1)} = e\tau\frac{\partial f_0}{\partial \varepsilon}v.\frac{A + (e\tau/m^*)^2(A.B)B + (e\tau/m^*)(A \times B)}{1 + (e\tau/m^*)^2B^2} \qquad \text{II.37}$$

II.2.4 Current and Energy Flux Densities

The current density can be written as:

$$j = \frac{e}{2\pi^3}\int v f(\vec{r},\vec{k})\,d^3\vec{k} = \frac{e}{2\pi^3}\int v f^{(1)}(\vec{r},\vec{k})\,d^3\vec{k} \qquad \text{II.38}$$

Substituting the value of $f^{(1)}(\vec{r},\vec{k})$,

$$j = \frac{e}{2\pi^3}\int \left(-\frac{\partial f_0}{\partial \varepsilon}\right)\tau v(v.\Xi)d^3\vec{k} \qquad \text{II.39}$$

The movement of charged particles not only carries a current but also transfers energy. The energy flux, i.e. the energy amount crossing a unit cross section per unit time is given by the expression:

$$j = \frac{1}{4\pi^3}\int \varepsilon(\vec{k})v f^{(1)}(r,k)\,d^3\vec{k} \qquad \text{II.40}$$

The expression, in terms of Ξ, is

$$j = \frac{1}{4\pi^3\hbar^2}\int \left(-\frac{\partial f_0}{\partial \varepsilon}\right)\varepsilon(\vec{k})\tau v(v.\Xi)d^3\vec{k} \qquad \text{II.41}$$

In the absence of magnetic fields,

$$\Xi = eE - \nabla\mu - \frac{\varepsilon - \mu}{\mathrm{T}}\nabla\mathrm{T} = \mathrm{E} \qquad \text{II.42}$$

The expression for the electric current becomes

$$j = \frac{1}{4\pi^3\hbar^2}\int \left(-\frac{\partial f_0}{\partial \varepsilon}\right)\varepsilon(\vec{k})\tau v\left(v.\left[E - \nabla\mu - \frac{\varepsilon - \mu}{\mathrm{T}}\nabla\mathrm{T}\right]\right)d^3\vec{k} \qquad \text{II.43}$$

For an isotropic medium,

$$j = \frac{4e}{3m^*}\int\left(-\frac{\partial f_0}{\partial \varepsilon}\right)\tau\varepsilon D(\varepsilon)\left(eE - \nabla\mu - \frac{\varepsilon-\mu}{\mathrm{T}}\nabla\mathrm{T}\right)d\varepsilon \quad \text{II.44}$$

Introducing the notation

$$l_{ij} = \frac{4}{3m^*}\int\left(-\frac{\partial f_0}{\partial \varepsilon}\right)\tau^i\varepsilon^i D(\varepsilon)d\varepsilon \quad \text{II.45}$$

The electrical current becomes

$$j = el_{11}\left(eE - T\nabla\frac{\mu}{T}\right) - el_{21}\nabla lnT \quad \text{II.46}$$

Similarly,

$$j_Q = el_{21}\left(eE - T\nabla\frac{\mu}{T}\right) - el_{31}\nabla lnT \quad \text{II.47}$$

From an isotropic medium equation and the definition of the transport coefficients, the electrical conductivity is:

$$e^2 l_{11} = \sigma \quad \text{II.48}$$

If there is no electrical current circulating through the semiconductor (open circuit), $j = 0$, and the electric field is

$$E = \frac{1}{e}\nabla\mu + \frac{l_{21} - \mu l_{11}}{el_{11}T}\nabla T \quad \text{II.49}$$

If there are no gradients of concentration, from the definition of the Seebeck effect, the Seebeck coefficient $S = dV / dT$ is given by

$$S = \frac{l_{21} - \mu l_{11}}{el_{11}T} \quad \text{II.50}$$

We can introduce in Eq. (1.51) the electrical current. The result is

$$j_Q = \frac{l_{21}}{el_{11}}j + \left(\frac{l_{21}^2 - el_{31}l_{11}}{el_{11}}\right)\nabla T = \prod j - \square_e \nabla T \quad \text{II.51}$$

Where the Peltier coefficient

$$\prod = \frac{l_{21}}{el_{11}} = ST \quad \text{II.52}$$

And the electron thermal conductivity

$$\kappa_e = \frac{l_{21}^2 - el_{31}l_{11}}{el_{11}} \quad \text{II.53}$$

The opposite relations are

$$l_{11} = \frac{\sigma}{e^2}, \qquad l_{21} = \frac{\sigma ST}{e}, \qquad l_{11} = ST - \kappa_e \quad \text{II.54}$$

And the transport coefficients can be written in terms of the relaxation time $\langle\tau\rangle$ as:

$$l_{ij} = \frac{n}{m^*}\varepsilon^i\tau^i \qquad \text{II.55}$$

II.2.5 The Thermal Conductivity in a Semiconductor

In semiconductors with parabolic bands, the relaxation time can be written as:

$$\tau = \tau_0\varepsilon^\lambda \qquad \text{II.56}$$

Where λ is a exponent which depends on the scattering mechanism. In terms of l_{ij} with the relaxation time ⟨τ⟩

$$l_{11} = \frac{n}{m^*}\langle\varepsilon\tau\rangle,\ l_{21} = \frac{n}{m^*}\langle\varepsilon^2\tau\rangle, \qquad l_{31} = \frac{n}{m^*}\langle\varepsilon^3\tau\rangle \qquad \text{II.57}$$

Following the expression for the electronic thermal conductivity, it can be written explicitly in terms of Γ −functions:

$$\kappa_e = \frac{n}{m^*}\frac{5k_B^2T\tau_0}{4}\left[7\frac{\Gamma(9/2+\lambda)}{\Gamma(9/2)} - 5\frac{\Gamma^2(7/2+\lambda)\Gamma(5/2)}{\Gamma^2(5/2+\lambda)(7/2)}\right] \qquad \text{II.58}$$

The expression of κe contains the unknown factor τ0, which is also included in the electrical conductivity. Actually, we can calculate the amount $\kappa_e\ /\ \sigma\ T\ = L$, the Lorentz number:

$$L = \frac{\kappa_e}{\sigma T} = \frac{l_{31}l_{11} - l_{21}^2}{e^2l_{11}^2T^2} = \frac{k_B^2}{e^2}(5/2+\lambda) \qquad \text{II.59}$$

This is independent ofτ_0. Thus, the thermal conductivity can be written in terms of the electrical conductivity and the Lorentz number:

$$\kappa_e = \sigma LT = \frac{k_B^2T^2}{e^2}(5/2+\lambda)\sigma \qquad \text{II.60}$$

In a semiconductor, the thermal conductivity of the electrons is proportional to the electronic conductivity. The expression $\kappa_e\ /\ \sigma\ =\ L\ T$ is known as Wiedemann–Franz law. As it is well known, in the case of metals, or a degenerate semiconductor, the Lorentz number is a constant:

$$L = \frac{\kappa_e}{\sigma T} = \frac{\pi^2}{3}\frac{k_B^2}{e^2} \qquad \text{II.61}$$

II.2.6 The Seebeck Coefficient in a Semiconductor

In the case of a metal or a degenerate semiconductor, the transport coefficients

$$l_{ij} = \frac{4}{3m^*}\int\left(-\frac{\partial f_0}{\partial\varepsilon}\right)\tau^i\varepsilon^iD(\varepsilon)d\varepsilon = \frac{4e^2}{3m^*}\tau^i(E_F)E_F^iD(E_F) \qquad \text{II.62}$$

And the Seebeck coefficient is zero. It is necessary to take the first term in the development of the Fermi integral, giving

$$S = \frac{\pi^2}{3}\frac{k_B^2}{e}\frac{\partial ln\sigma(\varepsilon)}{\partial \varepsilon}\Big|_{E=E_F} = \frac{\pi^2}{3}\frac{k_B^2}{eE_F} \qquad \text{II.63}$$

The Seebeck coefficient for a typical metal, Cu (E_F= 7. 0 eV), is $S = 1.05\mu V / K$ at 300 K.

Instead of the chemical potential, it is more useful to write the expression in terms of the electron concentration:

$$S = \frac{k_B}{e}\left[\frac{5}{2} + \lambda - ln\frac{N_C}{n}\right] \qquad \text{II.64}$$

We can quantify the Seebeck coefficient for a typical semiconductor. At low temperature $T = 100\,K$, $k_BT = 8.64\,meV$ If we assume for simplicity that, at this temperature, the chemical potential is 8.64 meV below the conduction band, and those impurities are the dominant scattering mechanisms$S = 5k_B / e = 0.4\,meV / K$. Typical values are at least one order of magnitude larger than in metals.

From the first term in the development of the Fermi integral, we can argue that the Seebeck coefficient, roughly, is proportional to:

$$S \propto \frac{\partial D(\varepsilon)}{\partial \varepsilon}\Big|_{E=E_F} \qquad \text{II.65}$$

If the density of states changes around the chemical potential, the Seebeck coefficient will be high. If the density of states is smooth around the chemical potential, the Seebeck coefficient will be low.

Bibliography

[1] R. Hoffmann, Angew. Chem. Int. Ed. Engl. , 26, 846, (1987).

[2]P. H OHENBERG, W. KOHN. "Inhomogeneous Electron Gas".*Phys. Rev.* 136, B864–B870,(1964).

[3]D.R. H ARTREE. "The Wave Mechanics of an Atom with a Non-Coulomb Central Field".*Proc. Cambridge Philos. Soc.* 24, 89–110,(1928).

[4] J.C. Slater. «A simplification of the Hartree-Fock method ».*Phys. Rev.* 81, 385–390,(1951).

[5]L.H. T HOMAS."The Calculations of Atomic Fields", *Proc. Camb.Phil. Soc.* 23,542,(1927).

[6] W. KOHN, L.J. S HAM. "Self-consistent Equations Including Exchange and Correlation Effects".*Phys. Rev.* 140, A1133–A1138,(1965).

[7]P. A. M. Dirac, Proc. Cambridge Philos. Soc. 26 376,(1930).

[8] J. P. Perdew, and A. Zunger, Phys. Rev. B 23, 5048, (1981)

[9] D. M. Ceperley, and B. J. Alder, Phys. Rev. Lett. 45, 566, (1980)

[10] A. D. Becke, Phys. Rev. A 38, 3098, (1988).

[11] J. P. Perdew, J. A. Chevary, S. H. Vosko, K. A. Jackson, M. R. Pederson, and C. Fiolhais, Phys. Rev. B 46, 6671, (1992).

[12] J. P. Perdew, K. Burke, and M. Ernzerhof, Phys. Rev. Lett. 77, 3865, (1996).

[13] N.W. Achcroft et N.D. Mermin, Solid State Physics, editions internationals Holt-Saunders,(Japon, 1981).

[14] J. C. Slater, *Wave Functions in a Periodic Potential*, Phys. Rev. 51, 846, (1937).

[15] O. K. Andersen, *Linear methods in band theory*, Phys. Rev. B 12, 3060, (1975).

[16] D. D. Koelling and G. O. Arbman, *Use of energy derivative of the radial solution inan augmented plane wave method: application to copper*, J. Phys. F (Metal Phys.) 5,2041, (1975).

[17] P.M.Marcus, *VariationalMethods in the Computation of Energy Bands*, Int. J. QuantumChem. Suppl. 1, 567, (1967).

Chapter III

III. Introduction

Thermoelectric materials have been widely studied over the past few decades due to their ability to convert waste heat into useful electricity. Among the various thermoelectric materials, skutterudite distinguishes itself in both space and terrestrial applications with its excellent thermoelectric performance, robust mechanical properties, and thermal stability. It is a promising candidate for mid-temperature range (400℃ - 900℃) applications.

The origin of the name skutterudite derives from its place of finding, namely the cobalt mines in Skutterud (Norway), where the naturally occurring mineral $CoAs_3$ was firstly discovered and described in 1845 [1,2].

It should be noted that K.F. Boebert (director of the cobalt mine in Skutterud in the early 19th century) stated in his work that he was assumable the first person who discovered the skutterudite materials [1].

They are typically opaque with a metallic luster and tin-white to silver-gray in color. Today, as an accessory mineral, they are found in many localities worldwide.

Fig. III.1: Naturally occurring skutterudite. (Rob Lavinsky, iRocks.com (http://www.irocks.com/)-CC-BY-SA-3.0)

III.1 Over view of properties of binary Skutterudite compounds MX_3

III.1.1 Crystallographic characteristic

The general formula of binary skutterudite is MX_3 (or more opportune: M_4X_{12}), where M is a transition metal (Co, Fe, Ir and Rh) and X is a pnictogen atom (As, Sb and P).

It comprises a cubic structure with 32 atoms and corresponds to the space group $Im\bar{3}$ (N^o.204). As shown in Fig. III.2, the transition metals occupy the 8*c*-sites $(1/4, 1/4, 1/4)$ and the X atoms the 24g sites$(0, y, z)$ [3]. Where the X atoms enclose the transition metals in octahedral coordination and form a rectangle (four-membered Sb_4 rings).

Oftedal assumed that this pnicogen rectangle is strongly constrained, (i.e.$y + z = 0.5$), which is not apparently the case in practice and therefore shows a little rectangular distortion [4].

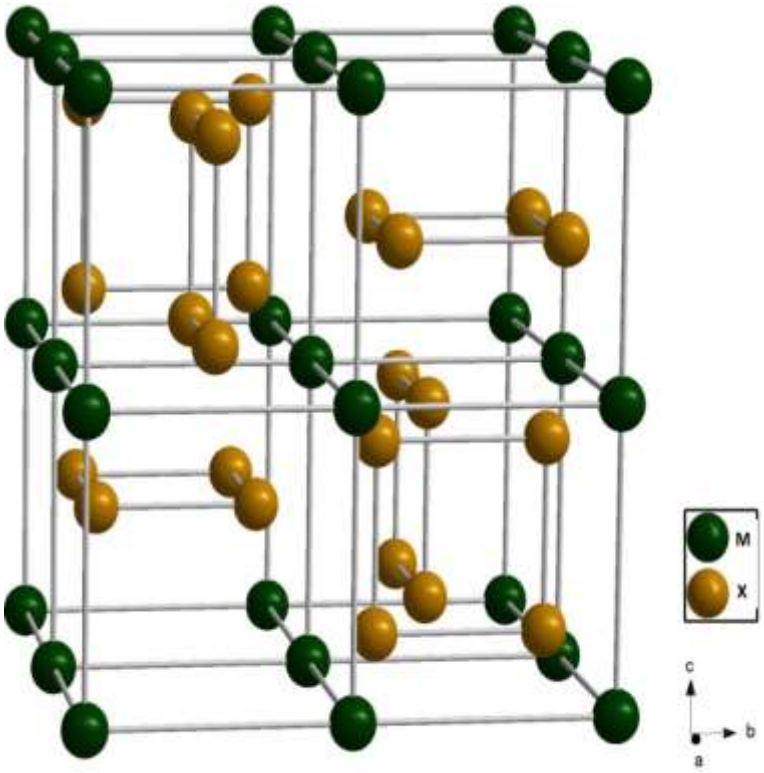

Fig. III.2: Crystal structure of binary skutterudites MX_3.

III.1.2 Computational details

The Kohn-Sham equation implemented in the Wien2k code was solved with the FP-LAPW method (Full Potential Linearized Augmented Plane Wave) [5]. The exchange

correlation potential was determined within the framework of the generalized gradient approximation (GGA-PBE) proposed by Perdew et *al*. LDA, PBE-Sol and TB-mBJ approximations to investigate the structural and electronic properties [6-8].

Before studying any material one must do a convergence test to get good results with the minimum amount of energy.

The following parameters: wave functionsψ, electronic densities ρ and potential v are developed in combination spherical harmonics multiply by radial functions around atomic sites l_{max}, and a Fourier series expansion in the interstitial region. This region is limited by a cutoff (cutoff radius) $R_{mt}^{min} * k_{max}$ (R is the smallest radius of the MT sphere, k_{max} is the cutoff of the wave vector for plane waves); this parameter is the norm of the largest wave vector used for the plane wave expansion of eigenfunctions.

To avoid the overlapping of the spheres (Muffin-tin) and to ensure the integration of the majority of the core electrons in the sphere (Muffin-tin), we must make the precise choice of the rays of Muffin-tin R_{mt} for the binary skutterudites compounds MX_3.

And we carried out convergence tests on the norm of the largest wave vector used for the plane wave expansion of the charge density G_{max} for binary skutterudite antimonide compounds; and the number of k-points to consider in the first irreducible Brillouin zone (IBZ). These parameters are collected for the investigated materials in Table III.1.

Table. III.1: The values of: R_{mt}, $R_{mt} * K_{max}$, l_{max} , G_{max} *et* K_{points} for binary skutterudites MX_3 compounds.

MSb_3	**R_{mt} (u.a)**					**$R_{mt} * K_{max}$**	**l_{max}**	**K_{points}**	**G_{max} ($Ry^{1/2}$)**
	Co	**Ir**	**Fe**	**Rh**	**Sb**				
$CoSb_3$	2.39	–	–	–	2.39	7.0	10	1000	12
$FeSb_3$	–	–	2.5	–	2.25	7.0	10	1000	12
$IrSb_3$	–	2.5	–	–	2.44	7.0	10	1000	12
$RhSb_3$	–	–	–	2.5	2.5	7.0	10	1000	12
MP_3	**R_{mt} (u.a)**					**$R_{mt} * K_{max}$**	**l_{max}**	**K_{points}**	**G_{max} ($Ry^{1/2}$)**
	Co	**Ir**	**Rh**	**P**					
CoP_3	2.21	–	–	1.96		7.0	10	1000	12
IrP_3	–	2.36	–	2.09		7.0	10	1000	12
RhP_3	–	–	2.35	2.09		7.0	10	1000	12
MAs_3	**R_{mt} (u.a)**					**$R_{mt} * K_{max}$**	**l_{max}**	**K_{points}**	**G_{max} ($Ry^{1/2}$)**
	Co	**Ir**	**Rh**	**As**					
$CoAs_3$	2.34	–	–	2.07		7.0	10	1000	12
$IrAs_3$	–	2.46	–	2.19		7.0	10	1000	12
$RhAs_3$	–	–	2.46	2.18		7.0	10	1000	12

III.1.3 Ground state properties

The crystalline structure of binary skutterudite compounds MX_3 is characterized by two free parameters: the lattice constant *a*, and the internal structure parameters of pnictogen atoms(u_X and v_X).

We have performed two sets of calculations. As a first step, starting from the experimental lattice parameters, we have optimized the internal parameters by relaxing the u_X and v_X coordinates of the pnictogen atoms until the forces on the ions were below a tolerance value taken as 0.001 eV/Å.

Secondly, by using the optimized internal parameters, the total energies are calculated at different volumes *V*, to obtain the absolute minimum in total energy for binary skutterudites: $RhSb_3$, CoP_3, $IrSb_3$, $IrAs_3$, $CoSb_3$, $CoAs_3$, $RhAs_3$, IrP_3, and RhP_3 compounds as shown in Figs. III(3)-(5). In the other hand, and in order to verify the phase stability of the binary skutterudite $FeSb_3$ compound the calculated total energies versus volumes for the both non-magnetic (NM) and ferromagnetic (FM) phases are presented in Fig. III.6.

Table III.2 summarizes the results obtained for the optimized lattice constant (a), lowest energies (E_0), internal parameters of pnictogen atoms(u_X and v_X), bulk modulus (B_0) and its first pressure derivative ($B^{'}$) were determined by adjusting the calculated total energy as a function of the cell volume to the Murnaghan equation of state [9].

From Fig. III.6, it is clear that the lowest energy values are reached in the case of ferromagnetic. This signifies that the ferromagnetic phase of binary skutterudite $FeSb_3$ compound is comparatively the most stable energetically than the non magnetic one.

One can observe also form table III.2 that our calculated values for the lattice constants, internal parameters of pnictogen atoms(u_X and v_X) and bulk modulus for binary skutterudites compounds are in good agreement with the results reported in numerous studies [10-14]. Due to the known overestimation of GGA, the obtained lattice constant values are slightly larger than the experimental findings [15].

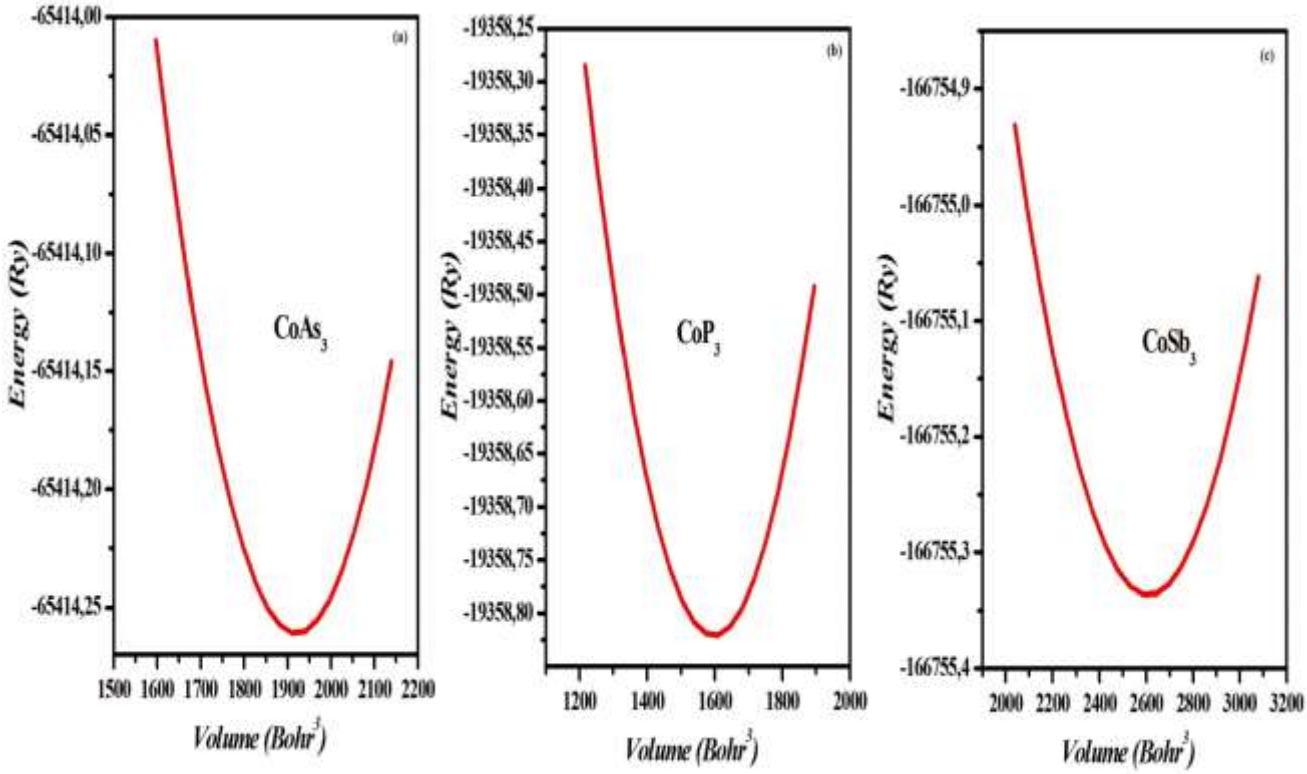

Fig. III.3: Calculated energy versus volume curves for binary skutterudites: (a) $CoAs_3$, (b) CoP_3 and (c) $CoSb_3$ compounds.

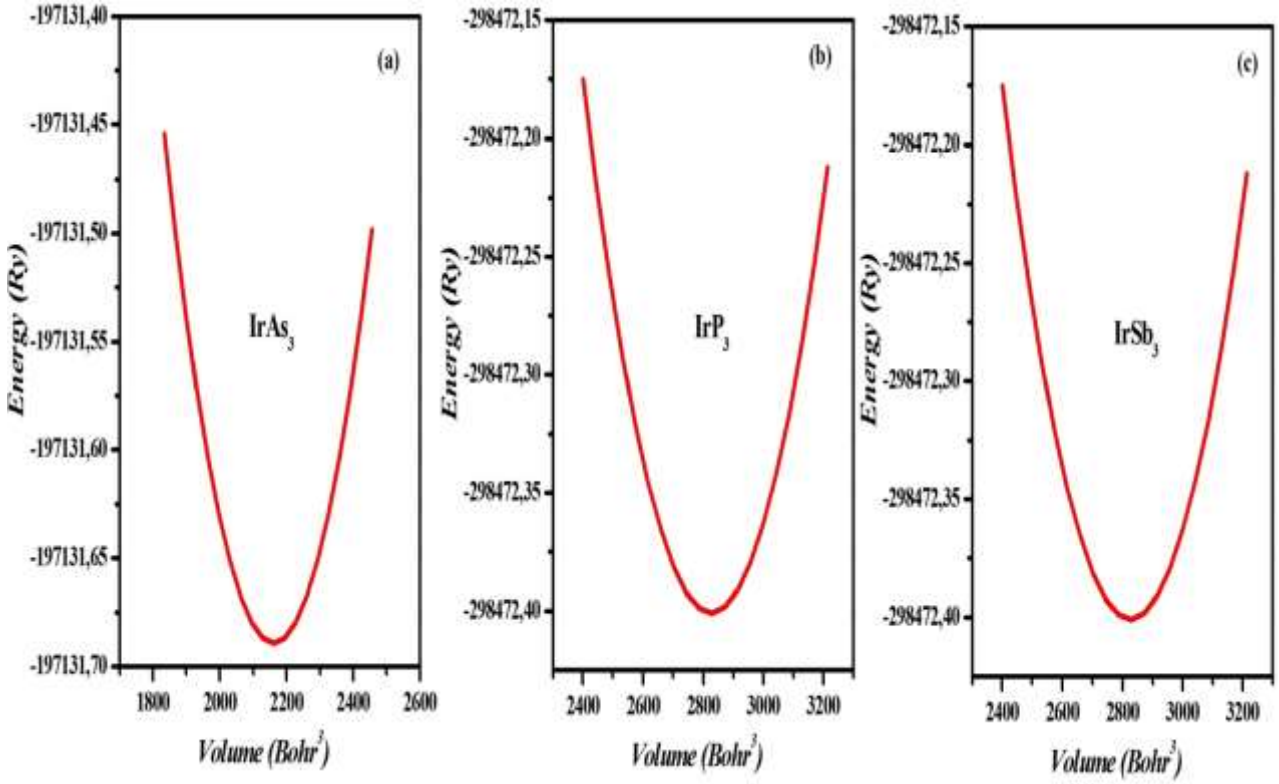

Fig. III.4: Calculated energy versus volume curves binary skutterudites: (a) $IrAs_3$, (b) IrP_3 and (c) $IrSb_3$ compounds.

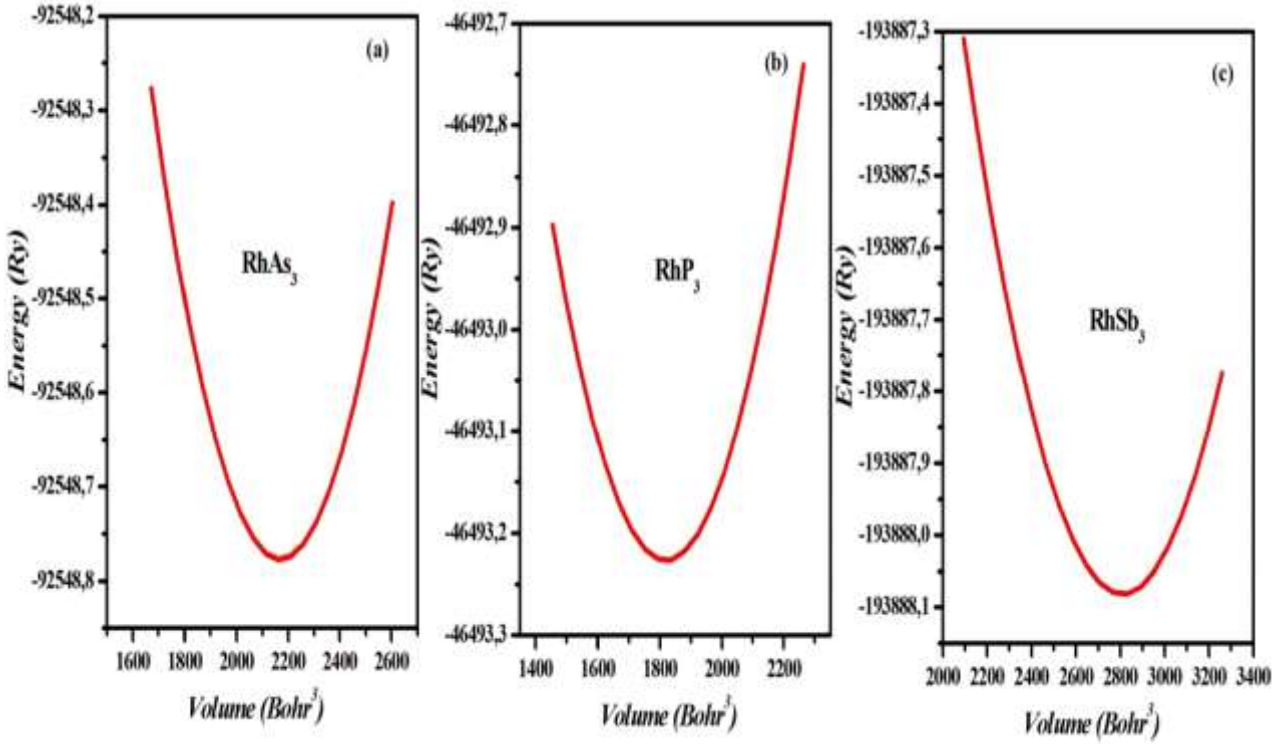

Fig. III.5: Calculated energy versus volume curves binary skutterudites: (a) $RhAs_3$, (b) RhP_3 and (c) $RhSb_3$ compounds.

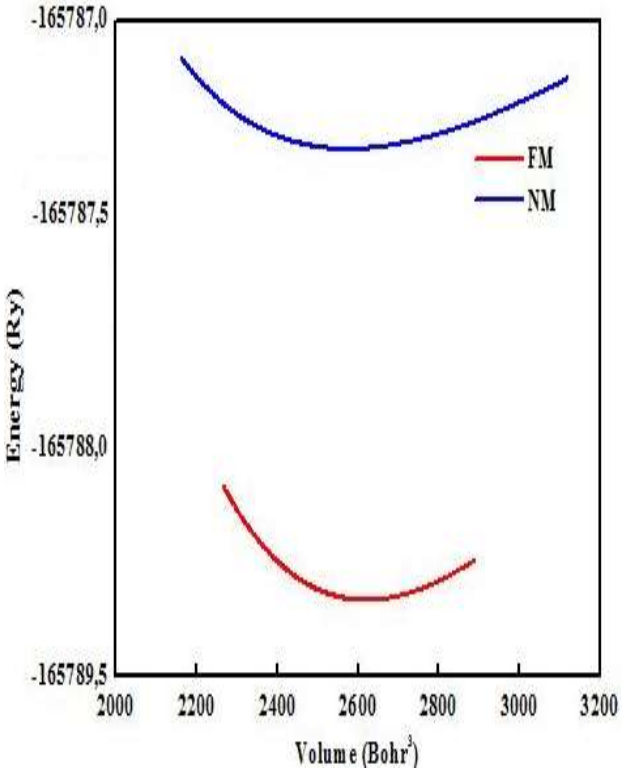

Fig. III.6: The calculated total energies versus volumes for the both non-magnetic (NM) and ferromagnetic (FM) phases for the binary skutterudite $FeSb_3$ compound.

Table. III.2: The experimental and theoretical lattice constants, positional parameters for Sb atom, and bulk modulus B_0 (in GPa) and its derivative B' for binary skutterudite compounds.

PBE-GGA		a(Å)	u	v	B_0 (GPa)	B'	E_0 (Ry)
$CoSb_3$		9.117 9.038[10] 8.927[15] 9.182[16] 8.923[17]	0.3353 0.3354[16]	0.15788 0.1579[16]	75.60 93.60[10] 81.09[11] 101.2[15] 97.65[17] 83.20[18]	4.79 –	-166755.332
$IrSb_3$		9.3563 9.2533[17]	0.3415 0.3407[17]	0.1507 0.1538[17]	100.35 112.4[19]	5.27 –	-29879.399
$RhSb_3$		9.379 9.2322[17]	0.3431 0.3420[17]	0.1526 0.1517[17]	90.80 92[17]	4.82 –	-193889.064
$CoAs_3$		8.270 9.2322[17]	0.3412 –	0.1519 0.1517[17]	115.05 –	4.57 –	-65414.257
$IrAs_3$		8.596 8.422[17]	0.3479 –	0.1458 –	133.166 –	4.91 –	-197131.689
$RhAs_3$		8.578 8.465[18]	0.3484 –	0.1465 –	117.71 –	4.56 –	-92548.772
CoP_3		7.751 7.654[18]	0.3480 –	0.1461 –	149.84 –	4.41 –	-19358.813
IrP_3		8.109 8.023[17]	0.3547 –	0.1394 –	177.29 –	4.55 –	-151076.237
RhP_3		8.091 8.002[18]	0.3558 –	0.1397 –	148.54 –	4.72 –	-46493.234
$FeSb_3$	*NM*	9.139	0.3319	0.1585	83.46	5.24	-165787.399
	FM	9.192	0.3319	0.1585	80.36	5.12	-165789.381
	Exp.	9.2116[18]	0.3402[18]	0.1578[18]	–	–	

Electronic properties

In this section we turn our attention to study the electronic properties of binary skutterudites compounds via calculating the electronic band structures, the projected density of states (DOS).

III.4.1 Band structures

One of the most fundamental parameter which describes many physical properties of a compound is the bandgap which is provides a detailed account of the optical, electronic, optoelectronic and thermoelectric properties of the material. Therefore, the knowledge of the electronic band structure of a material is necessary for its possible technological applications in various devices. In optoelectronics, we are mostly concerned with direct bandgap materials, where the gap value in the range of infrared (IR) to ultraviolet (UV) depends strictly upon the nature of application. Nevertheless, there are more stringent requirements for efficient thermoelectric materials but different to optically active materials; they require narrow bandgap compounds irrespective of their nature, direct or indirect. For that reasons and in order to understand the electronic properties in the investigated compounds, the electronic band structures are examined.

Figs. III(7)-(15) display the band structures of binary skutterudite compounds MX_3 (M= Co, Ir and Rh and X= As, P and Sb) with: (a) PBE-GGA and (b) TB-mBJ approximations. A broken line denotes the energy level of the highest occupied state (Fermi level E_F). Additionally, we have also plotted the spin resolved electronic band structures within the optimized lattice constant of $FeSb_3$ compound were calculated by (GGA-PBE) and (TB-mBJ) methods, respectively in Figs. III(16)-(17).

The calculated electronic band structures with the both approaches said above for binary skutterudites compounds MX_3 (M= Co, Ir and Rh, X= As, P and Sb) show that the first valence bands which are highly dispersive exhibit parabolic shapes; while the conduction bands minimum (CBM) are typified by doublet and singlet degenerated and unoccupied bands. It can be seen that the valence bands maximum (VBM) and the conduction bands minimum (CBM) in binary skutterudites: $CoSb_3$, $IrSb_3$, $CoAs_3$, $IrAs_3$ and $RhAs_3$ compounds lie at the same Γ point (Γ_V–Γ_C); this observation shows that the binary skutterudite compounds have semiconductors character with fundamentals narrowing directs band gaps. However, the conduction band minimum (CBM) occurs at the *H*-point resulting in indirect band gaps ($\Gamma \rightarrow H$) for the CoP_3, IrP_3 and $RhSb_3$ compounds. Whereas the both

electronic band structures in Fig. III.15 show a metallic behavior for the binary skutterudites RhP_3 compound.

As shown in Figs. III(16)-(17), the spin-up valence band maximum (VBM) for binary skutterudite $FeSb_3$ compound which exhibits parabolic form is touching the Fermi level, as well as the conduction band minimum (CBM) in the both cases of PBE-GGA and TB-mBJ approximations is located at the high symmetry Γ point. Thus, a direct band gap of 0.218 eV and 0.424 eV is observed, respectively. At the same time, the spin-down valence band maximum and conduction band minimum are separated by localized bands situated exactly at the Fermi level, giving rise to a pseudogap on both regions of VBM and CBM.

A wide range of experimental band gap values measured in different methods have been reported for binary Skutterudite $CoSb_3$ from 0.03 to 0.05 eV [19-21] to an intermediate of 0.31–0.35 eV [19,22] and also large values of 0.6–0.7 eV [23-26]. They would correspond to one of three theoretically identified band gaps including a direct pseudogap, an indirect pseudogap, and the direct gap [27]. The calculated band gaps are obtained depending on the methods used [10,12,29-35].

Table. III.3 presents the obtained bandgaps nature for binary skutterudites using PBE-GGA and regular TB-mBJ methods. Where in table. III.4 we regroup the calculated bandgaps (eV) using: PBE-GGA, PBEsol-GGA, LDA and regular TB-mBJ methods for binary skutterudites compounds (M= Co, Ir, Fe and Rh and X= As, P and Sb). One can noticed from these tables; our calculated bandgaps values agree well with those founded in literature [36].

Table. III.3: The obtained bandgaps nature for binary skutterudites using PBE-GGA and regular TB-mBJ methods.

Compounds		Band gap Nature		Work of Khan[36]	
				Band gap Nature	
		PBE-GGA	Regular TB-mBJ	Regular TB-mBJ	Non-regular TB-mBJ
$CoSb_3$		direct	direct	indirect	indirect
$IrSb_3$		direct	direct	indirect	indirect
$RhSb_3$		indirect	indirect	indirect	indirect
CoP_3		indirect	indirect	indirect	indirect
IrP_3		indirect	indirect	indirect	indirect
RhP_3		metal	metal	metal	metal
$CoAs_3$		direct	direct	indirect	indirect
$IrAs_3$		direct	direct	indirect	indirect
$RhAs_3$		direct	direct	indirect	indirect
$FeSb_3$	*Spin up*	direct	direct	–	–
	Spin dn	Pseudo direct	metal	–	–

Table. III.4: Calculated bandgaps (eV) using: PBE-GGA, PBEsol-GGA, LDA and regular TB-mBJ methods for binary skutterudites compounds.

Compounds		PBE-GGA	PBE-Sol	LDA	Regular TB -mBJ	Other works
$CoSb_3$		0.554	0.545	0.488	0.706	0.63[37] 0.61[7]
$IrSb_3$		0.396	0.456	0.406	0.674	1.4[38] 0.87[36]
$RhSb_3$		0.151	0.145	0.110	0.256	0.17[36] 0.80[38]
CoP_3		0.121	0.083	0.064	0.367	0[36],
IrP_3		0.416	0.421	0.406	0.824	0.61[36]
RhP_3		metal	metal	metal	metal	metal[36]
$CoAs_3$		0.379	0.358	0.329	0.604	0.65[36]
$IrAs_3$		0.516	0.509	0.436	0.796	0.9[36]
$RhAs_3$		0.109			0.285	0.38[37]
$FeSb_3$	***Spin up***	0.218	–	–	0.414	–
	Spin dn	metal	metal	–	–	–

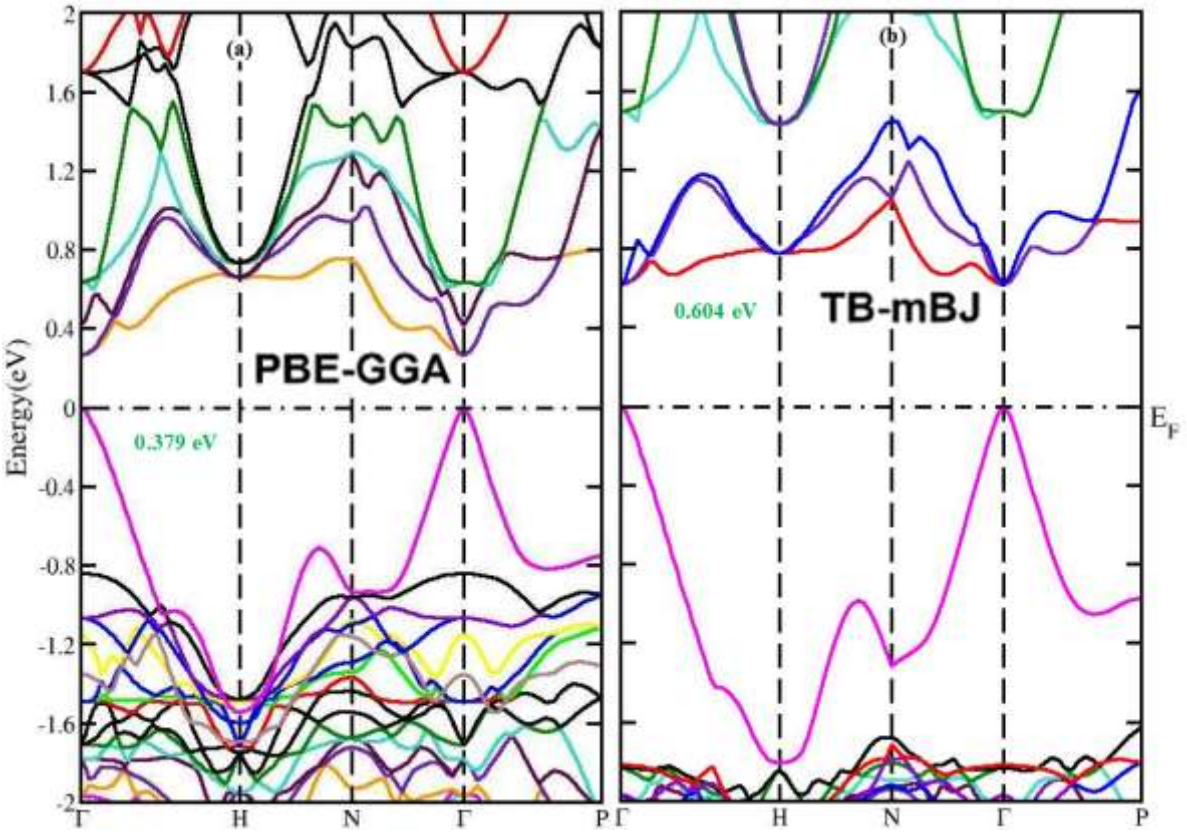

Fig. III.7: Band structures of $CoAs_3$ with: (a) PBE-GGA and (b) TB-mBJ approximations.

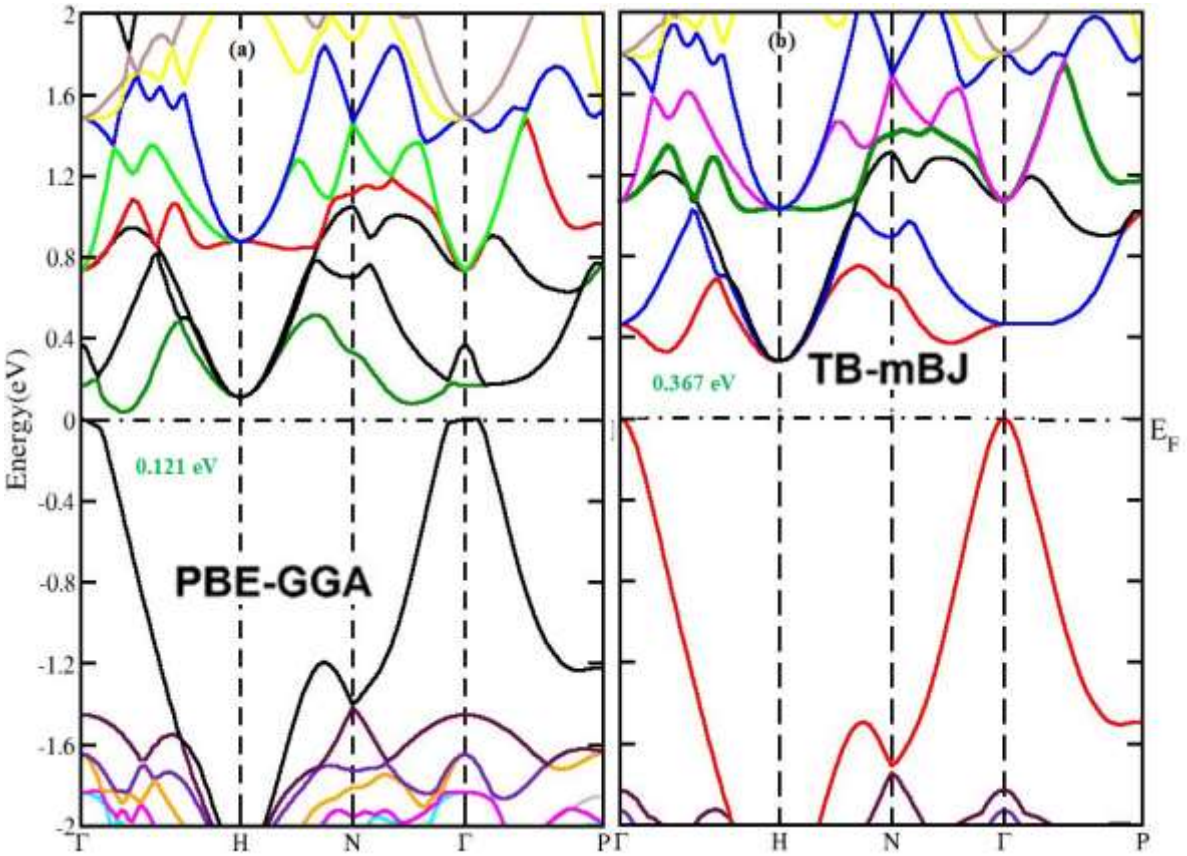

Fig. III.8: Band structures of CoP_3 with: (a) PBE-GGA and (b) TB-mBJ approximations.

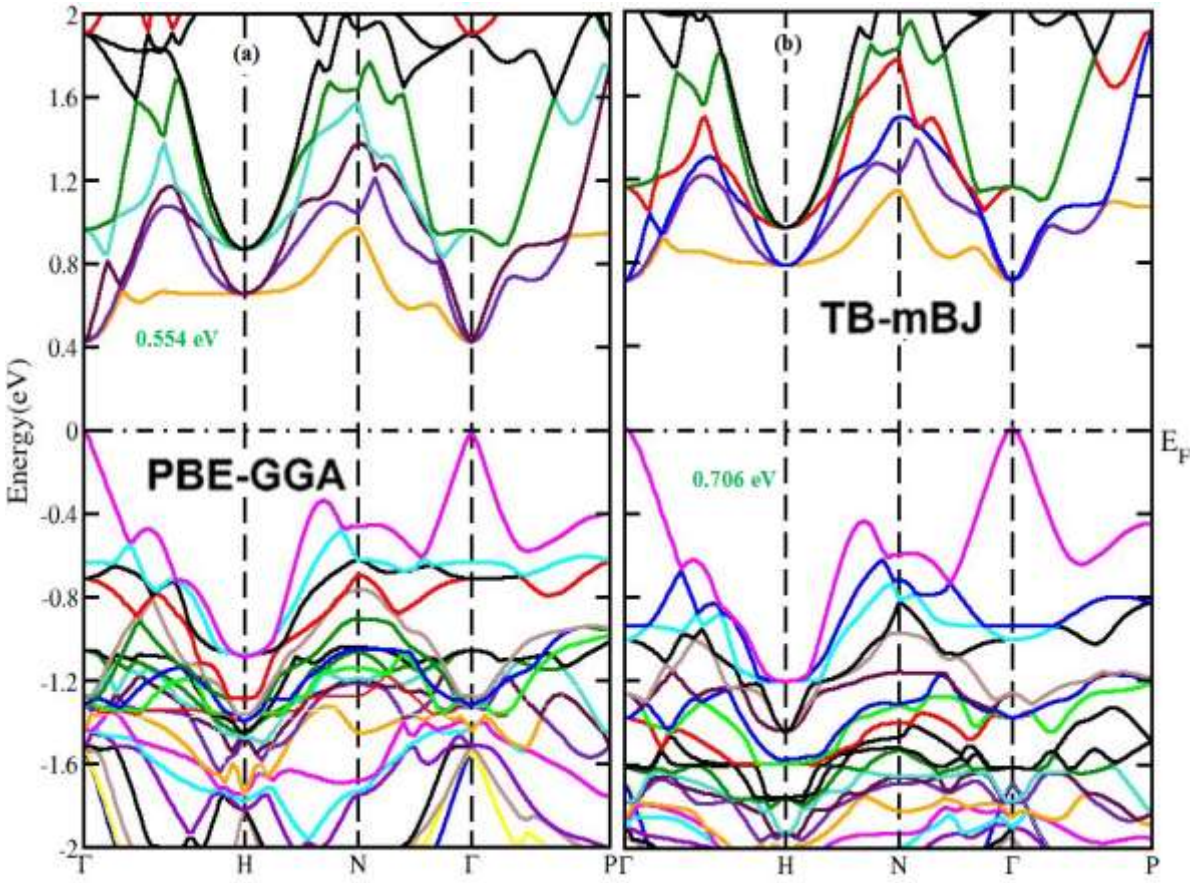

Fig. III.9: Band structures of $CoSb_3$ with: (a) PBE-GGA and (b) TB-mBJ approximations.

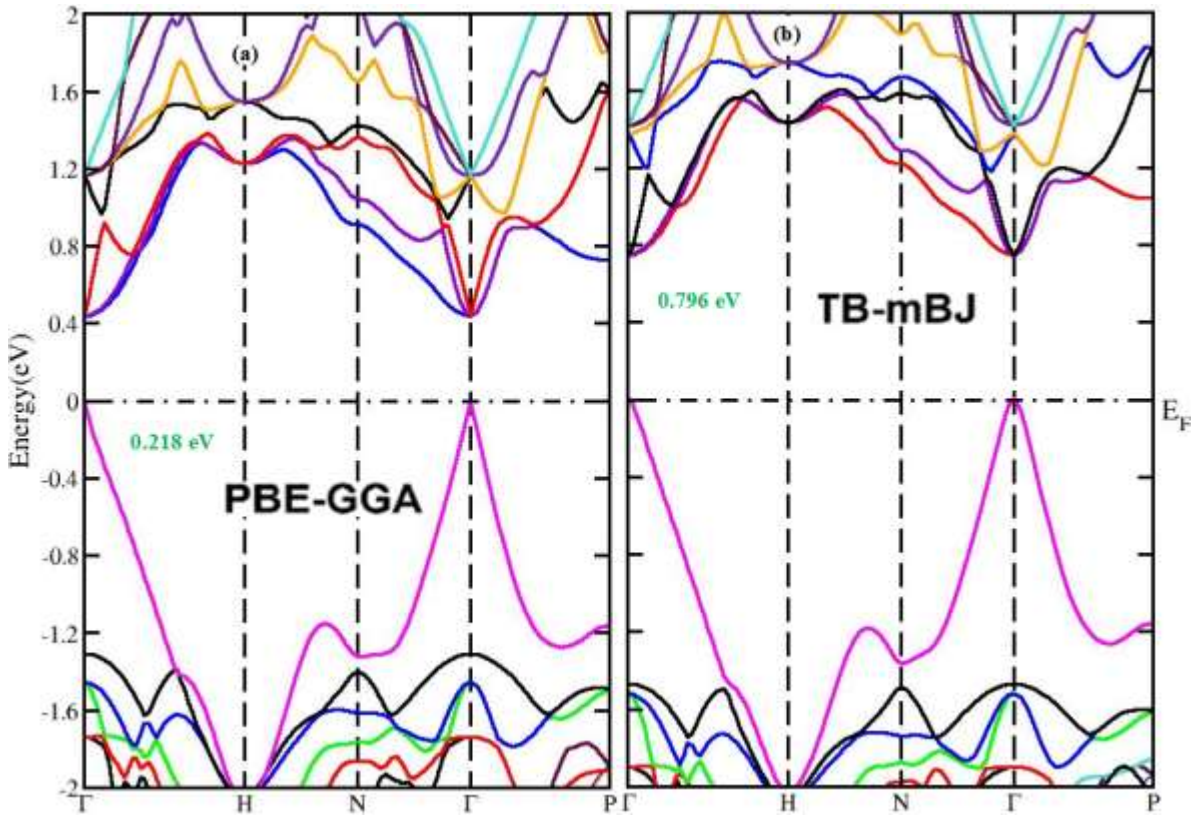

Fig. III.10: Band structures of $IrAs_3$ with: (a) PBE-GGA and (b) TB-mBJ approximations.

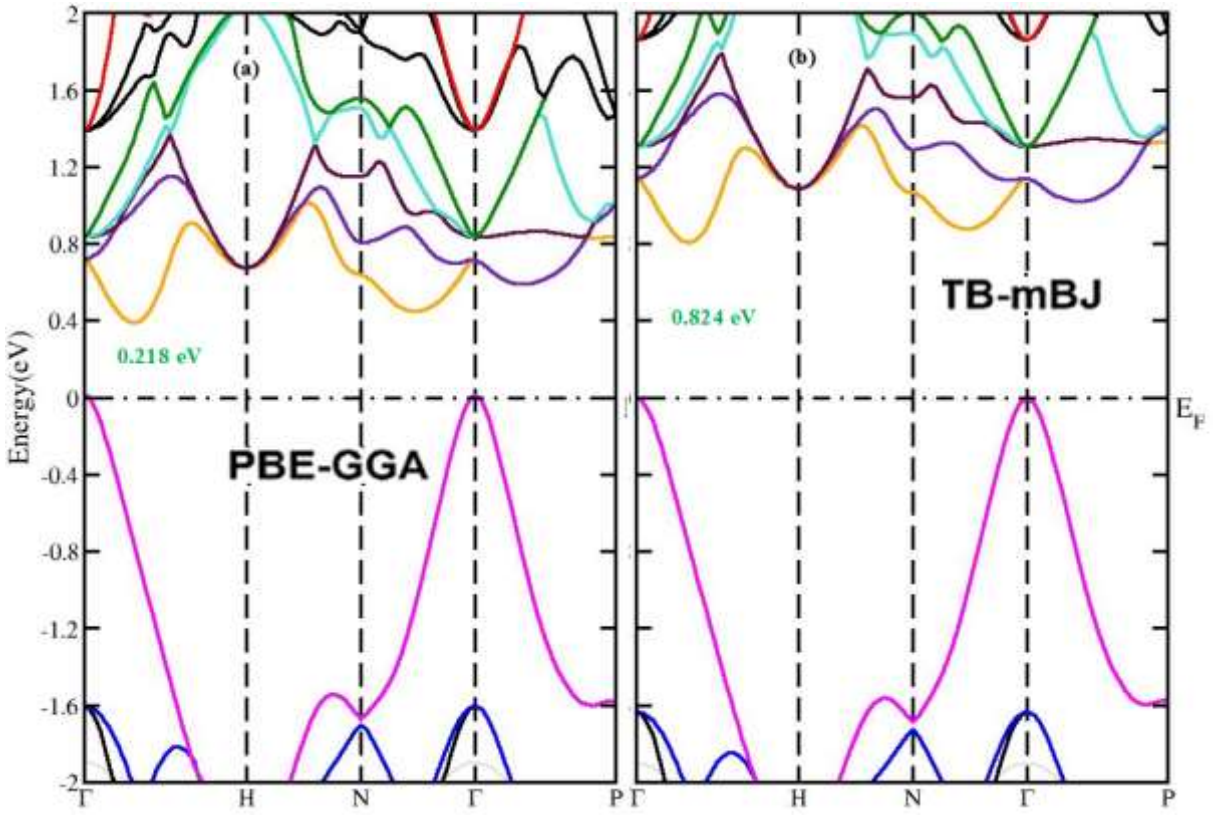

Fig. III.11: Band structures of IrP_3 with: (a) PBE-GGA and (b) TB-mBJ approximations.

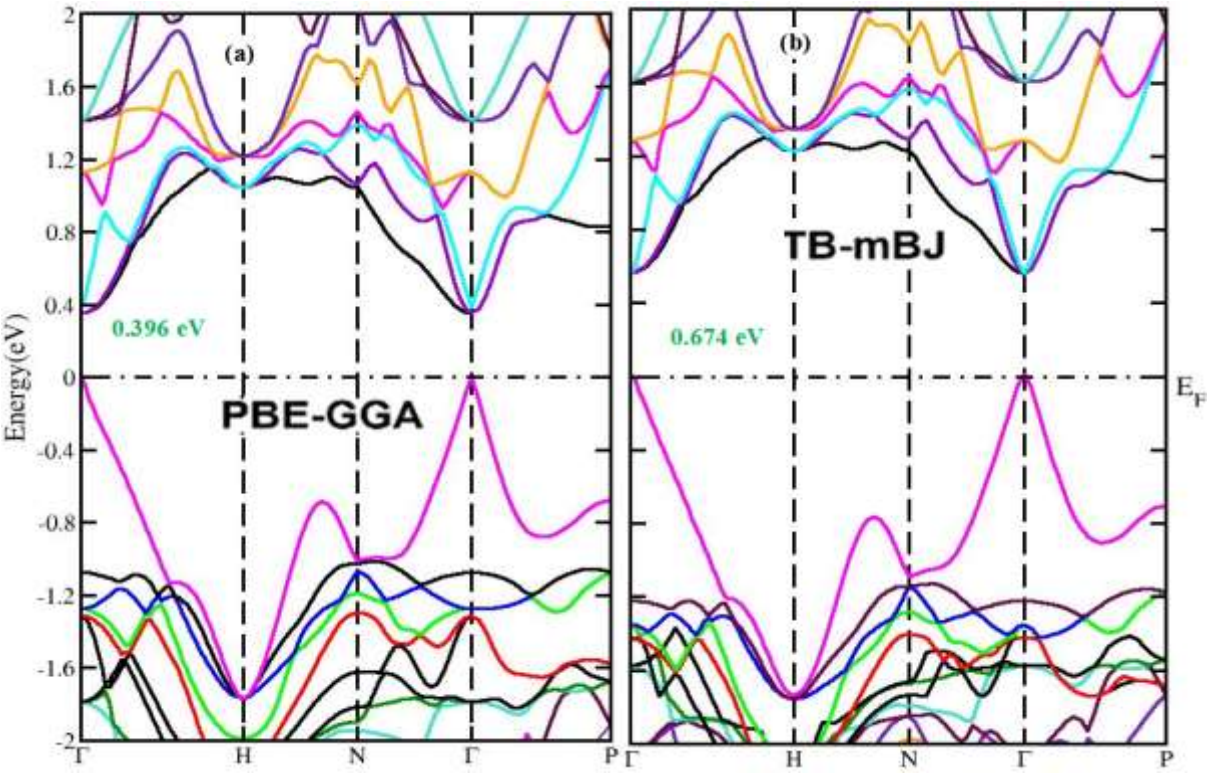

Fig. III.12: Band structures of $IrSb_3$ with: (a) PBE-GGA and (b) TB-mBJ approximations.

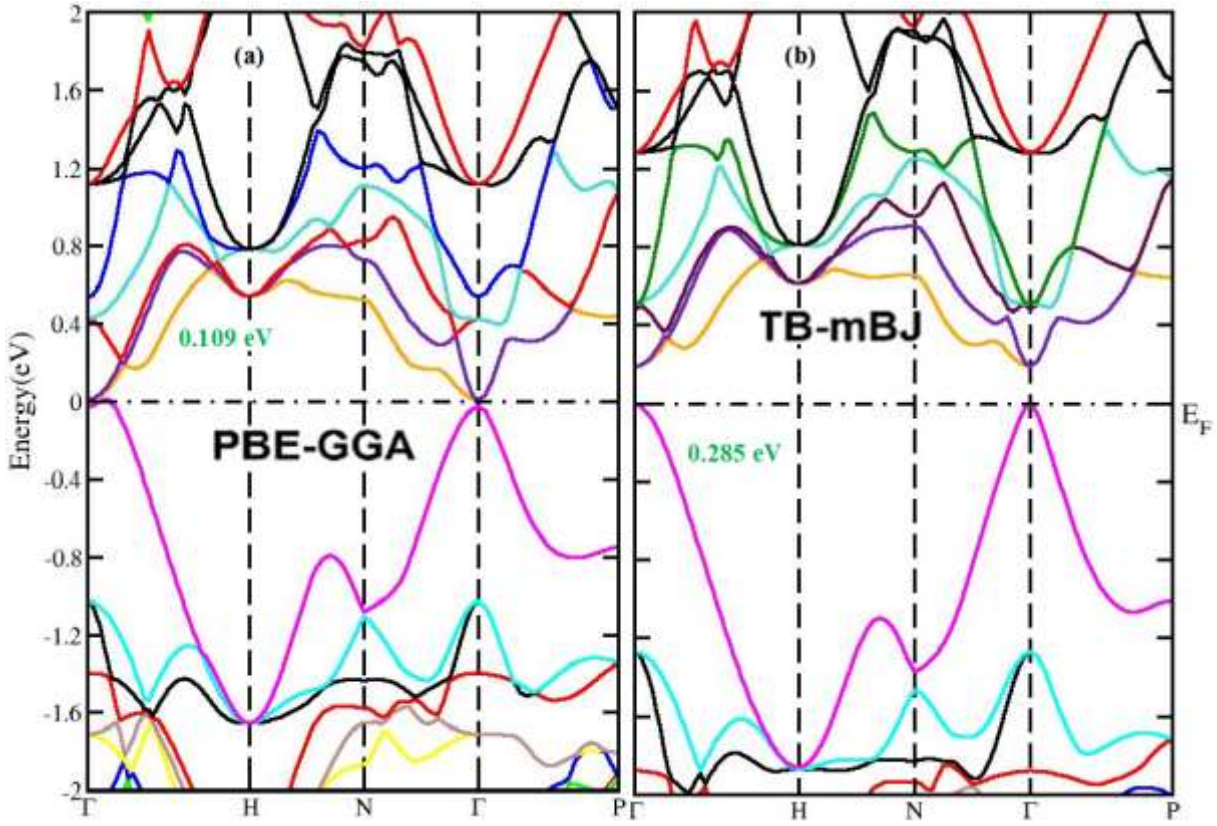

Fig. III.13: Band structures of $RhAs_3$ with: (a) PBE-GGA and (b) TB-mBJ approximations.

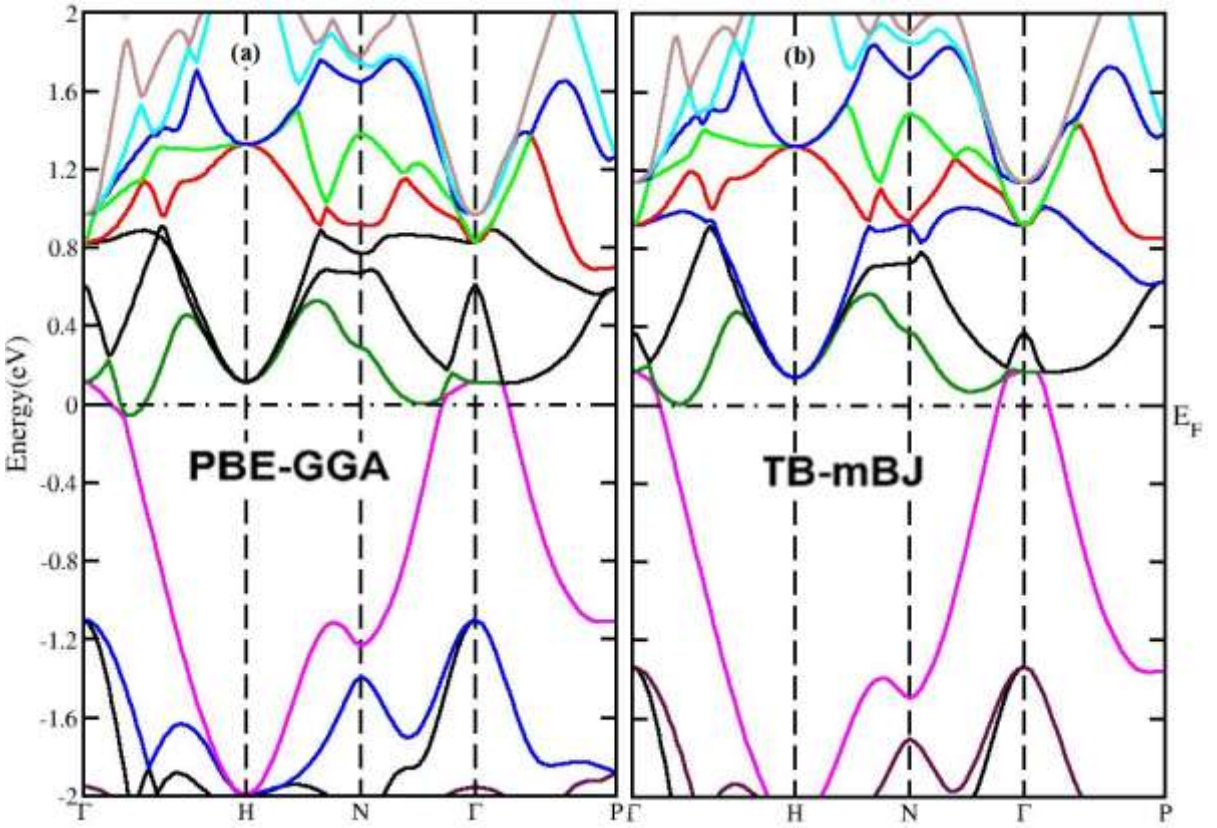

Fig. III.14: Band structures of RhP_3 with: (a) PBE-GGA and (b) TB-mBJ approximations.

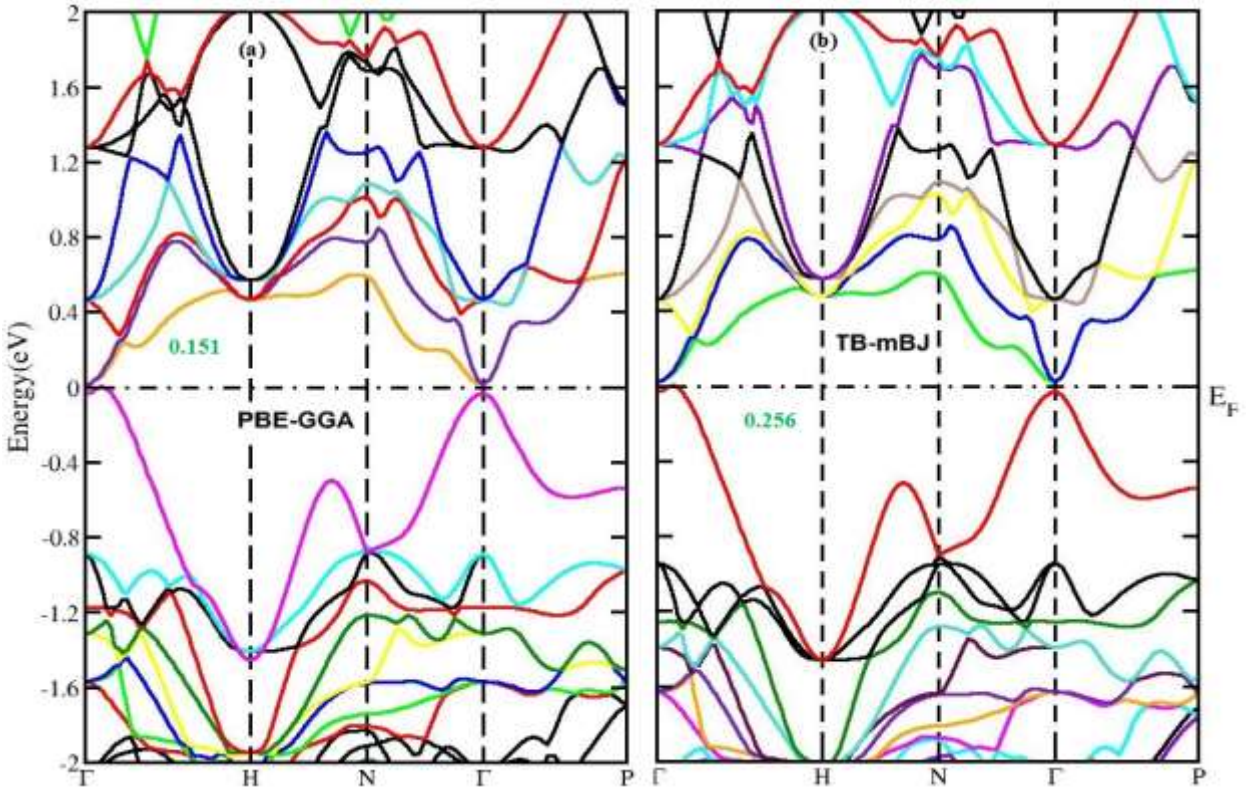

Fig. III.15: Band structures of $RhSb_3$ with: (a) PBE-GGA and (b) TB-mBJ approximations.

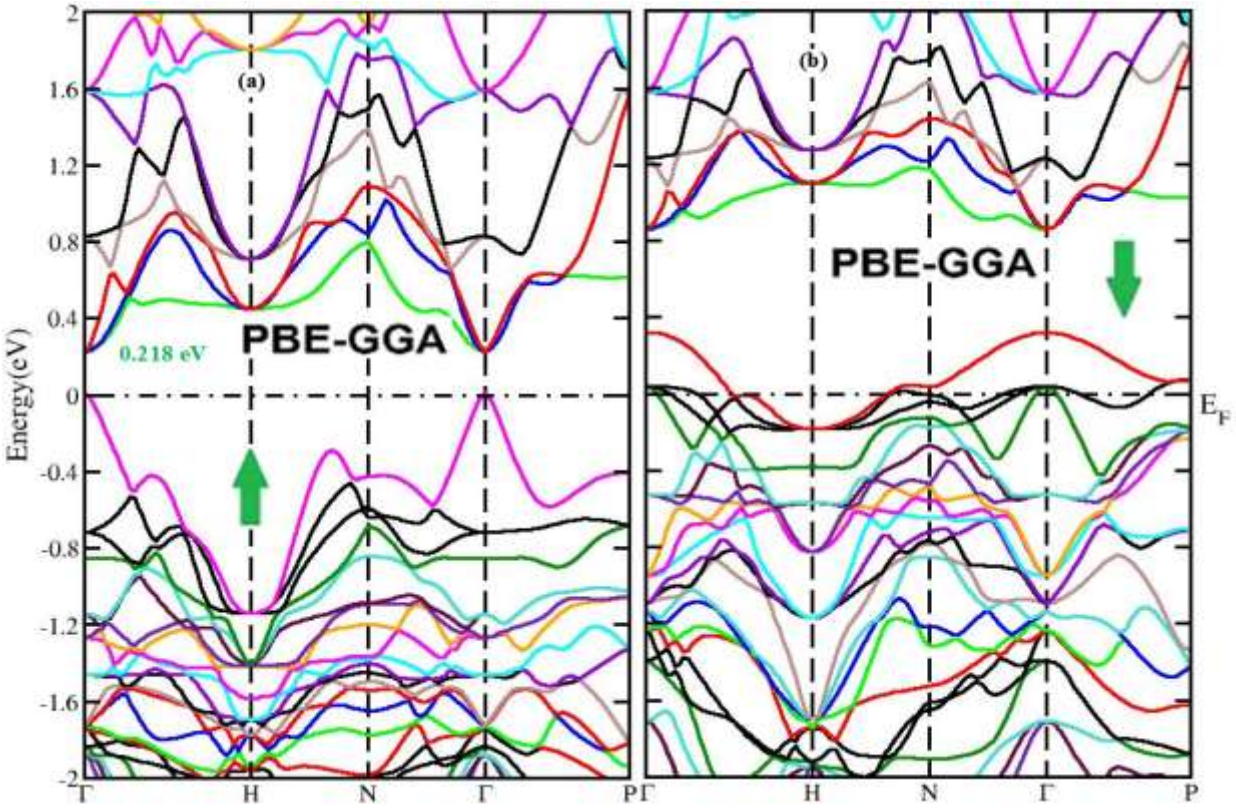

Fig. III.16: Band structures of $FeSb_3$ with PBE-GGA approximation: (a) spin up (b) spin down.

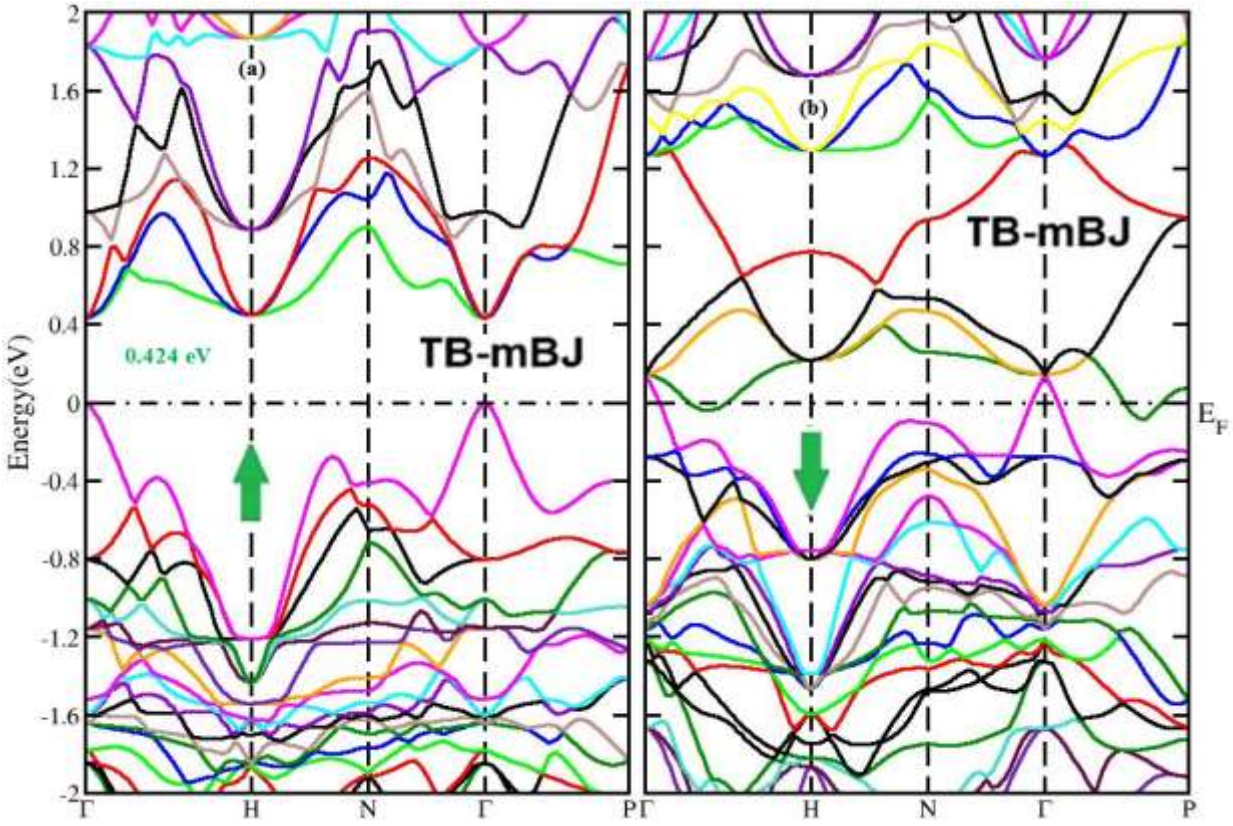

Fig. III.17: Band structures of $FeSb_3$ with TB-mBJ approximation: (a) spin up (b) spin down.

III.4.2 Densities of states (DOSs)

In Figs. III. (18)-(25), we plot the total and the partial projected densities of states for binary skutterudites compounds MX_3 (M= Co, Ir and Rh; X= As, P and Sb) with: (a) PBE-GGA and (b) TB-mBJ approximations. A broken line denotes the energy level of the highest occupied state (Fermi level E_F). It is important to note that each orbital of the both metals and pnictogen ions had been projected separately in order to find the total contribution attributed from each ion in the binary skutterudite compounds. Additionally, we have also plotted the spin resolved electronic densities of states of $FeSb_3$ compound were calculated by (TB-mBJ) method, respectively in Fig. III.26.

As can be seen from Figs. III. (18)-(25), the top of the valence bands at the vicinity of the Fermi level for the skutterudites compounds MX_3 (M= Co, Ir and Rh; X= As, P and Sb) are primarily composed from the extremely hybridization between the d-states of metal (M) atoms and p-states of their neighboring pnictogen (X) ions, confirming obviously the strong covalent combination between (M/X) bonds, although a small contribution of the both orbitals is contained in the conduction bands. And thus gives rise to the diamagnetic

character of these compounds. As shown in Fig. III(26), the top of the valence band at the vicinity of the Fermi level for the majority spin (spin up) is primarily composed from the extremely hybridization between the d-states of iron atoms (Fe) and the p-states of their neighboring Sb ions, confirming obviously the strong covalent combination between (Fe/Sb) bonds, although a small contribution of the both orbitals is contained in the conduction band. Whereas for the minority spin (spin down), the d-states of Fe ions provide the main contribution to the valence band above to the Fermi level, while a negligible contribution for the Sb orbitals is established. In the other hand, the conduction band is generally shaped by the p-states of Sb ions mixed with d-states of Fe atoms. In comparison with the DOS in the majority spin channel, the electronic DOS close to Fermi level in spin up channel is enhanced to about 23.7 electrons/eV. This is will be advantageous to the electrical conductivity due to the enhanced of bipolar diffusion at elevates temperature.

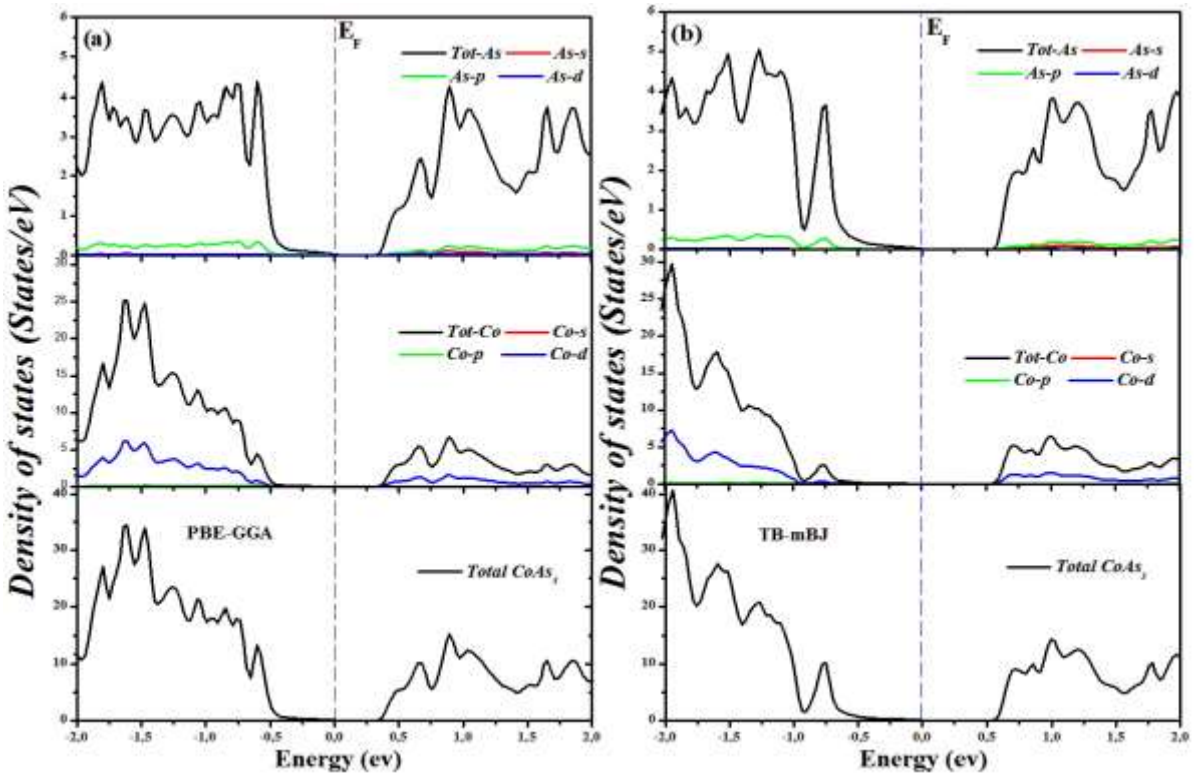

Fig. III.18: Densities of states for $CoAs_3$ with: (a) PBE-GGA and (b) TB-mBJ approximations.

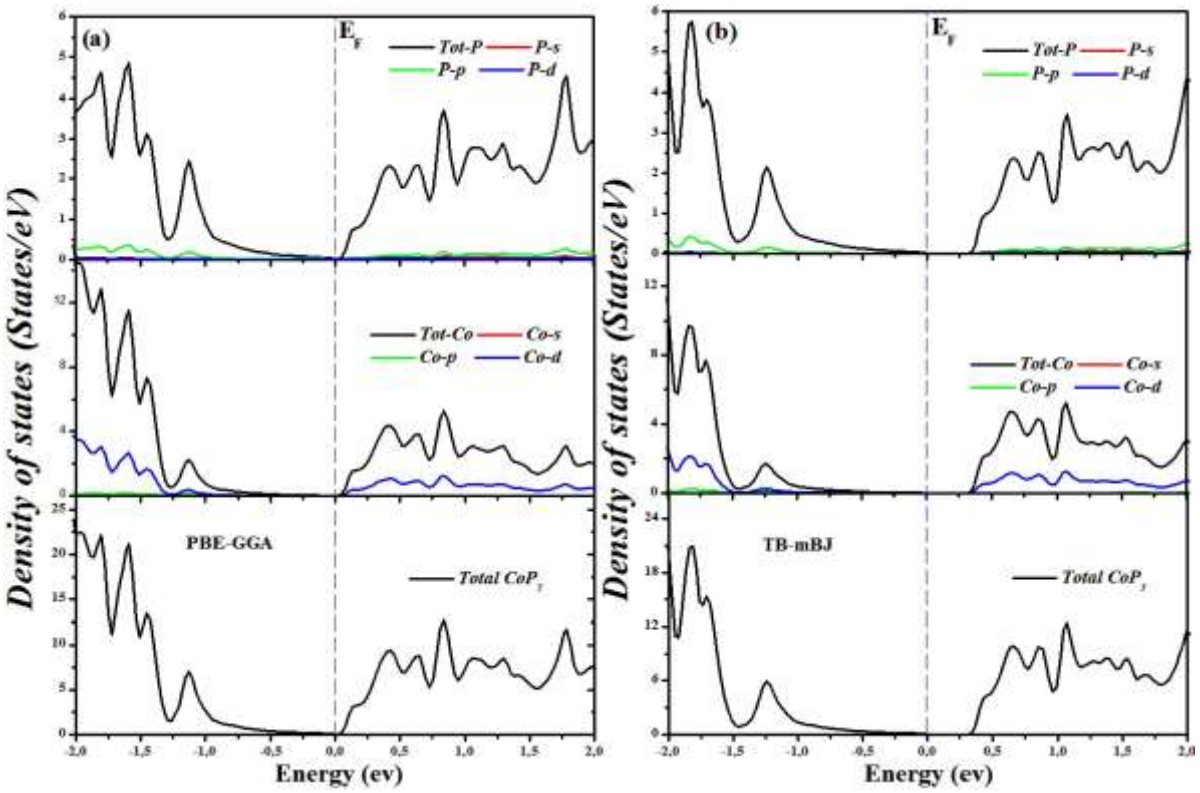

Fig. III.19: Densities of states for CoP_3 with: (a) PBE-GGA and (b) TB-mBJ approximations.

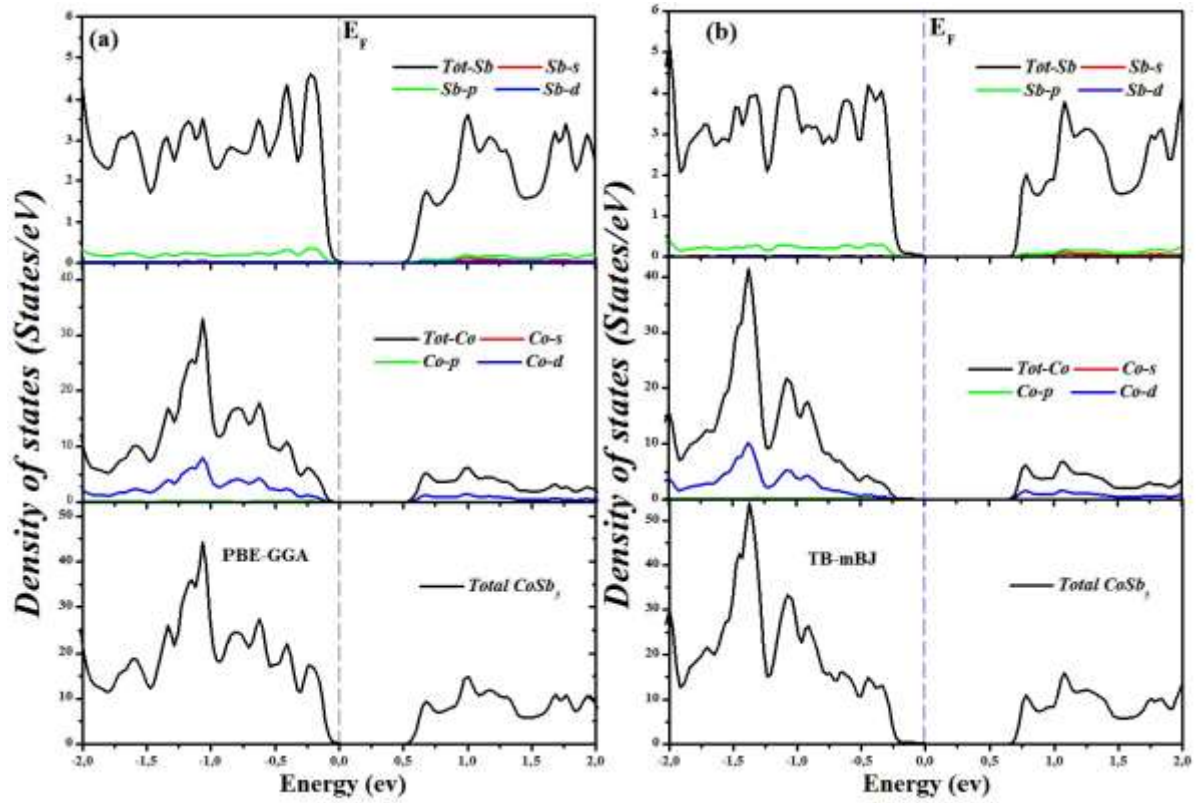

Fig. III.20: Densities of states for $CoSb_3$ with: (a) PBE-GGA and (b) TB-mBJ approximations.

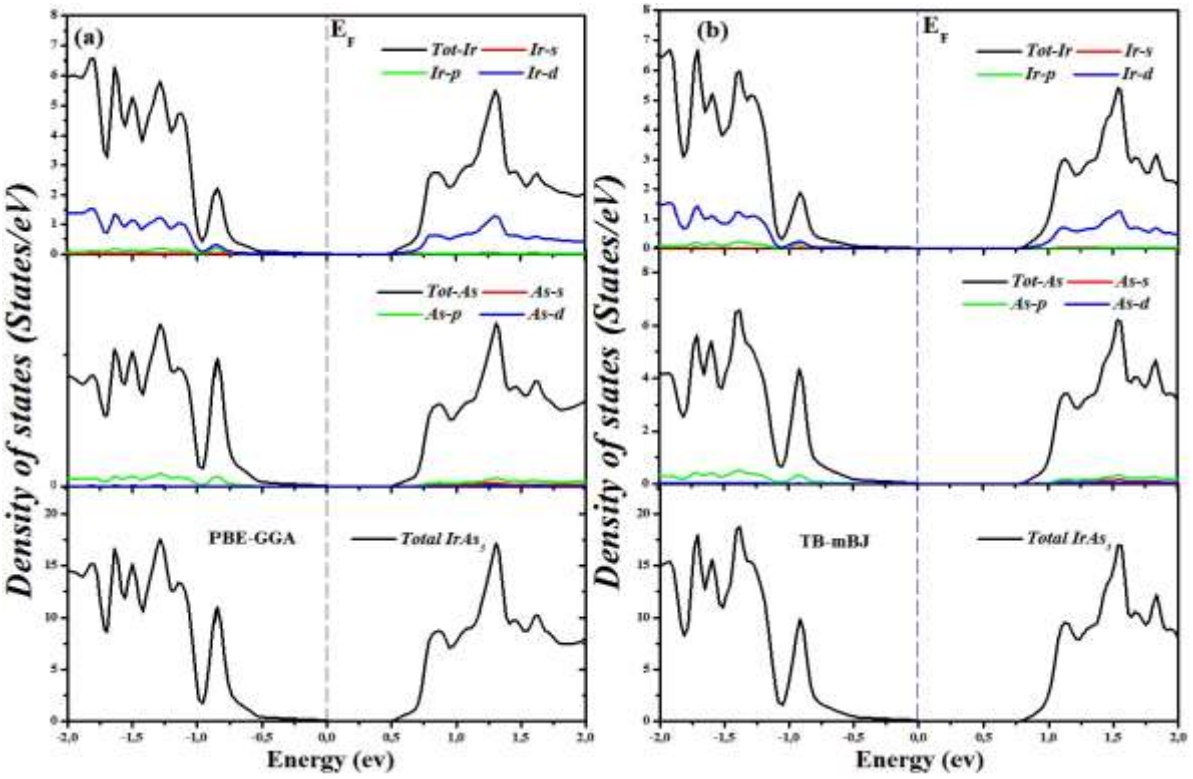

Fig. III.21: Densities of states for $IrAs_3$ with: (a) PBE-GGA and (b) TB-mBJ approximations.

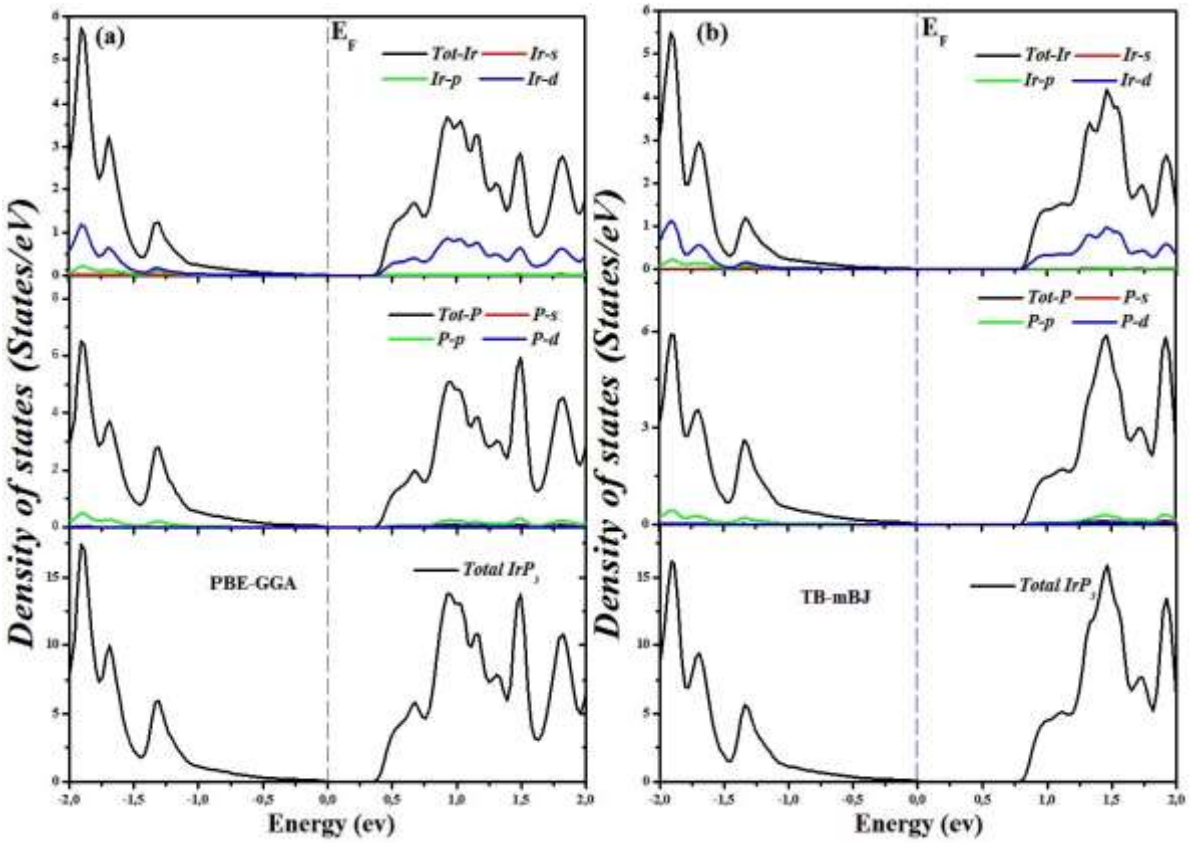

Fig. III.22: Densities of states for IrP_3 with: (a) PBE-GGA and (b) TB-mBJ approximations.

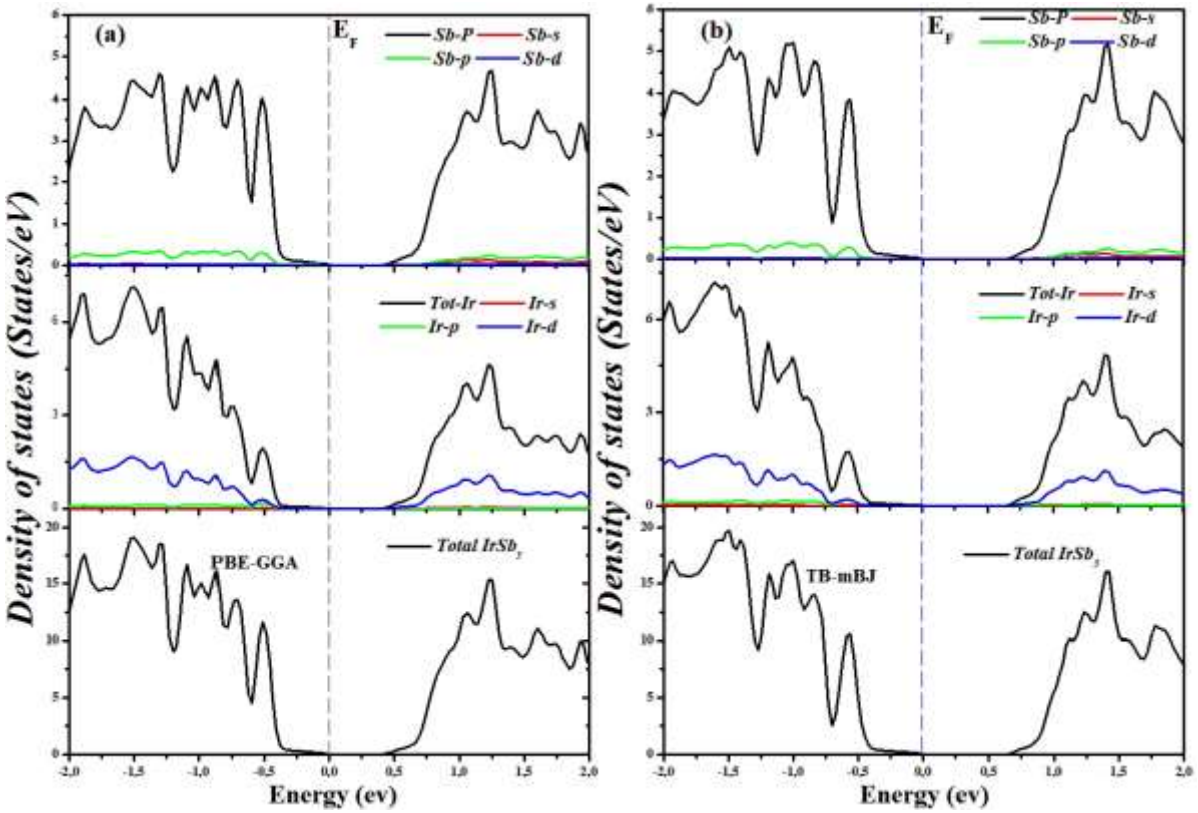

Fig. III.23: Densities of states for $IrSb_3$ with: (a) PBE-GGA and (b) TB-mBJ approximations.

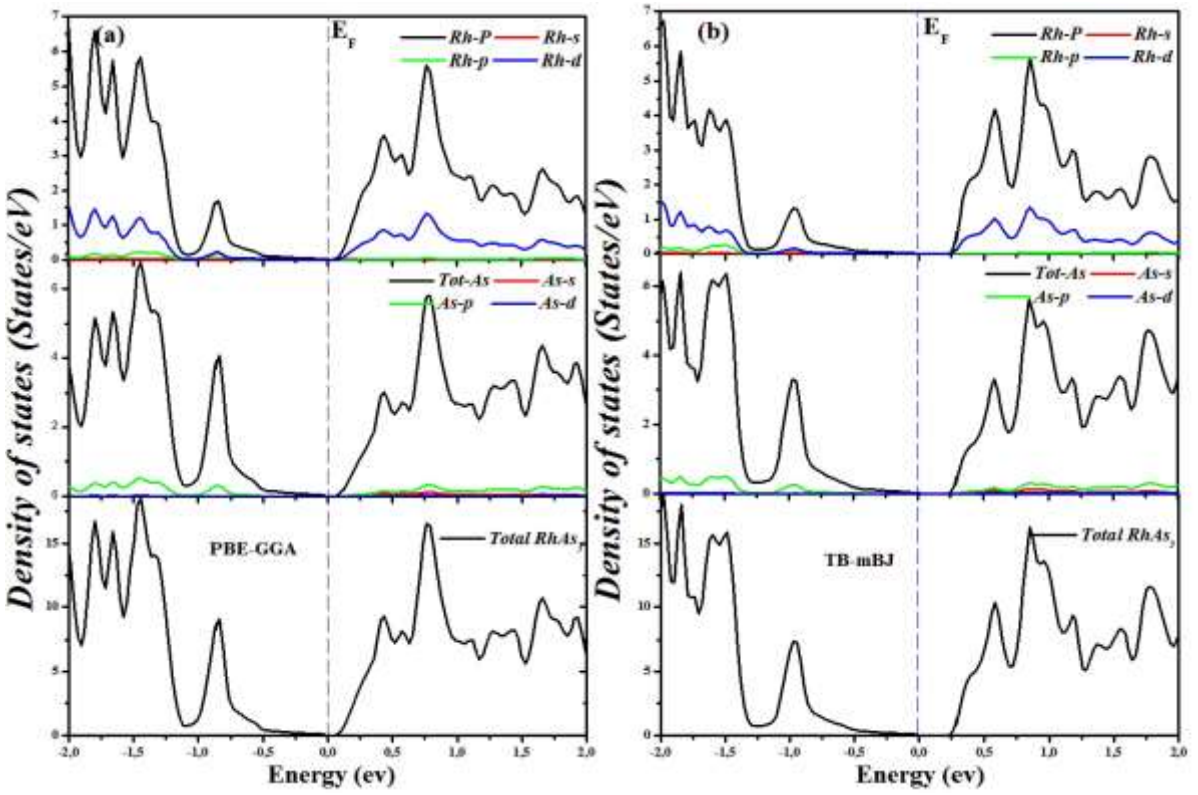

Fig. III.24: Densities of states for $RhAs_3$ with: (a) PBE-GGA and (b) TB-mBJ approximations.

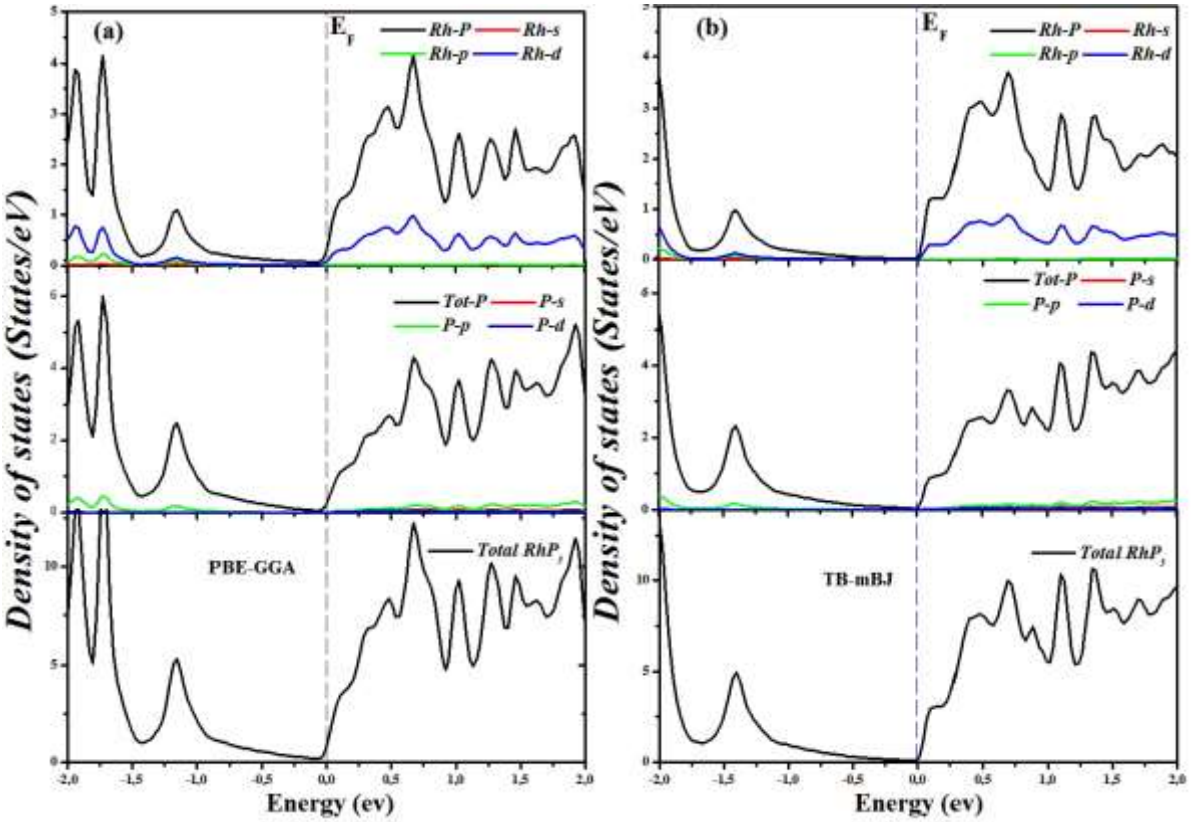

Fig. III.25: Densities of states for RhP_3 with: (a) PBE-GGA and (b) TB-mBJ approximations.

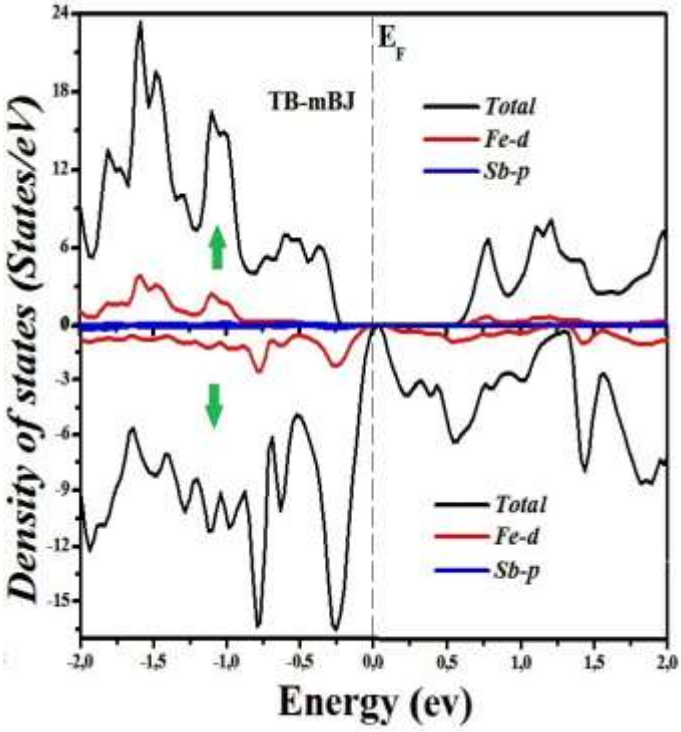

Fig. III.26: Densities of states for spin up and spin down channels of $FeSb_3$ compound with TB-mBJ approximations.

III.5. Thermoelectric properties

Now, we spotlight on the thermoelectric properties of binary skutterudites compounds MX_3 using the BoltzTrap code [39]. In general, the calculation of the thermoelectric properties is transition from first-principles to second-principles methods. The first principles method used here is the FP-LAPW whereas the second-principles are the BoltzTraP code. Usually, the thermoelectric properties of the system are calculated from the ground state within the limits of Boltzmann theory [40–42] and the constant relaxation time approximation as implemented in the BoltzTraP code. Regularly BoltzTraP code performs a Fourier expansion of the quantum chemical band energies which allows to obtain the electronic group velocity v and inverse mass tensor, as the first and second derivatives of the bands with respect to k. Applying v and to the semiclassical Boltzmann equations, the transport tensors can be evaluated. The both none and spin-polarized thermoelectric properties for binary skutterudites compounds are used. Where the spin-up and spin-down channels data of the transport coefficients are averaged through two-current model [50]. These models assume the resistivities from two spin channels as parallel resistors and are added as if no spin-flip process occurs. Therefore, the resulting average resistivity (ρ) and conductivity (σ) become,

$$\frac{1}{\rho} = \frac{1}{\rho\downarrow} + \frac{1}{\rho\uparrow} \qquad \textit{and} \qquad \sigma = \sigma\downarrow + \sigma\uparrow \qquad \text{III.1}$$

The effective electronic part of thermal conductivity (κ_e) is expressed as [43]:

$$\kappa_e = \kappa_e\uparrow + \kappa_e\downarrow \qquad \text{III.2}$$

The total Seebeck coefficient (S) from both the channels is weighted as [44,45]:

$$S = \left[\frac{S\uparrow\sigma\uparrow + S\downarrow\sigma\downarrow}{\sigma\uparrow + \sigma\downarrow}\right] \qquad \text{III.3}$$

Where ρ↑ and ρ↓, σ↑ and σ↓, κe↑ and κe↓, S↑ and S↓ are the resistivities, electrical conductivities, thermal (electronic part) conductivities and seebeck coefficients in spin-up and spin-down channels, respectively.

As we know, in semiconductor materials, a significant number of electrons can be excited to cross the band gap and this movement of such electrons is responsible for the conductivity of this material. Therefore, since in the semiconductor materials, the electrical conductivity depends on energy band gap [30,37], and the TB-mBJ approach has estimated the good value of the energy band gaps for our investigated materials, the thermoelectric properties including the electrical and the electronic thermal conductivities and the Seebeck

coefficient were calculated based on the calculated TB-mBJ band structures. We note here that the k-point has increased to 1000 000 k-points in the IBZ as the precise calculations of thermoelectric properties of metals require the dense sampling of the BZ.

III.5.1 Seebeck coefficient (S)

We know that the Seebeck coefficient (S) for semiconductors, which defines the relationship between the electrical potential and the temperature gradient ($S = \Delta V/\Delta T$) [46], is very sensitive to the number and type of Carrier concentrations. Figs. III.27(a)-(c) show the temperature dependence of the Seebeck coefficient (*S*) for binary skutterudite MX_3 compounds (M= Co, Rh and Ir and X= Sb, P, and As) compounds and the up/dn jointed with total Seebeck coefficient (S) as a function of temperature at a certain value of the chemical potential ($\mu = E_F$) for $FeSb_3$ compound are illustrated in Fig. III.27(d).

As shown in this Fig, the Seebeck coefficient values show positives signs for: $CoSb_3$, $IrSb_3$, $FeSb_3$, IrP_3, $RhAs_3$ and $CoAs_3$ compounds, which indicate that the major charge carries in these compounds are the holes and consequently, signifying the *p*-type conduction. While for the binary skutterudites CoP_3 and RhP_3 compounds, they show negatives values, suggesting that the major charge concentrations are electrons, and as results they confirm the n-type conductions.

Whereas in the both binary skutterudites $IrAs_3$ and $RhSb_3$ compounds the seebeck coefficient values exhibit mixed signs. They show *p*-type conductivity between temperatures ranges $100\ K$ and 600 K ($100\ K$ and 450 K) for $RhSb_3$ ($IrAs_3$) compounds respectively, and at about $T = 600\ K$ (450 K) for the both $RhSb_3$ ($IrAs_3$) compounds, there is a transition to *n*-type conductivity. This is possibly will be due to the existence of both holes and electrons at the vicinity of Fermi level. And thus is in concurrence with the complex electronic band structure (see Fig. III.15 and Fig. III.10).

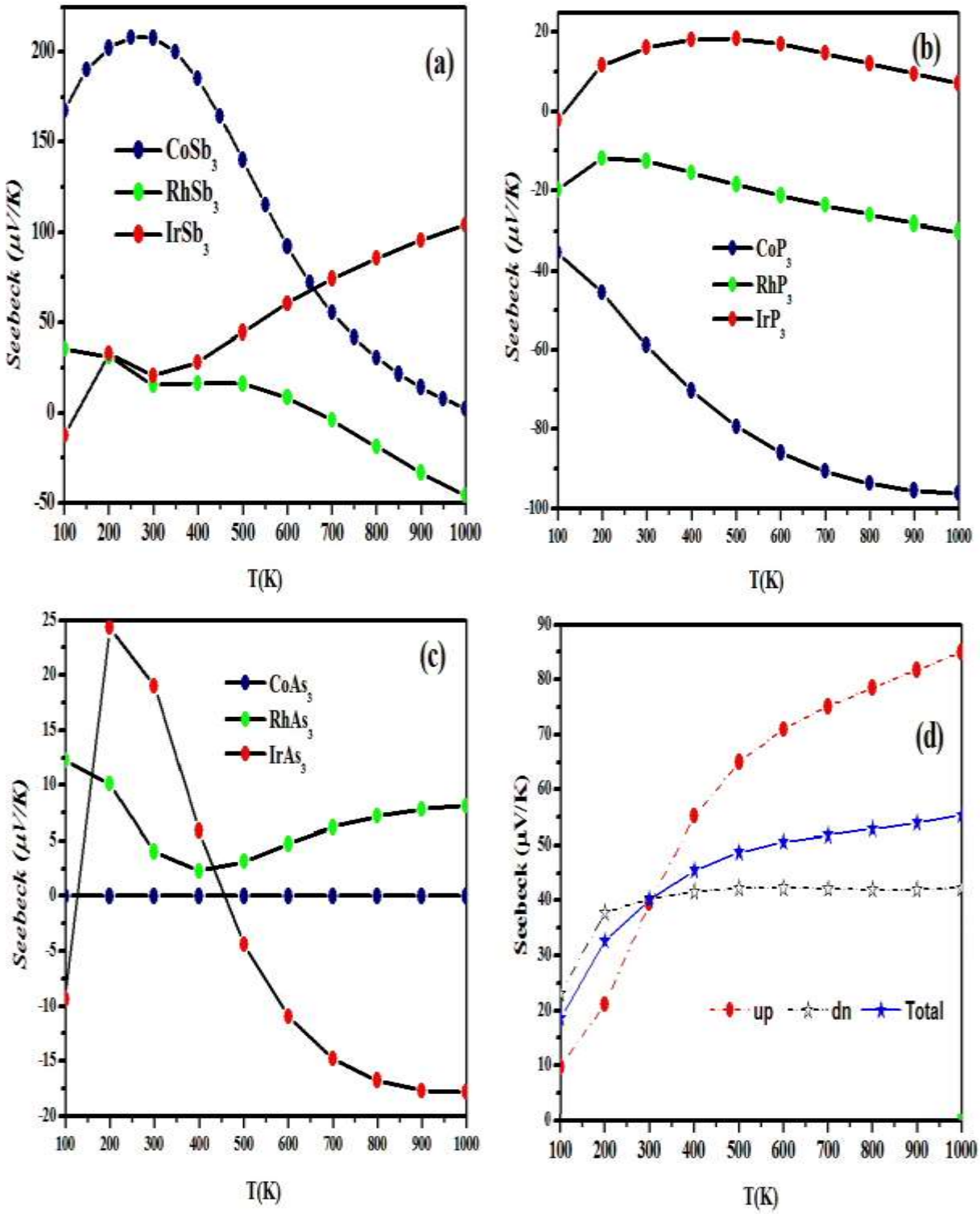

Fig. III.27: The temperature dependence of the seebeck coefficient of binary skutterudite compounds: (a)-(c) for MX_3 (M= Co, Ir, Rh and X= Sb, P, As) compounds and (d) for spin up and down channels for $FeSb_3$ compound.

III.5.2 Electrical conductivity (σ) and electronic thermal conductivity (κ_e)

Like that of the Seebeck coefficient, the electrical conductivity directly affects the figure of merit (ZT) of a thermoelectric material. Where the thermal conductivity inversely affects the thermoelectric performance (TE) of a material (i.e. it should be kept as low as possible to obtain a higher figure of merit).

Figs. III.28(a)-(c) present the temperature dependence of the calculated electrical conductivities over relaxation time $\left(\frac{\sigma}{\tau}\right)$ for binary skutterudite MX_3 compounds (M= Co, Rh and Ir and X= Sb, P, and As) compounds and the variation of $\left(\frac{\sigma}{\tau}\right)$ for the spin up/dn channels jointed with total $\left(\frac{\sigma}{\tau}\right)$ as a function of temperature at a certain value of the chemical potential ($\mu = E_F$) for $FeSb_3$ compound are illustrated in Fig.III.28(d).

As shown in this Figure, the calculated electrical conductivities over relaxation time $\left(\frac{\sigma}{\tau}\right)$ for binary skutterudites $CoSb_3$, $RhSb_3$, CoP_3, $IrSb_3$ and $FeSb_3$ compounds slightly increased with increasing temperature, which clearly indicates the highly degenerate nature of materials. Where the very low values at all examined temperatures reached for the binary skutterudite antimonide $CoSb_3$ compound. This is in accord with its calculated Seebeck coefficient values. Which suggest the usual character of degenerate semiconductor.

One can notice also, that the $\left(\frac{\sigma}{\tau}\right)$-T relationships for these compounds have roughly linear tendencies. It has been noticed that the calculated electrical conductivities over relaxation time $\left(\frac{\sigma}{\tau}\right)$ for binary skutterudites $CoAs_3$, $RhAs_3$, IrP_3, and RhP_3 compounds significantly decrease with increasing temperature range, showing typical character of heavily degenerated semiconducting behavior. These differs trends observations founded for binary skutterudites compounds are attributed to the carrier concentration, carrier's type and carrier's mobility.

The temperature dependence of the electronic part of thermal conductivities over relaxation time $\left(\frac{\kappa_e}{\tau}\right)$ for binary skutterudite MX_3 compounds (M= Co, Rh and Ir and X= Sb, P, and As) compounds are shown in Figs. III.29(a)-(c), where Fig. III.29(d) displays the variation of $\left(\frac{\sigma}{\tau}\right)$ for the spin up/dn channels jointed with total $\left(\frac{\sigma}{\tau}\right)$ as a function of temperature at a certain value of the chemical potential ($\mu = E_F$) for $FeSb_3$ compound.

The thermal conductivity is another important factor that determines the thermoelectric performance of the compound; it is a measure of its ability to conduct heat.

Generally, there are two kinds of conductive mechanisms, namely electronic κ_e and lattice thermal κ_{lat}, owing to the presence of electron and phonon respectively. Where the electronic thermal conductivity has been calculated from the Wiedemann-Franz law$\kappa_e = L\sigma T$, which states that the ratio of the electronic contribution of the thermal conductivity (κ_e) to the electrical conductivity (σ) of a metal is proportional to the temperature (T) [30]. Theoretically, the calculation of the proportionality constant L, known as the Lorenz number, requires an accurate band structure and knowledge of the energy-dependent scattering processes [24].

One can observe from Fig. III.29, the electronic thermal conductivities over relaxation time $\left(\frac{\kappa_e}{\tau}\right)$ for all the binary skutterudites compounds considerably increased with increasing the temperature range, they were found that the largely reduced electronic thermal conductivity over relaxation time $\left(\frac{\kappa_e}{\tau}\right)$ achieved in the binary skutterudite antimonide $CoSb_3$ compound. These findings are in consistence with the obtained results of electrical conductivities over relaxation time $\left(\frac{\sigma}{\tau}\right)$ (see Figs. III.28).

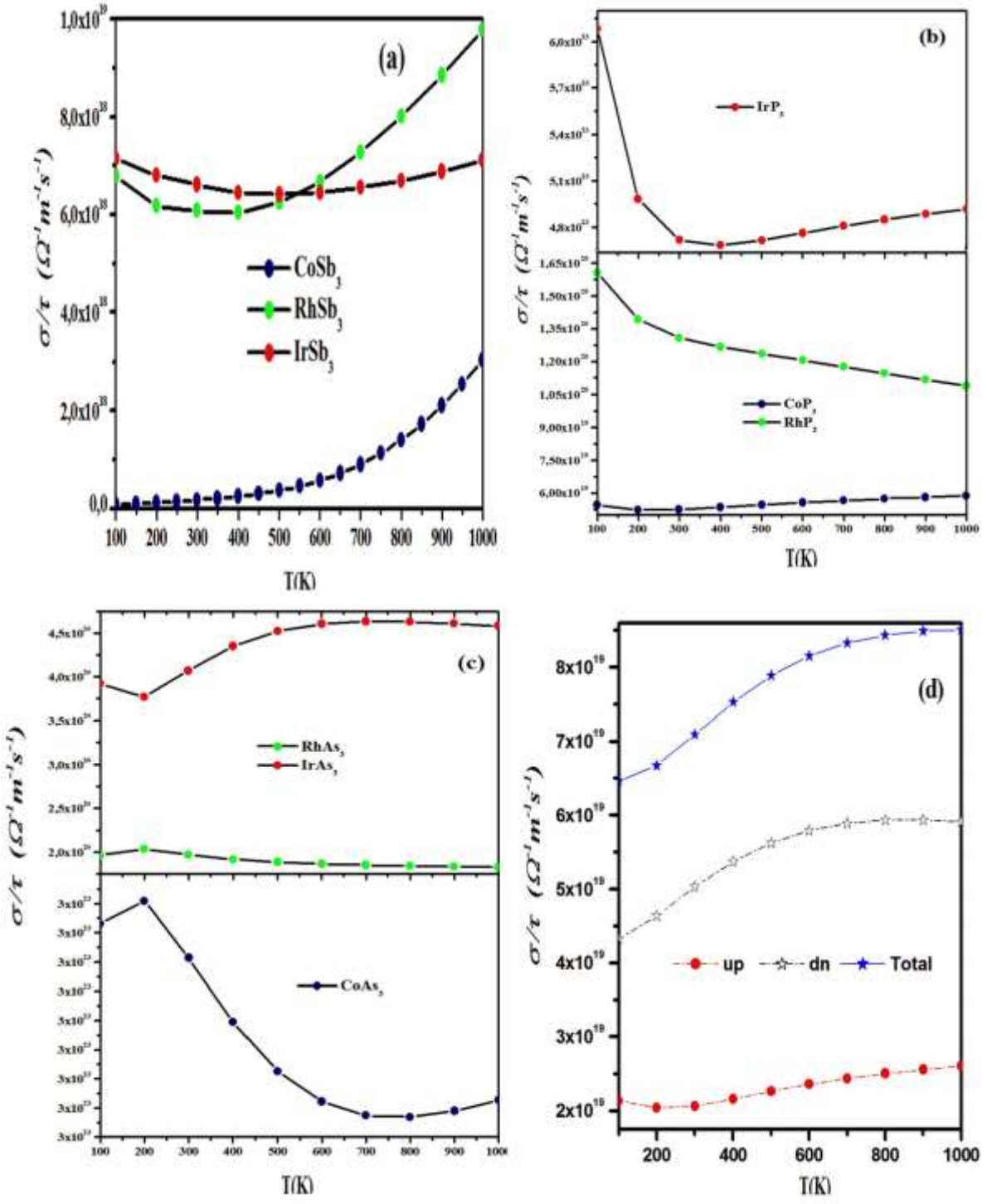

Fig. III.28: The calculated electrical conductivities over relaxation time $\left(\frac{\sigma}{\tau}\right)$ of binary skutterudite compounds: (a)-(c) for MX_3 (M= Co, Ir, Rh and X= Sb, P, As) compounds and (d) for spin up and down channels for $FeSb_3$ compound.

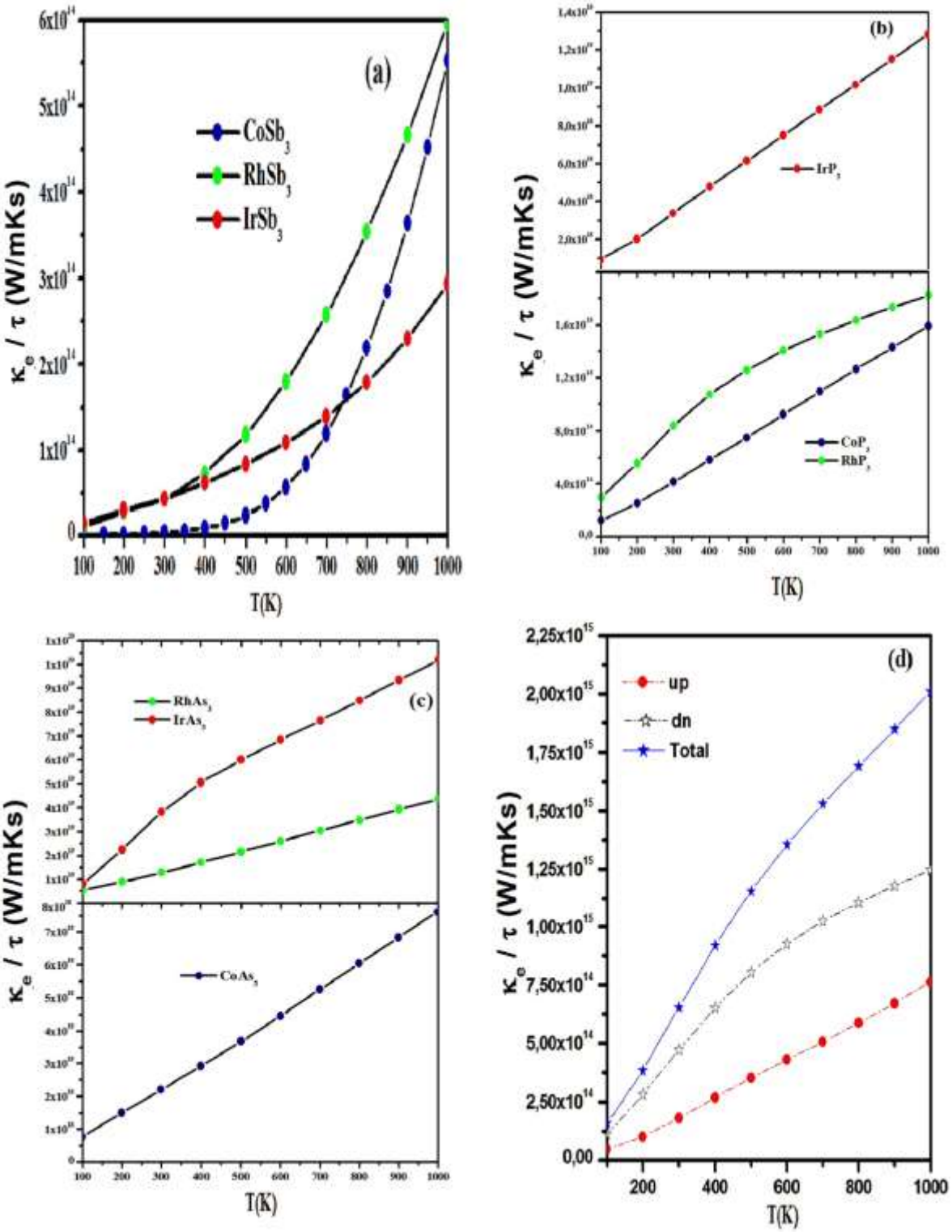

Fig. III.29: The temperature dependence of the electronic part of thermal conductivities over relaxation time $\left(\frac{\kappa_e}{\tau}\right)$ of binary skutterudite compounds: (a)-(c) for MX_3 (M= Co, Ir, Rh and X= Sb, P, As) compounds and (d) for spin up and down of $FeSb_3$ compound.

III.5.3 Electronic figure of merit (ZT_e)

Finally, we tried to figure out the figure of merit (ZT_e) defined as, $ZT = \frac{S^2\sigma}{\kappa} T$ [47]. Here the figure of merit is presented as a function of absolute temperature presented in the Figs. 30(b)-(d). The predicted ZT_e value reaches to a maximum of 0.67 at 201K for binary skutterudite antimonide $CoSb_3$. While as its value is 0at temperature 900 K.

Although, the ZT_e value increases on going from the lower to higher temperatures in $RhSb_3$, CoP_3, $IrSb_3$, $IrAs_3$, $FeSb_3$, $CoAs_3$, $RhAs_3$, IrP_3, and RhP_3 compounds, but the magnitude is quite low when compared to $CoSb_3$ compound. These results make the binary skutterudite $CoSb_3$ compound as most promising binary skutterudites. However, its ZT_e value stays low compared with state-of-the-art of thermoelectric materials.

The suitable doping substituent elements or filling various species can be an alternative to decrease the thermal conductivity while keeping the other parameters constrained. Since, thermoelectric materials are essentially nowadays investigated for the innovative renewable technology applications.

From the investigation of the thermoelectric properties, the $CoSb_3$ binary skutterudite compound has been found to have a large Seebeck coefficient, combined with high electrical conductivity, although it has a relatively high thermal conductivity, which apparently makes it less attractive as an applied thermoelectric material. So, an optimization of the carrier concentrations by filler or/and substitution might improve the thermoelectric performance of $CoSb_3$ binary skutterudite antimonide compound. This is will be the objective of the next sections.

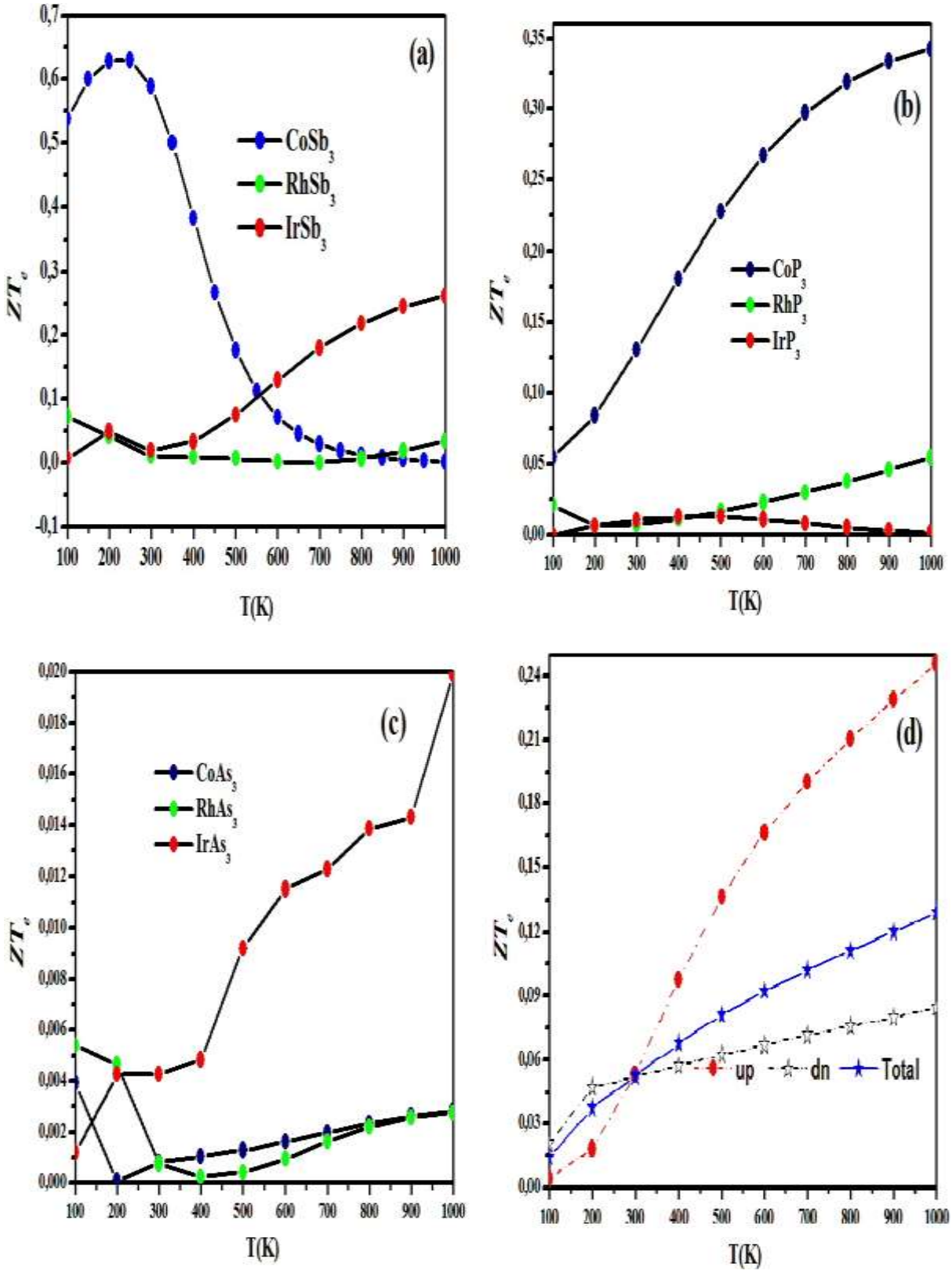

Fig. III.30: The temperature dependence of the electronic figure of merit values (ZT_e) of binary skutterudite compounds: (a)-(c) for MX_3 (M= Co, Ir, Rh and X= Sb, P, As) compounds and (d) for spin up and down of $FeSb_3$ compound.

Bibliography

[1] K.F. Boebert. Ueber das Modumer Blau farbenwerk in Norwegen. Archivfuer Mineralogie, Geognosie, Bergbau und Huettenkunde. G. Reimer, Berlin, (1847).

[2] A. Breithaupt. Uebereineneue Kies-Spezies von Skutterud. Annalen der Physik und Chemie, 9, 115 (1827).

[3] I. Oftedal. Die Kristallstruktur von Skutterudit und Speiskobalt-Chloanthit. Z. Kristallogr., A66, 517 (1928).

[4] D.M. Rowe. Thermoelectrics Handbook: Macro to Nano. CRC/Taylor & Francis, (2006).

[5] P. Blaha, K. Schwarz, G.K.H. Madsen, D. Kvasnicka, J. Luitz, Vienna University of Technology, Austria, (2001).

[6] J.P. Perdew, A. Ruzsinszky, G.I. Csonka, O.A. Vydrov, G.E. Cuseria, L.A. Constantin,X. Zhou and K. Burke, JPhys. Rev. Lett. 100, 136406 (2008).

[7] F. Tran and P. Blaha, J. Phys. Rev. Lett. 102, 226401 (2009).

[8] E.J. Walter, Optium- pseudo potential generation project.

[10] D. Velasco-Soto, E. Menendez-Proupin, R. Realyvazquez-Guevara, J.A. MatutesAquino, Mater. Res. Express 5, 025908 (2018).

[11] M. Christensen, B.B. Iversen, L. Bertini, C. Gatti, M. Toprak, M. Muhammed, E. Nishibori, J. Appl. Phys. 96, 3148 (2004).

[12] S. Sharma, S.K. Pandey, Comput. Mater. Sci. 85, 340 (2014).

[13] M. Rasander, M.A. Moram, J. Chem. Phys. 143 (14), 144104 (2015).

[14] A. Mochel, I. Sergueev, N. Nguyen, G.J. Long, F. Grandjean, D.C. Johnson, R. P. Hermann, Phys. Rev. B 84 (6), 064302 (2011).

[15] E. Arushanov, K. Fess, W. Kaefer, C. Kloc, E. Bucher, Phys. Rev. B 56, 911 (1997).

[16] T. Schmidt, G. Gliche, and H. D. Lutz, J. Acta. Crystallogr., Sect. C:Cryst. Struct. Commun. 43, 1678 (1987).

[17] A. Kjekshus and T. Rakke, J. Acta. Chem. Scand., Ser. A 28, 99 (1978).

[18] C. Artini,G. Zanicchi, G.A. Costa, M.M. Carnasciali, C. Fanciulli,and R. Carlini, J. Inorg. Chem. 55, 2574 (2016).

[19] D. Mandrus, A. Migliori, T.W. Darling, M.F. Hundley, E.J. Peterson, J. D. Thompson, Phys. Rev. B 52, 4926 (1995).

[20] E. Arushanov, M. Respaud, H. Rakoto, J.M. Broto, T. Caillat, Phys. Rev. B 61, 4672 (2000).

[21] J. Nagao, M. Ferhat, H. Anno, K. Matsubara, E. Hatta, K. Mukasa, Appl. Phys. Lett. 76, 3436 (2000).

[22] K. Matsubara, T. Iyanaga, T. Tsubouchi, K. Kishimoto, T. Koyanagi, AIP Conf. Proc. No. 316, AIP, New York, p. 226, (1995).

[23] J.W. Sharp, E.C. Jones, R.K. Williams, P.M. Martin, B.C. Sales, J. Appl. Phys. 78, 1013 (1995).

[24] G.S. Nolas, G.A. Slack, T. Caillat, G.P. Meisner, J. Appl. Phys. 79, 2622 (1996).

[25] T. Caillat, A. Borshchevsky, J.P. Fleurial, J. Appl. Phys. 80, 4442 (1996).

[26] L.D. Dudkin, N. KhAbrikosov, Sov. Phys. Solid Stat 1, 126 (1959).

[27] C. Hu, X. Zeng, Y. Liu, M. Zhou, H. Zhao, T.M. Tritt, J. He, J. Jakowski, P.R.C. Kent, J. Huang, B.G. Sumpter, Phys. Rev. B 95, 165204 (2017).

[28] A.C. Kraemer, M.R. Gallas, J.A.H. Da Jornada, C.A. Perottoni, Phys. Rev. B 75, 024105 (2007).

[29] H.A. Rahnamaye Aliabad, M. Ghazanfari, Iftikhar Ahmed, M.A. Saeed, Comput. Mater. Sci. 65, 509 (2012).

[30] D.J. Singh, W.E. Pickett, Phys. Rev. B 50, 11235 (1994).

[31] J.O. Sofo, G.D. Mahan, Phys. Rev. B 58, 15620 (1998).

[32] E.Z. Kurmaev, A. Moewes, I.R. Shein, L.D. Finkelestein, A.L. Ivanovskii, A. Anno, J. Phys. Condens. Matter 16, 979 (2004).

[33] K. Koga, K. Akai, K. Oshiro, M. Matsuura, Phys. Rev. B 71, 155119 (2005).

[34] P.X. Lu, Z.G. Shen, X. Hu, Physica B 405, 1740 (2010).

[35] K. Takegahara, H. Harima, Physica B 328, 74 (2003).

[36] J.-P. Fleurial, T. Caillat and A. Borshchevsky, Proceedings ICT '97. XVI International Conference on Thermoelectrics IEEE, Dresden, Germany, August 26-29, 1-11 (1997).

[37] B. Khan, H.A.R. Aliabad, Saifullah, S. Jalali-Asadabadi, I. Khan, I. Ahmad, J. Alloy.Compound.10, 1016 (2015).

[38] G.A. Slack and V.G. Tsoukala, J. Appl. Phys. 76 1665 (1994).

[39] J. Ackermann and A. Wold, J. Phys. Chem. Solids 38, 1013(1977).

[40] G.K.H. Madsen, D. Singh, J. Comput. Phys. Commun. 175, 67 (2006).

[41] P. B. Allen, in Quantum Theory of Real Materials, ed. J. R.Chelikowsky and S. G. Louie, Kluwer, Boston, 219 (1996).

[42] J. M. Ziman, Electrons and Phonons, Clarendon, Oxford, (2001).

[43] C. M. Hurd, The Hall Effect in Metals and Alloys, Plenum, New York, (1972).

[44] A.S. Botana, P.M. Botta, C. de la Calle, A. Piñeiro, V. Pardo, D. Baldomir, J.A. Alonso, Phys. Rev. B 83, 184420 (2011).

[45] G.E.W. Bauer, E. Saitoh, B.J. van Wees, Nat. Mater. 11, 391 (2012).

[46] S.O. Kasap, Thermoelectrical Effects in Metals: Thermocouples, e-Booklet, 1990-2001.

[47] S.A. Khandy, D.C. Gupta, J. Magn. Mag. Mater. 458, 176 (2018).

Chapter IV

Chapter IV: Role of filler elements on thermoelectric performance of $CoSb_3$ based skutterudites

IV.1 Introduction

Considering defect in thermoelectrics shows that certain materials tend to have opening sites or interstitial occupancies. This opens up new routes for exploring the intrinsic defect chemistry of thermoelectric materials and controlling transport at different temperatures. Among them, we have the class of skutterudite compounds.

Their structure can be modified by the insertion of variety of guest atoms, which fill the 2*a* vacant sites (0,0,0) of the unit cell and occupy a body-centered position in the cubic structure [1] (see Fig. IV.1), and the general formula of the compounds becomes RM_4X_{12} referred to as filled skutterudites.

This filling makes the class of the skutterudite materials as a perfect example of the phonon glass electron crystal (PGEC) concept, proposed by Slack [2].

The filler elements can be lanthanides, actinides, alkaline (earths) metals, and certain elements from the Bromine and carbon groups [3-5]. The filler atomic size, charge state, electronegativity and the filling fraction limit (FFL) have been considered to involve a thermodynamically stable compound.

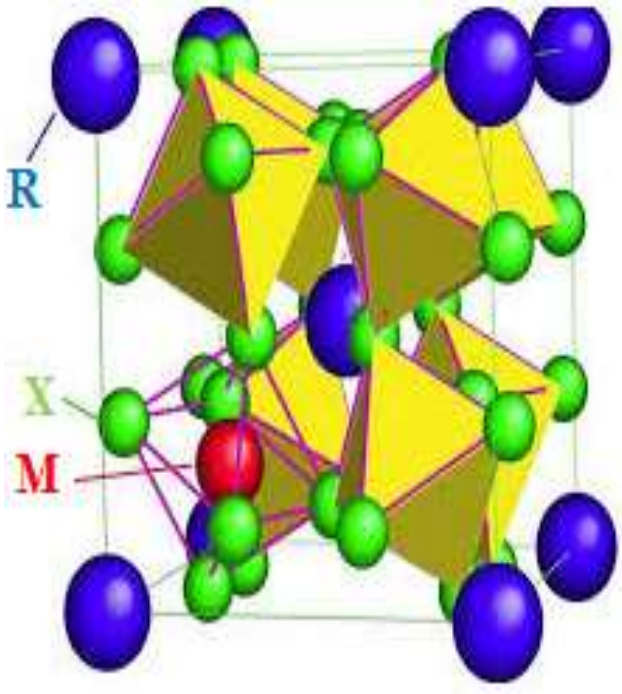

Fig. IV.1: Crystal structure of filled skutterudites (RMX_3).

IV.2. *N*-type filled $CoSb_3$-based skutterudites $R_yCo_4Sb_{12}$ (with R= AM, EM and RE with $x \leq 0.5$)

Fourth types of skutterudite structures were calculated, including (i) alkali metals fully filled $CoSb_3$, (ii) Na partially filled $CoSb_3$, (iii) Ba partially filled $CoSb_3$ and (iv) Yb partially filled $CoSb_3$.

For alkali metals fully filled $CoSb_3$, the simple cubic cell (Co_8Sb_{24}) was used for the calculations of structural optimizations, while the bcc primitive cell (Co_4Sb_{12}) and the bcc 1 × 1 × 2 supercell ($Co_{16}Sb_{48}$) were used to calculate the electronic structures of the partially filled $CoSb_3$ compounds. The bcc supercell contains four dodecahedron voids, each enclosed by eight Co atoms and six pairs of Sb atoms.

The structure of partially filled $CoSb_3$ was constructed by filling one and two of the four voids in the bcc supercell, giving $RCo_{16}Sb_{48}$ ($R_{0.5}Co_{16}Sb_{48}$) or equivalently to $R_{0.5}Co_4Sb_{12}$ ($R_{0.25}Co_4Sb_{12}$), which correspond to the filling fraction of 50% (25%), respectively.

IV.2.1. Structural features

We begin with presenting the global structural effect of filling on $CoSb_3$ based skutterudites by reporting changes in the lattice parameters which are provided in Table IV.1. The calculated lattice parameters at equilibrium (a_0) for the partially filled skutterudite $R_yCo_4Sb_{12}$ (R= Yb, Na and Ba with $x \leq 0.5$) and alkali metals fully filled $CoSb_3$ based skutterudites compounds are in good agreement with those reported in literature [6-9].

One can notice from Table IV.1, the equilibrium lattice parameter a_0 increases as the increase of the both filling fraction (FF) and the size of the filler ions. These findings are consistent with the investigated results in filled pnictogen-substituted skutterudites [10-14].

Table .IV.1 regroups the calculated equilibrium structural parameters for partially filled skutterudite $R_yCo_4Sb_{12}$ (R= Yb, Na and Ba with $x \leq 0.5$) and alkali metals fully filled $CoSb_3$ based skutterudites compounds.

Table .IV.1: The equilibrium structural parameters for partially filled skutterudite $R_yCo_4Sb_{12}$ (R= Yb, Na and Ba with $x \leq 0.5$) and alkali metals fully filled $CoSb_3$ based skutterudites compounds.

Compounds	a(Å)	B_0 (GPa)	B'
$NaCo_4Sb_{12}$	9.250	85.24	4.67
$CsCo_4Sb_{12}$	9.252	82.27	5.08
KCo_4Sb_{12}	9.200	77.80	5.05
$LiCo_4Sb_{12}$	9.154	84.92	5.09
$RbCo_4Sb_{12}$	9.220	82.476	5.03
$Na_{0.5}Co_4Sb_{12}$	9.191	83.79	4.31
$Yb_{0.5}Co_4Sb_{12}$	9.270	86.46	4.53
$Ba_{0.5}Co_4Sb_{12}$	9.176	95.64	3.24
$Na_{0.25}Co_4Sb_{12}$	9.152	89.48	3.85
$Yb_{0.25}Co_4Sb_{12}$	9.275	84.97	4.59
$Ba_{0.25}Co_4Sb_{12}$	9.121	82.05	4.79

IV.2.2. Electronic properties

First-principles band structure calculations have been carried out to shed light on the band variations caused by the introduction of alkali metals (Na), alkali earth metals (Ba) and rare earth (Yb) in to the 2a sites of the $CoSb_3$ based skutterudites compound.

Due to the similarity between band structures of alkali metals filled $CoSb_3$ based skutterudites, only the results on Na filled systems are shown in Fig. IV.2(a) (b).

IV.2.2.a. Electronic band structure

Fig. IV.2 shows the band structures around the Fermi levels (zero energy points) for (a) $Na_{0.5}Co_4Sb_{12}$, (b) $Na_{0.25}Co_4Sb_{12}$, (c) $Yb_{0.5}Co_4Sb_{12}$, (d) $Yb_{0.25}Co_4Sb_{12}$, (e) $Ba_{0.5}Co_4Sb_{12}$ and (f) $Ba_{0.25}Co_4Sb_{12}$ partially filled $CoSb_3$ based skutterudites compounds. As estimated based on the electronic structures of the bcc supercell shown below, the low R filling fraction largely serves to raise the Fermi energy to a position slightly above the bottom of the valley

bands (second conduction bands); suggesting that these compounds are heavily doped *n*-type degenerate semiconductors.

These results are generally owing to the charge transfer from the guest filling atoms towards $CoSb_3$ matrix. Because each of the type fillers donates roughly two electrons to the host matrix of parent compound, and hence the Fermi levels in partially filled skutterudites shift up beyond the energy gap.

If these filled compounds are physically synthesized for thermoelectric applications, they will be additionally doped in order to rearrange the Fermi level somewhere near the energy gap [15].

From the structural results, we found that filling generally induces the increase of the lattice parameter; thus making the bond lengths become larger, and consequently decreasing the pseudo band gaps of $Na_{0.5}Co_4Sb_{12}$, $Na_{0.5}Co_4Sb_{12}$, $Yb_{0.5}Co_4Sb_{12}$ and $Yb_{0.25}Co_4Sb_{12}$ as results. With exception for the case of $Ba_{0.5}Co_4Sb_{12}$ and $Ba_{0.25}Co_4Sb_{12}$ partially filled Co_4Sb_{12} skutterudites compounds, the pseudo band gaps become larger than that of the corresponding unfilled Co_4Sb_{12} compound (see Figs. IV.2(a)-(f)). Similar results are reported by Yang et *al*. [16].

Following Fig. IV.2(c)-(d), we can also find that the change of the band structure for the Yb guest filling atom around the conduction band maximum (CBM) is more pronounced than that for Na and Ba guest atoms.

In addition, it can be observed from Figs. IV.2(a)-(f) that the lowest degenerate conduction bands are relatively flat, which leads to an increase in the effective mass. Where, the highly dispersive nature of the top of their highest valence bands should be advantageous to the increase in their electrical conductivities.

Also, it is obvious from the band structures of partially filled skutterudite, that the shape of the CBM is strongly dependent on the filling fraction of the guest fillers.

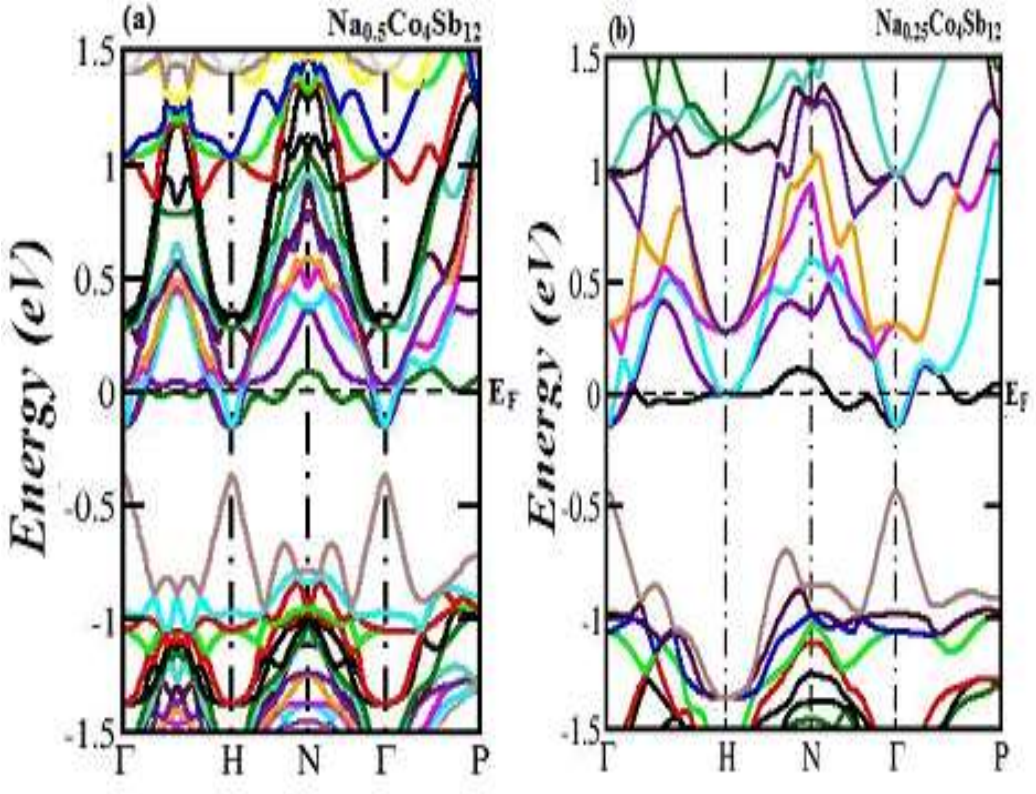

Fig. IV.2: The electronic band structures around the Fermi levels (zero energy points) for (a) $Na_{0.5}Co_4Sb_{12}$, (b) $Na_{0.25}Co_4Sb_{12}$.

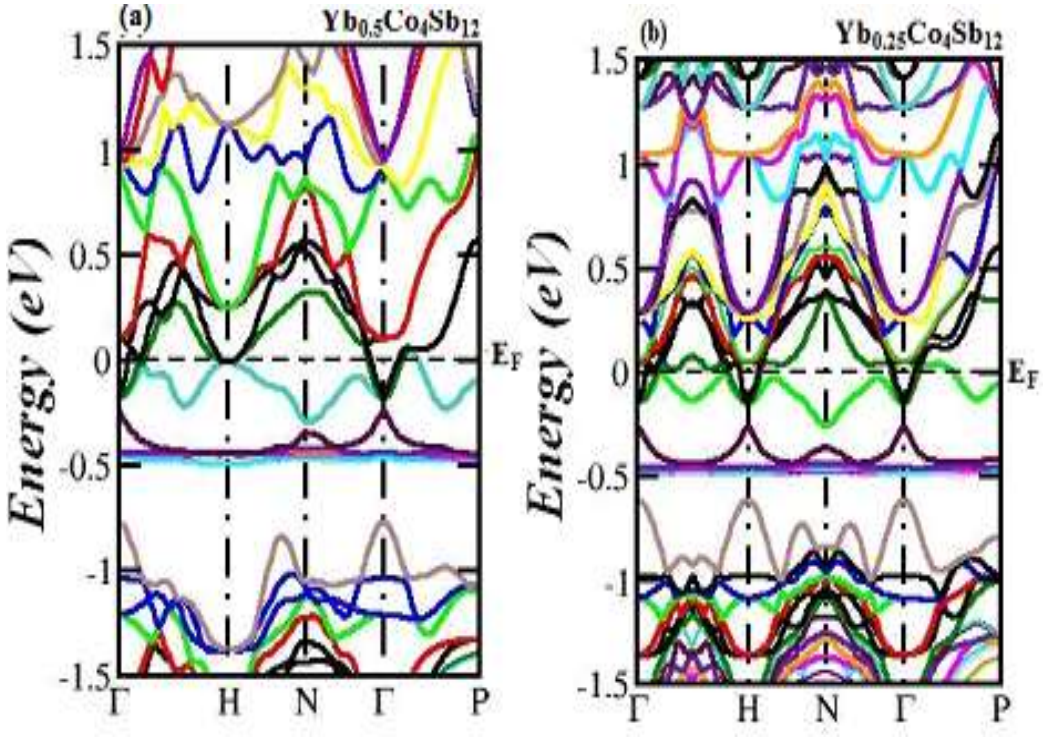

Fig. IV.3: The electronic band structures around the Fermi levels (zero energy points) for (a) $Yb_{0.5}Co_4Sb_{12}$, (b) $Yb_{0.25}Co_4Sb_{12}$.

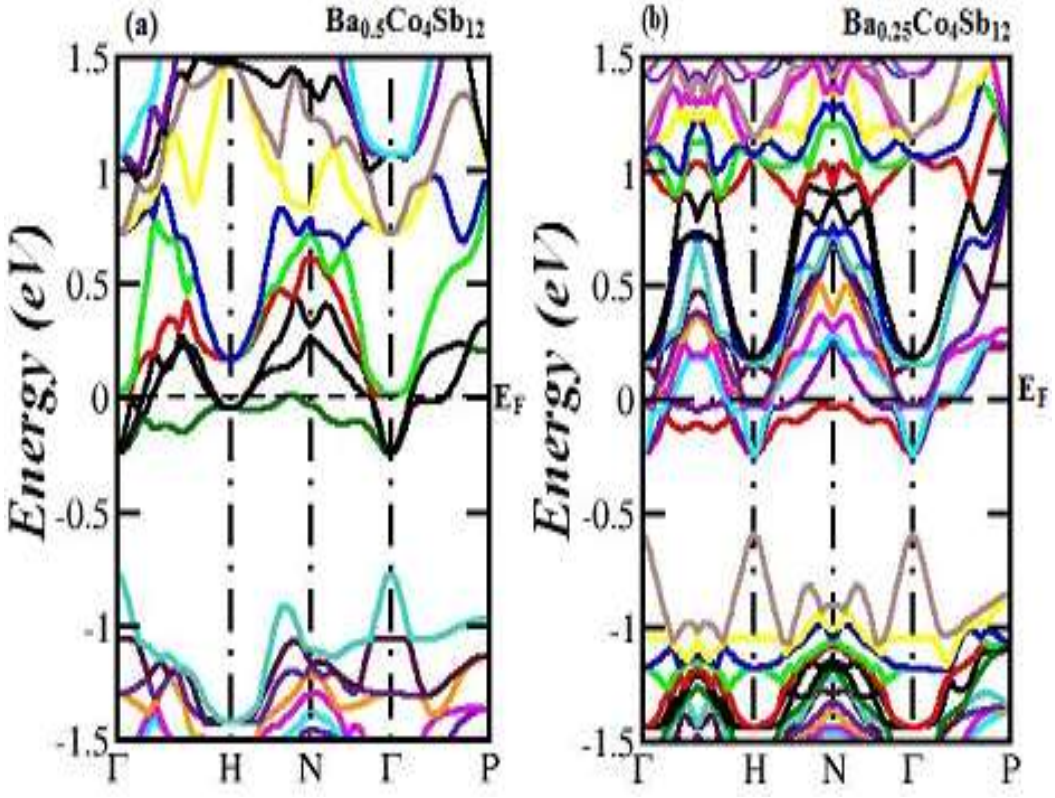

Fig. IV.4: The electronic band structures around the Fermi levels (zero energy points) for (a) $Bab_{0.5}Co_4Sb_{12}$, (b) $Ba_{0.25}Co_4Sb_{12}$.

IV.2.2.b. Electronic density of states (DOS)

Since a similar tendencies in the calculated total electronic and partial projected densities of states (TDOSs and PDOSs) were found among all the compounds studied here, the total electronic density of states and the partial projected density of states of only Ba partially filled Co_4Sb_{12} based skutterudite ($Ba_{0.25}Co_4Sb_{12}$) compound are shown in Figs. III.9. According to the electronic density of states in Figs. III.9. we notice that the states projected onto the transition metal Co show very heavy presence of Co-d orbitals in the valence band in the partially filled skutterudite $Ba_{0.25}Co_4Sb_{12}$ compound with a little admixture of p orbitals of both Sb and Ba atoms. On the other hand, the conduction band mainly comes from the Ba-d orbitals, while a negligible contribution from the Co orbitals is observed. The additional conduction bands come from the contributions of Ba-p and Sb-p orbitals.

So altering the framework chemistry of skutterudites compounds (introducing guest elements) is responsible for the modification of the curvature and the position of the existing bands.

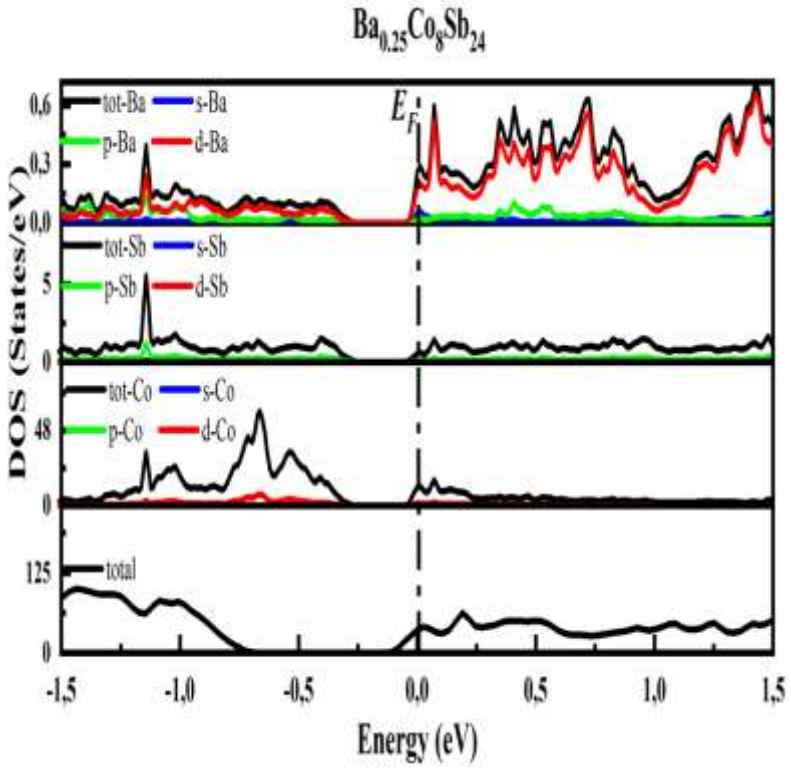

Fig. IV.5: Total and partial electronic densities of states for Ba partially filled skutterudite $Ba_{0.25}Co_8Sb_{24}$ compound.

IV.2.3. Thermoelectric properties

IV.2.3.1. Electrical transport properties

Starting from the band structure, we can estimate the electrical transport properties using a semi classical Boltzmann transport approach with the constant relaxation-time approximation [16].

IV.2.3.1.a. Seebeck coefficient (S)

Figs. IV(6)-(7) show the temperature dependence of the seebeck coefficient values for the partially filled skutterudite $R_yCo_4Sb_{12}$ (R= Yb, Na and Ba with $x \leq 0.5$) and alkali metals fully filled skutterudites, respectively. In these Figs., negative Seebeck coefficient values are obtained for the both fully and partially filled Co_4Sb_{12} based skutterudites compounds, which indicates that electrons are the majority carriers, and thus confirms that these compounds are *n*-type materials. These results are in good agreement with those reported in literatures [17,18].

As shown in Figs. IV.5, the Seebeck coefficient is affected by filling fraction (FF) of Ba, Yb and Na atoms, it decreases with increasing FF of the filler types, this is mostly due to the increase in the Hall carrier concentration (n_H). Accordingly these results are regular trend in thermoelectric materials. And they strongly depend on the electronic band structures near the Fermi level (see Figs. IV (2)–(4)). Our results are in good agreement with the results reported in numerous studies [19,20].

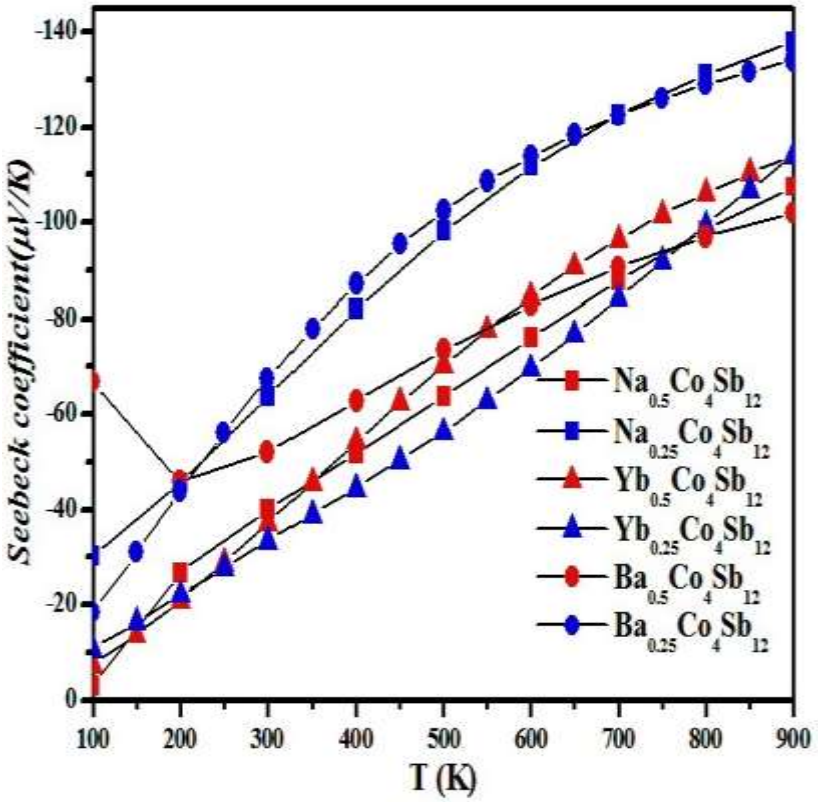

Fig. IV.5: The temperature dependence of the seebeck coefficient values for the partially filled skutterudites $R_yCo_4Sb_{12}$ (R= Yb, Na and Ba with $x \leq 0.5$).

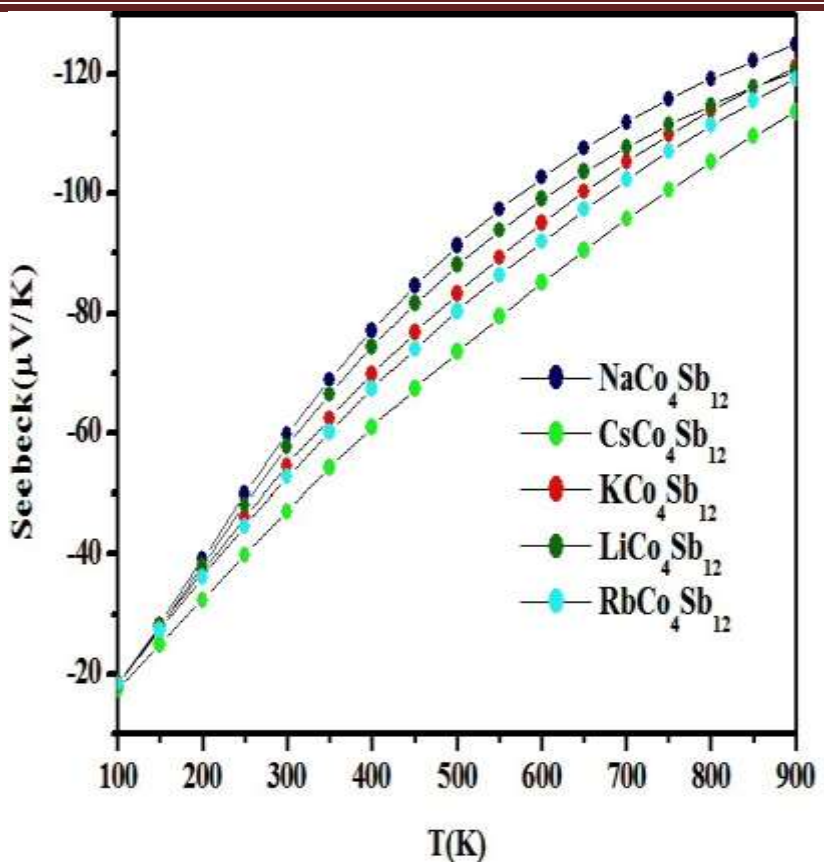

Fig. IV.6: The temperature dependence of the seebeck coefficient values for the alkali metals fully filled skutterudites (Na, Cs, K, Li and Rb).

IV.2.3.1.b. Electrical conductivity (σ)

Fig. IV.7 and Fig. IV.8 show the temperature dependence of the electrical conductivities over relaxation time $\left(\frac{\sigma}{\tau}\right)$ for the partially filled skutterudite $R_yCo_4Sb_{12}$ (R= Yb, Na and Ba with $x \leq 0.5$) and the alkali metals fully filled skutterudites, respectively.

From these Figs.; we notice that the electrical conductivities over relaxation time $\left(\frac{\sigma}{\tau}\right)$ of our investigated compounds increased with increasing temperature. This means that the filler atoms have an influence on the reduction of the electrical resistivities.

One can observe also from Fig. IV.7, the electrical conductivities decrease with decreasing filling fraction, and thus are in concord with the increase of the absolute Seebeck coefficient values (Fig. IV.5).

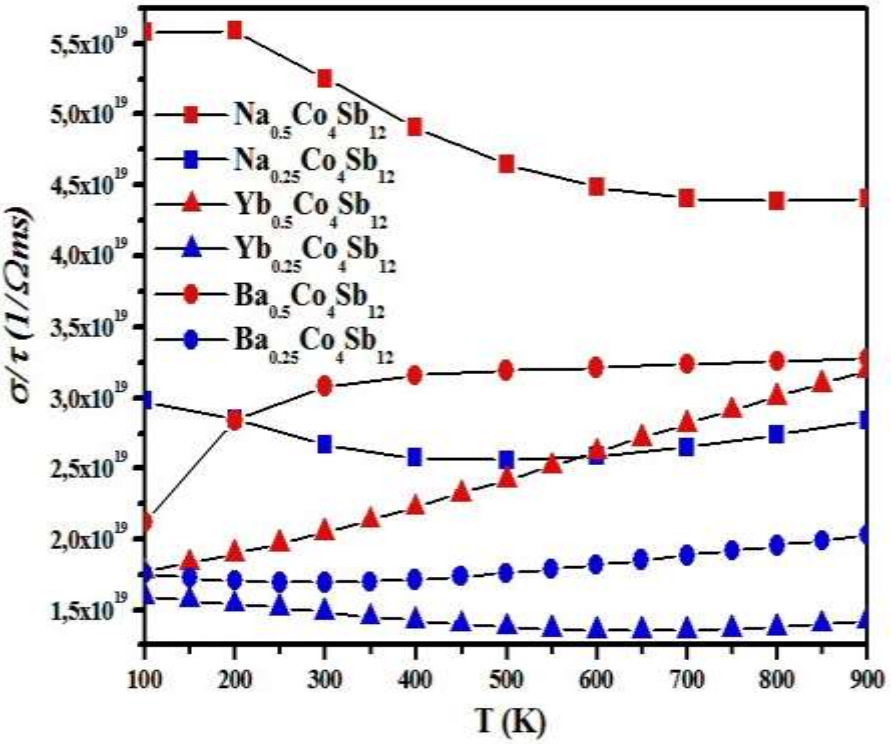

Fig. IV.7: The temperature dependence of the electrical conductivities over relaxation time $\left(\frac{\sigma}{\tau}\right)$ for the partially filled skutterudites $R_yCo_4Sb_{12}$ (R= Yb, Na and Ba with $x \leq 0.5$).

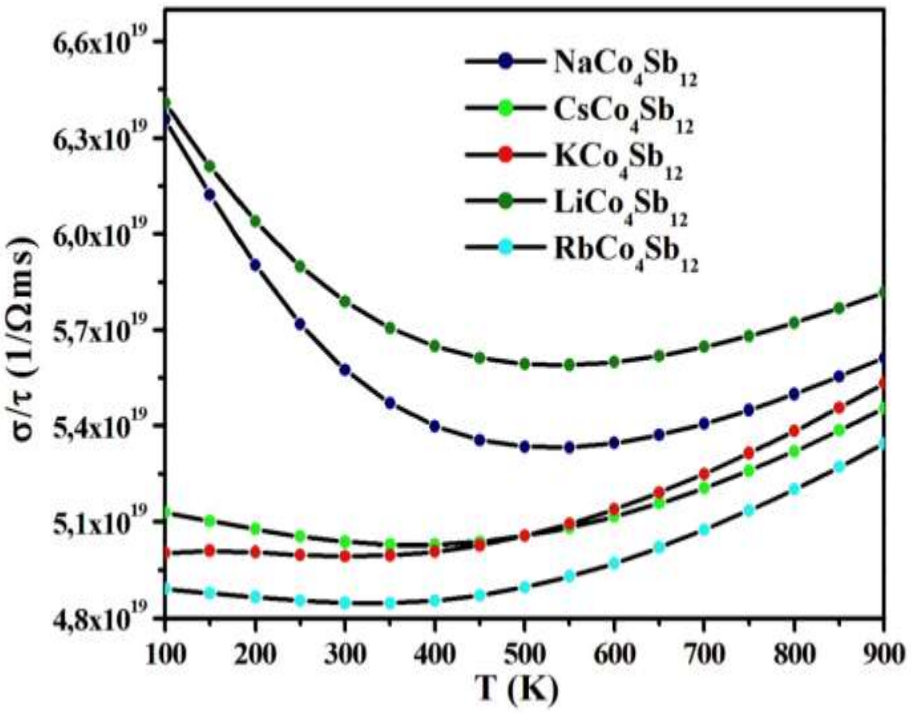

Fig. IV.8: The temperature dependence of the electrical conductivities over relaxation time $\left(\frac{\sigma}{\tau}\right)$ for the alkali metals fully filled skutterudites (Na, Cs, K, Li and Rb).

IV.2.3.1.c. Power factor (PF)

Fig. IV.9 and Fig. IV.10 show the temperature dependence of the power factor by relaxation time $\left(\frac{PF}{\tau}\right)$ for the partially filled skutterudite $R_yCo_4Sb_{12}$ (R= Yb, Na and Ba and$x <$ 0.5) and the alkali metals fully filled skutterudites, respectively.

The power factor is defined as a composed effect of thermo power and electrical conductivity. As shown in Fig. IV.9, the maximum power factor is reached when 0.5 electrons per unit cell are introduced into the conduction band, given the two free electrons (+2 charge state). In further terms, In Ba filled $CoSb_3$; the maximum power factor is achieved for $Ba_{0.25}Co_4Sb_{12}$ at high temperatures.

Detailed inspection proves that the rule of ‘‘0.5 electrons per unit cell’’ is valid for all our selected filled skutterudites.

This rule is further validated by many experimental results in various filled $CoSb_3$ skutterudites and Te-doped unfilled $CoSb_3$ [21–23]. Based on these results, we consider that (0.5 electrons per unit cell) is the optimized doping level for achieving optimal electrical transport performance for *n*-type $CoSb_3$ skutterudites.

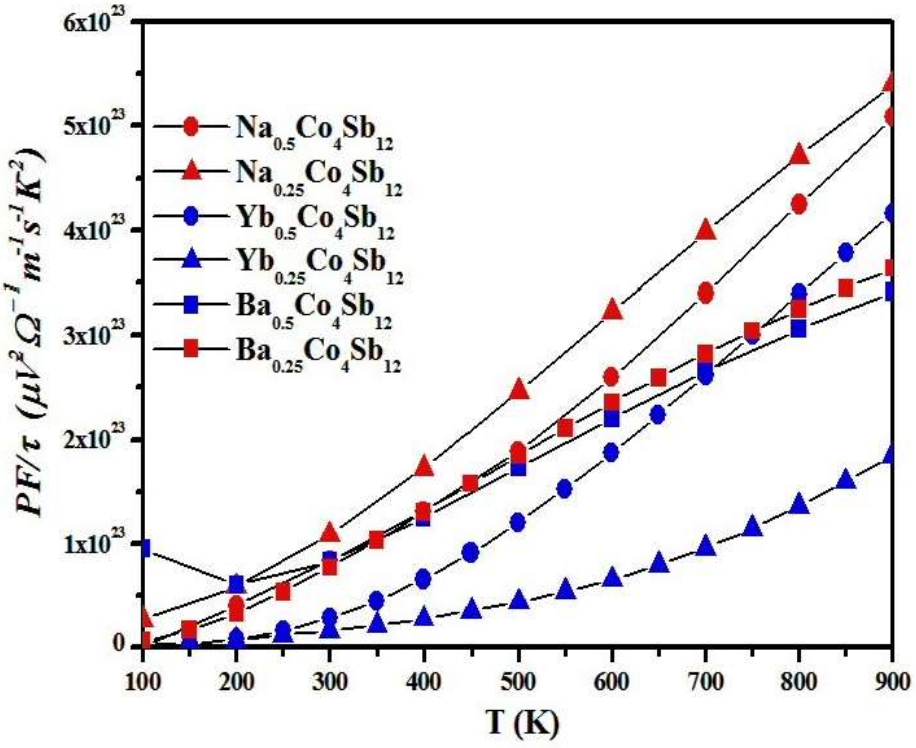

Fig. IV.9: The temperature dependence of the power factor by relaxation time $\left(\frac{PF}{\tau}\right)$ for the partially filled skutterudite $R_yCo_4Sb_{12}$ (R= Yb, Na and Ba with $x \leq 0.5$).

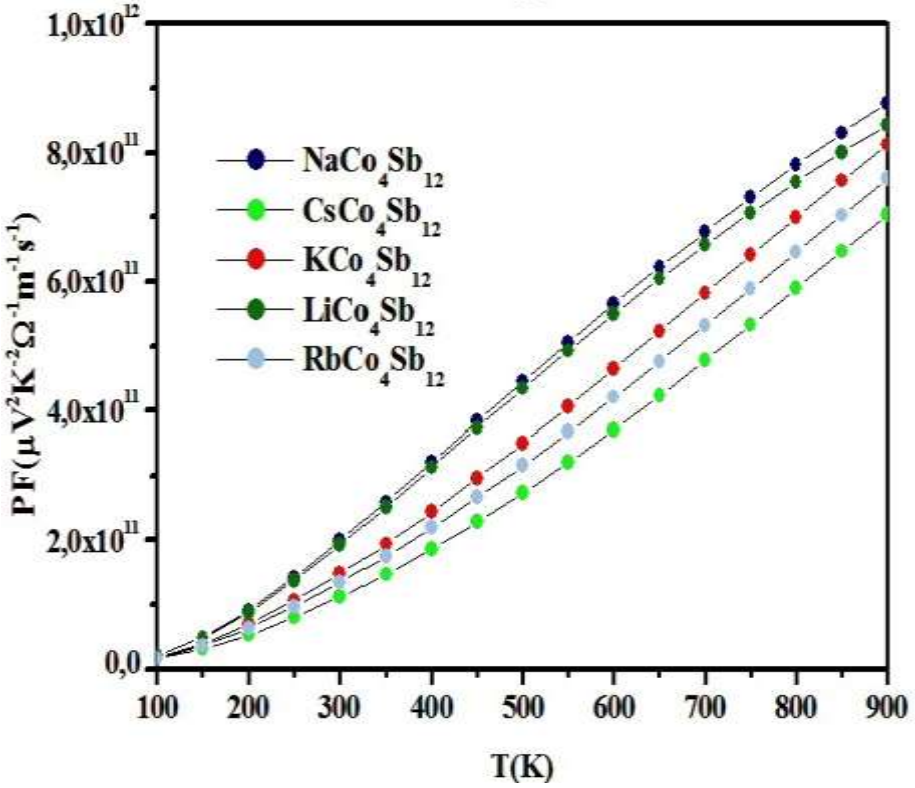

Fig. IV.10: The temperature dependence of the power factor by relaxation time $\left(\frac{PF}{\tau}\right)$ for the alkali metals fully filled skutterudites (Na, Cs, K, Li and Rb).

IV.2.3.2. Electronic thermal transport properties

The variation of the calculated electronic thermal conductivity over relaxation time $\left(\frac{\kappa_e}{\tau}\right)$ values for the partially filled skutterudites $R_yCo_4Sb_{12}$ (with $x \leq 0.5$) and the alkali metals fully filled skutterudites as a function of temperature are shown in Figs. IV(11)-(12), respectively.

It should be noted that the calculated electronic thermal conductivity over relaxation time $\left(\frac{\kappa_e}{\tau}\right)$ values for the partially filled skutterudites $R_yCo_4Sb_{12}$ (with $x \leq 0.5$) and the alkali metals fully filled skutterudites are lower than those reported with other compositions.

The ultimate cause of the decrease in the electronic thermal conductivity over relaxation time $\left(\frac{\kappa_e}{\tau}\right)$ for these compounds is due to a sensitive interaction between the electropositive filler atoms and the host lattice.

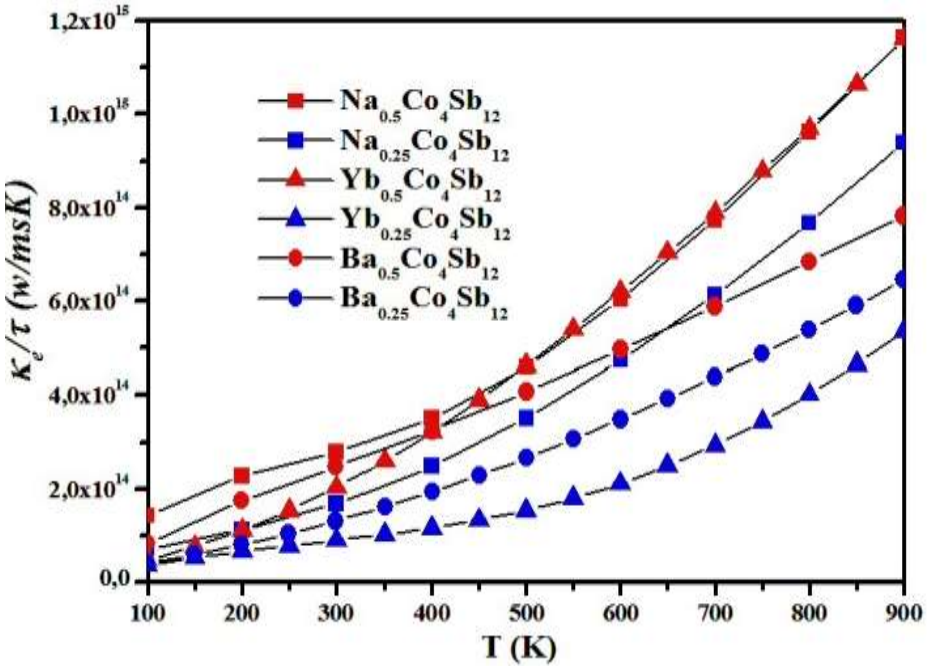

Fig. IV.11: The temperature dependence of the electronic thermal conductivities by relaxation time $\left(\frac{PF}{\tau}\right)$ for the partially filled skutterudite $R_yCo_4Sb_{12}$ (R= Yb, Na and Ba with $x \leq 0.5$).

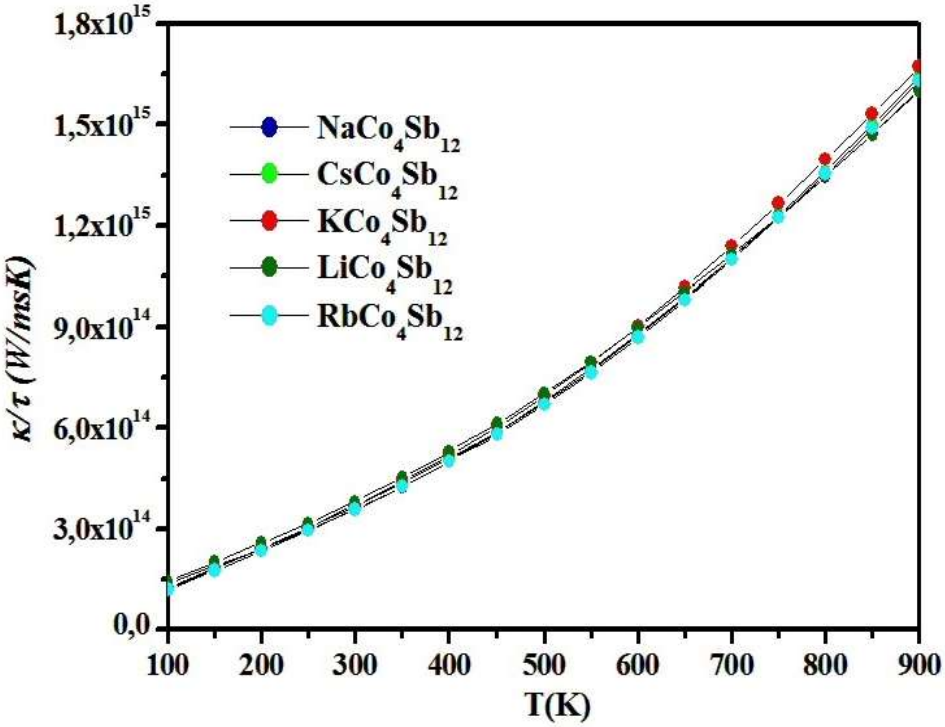

Fig. IV.12: The temperature dependence of the electronic thermal conductivities by relaxation time $\left(\frac{PF}{\tau}\right)$ for the alkali metals fully filled skutterudites (Na, Cs, K, Li and Rb).

IV.2.3.3. Dimensionless electronic merit factor (ZT_e)

The variation of the electronic figure of merit values (ZT_e) for the partially filled skutterudites $R_yCo_4Sb_{12}$ (with $x \leq 0.5$) and the alkali metals fully filled skutterudites as a function of temperature are shown in Figs. IV(13)-(14), respectively.

According to Fig. IV.13, the highest values of the electronic figure of merit ZT_e reached when the filling ratio is equal to y= 0.25, where the $Na_{0.25}Co_4Sb_{12}$ and $Ba_{0.25}Co_4Sb_{12}$ attained roughly the same maxima.

As shown in Fig. IV.14, the Na fully filled Co_4Sb_{12} based skutterudite ($NaCo_4Sb_{12}$) reaches the highest values of the electronic figure of merit ZT_e among the alkali metals fully filled Co_4Sb_{12} based skutterudites.

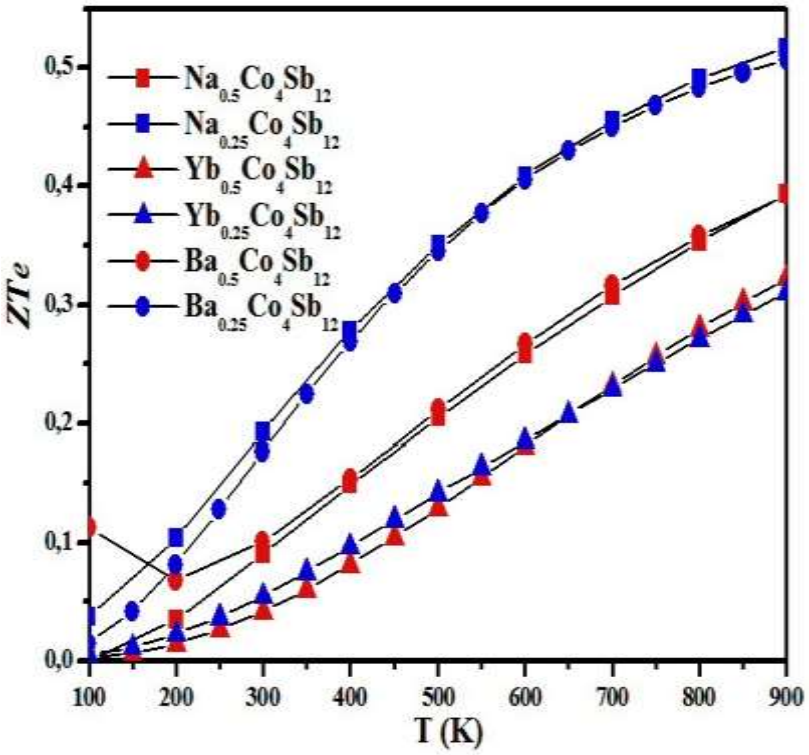

Fig. IV.13: The temperature dependence of the electronic figure of merit ZT_e for the partially filled skutterudite $R_yCo_4Sb_{12}$ (R= Yb, Na and Ba with $x \leq 0.5$).

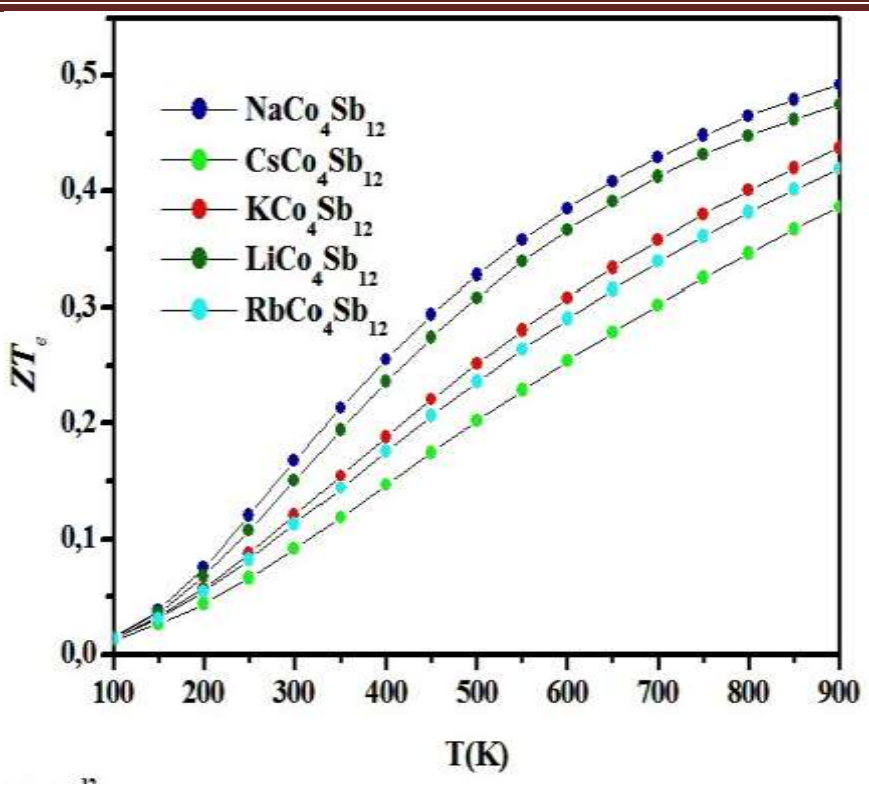

Fig. IV.14: The temperature dependence of the electronic figure of merit ZT_e for the alkali metals fully filled skutterudites (Na, Cs, K, Li and Rb).

IV.3. *P*-type filled $CoSb_3$-based skutterudites ($BrCo_4Sb_{12}$)

Recently, the findings of electronegative filling in CoSb3-based skutterudites provide a new perspective for guest-filling in skutterudites materials [25,26]. For this reason, in this section we spotlight on the study of structural, electronic properties and thermoelectric performance of Bromine fully filled $CoSb_3$ based skutterudite ($BrCo_4Sb_{12}$) compound.

IV.3.1. Structural properties

Table IV.2 summarizes the calculated equilibrium lattice parameter a_0, bulk modulus and its derivative for Bromine fully filled $CoSb_3$ skutterudite ($BrCo_4Sb_{12}$) compound.

The calculated lattice constant a_0 for the bcc primitive cell of Bromine fully filled $CoSb_3$ skutterudite ($BrCo_4Sb_{12}$) compound was optimized to be 9.047°A, as shown in table IV.2. This result is in good agreement with the experiment data [26] and it is in reasonable agreement compared with other filled skutterudites [10-12]. However, no theoretical information's are available for the comparison.

Table IV.2: Structural properties of bromine fully filled $CoSb_3$ based skutterudite ($BrCo_4Sb_{12}$) compound.

$BrCo_4Sb_{12}$	a_0 (Å)	B (GPa)	B'
Present work	9.047	9.044	5.09
Exp.	9.044[26]	–	–

IV.3.2. Electronic properties

The optimized crystal structure of $BrCo_4Sb_{12}$ compound was subjected to static band structure calculation with the GGA-PBE functional. The electronic properties, such as the electronic band structure and the electronic density of states of Bromine fully filled Co_4Sb_{12} skutterudite ($BrCo_4Sb_{12}$) are presented in Figs. IV(15) and (16), respectively.

As shown in Figs. IV(15) and (16), the electronic band structure and the electronic DOS of $BrCo_4Sb_{12}$ bear a large degree of similarity to the electronic structure of its parent structure (Co_4Sb_{12}) with the exception of the shifted down of the Fermi energy; therefore, the compound becomes a heavily doped *p*-type degenerate semiconductor.

IV.3.2.a. Electronic band structure

According to the obtain results in Fig. IV.15, the main effect observed for the electronic band structure for the electronegative Bromine fully filled Co_4Sb_{12} based skutterudites around the Fermi levels (zero energy points) is the slight increase of the pseudo direct band gap which is induced by the extra free electrons donated from the Bromine filler atom to the host matrix of $CoSb_3$. This observation signifies that the bands of the parent structure are rigid, allowing the quasi-Dirac band to survive the Br filling atoms and consequently give rise to *p*-type degenerated semiconductor behavior.

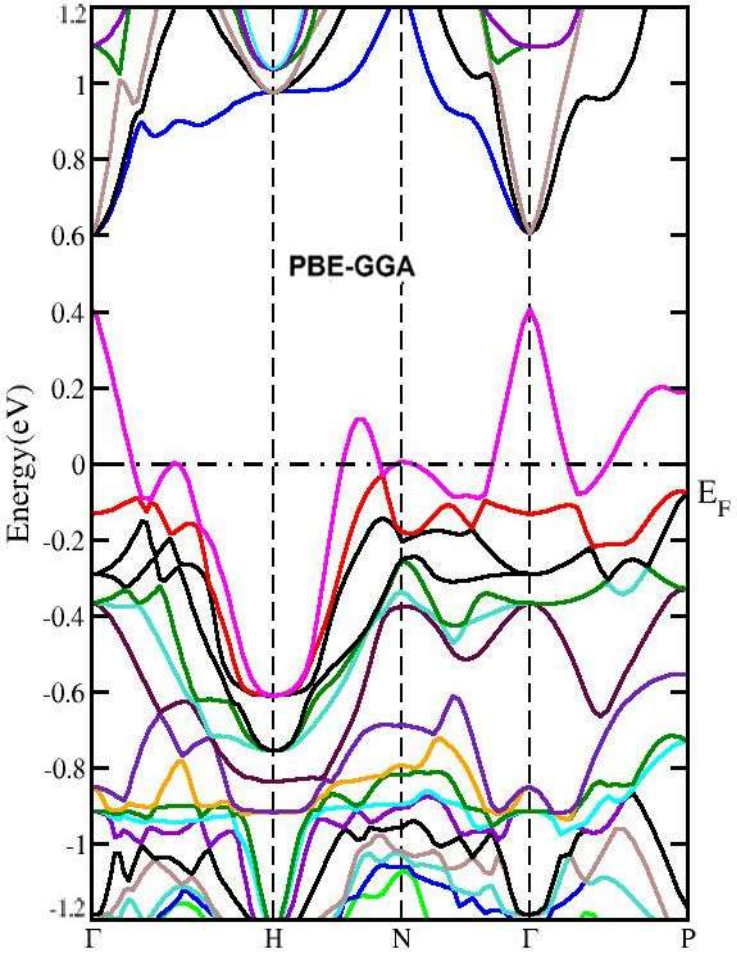

Fig. IV.15: The electronic band structure for *p*-type Br fully filled skutterudite ($BrCo_4Sb_{12}$).

IV.3.2.a. Electronic density of state (DOS)

The total and partial projected electronic densities of states of each atom (TDOSs and PDOSs) for Br fully filled skutterudite ($BrCo_4Sb_{12}$) are shown in Fig. IV.21. It is important to note that each orbital of each ion had been projected separately in order to find the total contribution attributed from each ion.

From Fig. IV.21**,** we can remark that there are two separated ranges in the total electronic densities of states. Following this Fig., the d-states of Co and p-states of Br ions provide the main contribution to the valence bands above the Fermi level with about a similar magnitude, whereas a negligible contribution for the Sb orbitals is established in this region. In the other hand, the conduction band is generally shaped by the d-states of Cobalt (Co) atom mixed with p-states for the both Sb and Br ions. To our knowledge, there are not results to compare them.

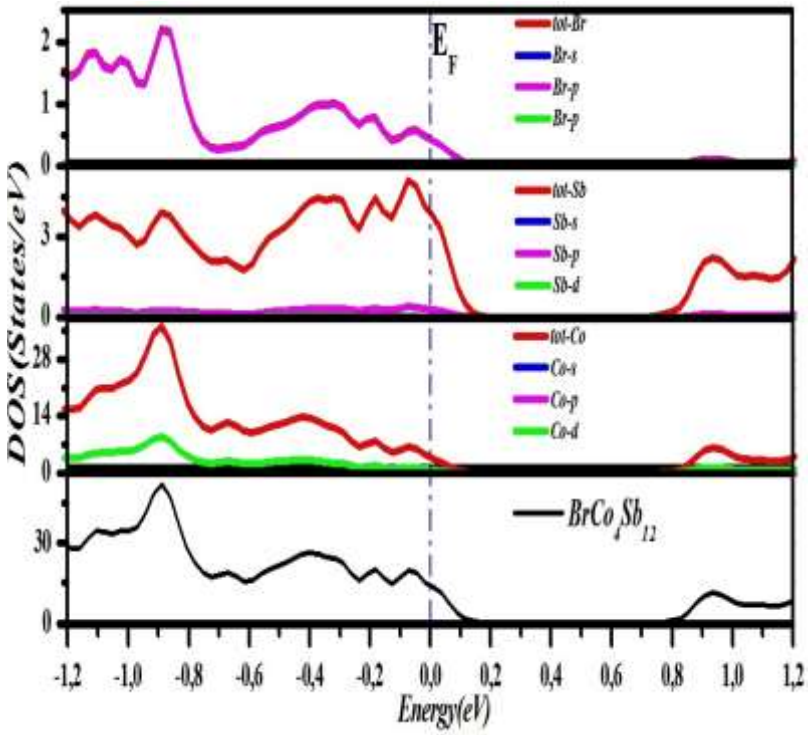

Fig. IV.16: The electronic density of states for p-type Br fully filled skutterudite ($BrCo_4Sb_{12}$).

IV.3.3. Thermoelectric properties

Fig. IV.17 shows the temperature dependence of the thermoelectric properties for *p*-type Bromine fully filled skutterudite compound ($BrCo_4Sb_{12}$).

We have calculated the Seebeck coefficient or thermo power (S) for Bromine fully filled skutterudite ($BrCo_4Sb_{12}$) as a function of temperature at a certain value of chemical potential ($\mu = E_F$) as shown in Fig. IV.17(a). The positive values obtained for the Seebeck coefficient along the temperature range suggests that the holes are extremely dominant charge carriers in this investigated compound, confirming the presence of the *p*-type conduction; this result is in concurrence with the experiment results obtained by Ortiz et *al.* [26].

Moreover, we notice that the variation in the Seebeck coefficient with temperature exhibited an increasing trend from a very low value to$\sim 90\ \mu V/K$, as shown in this Fig.

The temperature dependence of the electrical conductivities over relaxation time $\left(\frac{\sigma}{\tau}\right)$ for Bromine fully filled skutterudite ($BrCo_4Sb_{12}$) compound is shown in Fig. IV.17(b). The electrical conductivity over relaxation time $\left(\frac{\sigma}{\tau}\right)$ for studied compound shrinks totally with increasing temperature. This foundation is an indicative character of degenerate semiconductor material. Also, we observe a tendency of decline slow down at higher temperature. Which is an anomaly finding for semiconductors characteristic.

The temperature dependence of the electronic thermal conductivity over relaxation time $\left(\frac{\kappa_e}{\tau}\right)$ values for the *p*-type Bromine fully filled skutterudite ($BrCo_4Sb_{12}$) is shown in Fig. IV.17(c). The figure shows that the electronic thermal conductivity over relaxation time $\left(\frac{\kappa_e}{\tau}\right)$values increase with the increasing temperature.

In Fig. IV.17(d), we present the electronic figure of merit as a function of the temperature (T) for *p*-type Bromine fully filled skutterudite ($BrCo_4Sb_{12}$). The value of temperature at which the electronic figure of merit achieves the maximum is about $T = 900\,K$ which corresponds to the maximum temperature. Thermoelectric materials must withstand high temperatures because there may be a possibility of cracking due to thermal fatigue and thermal stress.

However, no data are available regarding thermal fatigue damage for thermoelectric materials. Therefore, our compound considered in this study has adequate ZT_e at high temperature, thereby making them resistant to thermal fatigue and thermal stress and consequently suitable material for use in thermoelectric devices.

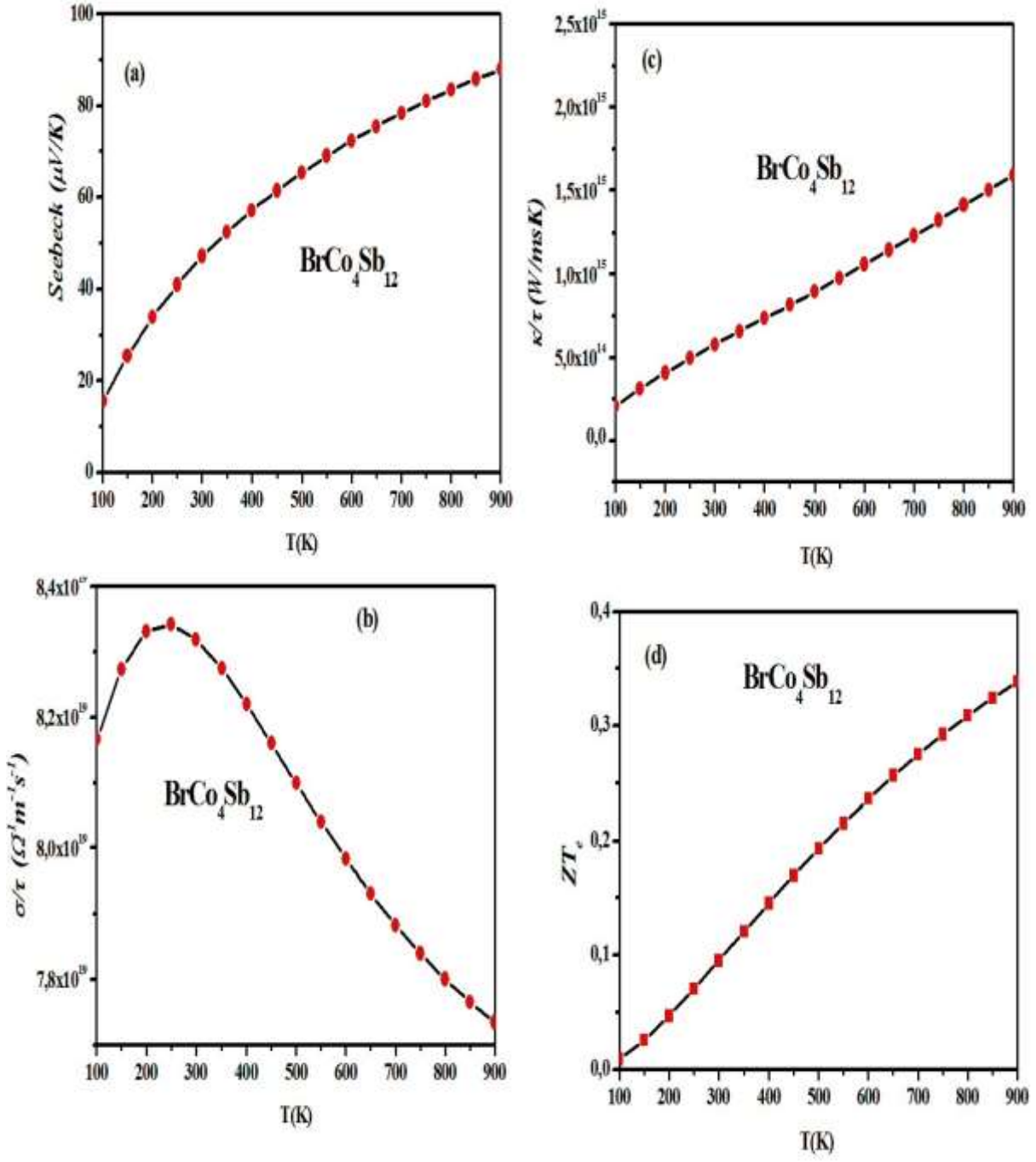

Fig. IV.17: Thermoelectric properties of bromine fully filled skutterudites ($BrCo_4Sb_{12}$) compound as function of temperature (T).

In comparison with *n*-type filler elements, *p*-type Bromine fully filled skutterudite ($BrCo_4Sb_{12}$) compound has lower peak ZT_e value than their *n*-type counterparts (see Figs. IV(13)(14)). This difference can largely be viewed in terms of electronic transport; modifications to the valence band dispersion and charge carrier scattering thus represent critical opportunities that have begun to be explored.

Bibliography

[1] W. Jeitschko and D. Braun.J. Acta Crystallographica Section B, 33(11) 3401 (1977).

[2] G. A. Slack, CRC Handbook of Thermoelectrics. 407 (CRC Press, 1995).

[3] X. Shi, W. Zhang, L. D. Chen, and J. Yang. J. Phys. Rev. Lett., 95(18), 185503 (2005).

[4] H.J. Goldsmid, Electronic Refrigeration, Pion Limited, London (1986).

[5] A.F. Ioffe, Semiconductor Thermoelements and Thermoelectric Cooling, Info search, London (1957).

[6] D. Kim, K. Kurosaki, Y. Ohishi, H. Muta, and S. Yamanaka, J. APL Materials 1, 032115 (2013).

[7] Yb in Yb-CoSb3 Skutterudite and its Effect on Preparation, Optimization and Life time of Thermoelectrics" J. Materiomics 1, 75 (2015).

[8] S. Wang, J.R Salvador, J. Yang, P. Wei, B. Duan and J. Yang, NPG Asia Materials, 8, 285 (2016).

[9] J. Yang, L. Xi, W. Zhang, L.D. Chen, and J. Yang, J. Electr. Mater, 38, 7 (2009).

[10] J. W. G. Bos, R. J. Cava, J. Solid State Commun. 141 38 (2007).

[11] F. Laufek, J. Návrátil, V. Goliáš, Powder Diffr. 23 15 (2008).

[12] P. Vaqueiro, G. G. Sobany, M. Stindl, J. Solid State Chem. 181 768 (2008).

[13] F. Laufek, J. Návrátil, J. Plášil, T. Plecháček, Č. Drašar, J. Alloys Compd. 479, 102 (2009).

[14] P. Vaqueiro, G. G. Sobany, A. V. Powell, Dalton Trans. 39, 1020 (2010).

[15] J. Yang, G.P. Meisner, W. Chen, J.S. Dyck, C. Uher, in: Proceedings ICT2001. 20th International Conference on Thermoelectrics, 73, (2001).

[16] G.K.H. Madsen, D. Singh, Comput. Phys. Commun. 175, 67 (2006).

[17] L. Deng, J. Ni, L.B. Wang, X.P. Jia, J.M. Qin, B.W. Liu, J. Alloy. Comp. 10, 1016 (2017).

[18] H. Luo, J.W. Krizan, L. Muechler, N. Haldolaarachchige, T. Klimczuk, W. Xie, M.K. Fuccillo, C. Felser and R.J. Cava, J. Nat. Comms, 10, 1038 (2015).

[19] J. Yang, D.T. Morelli, G.P. Meisner, W. Chen, J.S. Dyck, and C. Uher, Phys. Rev. B 67, 165207 (2003).

[20] G.A. Lamberton Jr., S. Bhattacharya, R.T. Littleton IV,M.A. Kaeser, R.H. Tedstrom, T.M. Tritt, J. Yang, and G.S. Nolas, Appl. Phys. Lett. 80, 598 (2002).

[21] L.D. Chen, T. Kawahara, X.F. Tang, T. Goto, T. Hirai, J.S.Dyck, W. Chen, and C. Uher, J. Appl. Phys. 90, 1864 (2001).

[22] Y.Z. Pei, L.D. Chen, W. Zhang, X. Shi, S.Q. Bai, X.Y. Zhao, Z.G. Mei, and X.Y. Li, Appl. Phys. Lett. 89, 221107 (2006).

[23] X. Shi, H. Kong, C.-P. Li, C. Uher, J. Yang, J.R. Salvador, H. Wang, L. Chen, and W. Zhang, Appl. Phys. Lett. 92, 182101 (2008).

[24] J. Yang, L. Zhang, Y. Liu, J. Appl. Phys. 113, 113703 (2013).

[25] X. Li, , B. Xu, L. Zhang et al. J. Alloys Compd. 615, 177 (2014).

[26] B.R. Ortiz, C.M. Crawford, R.W. McKinney, P.A. Parillab and E.S. Toberer, J. Mater. Chem. A 10, 1039 (2016).

Chapter V

V.1. Introduction

Modifications to the $CoSb_3$ framework allow carrier concentration tuning alter the electronic structure and decrease the lattice thermal conductivity through phonon scattering. For this reason, understanding the outsider defects in pure $CoSb_3$ binary skutterudite compound considered as an important approach to understanding how the Fermi level varies.

Recent calculations have estimated defect populations from the internal formation energetic and the chemical potential of the elemental constituents [1]. The cobalt site in $CoSb_3$ binary skutterudite compound can be replace with equal fractions of iron (Fe) and nickel (Ni) [2,3]. Similar strategies have been adopted with the antimony through substitution with diverse levels of group 14 or group 16 elements [4]; when substituted in equal ratio, the carrier concentration is nominally unaffected.

V.2. Effect of substitution on the electronic properties and thermoelectric performance of $CoSb_3$-based Skutterudite compounds

V.2.a. Substituted elements at the Cobalt site

V.2.a.1. Structural properties

The lattice parameter and bulk modulus have been calculated by computing the total energy for different volumes and fitted to Murnaghan's equation of state [5]

$$P(V) = \frac{B_0}{B_0'}\left[\left[\frac{V}{V_0}\right]^{-B_0'} - 1\right] \qquad \text{V.1}$$

Where P is the hydrostatic pressure, V is the distorted volume, V_0 is the equilibrium volume and B_0 is isothermal bulk modulus, and B_0' is the derivative of isothermal bulk modulus with respect to hydrostatic pressure, defined at zero pressure. Figs. V(1)-(2) present the calculated total energies versus volumes for Fe substituted Co_4Sb_{12} based skutterudite $Co_{4-x}Fe_xSb_{12}$ ($x < 0.5$) compounds. The calculated lattice constants, bulk modulus, and its derivative are summarized in Table V.I.

Table V.1: the calculated structural parameters for $Co_{4-x}Fe_xSb_{12}$ ($x < 0.5$) compounds.

Compounds	a(Å)	B_0 (GPa)	B'
$Co_{3.875}Fe_{0.125}Sb_{12}$	9.135	86.840	4.66
$Co_{3.75}Fe_{0.25}Sb_{12}$	9.139	86.767	4.72

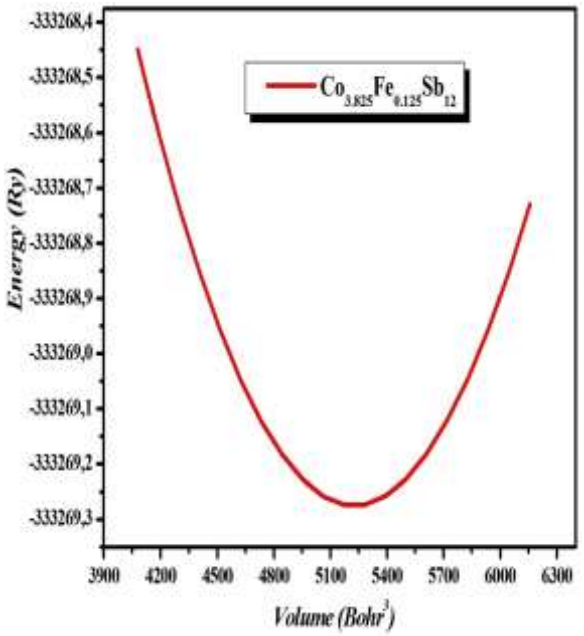

Fig. V.1: Energy versus volume curves for Fe doped $CoSb_3$ based Skutterudite compound ($Co_{3.825}Fe_{0.125}Sb_{12}$).

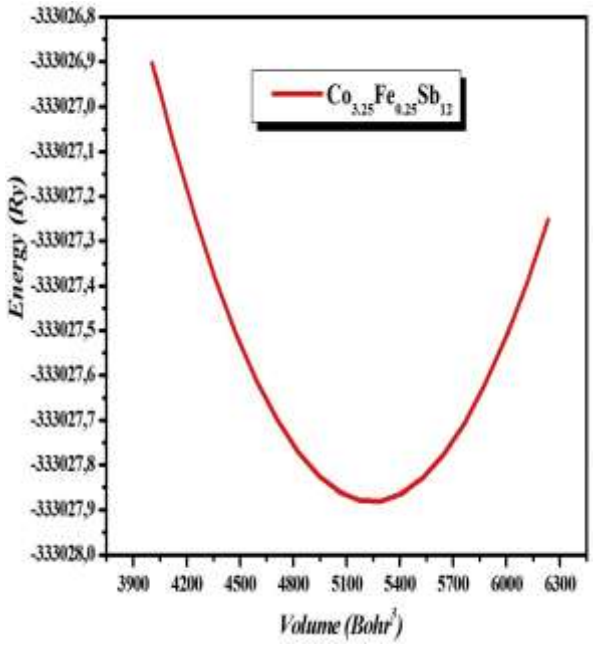

Fig. V.2: Energy versus volume curves for Fe doped $CoSb_3$ based Skutterudite compound ($Co_{3.25}Fe_{0.25}Sb_{12}$).

The calculated lattice constants of Fe substituted Co_4Sb_{12} based skutterudite $Co_{4-x}Fe_xSb_{12}$ $(x < 0.5)$ compounds at zero pressure are about 9.139 Å and 9.135 Å for $Co_{3.875}Fe_{0.125}Sb_{12}$ and $Co_{3.25}Fe_{0.25}Sb_{12}$ compounds, respectively. These values are close to the previous theoretical results and experiments data [6-9].

V.2.a.2. Electronic properties

The electronic band structure and the density of states are of the central interest in the study of the electronic properties of materials.

V.2.a.2.1. Electronic band structure

The results of the electronic band structures for Fe substituted Co_4Sb_{12} based skutterudite $Co_{4-x}Fe_xSb_{12}$ $(x < 0.5)$ are shown in Figs. V(3)-(4), respectively.

As shown in Figs. V(3) and (4), the most important significant modifications in the electronic band structures of $Co_{4-x}Fe_xSb_{12}$ $(x < 0.5)$ compounds are the shift of the two first valence states above the Fermi level, whereby a number of holes are introduced and consequently; generating an acceptor states.

The substitution of the Fe atoms at Co sites cause the Fermi level goes deeper in the valence bands and to shift it significantly as a result of the increase in the Fe concentration. Thus gives chance to heavily doped *p*-type degenerate semiconductor. Our calculated band structure for $Co_{3.75}Fe_{0.25}Sb_{12}$ compound is in concurrence with those reported by Bhardwaj et *al.* [8].

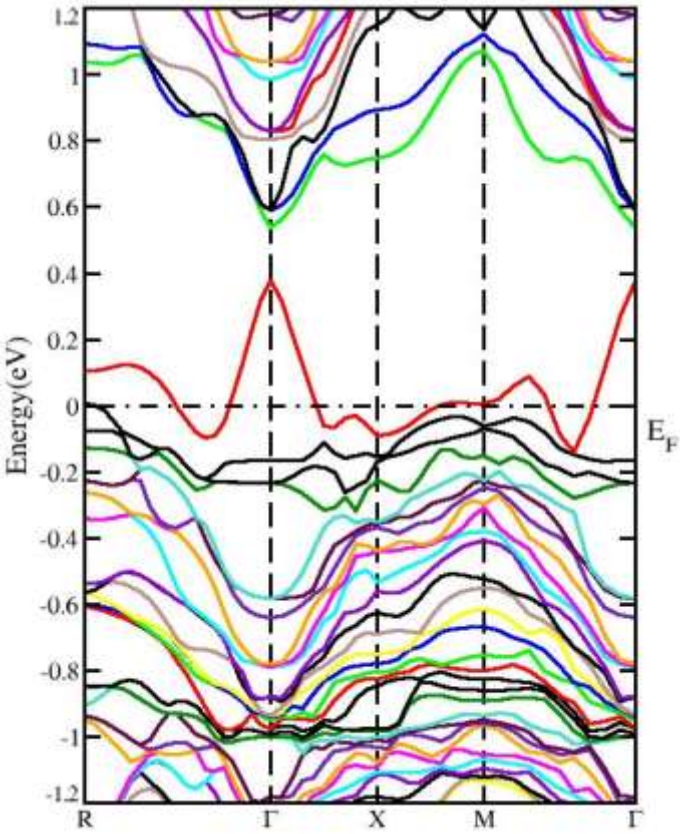

Fig. V.3: The electronic band structure for $Co_{3.875}Fe_{0.125}Sb_{12}$ compound.

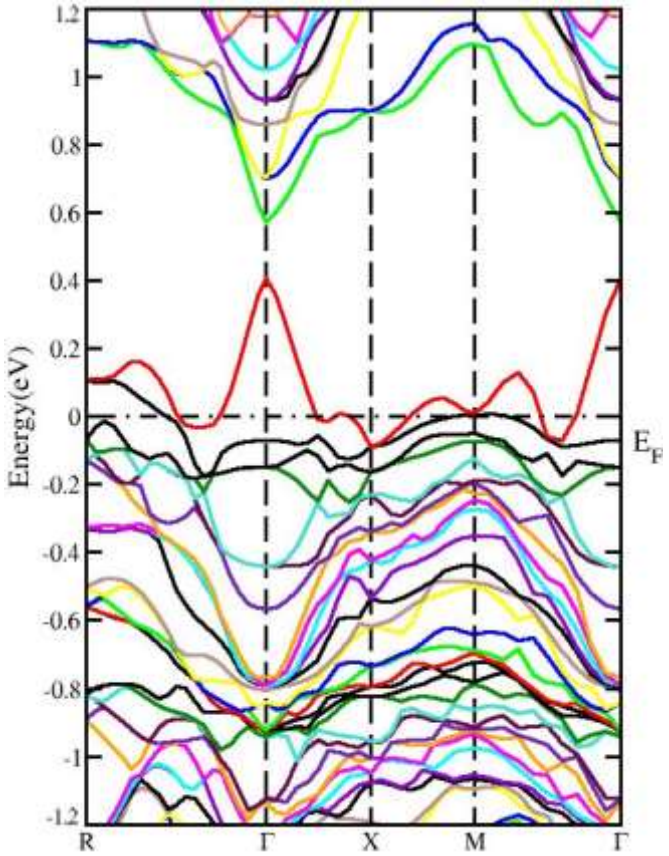

Fig. V.4: The electronic band structure for $Co_{3.75}Fe_{0.25}Sb_{12}$ compound.

V.2.a.2.2. Electronic density of states (DOS)

The total and partial projected electronic densities of states of each atom (TDOSs and PDOSs) for $Co_{3.875}Fe_{0.125}Sb_{12}$ and $Co_{3.75}Fe_{0.25}Sb_{12}$ compounds are shown in Figs. V(5) and (6), respectively. From these Figs.**,** we can observe that there are two separated ranges in the total electronic densities of states. Following the both Figs., we remark that the d-states of Cobalt (Co) and iron (Fe) ions provide the main contributions to the valence bands above to the Fermi level with roughly the similar magnitude, whereas a negligible contribution for the Sb orbitals is established. In the other hand, the conduction band is commonly formed by the p-states of Sb ions mixed with d-states of Co atom and its substituting iron atoms (Fe). Our obtained electronic density of states in Fig. V.6 is comparable to that found by Bhardwaj et *al.* [8].It can be found also that additional conduction bands hold contributions from the Sb-s orbitals.

In comparing with $CoSb_3$, the TDOS of $Co_{4-x}Fe_xSb_{12}$ $(x < 0.5)$ compounds near the Fermi energy reduce to about 28 and 34 electrons/eV for x= 0.125 and x= 0.25, respectively. This will be a restriction to further improve their electrical properties.

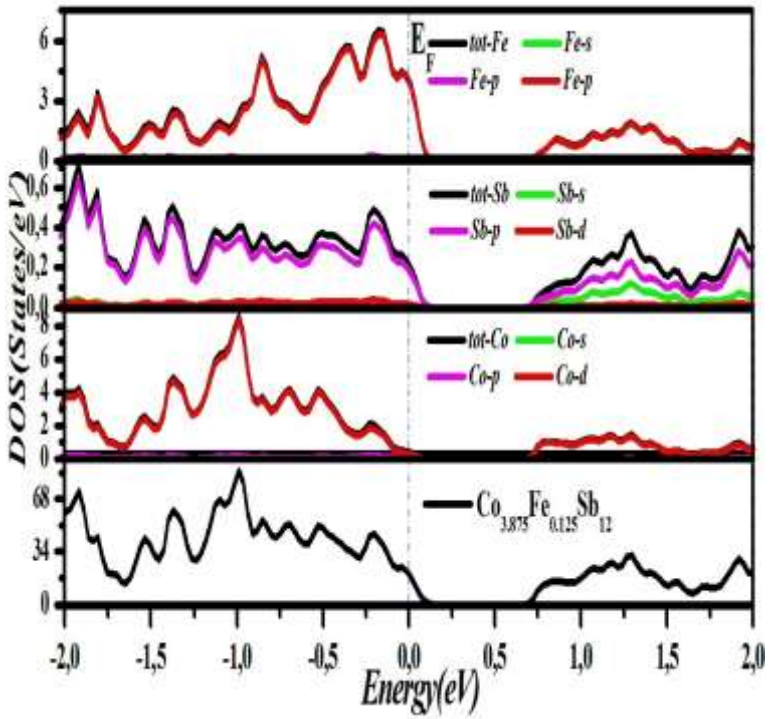

Fig. V.5: The electronic total and partial densities of states for $Co_{3.875}Fe_{0.125}Sb_{12}$ compound.

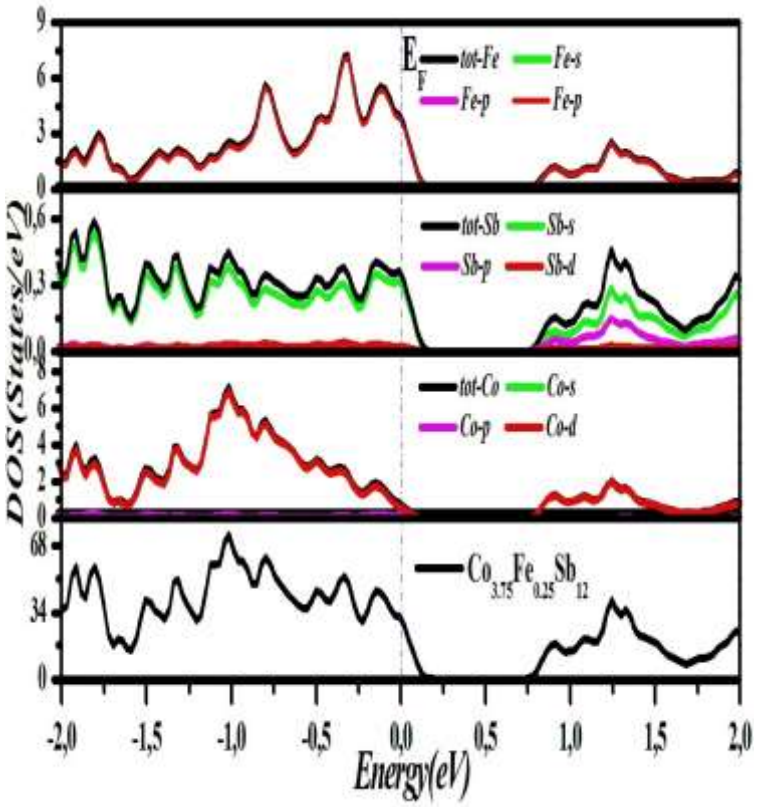

Fig. V.6: The electronic total and partial densities of states for $Co_{3.75}Fe_{0.25}Sb_{12}$ compound.

V.2.a.3. Thermoelectric transport properties

V.2.a.3.1. Seebeck coefficient (S)

The temperature dependence of the seebeck coefficient values of $Co_{4-x}Fe_xSb_{12}$ ($x < 0.5$) compounds are shown in Fig. V(7). The both compounds exhibit positive seebeck coefficient values, indicating that Fe substitution has generated an acceptor energy level. Thus is indicative of a *p*-type behavior.

One can notice also from this Fig. that at the same temperature the coefficient values for the both $Co_{3.875}Fe_{0.25}Sb_{12}$ and $Co_{3.25}Fe_{0.25}Sb_{12}$ compounds increase with decreasing Fe content, which could be explained in terms of the charge carrier.

The iron substituted $CoSb_3$ based skutterudite compounds shows worst Seebeck coefficient with values below 150µV/K up to temperature 900 K. The same conclusion can be drawn from the experimental finding [8].

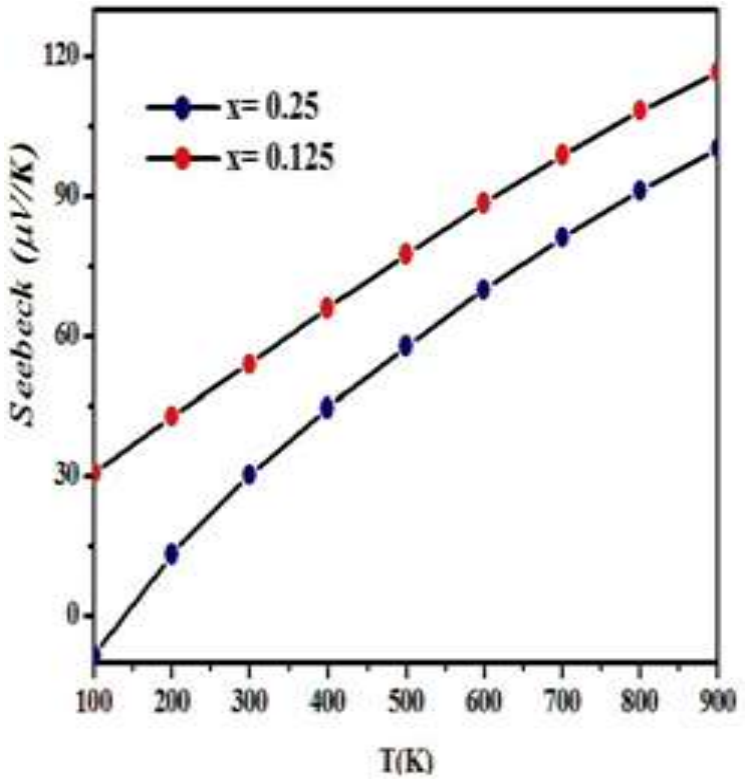

Fig. V.7: The temperature dependence of the seebeck coefficient values of $Co_{4-x}Fe_xSb_{12}$ $(x < 0.5)$ compounds.

V.2.a.3.2. Electrical conductivity (σ)

Fig. V.8 shows the calculated electrical conductivities over relaxation time $\left(\frac{\sigma}{\tau}\right)$ for $Co_{4-x}Fe_xSb_{12}$ $(x < 0.5)$ compounds at the temperature range $100\ K$ to$900\ K$.

At the same temperature the calculated electrical conductivities over relaxation time $\left(\frac{\sigma}{\tau}\right)$ for the both $Co_{3.875}Fe_{0.25}Sb_{12}$ and $Co_{3.25}Fe_{0.25}Sb_{12}$ compounds increase with increasing Fe content, which could be explained in terms of carrier concentration.

In general electrical conductivity increases with increasing carrier concentration, thereby the calculated $\left(\frac{\sigma}{\tau}\right)$ values increase with increasing Fe concentration.

Since Fe has one less valence electron than Co, the hole concentration increases with increasing Fe content.

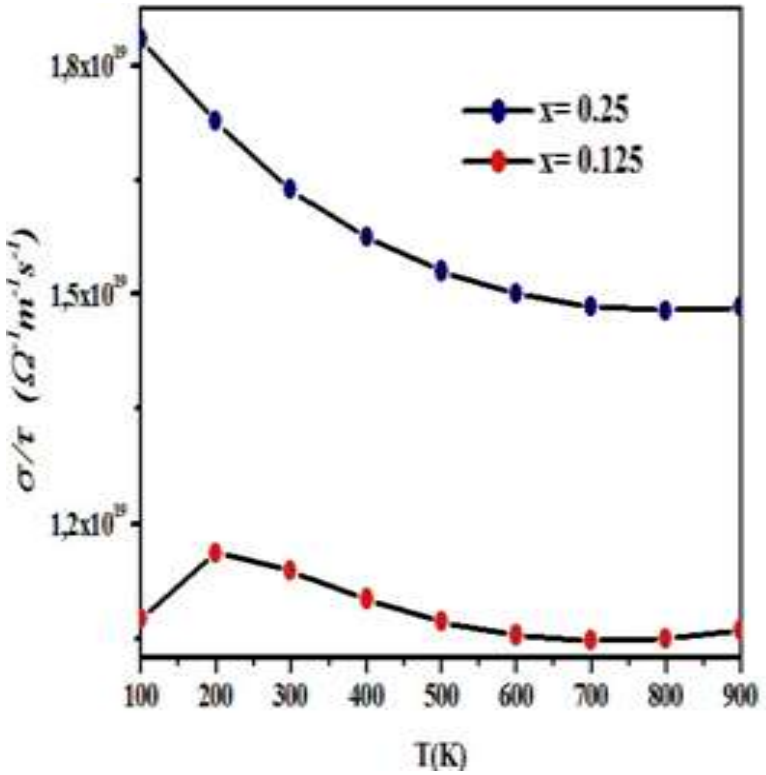

Fig. V.8: The calculated electrical conductivities over relaxation time $\left(\frac{\sigma}{\tau}\right)$ for $Co_{4-x}Fe_xSb_{12}$ ($x < 0.5$) compounds as function of temperature (T).

V.2.a.3.3. Electronic thermal conductivity (κ_e)

The variation of the calculated electronic thermal conductivities over relaxation time $\left(\frac{\kappa_e}{\tau}\right)$ values for $Co_{4-x}Fe_xSb_{12}$ (with $x < 0.5$) compounds as a function of temperature are shown in Fig. V(9).

It should be noted that the calculated electronic conductivities over relaxation time $\left(\frac{\kappa_e}{\tau}\right)$ values for $Co_{4-x}Fe_xSb_{12}$ (with $x < 0.5$) compounds are lower than those reported with similar composition due to the relatively low density. It could be seen also that $\left(\frac{\kappa_e}{\tau}\right)$ is almost independent on temperature and it increases a little with the augmentation of Fe substitution.

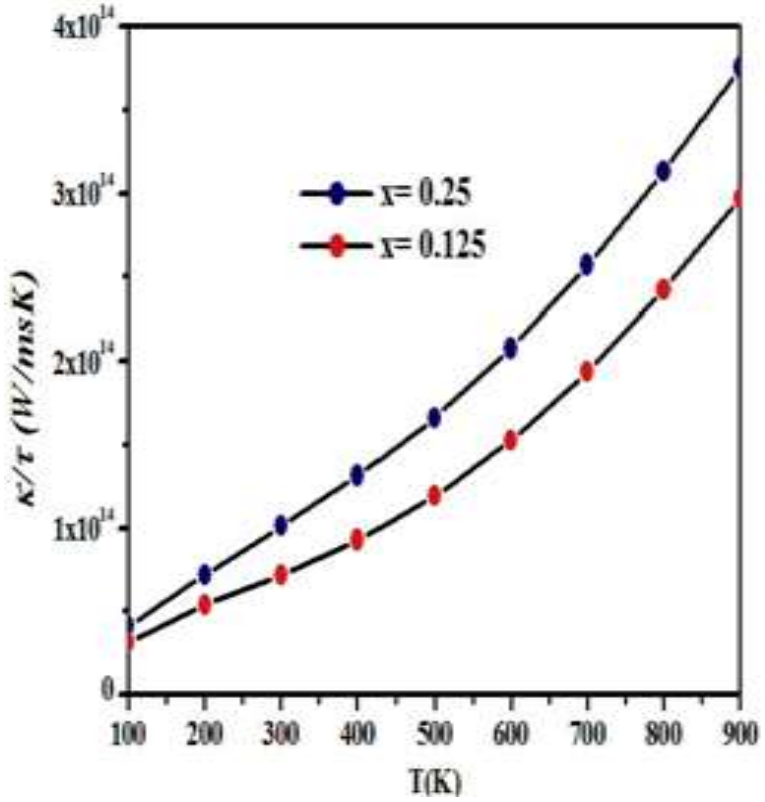

Fig. V.9: The variation of the calculated electronic thermal conductivities over relaxation time $\left(\frac{\kappa_e}{\tau}\right)$ values for $Co_{4-x}Fe_xSb_{12}$ (with $x < 0.5$) compounds as a function of temperature (T).

V.2.a.3.4. Electronic dimensionless figure of merit (ZT_e)

The electronic dimensionless figure of merit values (ZT_e) for $Co_{4-x}Fe_xSb_{12}$ (with $x <$ 0.5) compounds are shown in Fig. V10.

Fe substituted Co_4Sb_{12} based skutterudites makes the ZT_e values increase remarkably. One also can notice from this figure, that the ZT_e values of $Co_{3.75}Fe_{0.25}Sb_{12}$ compound are lower than that of $Co_{3.875}Fe_{0.125}Sb_{12}$ compound after temperature$T = 570\ K$.

Additionally, the temperatures corresponding to the maximal ZT_e values for the studied compounds shift to the elevated temperature. Among the investigated materials a maximal ZT_e value of 0.44 is obtained for $Co_{3.375}Fe_{0.125}Sb_{12}$ compound at temperature$T =$ $900\ K$. With is higher the values obtained by Tafti et al. for the same samples [10].

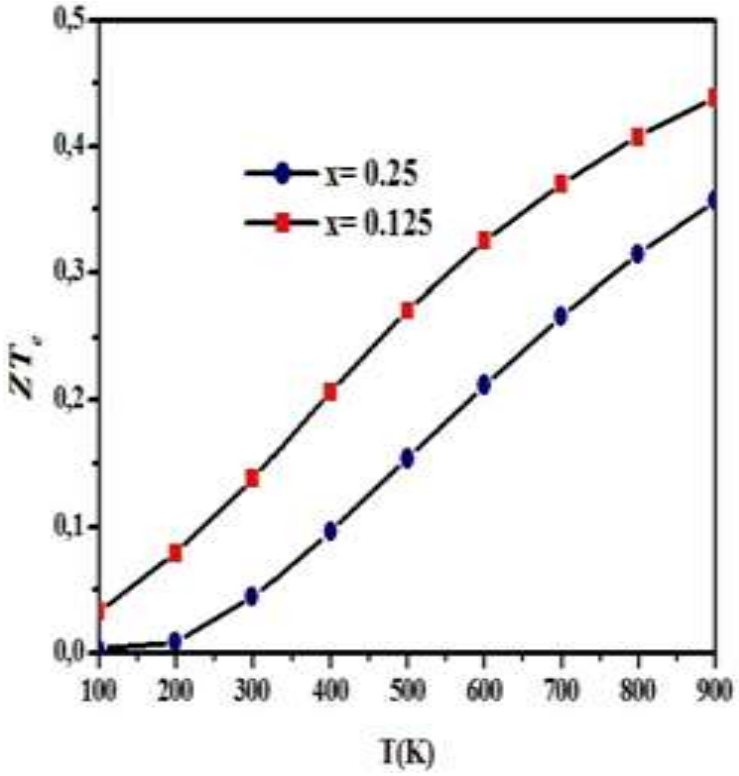

Fig. V.10: The calculated electronic dimensionless figure of merit values (ZT_e) for $Co_{4-x}Fe_xSb_{12}$ (with $x < 0.5$) compounds

V.2.b. Substituted elements at the antimony site (Sb)

V.2.b.1. *P*-type substituted element at the Sb site

V.2.b.1.1. Effect of Ge substitution on the electronic and thermoelectric transport properties of $CoSb_3$-based Skutterudite compound ($Co_4Sb_9Ge_3$)

First-principles calculations have been performed to investigate the structural, electronic properties and related transport properties of Ge doped Co_4Sb_{12} based skutterudite compound ($Co_4Sb_9Ge_3$).

V.2.b.1.1.a. Structural properties

The compound $Co_4Sb_9Ge_3$ obtained by substituting there of the 24 Sb atoms in the primitive bcc unit cell for three of Ge ions.

The equilibrium lattice parameter was calculated for Ge doped $CoSb_3$-based Skutterudite compound ($Co_4Sb_9Ge_3$) by determining the dependence of the total energy as a function of the volume the energy as a function of the volume of the primitive bcc unit cell of $CoSb_3$ as shown in Fig. V.11.

The obtained equilibrium parameters including lattice constant, bulk modulus B_0 (GPa) and its derivative B' as given in Eq. V.1 are regrouped in table V.2. To our knowledge there is not theoretical or experiments results for comparison.

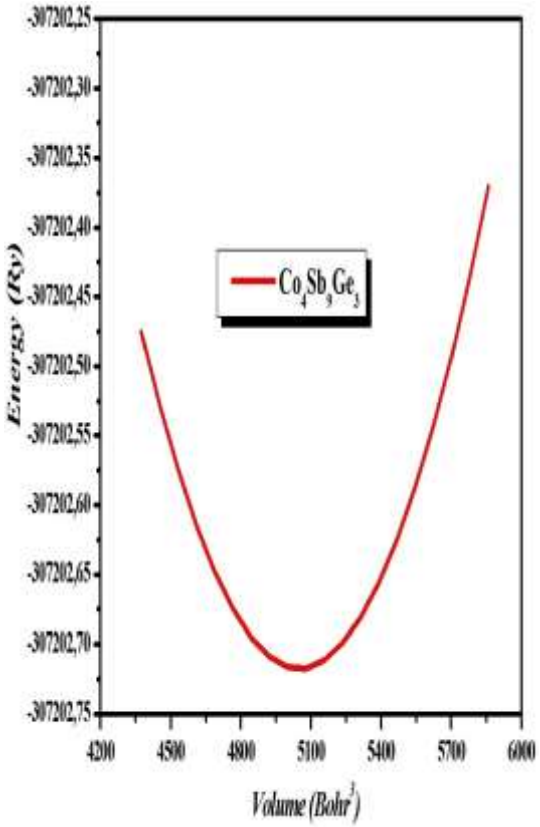

Fig. V.11: Energy versus volume curves for Ge doped $CoSb_3$-based Skutterudite compound ($Co_4Sb_9Ge_3$).

Table V.2: The calculated equilibrium parameters for Ge doped $CoSb_3$-based Skutterudite compound ($Co_4Sb_9Ge_3$).

$Co_4Sb_9Ge_3$	***Present work***
a(Å)	9.049
B_0 (GPa)	86.990
B'	5.078

V.2.b.1.1.b. Electronic properties

The relaxed structures were done using a denser grid of K-points (10×10×10) followed by the calculations of the band structure and the density of states (DOS).

V.2.b.1.1.b.1. Electronic band structure

The band structure was computed on the path Γ(0,0,0), H(0.5,0.5,0.5), N (0,0,0.5), Γ(0,0,0) and R (0.25,0.25,0.25). Fig. V.12 shows the electronic band structure at the vicinity of the Fermi level (zero energy point) for *p*-type Ge doped Co_4Sb_{12} skutterudite compound ($Co_4Sb_9Ge_3$).

One can observe from the electronic band structure in Fig. V.12 is the creation of new valence bands near the Fermi level. In addition, the Fermi level descends in the deep of the valence band, thus mainly due to the charge transfer from the Ge atoms towards $CoSb_3$ matrix and as a result the compound becomes a heavily doped *p*-type degenerate semiconductor. This is in accord with the results obtained by Velasco-Soto et *al*. [11] and comparable to those founded by Zhao et *al*. [12].

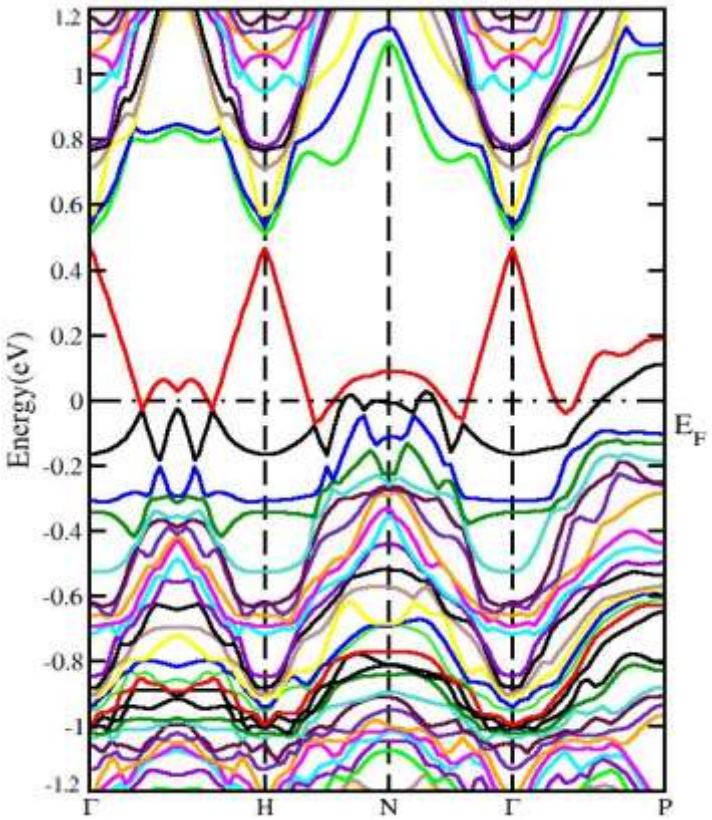

Fig. V.12: The electronic band structure for *p*-type Ge doped Co_4Sb_{12} skutterudite ($Co_4Sb_9Ge_3$)

V.2.b.1.1.b.2. Electronic density of states (DOS)

We present in Fig. V.13 the total and the partial projected electronic densities of states of each atom (TDOS and PDOS) for $Co_4Sb_9Ge_3$ compound were calculated by employing the GGA-PBE formalism.

According to the electronic density of states in this Fig., the valence band in *p*-type Ge doped Co_4Sb_{12} skutterudite ($Co_4Sb_9Ge_3$) compound is mainly formed by p orbitals of both Sb and Ge atoms with little admixture of Co-d orbitals. In contrast, the conduction band mainly comes from the Co-d orbitals, while a negligible contribution from the Ge orbitals is observed. The additional conduction bands come from contributions of both Sb-s and Sb-p orbitals.

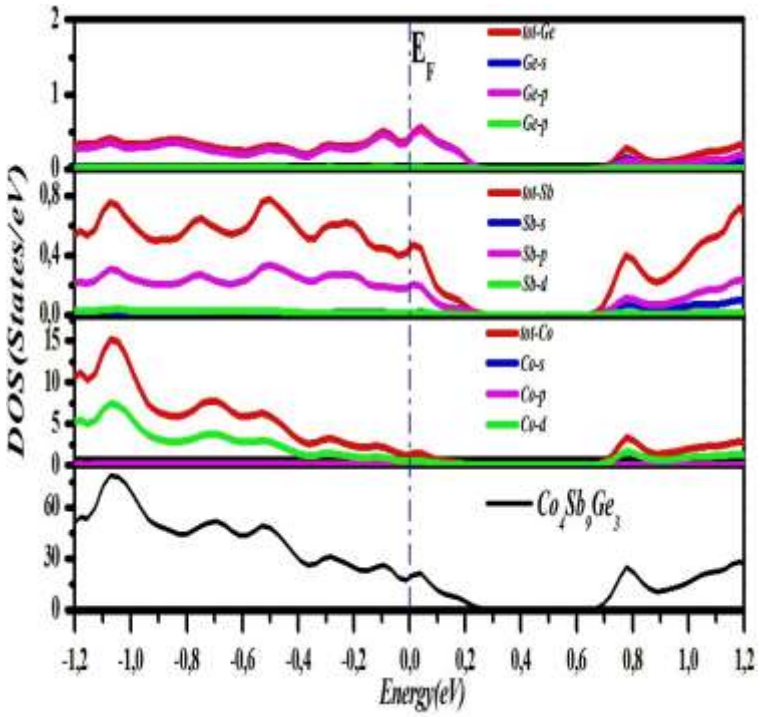

Fig. V.13: The electronic density of states for p-type Ge doped Co_4Sb_{12} skutterudite ($Co_4Sb_9Ge_3$) compound.

V.2.b.1.1.c. Thermoelectric properties

The corresponding intrinsic thermoelectric transport properties of Ge doped Co_4Sb_{12} skutterudite ($Co_4Sb_9Ge_3$) at different temperatures ranging from $100\,K$ to $900\,K$ were calculated to furnish deeper insights into the results of the Seebeck coefficient and the both electric and electronic thermal conductivities quantities.

The calculations are based on the optimized and relaxed structural parameters. Figs. V(14)-(17) display the temperature dependence of the calculated thermoelectric quantities of our investigated compound ($Co_4Sb_9Ge_3$).

V.2.b.1.1.c.1. Electrical and electronic thermal conductivities

Figs. V(14) and (15) show The temperature dependence of the calculated electrical and electronic thermal conductivities over relaxation time for Ge doped Co_4Sb_{12} skutterudite ($Co_4Sb_9Ge_3$) compound, respectively. From these Figs one can observe that with increasing temperature the both $\left(\frac{\kappa_e}{\tau}\right)$ and $\left(\frac{\sigma}{\tau}\right)$ quantities augment monotonically and reach their highest values at elevated temperature of about T= 900 K.

As results the calculated electrical and electronic thermal conductivities over relaxation time basically exhibit metallic behavior.

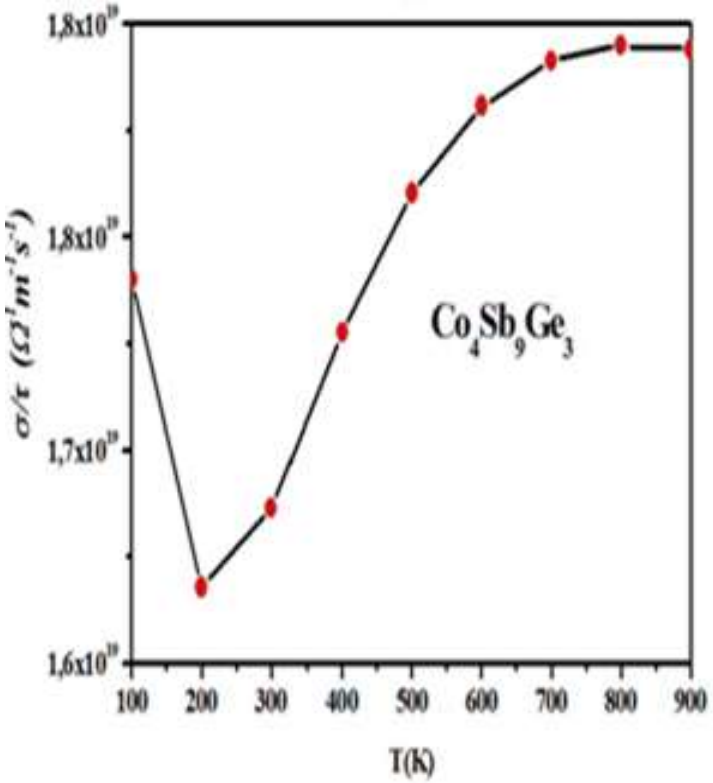

Fig. V.14: The temperature dependence of the calculated electrical conductivity over relaxation time for Ge doped Co_4Sb_{12}

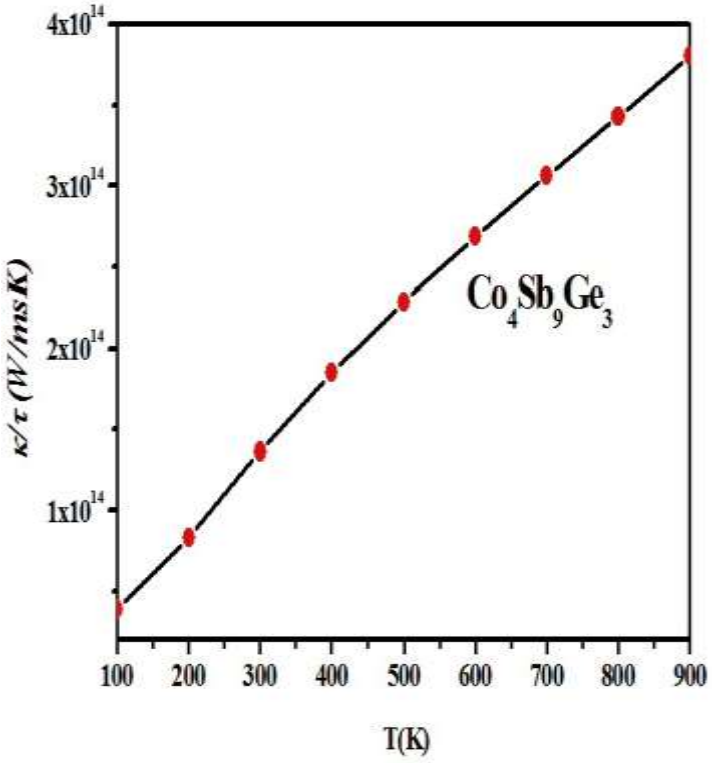

Fig. V.15: The temperature dependence of the calculated electronic thermal conductivity over relaxation time for Ge doped Co_4Sb_{12}

V.2.b.1.1.c.2. Seebeck coefficient and electronic dimensionless figure of merit

The temperature dependence of Seebeck coefficients for Ge doped Co_4Sb_{12} skutterudite ($Co_4Sb_9Ge_3$) compound is shown in Fig. V.16.

One can observe from this Fig., that the Ge doped Co_4Sb_{12} skutterudite ($Co_4Sb_9Ge_3$) compound is typical *p*-type transport behavior because it exhibits positive seebeck coefficient values. This result is in concurrence with those reported by Velasco-Soto [11].

According to the considered Seebeck coefficient, electrical and electronic thermal conductivities over relaxation time, the electronic dimensionless figure of merit ZT_e values are calculated and shown in Fig. V.17.

The ZT_e values of Ge doped Co_4Sb_{12} skutterudite ($Co_4Sb_9Ge_3$) compound increase with the increasing of temperature and the maximum value of about (0.27) is obtained at $T = 900\ K$.

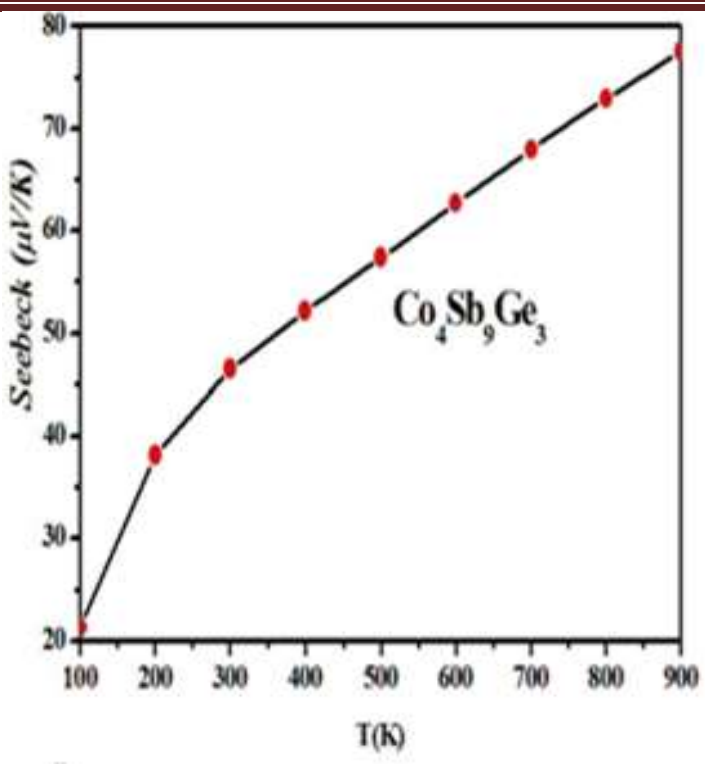

Fig. V.16: The temperature dependence of Seebeck coefficients for Ge doped Co_4Sb_{12} skutterudite ($Co_4Sb_9Ge_3$) compound.

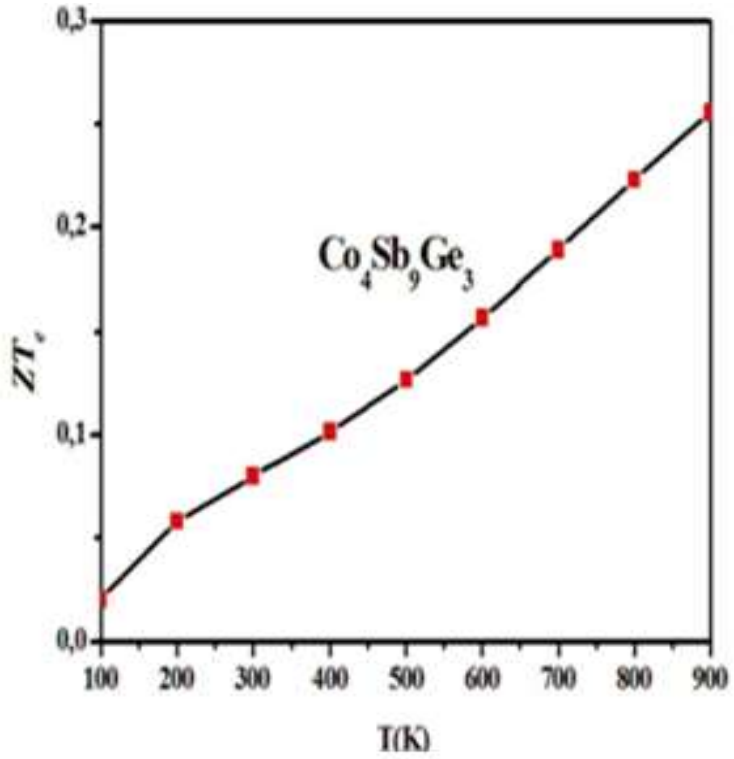

Fig. V.17: The temperature dependence of the electronic dimensionless figure of merit (ZT_e) for Ge doped Co_4Sb_{12} skutterudite ($Co_4Sb_9Ge_3$) compound.

V.2.b.2. *N*-type substituted elements at the Sb site

V.2.b.2.1 Effect of Te substitution on the electronic and thermoelectric transport properties of $CoSb_3$-based Skutterudite compound ($Co_4Sb_9Te_3$)

V.2.b.2.1.a. Structural properties

The compound $Co_4Sb_9Te_3$ obtained by substituting three of the 24 Sb atoms in the primitive bcc unit cell for three of Te ions.

The equilibrium lattice parameter was calculated for Te doped $CoSb_3$-based Skutterudite compound ($Co_4Sb_9Te_3$) by determining the dependence of the total energy as a function of the volume the energy as a function of the volume of the primitive bcc unit cell of $CoSb_3$ as shown in Fig. V.18.

The obtained equilibrium parameters including lattice constant, bulk modulus B_0 (GPa) and its derivative B' as given in Eq. V.1 are regrouped in table V.3.

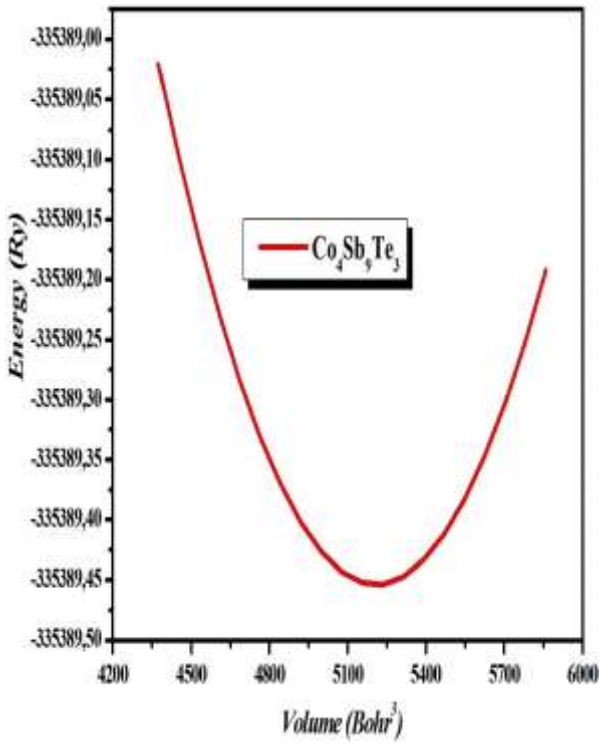

Fig. V.18: Energy versus volume curves for Te doped $CoSb_3$-based Skutterudite compound ($Co_4Sb_9Te_3$).

Table V.3: The calculated equilibrium parameters for Te doped $CoSb_3$-based Skutterudite compound ($Co_4Sb_9Te_3$).

$Co_4Sb_9Te_3$	***Present work***
a(Å)	9.049
B_0 (GPa)	86.990
B'	5.078

V.2.b.2.1.b. Electronic properties

First-principles calculations have been performed to investigate the electronic properties and related transport properties of Te doped Co_4Sb_{12} based skutterudite compound ($Co_4Sb_9Te_3$). Figs. V(19) and (20) show the electronic band structure and the calculated total and partial projected electronic densities of states for Te doped Co_4Sb_{12} skutterudite ($Co_4Sb_9Te_3$) compound.

Starting from the electronic band structure, Te atoms at the Sb substitution sites add extra electrons compared to pure $CoSb_3$. As a result, Te atom substituting for Sb leads to imbalanced charge and pushes up three Sb-based bands above the Fermi level, which carries the system to an unstable state at no charge compensation.

From the partial PDOS, we are able to distinguish the sharp force character of the Te doped Co_4Sb_{12} skutterudite (Co_4Sb_9 Te_3) compound. The part of the conduction band is mainly originated from the Co–*d* states admixed with an identical contribution from Sb–*s*+*p*, and Te–*s*+*p* states. Whereas the Co–*d* states combined with a significant contribution from Sb–p and Te–p states take the major place in the valence band.

Our electronic density of states is comparable to that shown by Velasco-Soto et *al* [11].

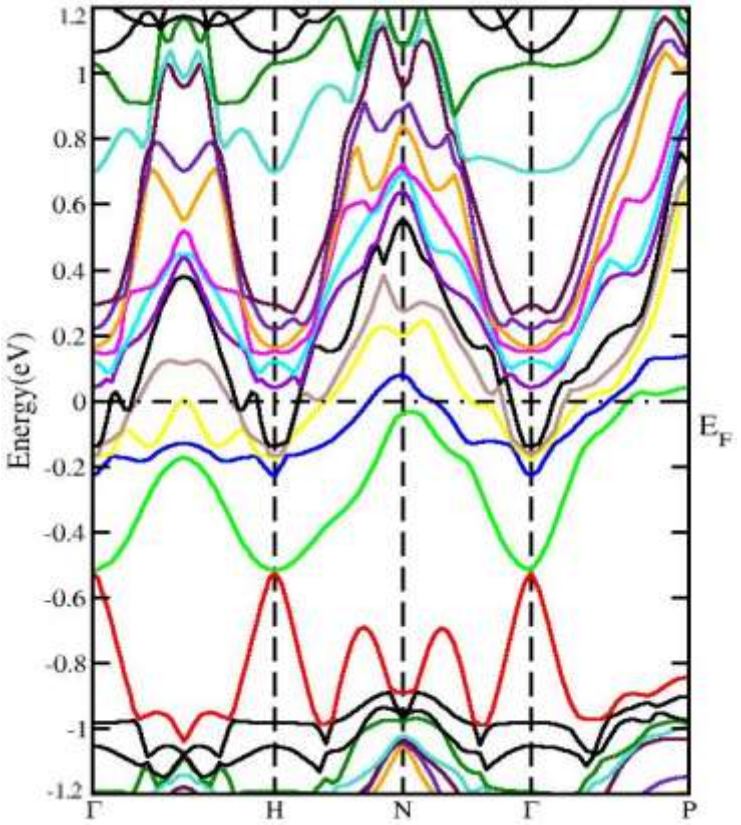

Fig. V.19: The electronic band structure for *n*-type Te doped Co_4Sb_{12} skutterudite ($Co_4Sb_9Te_3$).

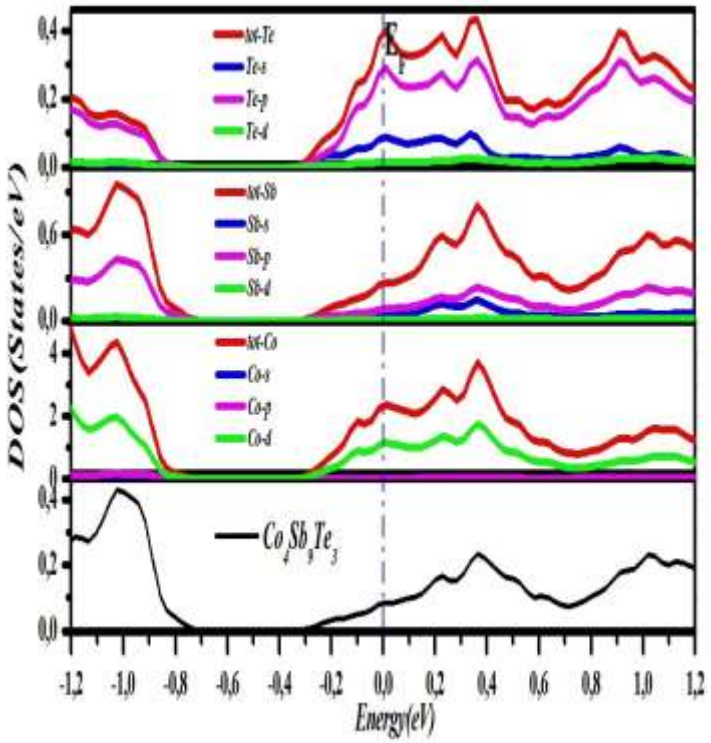

Fig. V.20: The electronic density of states for *n*-type Te doped Co_4Sb_{12} skutterudite ($Co_4Sb_9Te_3$).

V.2.b.2.1.c. Thermoelectric properties

The achieved results for the Seebeck coefficient, the both electrical and electronic thermal conductivities versus relaxation time and the electronic figure of merit are depicted in Figs. V(21)-(24) with respect to the temperature range of 100 K to 900 K. Due to the unidentified relaxation time parameter, a direct comparison with the experiment is only possible for the Seebeck coefficient.

V.2.b.2.1.c.1. Electrical transport properties

Fig. V.21 presents the temperature dependence of seebeck coefficient of Te doped $CoSb_3$ based skutterudite ($Co_4Sb_9Te_3$) compound. According to the results attained in this Fig., the negative Seebeck coefficient values indicate that electrons are the principle charge carriers in the investigated compound. The maximum absolute value of the Seebeck coefficient of Te doped $CoSb_3$ based skutterudite is about $-93\ \mu V/K$ at $T = 900\ K$. This value is in good agreement with the reported results for Te-doping skutterudite compounds [12].

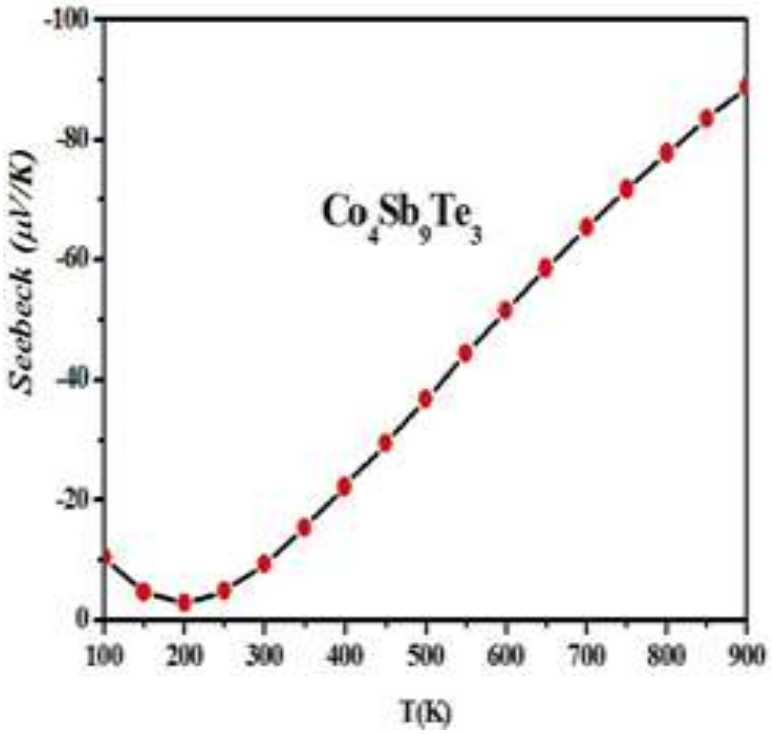

Fig. V.21: The temperature dependence of seebeck coefficient of Te doped $CoSb_3$ based skutterudite ($Co_4Sb_9Te_3$) compound.

Fig. V.22 shows the temperature dependence of the calculated electrical conductivity over relaxation time $\left(\frac{\sigma}{\tau}\right)$ for Te doped Co_4Sb_{12} skutterudite ($Co_4Sb_9Te_3$) compound, respectively. From this Figs one can observe that with increasing temperature the $\left(\frac{\sigma}{\tau}\right)$ quantities augment monotonically and reach their highest values at high temperature of about T= 900 K. As results the calculated electrical and electronic thermal conductivities over relaxation time basically exhibit metallic behavior. This is mainly because that the Te elements give two electrons, raise the carrier concentration of *p*-type Co_4Sb_{12} skutterudite. For that reason, the electrical conductivity values of Te doped Co_4Sb_{12} compound is increased in comparison with those of the Ge-doping skutterudite.

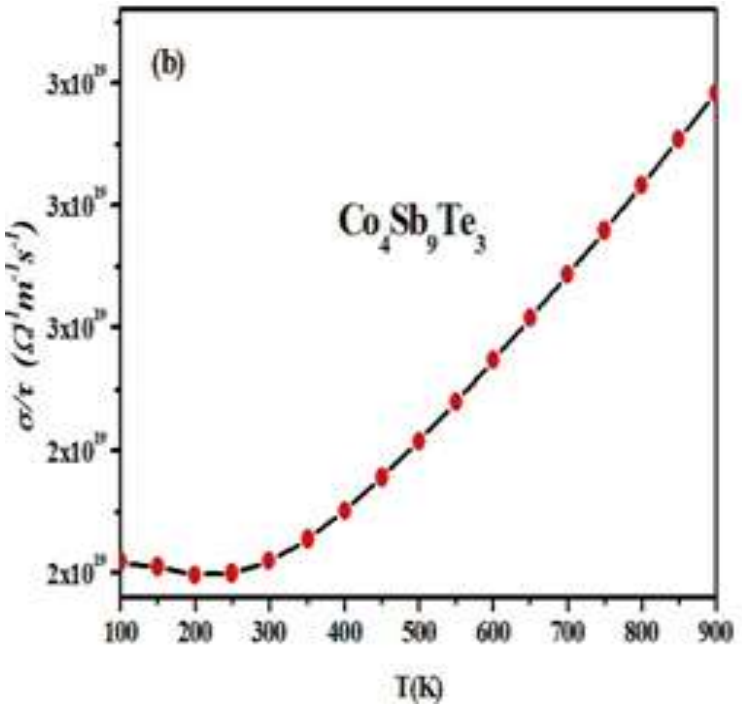

Fig. V.22: The temperature dependence of the calculated electrical conductivity over relaxation time $\left(\frac{\sigma}{\tau}\right)$ for Te doped Co_4Sb_{12} skutterudite ($Co_4Sb_9Te_3$) compound.

V.2.b.2.1.c.2. Electronic thermal transport properties

Fig. V.23 displays the variation of the electronic thermal conductivity over relaxation time $\left(\frac{\kappa_e}{\tau}\right)$ of Te doped Co_8Sb_{24} based skutterudite ($Co_4Sb_9Te_3$) compound as function of temperature (T).

Following this figure, we noticed that the electronic thermal conductivities over relaxation time $\left(\frac{\kappa_e}{\tau}\right)$ increased with increasing the temperature range from 100 K to 900 K.

this results is in concord with the obtained results of the electrical conductivity. And thus is regular trend for degenerated semiconductor materials.

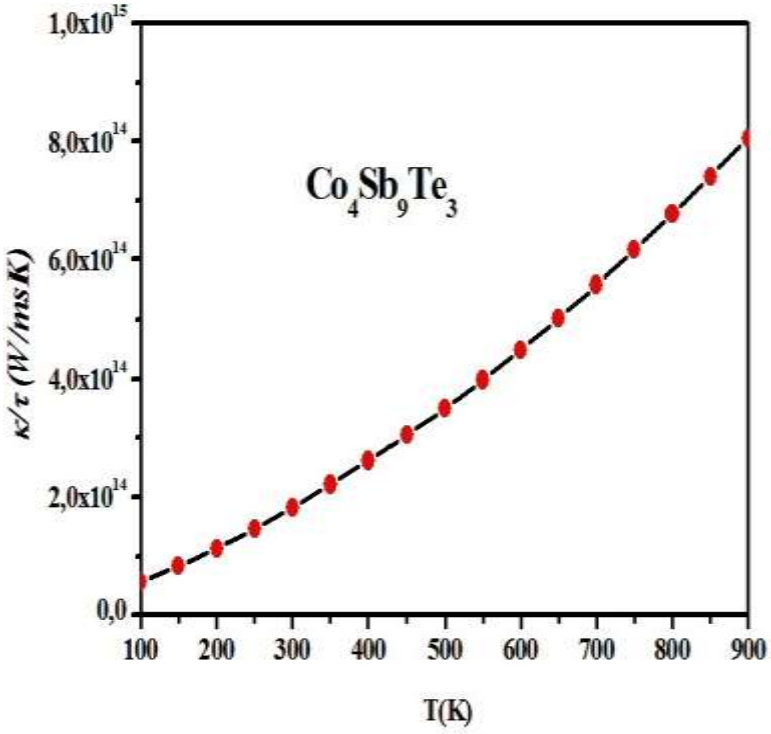

Fig. V.23: The temperature dependence of the calculated electronic thermal conductivity over relaxation time $\left(\frac{\kappa}{\tau}\right)$ for Te doped Co_4Sb_{12} skutterudite ($Co_4Sb_9Te_3$) compound.

V.2.b.2.1.c.3. Electronic dimensionless figure of merit

On the basis of the electrical and electronic thermal conductivities over relaxation time, and Seebeck coefficient, the electronic dimensionless figure of merit values are calculated, as shown in Fig. V.(24). The highest value of the electronic figure of merit is reached at elevated temperature$T = 900\ K$.

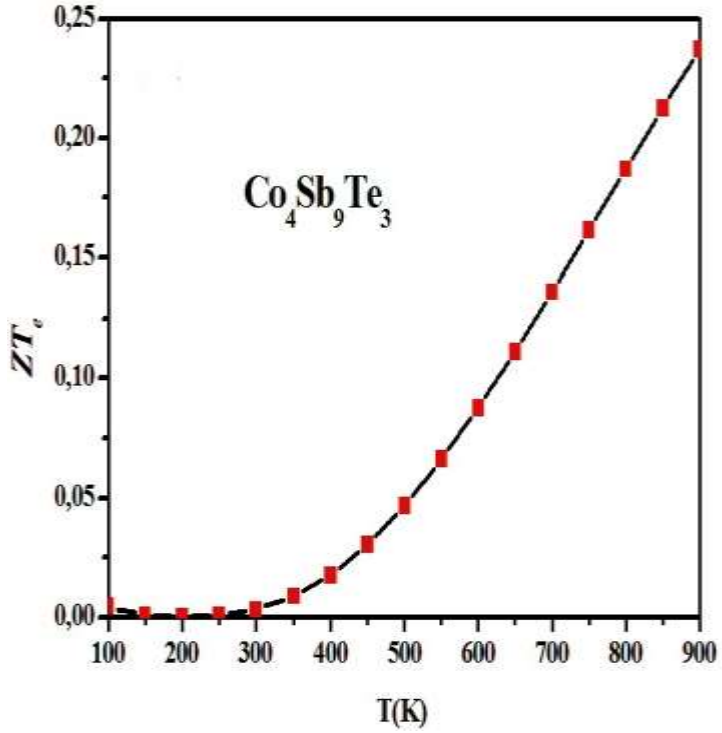

Fig. V.24: The temperature dependence of the calculated electronic dimensionless figure of merit for Te doped Co_4Sb_{12} skutterudite ($Co_4Sb_9Te_3$) compound.

Bibliography

[1] C.H. Park, and Y.S. Kim. J. Phys. Rev. B 81, 085206 (2010).

[2] G. Rogl, A. Grytsiv, E. Royanian, J. Acta. Mater. 61, 4066 (2013).

[3] A. Kaltzoglou, P. Vaqueiro, K.S. Knight, and A.V. Powell. J. Solid State Chem. 36, 193 (2012).

[4] Tan, G.S. Wang, and X. Tang. J. Sci. Adv. Mater. 5, 1974 (2013).

[5] F.D. Munrnaghan, Proc. Natl. Acad. Sci. USA 30, 244 (1944).

[6] Sedat Ballikaya a,b, Ctirad Uher J. Alloy. Compound., 585, 168(2014).

[7] I.H. Kim, S.C. Ur, J. Mater. Lett., 61, 2446 (2007).

[8] R. Bhardwaj, B. Gahtori, K.K. Johari, S. Bathula, N.S. Chauhan, A. Vishwakarma, S. R. Dhakate, S. Auluck and A. Dhar, J. Appl. Energy Mater,10, 1021 (2019).

[9] Y. Liu, X. Li, Q. Zhang; C. Chen, J. Li, L. Zhang, D. Yu, Y. Tian, B. Xu, J. Mater. Sci. Mater. Electron., 27, 6433 (2016).

[10] M.Y. Tafti, M. Saleemi, M.S. Toprak, M. Johnsson, A. Jacquot, M. Jägle, M. Muhammed, Open Chemistry, 13 (2015).

[11] D. Velasco-Soto, E. Menéndez-Proupin, R. Realyvazquez-Guevara, J.A. MatutesAquino, Mater. Res. Express 5, 025908 (2018).

[11] A. Zhou, L. S. Liu, C.C. Shu. J. Electron. Mater. 40, 974 (2011).

[12] R. Chetty a, J. Tobola b, P. Klimczyk c, L. Jaworska c, K.T. Wojciechowski, J. Alloy. Compound, 809, 151477 (2019).

Chapter VI

Chapter VI: Effect of charge balance on thermoelectric properties of $CoSb_3$ based skutterudites

VI.1. Introduction

Filling guest atoms into the voids of skutterudite materials is the mostly motivating one for the reduction of κ_l, though; these filler introduce further electrons that affect the behavior of the compound. This was confirmed by many studies reported in the literature [1-2]. The excess of electrons involves compensation by another lattice defect somewhere else in the structure to ensure charge balance according to the electro-neutrality condition. This phenomenon contributes to create further lattice disorders that are able to increase phonon scattering [1,3-5]. Liu et *al*. observed a reduction of the lattice thermal conductivity of $1.1 Wm^{-1}K^{-1}$ for Fe compensating Gd filled skutterudites ($Gd_{0.41}Fe_{1.48}Co_{2.52}Sb_{12}$), reaching a maximum ZT value of 0.83 at 700K [6]. Also, Prado-Gonjal et *al*. demonstrated that Fe compensating (Ce,Yb) double filled skutterudites reduces the lattice thermal conductivity κ_L, and the ZT reached a values of 0.68 at 773K, and of 0.93 at 823K for both $Ce_{0.8}Fe_3CoSb_{12}$ and $Ce_{0.5}Yb_{0.5}Fe_{3.25}Co_{0.75}Sb_{12}$, respectively [7]. Moreover, Duan et *al*. obtained low thermal conductivity of 1.34 $Wm^{-1}K^{-1}$ in $Nd_{0.6}Fe_2Co_2Sb_{11.6}Sn_{0.4}$ corresponding to 30% improvement of *ZT* for the same compound compared to that of Sn-free sample [8]. Recently some electronegative elements such as S, Se, Cl and Br have been filled into the voids in $CoSb_3$ with a small amount of n-type dopant Te on the Sb sites. In this case, the formation enthalpy is greatly reduced to form such charge compensated skutterudite materials [9].

VI.2. Thermoelectric performance of Sn compensated Ba partially filled *p*-type $CoSb_3$ based skutterudites ($Ba_{0.5}Co_8Sb_{24-x}Sn_x$)

With the existence of two relatively large voids in the skutterudite structure, it can be occupied by filler atoms (i.e. Ba) to represent Barium filled skutterudite with the general formula $Ba_yCo_4Sb_{12}$. By considering a $1 \times 1 \times 2$ supercell construction of Co_8Sb_{24} (consisting of 64 atoms), the number of voids becomes four. Our approach is to fill the voids in the skutterudite structure assuming that the optimally filling fraction for Ba approximates $y = 0.25$ ($Ba_{0.24}Co_4Sb_{12}$), which corresponds to the highest reported value of figure of merit for *n*-type filled skutterudites [10]. Therefore, only one of voids is filled with a Ba atom, and the formula becomes $BaCo_{16}Sb_{48}$ (or $Ba_{0.5}Co_8Sb_{24}$). The substitution of Sb atoms with Sn atoms will lead to different concentrations of Sn and Sb, yielding 64 atom supercells with four formulas $Ba_{0.5}Co_8Sb_{24-x}Sn_x$ ($x = 1, 2, 3$ and 4), which were taken to reflect the calculated structures as shown in Fig. VI.1(a)-(d).

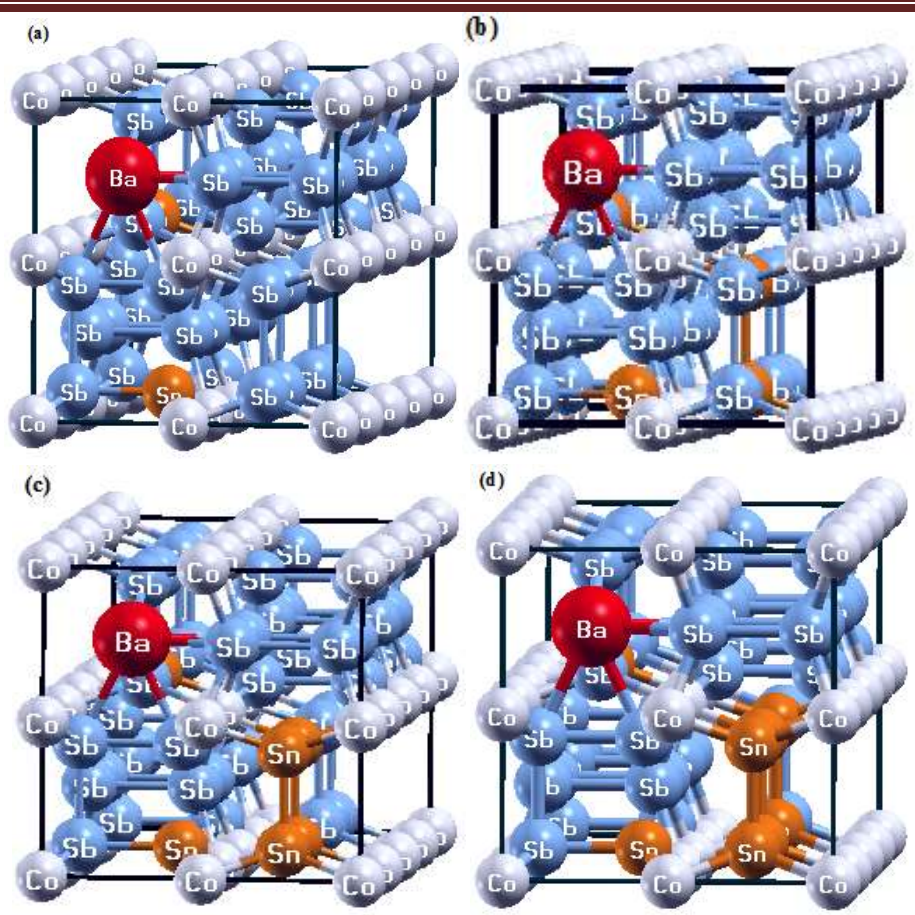

Fig. VI.1: The unit cell structures of Sn substituted partially filled skutterudites ($Ba_{0.5}Co_8Sb_{24-x}Sn_x$): (a) x= 1, (b) x= 2, (c) x= 3, and (d) x= 4.

TableVI.1. regroups the values of the following parameters: R_{mt}, $R_{mt} * K_{max}$, l_{max} , G_{max} et K_{points} for $Ba_{0.5}Co_8Sb_{24-x}Sn_x$ compounds.

Table VI.1: The values of: R_{mt}, $R_{mt} * K_{max}$, l_{max} , G_{max} et K_{points} for $Ba_{0.5}Co_8Sb_{24-x}Sn_x$ compounds.

GGA-PBE	R_{mt} (u.a)				$R_{mt} * K_{max}$	l_{max}	G_{max}	K_{points}
	Ba	Co	Sb	Sn				
$Ba_{0.5}Co_8Sb_{23}Sn$	2.5	1.78	1.71	1.51	6	10	12	1000
$Ba_{0.5}Co_8Sb_{22}Sn_2$	2.5	2.03	1.61	1.43	6	10	12	1000
$Ba_{0.5}Co_8Sb_{21}Sn_3$	2.5	2.03	1.61	1.43	6	10	12	1000
$Ba_{0.5}Co_8Sb_{20}Sn_4$	2.5	2.03	1.61	1.43	6	10	12	1000

Chapter VI: Effect of charge balance on thermoelectric properties of $CoSb_3$ based skutterudites

VI.2.1. Structural properties and total energies

The equilibrium structural parameters of Sn substitution in partially filled skutterudite $Ba_{0.5}Co_8Sb_{24-x}Sn_x$ (x =1, 2, 3 and 4) are determined by using the calculation of the total energies as a function of the cell volumes.

To evaluate the thermodynamic stability of the substituted compounds, we calculate the enthalpy of formation ΔE as follows:

$$\Delta E = E_0(Ba_{0.5}Co_8Sb_{24} - xSn_x) - E_0(Ba_{0.5}Co_8Sb_{24}) - x.E_0(Sb) + x.E_0(Sn) \quad \text{VI.1}$$

Where E_0 is the lowest energy of the compound and x is the number of Sn that replace the Sb atoms. $E_0(Sb)$ and $E_0(Sn)$ are energies per atom of the constituents in their ground state phases.

Table VI.2 summarizes the results obtained for the optimized lattice constants and bulk modulus, its derivative and relatives formation energies of the studied compounds.

The diamond structure, which crystallizes in the cubic $Fd-3m$ space group, and the alpha-Sb structure, which crystallizes in the trigonal $R\bar{3}m$ space group, was assumed to be ground state phases for Sn and Sb atoms, respectively. The results as a function of different levels of substituted Sn in partially filled skutterudite $Ba_{0.5}Co_8Sb_{24-x}Sn_x$ (x =1, 2, 3 and 4) are given in table VI.2.

The negative enthalpy of formation indicates the stability of the composition. table VI.2 shows that the enthalpy of formation decreases when the degree of Sn substitution decreases from $Ba_{0.5}Co_8Sb_{20}Sn_4$ to $Ba_{0.5}Co_8Sb_{21}Sn_3$, $Ba_{0.5}Co_8Sb_{22}Sn_2$ and $Ba_{0.5}Co_8Sb_{23}Sn$, respectively, which indicates that the $Ba_{0.5}Co_8Sb_{23}Sn$ compound is comparatively most stable than the other compounds.

The values calculated for the lattice constant of Sn substituted in partially filled skutterudite $Ba_{0.5}Co_8Sb_{24-x}Sn_x$ (x =1, 2, 3 and 4) are slightly larger than the calculated values for the lattice constant of binary skutterudite (Co_8Sb_{24}) (see Chap. III) and partially filled $Ba_{0.5}Co_8Sb_{24}$ (see Chap. IV) compounds. They increase as a function of the increase in Sn substitution. This is mainly because the atomic radius of the Sb atoms is smaller than that of the Sn anions.

Table VI.2: The calculated equilibrium structural parameters of Sn substituted in partially filled skutterudite $Ba_{0.5}Co_8Sb_{24-x}Sn_x$ (x= 1, 2, 3 and 4) compounds and their relative formation energies.

$B_{0.5}Co_8Sb_{24-x}Sn_x$	Lattice constant a(Å)	B (GPa)	B'	ΔE (meV)
x=1	11.520	85.13	5.08	-0.263
x=2	11.523	84.47	5.12	-0.017
x=3	11.530	87.95	3.42	0.233
x=4	11.536	84.67	4.56	0.481

VI.2.2. Electronic properties

In order to understand the electronic properties and to control the charge balance in the investigated compounds, the band structures and projected density of states (DOS) are examined.

VI.2.2.a. Electronic band structure

Fig. VI.2 shows the band structures for the equilibrium geometries of Sn substituted in partially filled skutterudite $Ba_{0.5}Co_8Sb_{24-x}Sn_x$ for: (a) x = 1,(b) x =2, (c) x =3 and (d) x = 4 compounds along the high-symmetry points R-Γ-X-M-Γ in the first Brillion zone. It can be seen that the valence band maximum (VBM) and the conduction band minimum (CBM) in Fig. VI.2 lie at the same Γ point (Γ_V–Γ_C); this shows that the compounds investigated have a semiconductor character with fundamental narrow direct band gaps.

Following Figs. VI.2(a)–(d), the most important significant changes in the band structures of $Ba_{0.5}Co_8Sb_{24-x}Sn_x$ (x = 2, 3 and 4) are the shift of the further valence states above the Fermi level, whereby a number of holes are introduced and generate acceptor states, with the exception of $Ba_{0.5}Co_8Sb_{23}Sn$ which correspond to the level substitution of x = 1, in which all valence bands are below the Fermi level. This is mainly due to the balanced charge in the compound. The substitution of the Sn atom at Sb sites causes the Fermi level in the valence bands to shift significantly as a result of the increase in the Sn concentration. In addition, it

can be seen from Fig. VI.2(a)–(d) that the degeneracy of the CBM is distorted by Sn substitution, this result shows similarity to that obtained in Ga-containing thermoelectric skutterudites [11].

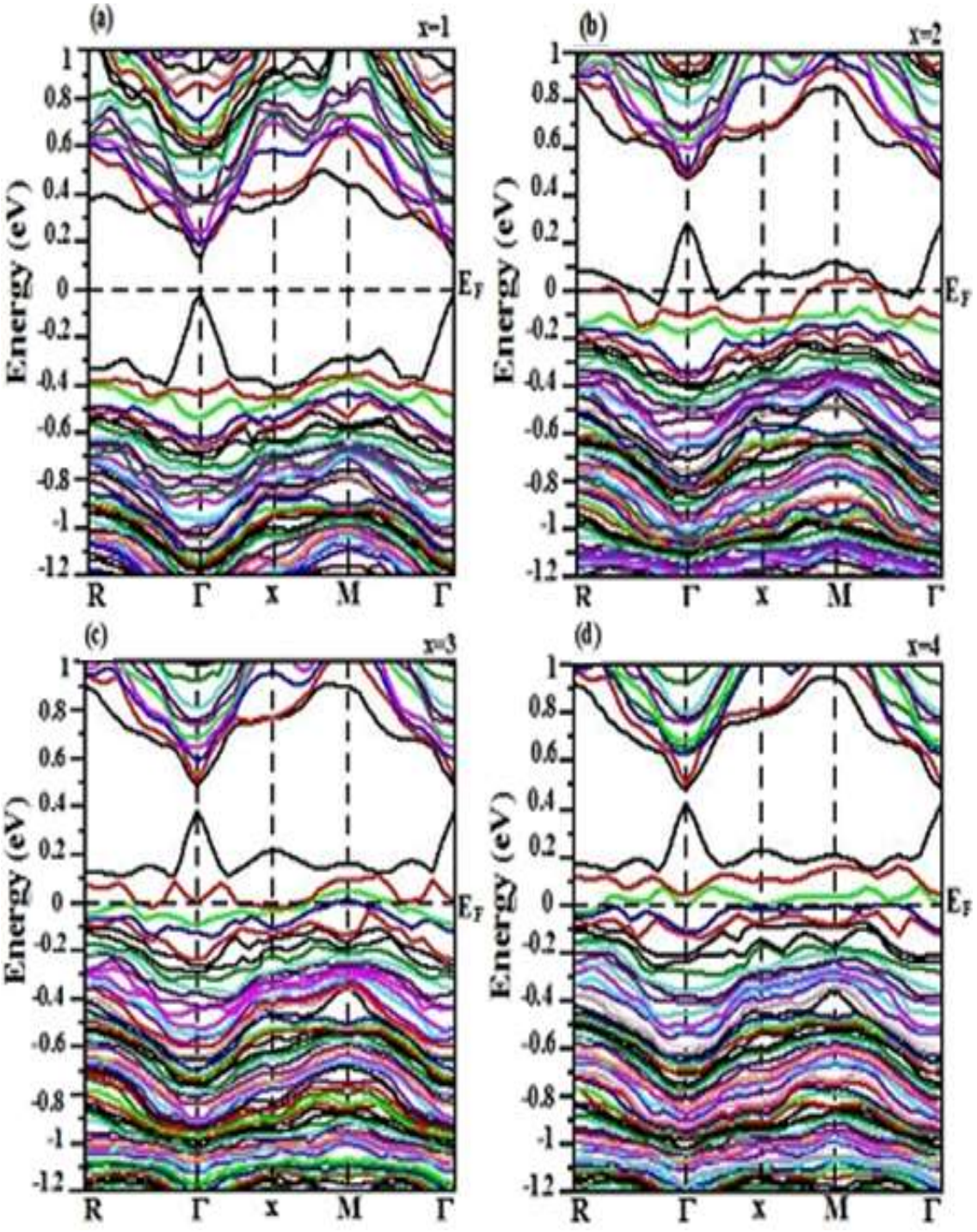

Fig. VI.2: Calculated band structures within GGA formalism for: (a) $Ba_{0.5}Co_8Sb_{23}Sn$ (x= 1), (b) $Ba_{0.5}Co_8Sb_{22}Sn_2$ (x= 2), (c) $Ba_{0.5}Co_8Sb_{21}Sn_3$ (x= 3) and (d) $Ba_{0.5}Co_8Sb_{20}Sn_4$ (x= 4) compounds.

VI.2.2.b. Electronic density of states (DOS)

In order to obtain a basic understanding of the electronic structure, the total and partial projected densities of states of each atom (TDOSs and PDOSs) in the examined compounds were calculated as shown in Fig. VI.3. It is important to note that each orbital of each atom is projected separately to determine the total contribution associated with each atom. From this figure we can conclude that there are two different ranges in the total electronic densities of states (TDOS), which are separated by energy gaps.

As shown in Figs. IV.3(c)–(d), the p-orbitals of both the Sb and Sn atoms make the major contribution to the valence band above the Fermi level with approximately the same amount. While the valence band near the Fermi level for the $Ba_{0.5}Co_8Sb_{23}Sn$ compound mainly results from extremely hybridized contributions between p-orbitals of pnictogen (Sb/Sn) atoms and d orbitals of Ba and Co atoms mixed with Ba-s and d-orbitals of pnictogen (Sb/Sn) atoms (see Fig. VI.3(a)). This obviously confirms the covalent nature of filler-pnictogen (Ba–Sb/Sn) and metal-pnictogen (Co-(Sb/ Sn)) bonds in the $Ba_{0.5}Co_8Sb_{23}Sn$ compound. It follows from Figs. VI.3(a)–(d) that the conduction bands for $Ba_{0.5}Co_8Sb_{24-x}Sn_x$ (x = 1, 2, 3 and 4) compounds are generally shaped by the both p- and s-orbitals of pnictogen (Sb/Sn) atoms mixed with d-orbitals of Ba and Co atoms.

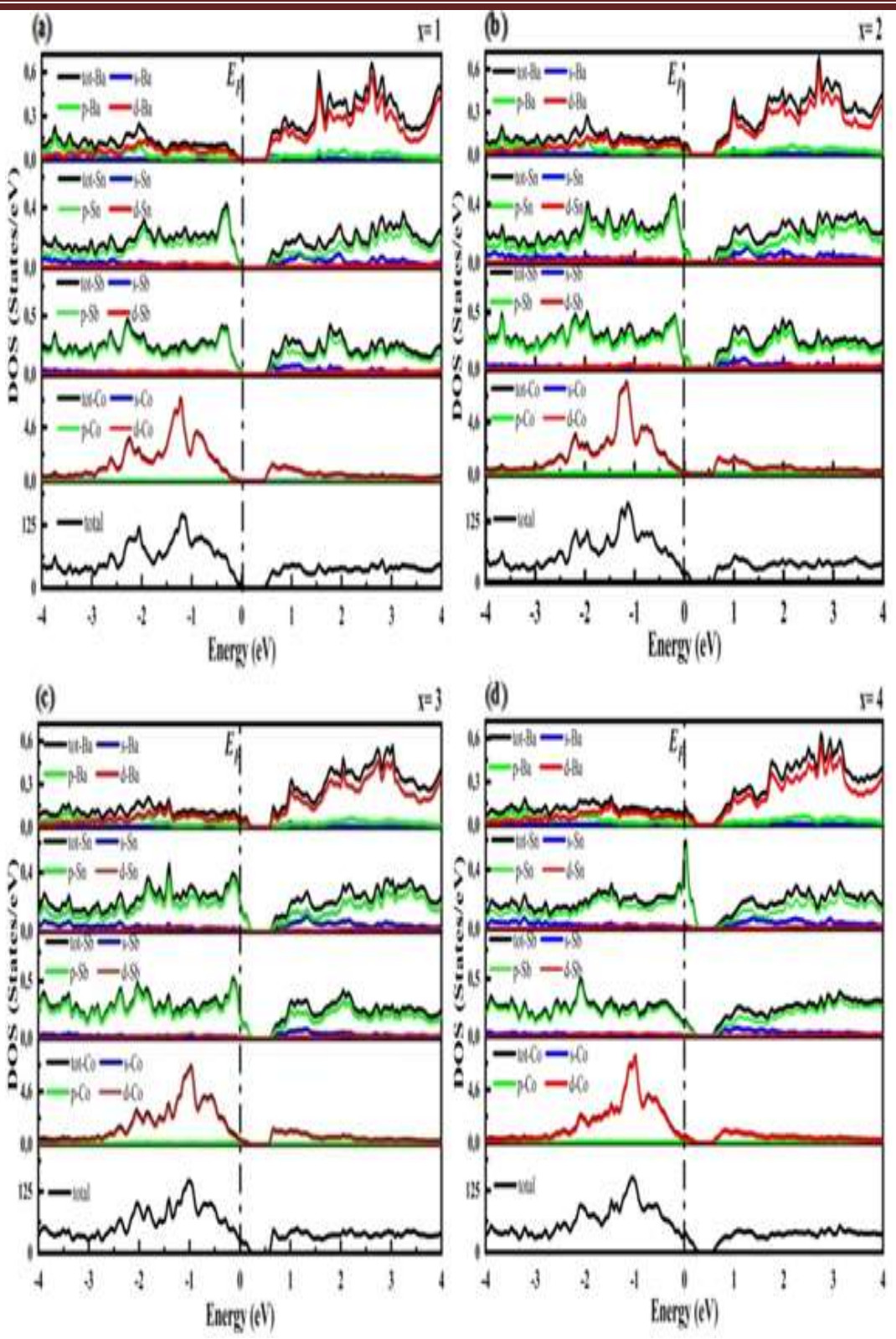

Fig. VI.3: Total and partial electronic densities of states for: (a) $Ba_{0.5}Co_8Sb_{23}Sn$ (x= 1), (b) $Ba_{0.5}Co_8Sb_{22}Sn_2$ (x= 2), (c) $Ba_{0.5}Co_8Sb_{21}Sn_3$ (x= 3) and (d) $Ba_{0.5}Co_8Sb_{20}Sn_4$ (x= 4) compounds.

VI.2.3. Thermoelectric properties

In this section we focus on the thermoelectric properties of the binary skutterudite Co_8Sb_{24}, of the partially filled skutterudite compound $Ba_{0.5}Co_8Sb_{24}$ and Sn substituted in partially filled skutterudite $Ba_{0.5}Co_8Sb_{24-x}Sn_x$ compounds (x = 1, 2, 3 and 4). The thermoelectric properties, including the electrical and electronic thermal conductivities and the Seebeck coefficient, were calculated using the BoltzTraP code [12], which is based on the semi-classical Boltzmann theory and the Fourier interpolation of the calculated bands. The band energies were differentiated to determine the group velocities of the electrons.

VI.2.3.a.Seebeck coefficient (S)

Figs. VI.4(a)-(b) show the temperature dependence of the Seebeck coefficients for binary Skutterudite Co_8Sb_{24}, which are associated with the plots of Sn substituted in partially filled Skutterudite $Ba_{0.5}Co_8Sb_{24-x}Sn_x$ (x = 1, 2, 3 and 4) compounds and the partially filled Skutterudite $Ba_{0.5}Co_8Sb_{24}$, respectively.

In Fig. VI.4(b), negative Seebeck coefficient values are obtained for the partially filled skutterudite $Ba_{0.5}Co_8Sb_{24}$, which indicates that electrons are the majority carriers, and thus confirms that this is an *n*-type material. However, opposite signs of S values can be observed in Fig. VI.4(a), which means that both compounds of binary skutterudite Co_8Sb_{24} and Sn substituted in partially filled skutterudite $Ba_{0.5}Co_8Sb_{24-x}Sn_x$ (x = 1, 2, 3 and 4) are *p*-type materials.

As shown in Fig. VI.4(a), the Seebeck coefficient is affected by Sn substitution; it decreases with increasing Sn substitution. The specific values are $252.88\,\mu VK^{-1}$ for $Ba_{0.5}Co_8Sb_{23}Sn$, $52.77\mu VK^{-1}$ for $Ba_{0.5}Co_8Sb_{22}Sn_2$, $24.60\,\mu VK^{-1}$ for $Ba_{0.5}Co_8Sb_{21}Sn_3$ and $14.55\,\mu VK^{-1}$ for $Ba_{0.5}Co_8Sb_{20}Sn_4$ at one temperature $T = 500K$. This is mainly due to the increase in the Hall carrier concentrations of $6.23 \times 10^{18}cm^{-3}$, $8.32 \times 10^{20}cm^{-3}$, $6.32 \times 10^{21}cm^{-3}$ to $4.24 \times 10^{22}cm^{-3}$ for $Ba_{0.5}Co_8Sb_{23}Sn$, $Ba_{0.5}Co_8Sb_{22}Sn_2$, $Ba_{0.5}Co_8Sb_{21}Sn_3$ to $Ba_{0.5}Co_8Sb_{20}Sn_4$, respectively This is a regular trend in thermoelectric materials.

These results strongly depend on the electronic DOSs near the Fermi level (see Fig. VI.3(c)–(f)). While the Seebeck coefficient in Fig. VI.4(b) for partially filled skutterudite $Ba_{0.5}Co_8Sb_{24}$ reached the value of $105.27\mu VK^{-1}$ at the same temperature. This value agrees with the values given in Ref. [10].

The largely moderate Seebeck coefficient values in $Ba_{0.5}Co_8Sb_{23}Sn$ can originate from the balance between the *n*-type and *p*-type carriers. In addition, the Seebeck coefficient for this compound increases with increasing temperature. They have a broad peak centered at around $T = 500\ K$ and begin to drop at $T > 500\ K$. This is an alleged feature of the bipolar effect that results from the excitation of electrons from valence bands to conduction bands at a finite temperature leaving holes in the valence band. Both electrons and holes can be excited, whereby the conduction bands or valence bands are filled near the Fermi level, which indicates the occurrence of a transition to intrinsic semiconductor behavior [13,14].

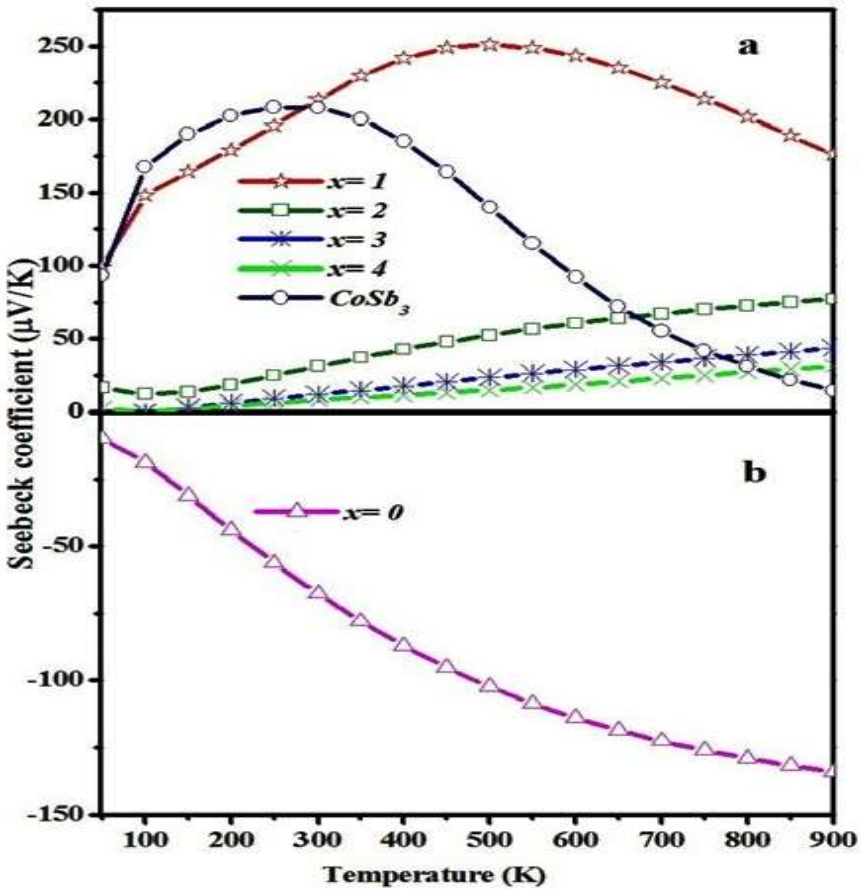

Fig. VI.4: Calculated Seebeck coefficient values as functions of temperature for: (a) binary skutterudite Co_8Sb_{24} and Sn substituted in partially filled skutterudite $Ba_{0.5}Co_8Sb_{24-x}Sn_x$ (x= 1, 2, 3 and 4) compounds, and (b) partially filled skutterudite $Ba_{0.5}Co_8Sb_{24}$.

VI.2.3.b.Electrical conductivity (σ)

Under Boltzmann transport theory, electrical conductivity σ is given by [15]

$$\sigma = \frac{e^2}{4\pi^3 k_B T}\int \tau v_x^2 f_0(1-f_0)d^3k \qquad \text{VI.2}$$

Where k_B is the Boltzmann constant, T the absolute temperature, f_0 the Fermi-Dirac distribution, τ the electron relaxation time, v_x the electron velocity along temperature gradient. The integral is performed in wave-vector space k and summation is performed for all valleys related to the electrical conduction.

Fig. VI.5 presents the calculated electrical conductivities over relaxation time $\left(\frac{\sigma}{\tau}\right)$ in temperature interval from $100K$ to $900K$, for binary skutterudite Co_8Sb_{24}, partially filled skutterudite $Ba_{0.5}Co_8Sb_{24}$ and Sn substituted in partially filled skutterudite $Ba_{0.5}Co_8Sb_{24-x}Sn_x$ (x= 1, 2, 3 and 4) compounds.

From Fig. VI.5, we can see that the electrical conductivity over relaxation time $\left(\frac{\sigma}{\tau}\right)$ values for partially filled skutterudite $Ba_{0.5}Co_8Sb_{24}$ increases with increasing temperature, indicating a typical behavior of the metal materials.

On the other hand, the electrical conductivities over relaxation time $\left(\frac{\sigma}{\tau}\right)$ values for $Ba_{0.5}Co_8Sb_{24-x}Sn_x$ compounds increase with increasing the number of Sn in partially filled skutterudite, where as the Fermi level is clearly controlled by partially Ba-filling and Sn/Sb proportion (see Figs. VI.2(a)-(d)).

These results are extremely concurring with the difference in the electronic density of states close to Fermi level in Figs. VI.3(a)-(d).The minimum values of $\left(\frac{\sigma}{\tau}\right)$ are reached for both Co_8Sb_{24} and $Ba_{0.5}Co_8Sb_{23}Sn$ compounds due to their relatively small number of holes carriers; this is in accord with their calculated Seebeck coefficient values (see Fi. VI.4(a)).

One can notice also, that the $\left(\frac{\sigma}{\tau}\right)$-T relationships for $Ba_{0.5}Co_8Sb_{24-x}Sn_x$ (x= 2, 3 and 4) compounds have roughly linear tendencies. They decrease with increasing temperature range, showing the typical character of heavily degenerated semiconducting behavior.

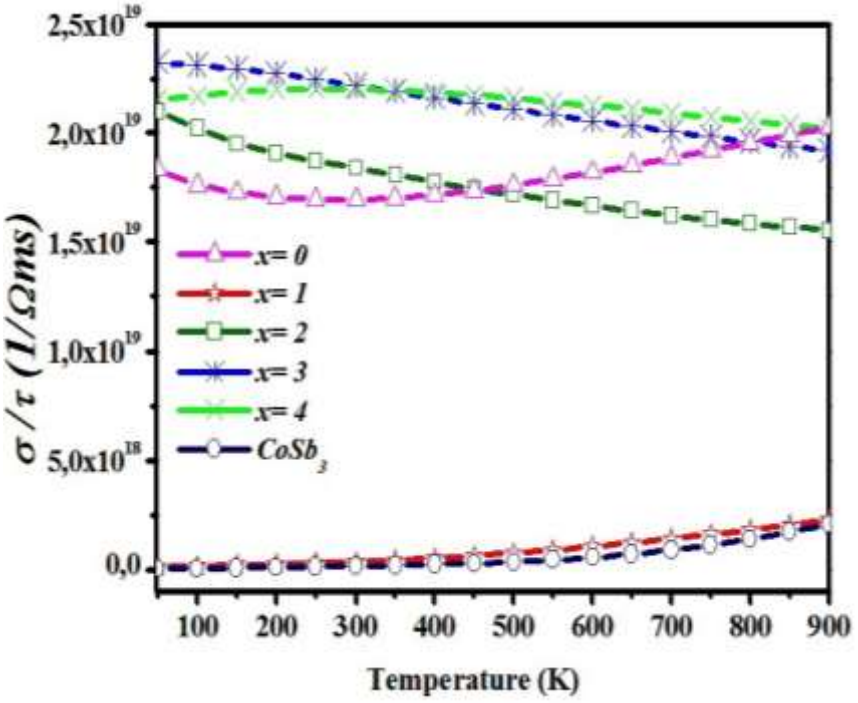

Fig. VI.5: Calculated electrical conductivities over relaxation time $\left(\frac{\sigma}{\tau}\right)$ as functions of temperature for Co_8Sb_{24}, $Ba_{0.5}Co_8Sb_{24}$ and $Ba_{0.5}Co_8Sb_{24-x}Sn_x$ (x= 1, 2, 3 and 4) compounds.

VI.2.3.c.Electronic thermal conductivity (κ_e)

The temperature dependence of the electronic part of thermal conductivities over relaxation time $\left(\frac{\kappa_e}{\tau}\right)$ for the binary skutterudite Co_8Sb_{24}, the partially filled skutterudite $Ba_{0.5}Co_8Sb_{24}$ and for the Sn substituted in partially filled skutterudite $Ba_{0.5}Co_8Sb_{24-x}Sn_x$ (x= 1, 2, 3 and 4) compounds are shown in Fig. VI.6. It was found that the electronic thermal conductivities over relaxation time of the partially filled skutterudite $Ba_{0.5}Co_8Sb_{24}$ were drastically reduced by the Sn substitution. The largely reduced $\left(\frac{\kappa_e}{\tau}\right)$ values were found in the $Ba_{0.5}Co_8Sb_{23}Sn$ compound. This is mainly because of the decrease on the charge carrier's concentrations, which are related directly with the electronic part of thermal conductivity, according to the following equation [16]:

$$\kappa_e = \frac{n\pi^2 T k_b^2}{3m^* v_e} \qquad \text{VI.3}$$

Where k_b is the Boltzmann constant, T is the absolute temperature, n is the concentration of charge carries, m^* is the effective mass, and v_e is the electron velocity.

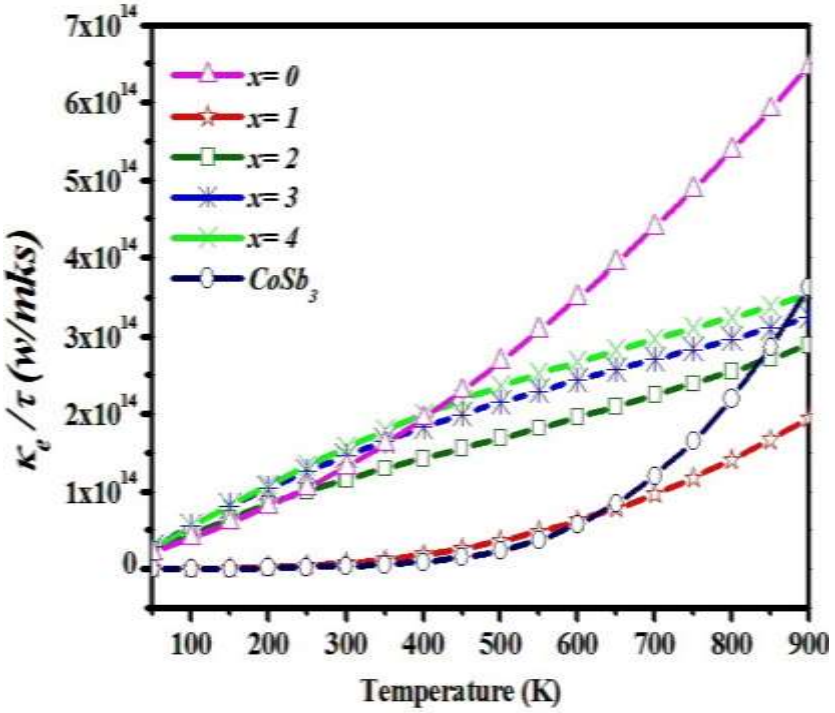

Fig. VI.6: Calculated electronic thermal conductivities over relaxation time $\left(\frac{\kappa_e}{\tau}\right)$ as functions of temperature for binary skutterudite Co_8Sb_{24}, partially filled skutterudite $Ba_{0.5}Co_8Sb_{24}$ and Sn substituted in partially filled skutterudite $Ba_{0.5}Co_8Sb_{24-x}Sn_x$ (x= 1, 2, 3 and 4) compounds.

VI.2.3.d.Dimensionless electronic figure of merit (ZT_e)

On the basis of Seebeck coefficient, electrical conductivities and electronic thermal conductivities per relaxation time result; the dimensionless electronic figure of merit values, ZT_e for the binary skutterudite Co_8Sb_{24}, the partially filled skutterudite $Ba_{0.5}Co_8Sb_{24}$ and the Sn substituted in partially filled skutterudite $Ba_{0.5}Co_8Sb_{24-x}Sn_x$ (x= 1, 2, 3 and 4) as functions of temperature are displayed in Fig. VI.7.

It can be seen that the ZT_e values improved via decreasing Sn substitution. For Sn substituted in partially filled skutterudite $Ba_{0.5}Co_8Sb_{24-x}Sn_x$, the maximum ZT_e value of 0.67 has been attained for $Ba_{0.5}Co_8Sb_{23}Sn$ compound at temperature of 500K, which is bigger than the ZT_e value in partially filled skutterudite $Ba_{0.5}Co_8Sb_{24}$ at the same temperature.

The main reason for the enhancement of the dimensionless electronic figure of merit ZT_e in the $Ba_{0.5}Co_8Sb_{23}Sn$ compound is due to its high Seebeck coefficient and its low electronic thermal conductivity per relaxation time.

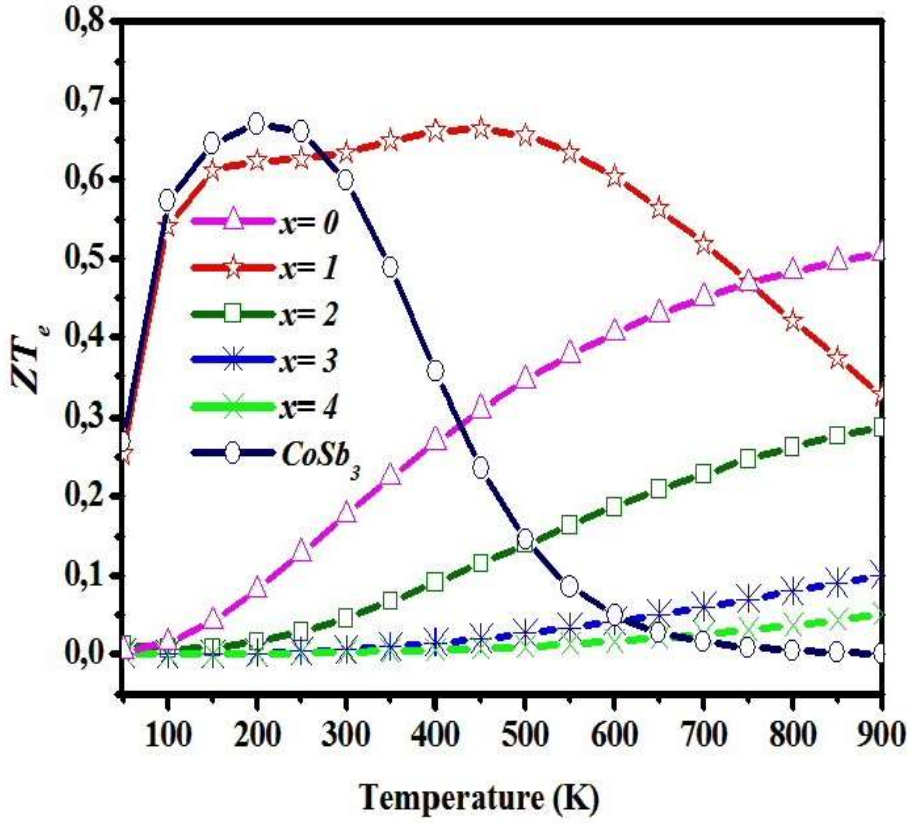

Fig. VI.7: Calculated dimensionless electronic figure of merit values, ZT_e for binary skutterudite Co_8Sb_{24}, partially filled skutterudite $Ba_{0.5}Co_8Sb_{24}$ and Sn substituted in partially filled skutterudite $Ba_{0.5}Co_8Sb_{24-x}Sn_x$ (x= 1, 2, 3 and 4) compounds as functions of temperature.

VI.3. Thermoelectric performance of Te compensated Fe doped $CoSb_3$ based skutterudite ($Fe_xCo_{8-x}Sb_{24-y}Te_y$) compounds.

VI.3.1. Structural properties

The equilibrium structural parameters including the optimized lattice constant (a), the isothermal bulk modulus B_0, and the derivative of isothermal bulk modulus B_0' of Fe and Te co-doped $CoSb_3$ based skutterudite compounds were determined by adjusting the calculated total energies as a function of the cell volumes to the Murnaghan equation are summarized in table VI.3.

From table VI.3; one can observe that the lattice constant are slightly larger than the calculated values for the lattice constant of binary skutterudite (Co_8Sb_{24}) (see Chap. III) and Fe doped $CoSb_3$ based skutterudite compounds (see Chap. V) with 1% and 2% deviations.

This is mainly due to the fact that the atomic radius of Co (Sb) ions is smaller (larger) than in Fe (Te) ions.

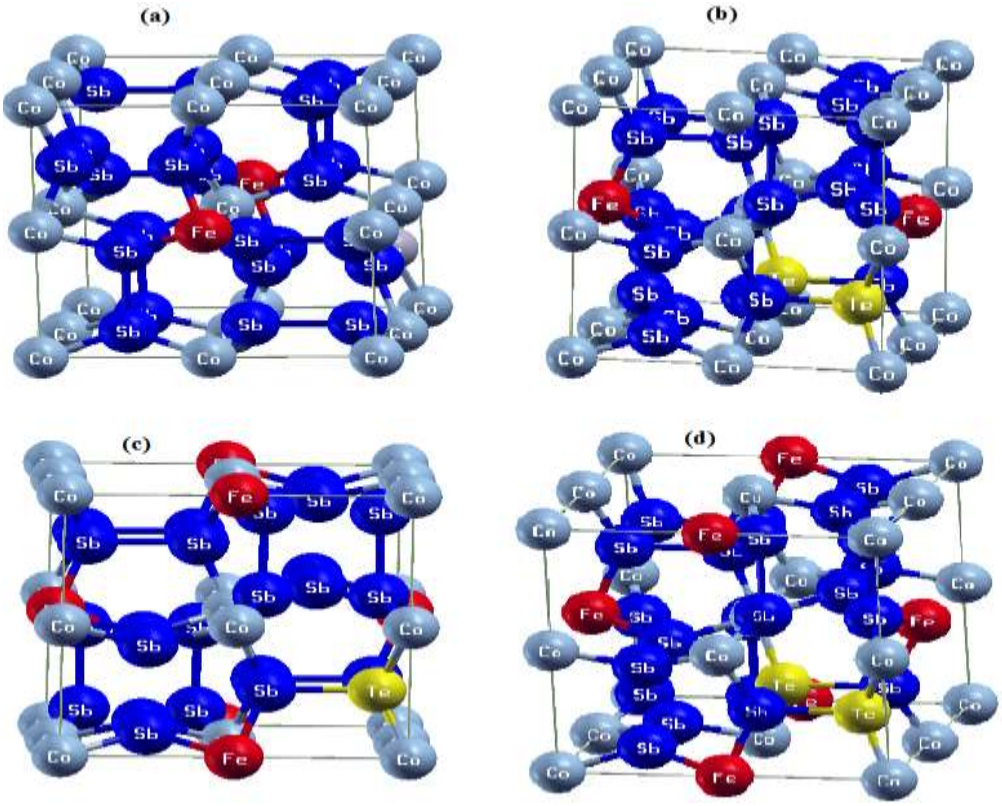

Fig. VI.8: The unit cell structures of Fe and Te co-doped $CoSb_3$ based skutterudite compounds ($Fe_xCo_{8-x}Sb_{24-y}Te_y$): (a) x= 1, y= 1, (b) x= 1, y= 2, (c) x= 2, y= 1 and (d) x= 2, y= 2.

Table VI.3: The calculated equilibrium structural parameters of Fe and Te co-doped $CoSb_3$ based skutterudite compounds.

$Fe_xCo_{8-x}Sb_{24-y}Te_y$	Lattice constant a(Å)	B (GPa)	B'
x= 1, y= 1	9.1396	86.14	4.16
x= 1, y= 2	9.1492	84.63	4.91
x=2, y= 1	9.1390	86.32	5.13
x= 2, y= 2	9.1396	84.79	5.23

VI.3.2. Electronic properties

VI.3.2.a. Electronic band structure

Fig. VI.9 shows the band structures for the equilibrium geometries of Fe and Te co-doped $CoSb_3$ based skutterudite compounds for: (a) x =1, y= 1, (b) x =1, y= 2, (c) x = 2, y= 1 and (d) x = 2, y= 2 compounds along the high-symmetry points R-Γ-X-M-Γ (where Γ(0,0,0), M(0.5,0.5,0.5), X (0,0,0.5) and R (0.25,0.25,0.25)) in the first Brillion zone.

Following Figs. VI.9(b) and (c), the most important significant variations in the electronic band structures of $Fe_xCo_{8-x}Sb_{24-y}Te_y$ systems caused by Fe (Te) dopants are the shift of the further valence (conduction) states above (below) the Fermi level, whereby a number of holes (electrons) are introduced and generate acceptor (donors) states, with the exception of $FeCo_7Sb_{23}Te$ and $Fe_2Co_6Sb_{22}Te_2$ compounds which correspond to the level doping of x =1, y= 1 and x = 2, y= 2, respectively (Fig.VI.9(b) and (d)), in which the Fermi level is controlled and all valence bands are below it. This last finding is typically due to the balanced charge in the both investigated compounds.

The substitution of the Fe (Te) atoms at Co (Sb) sites causes the Fermi level in the valence (conduction) bands to shift it significantly as a result of the raise in the Fe (Te) fraction. Moreover, it can be seen from Fig. VI.9(a)–(d) that the degeneracy of the first conduction band is distorted by Fe/Te dopants, this result shows similarity to that obtained in Ga compensated thermoelectric skutterudite materials [11].

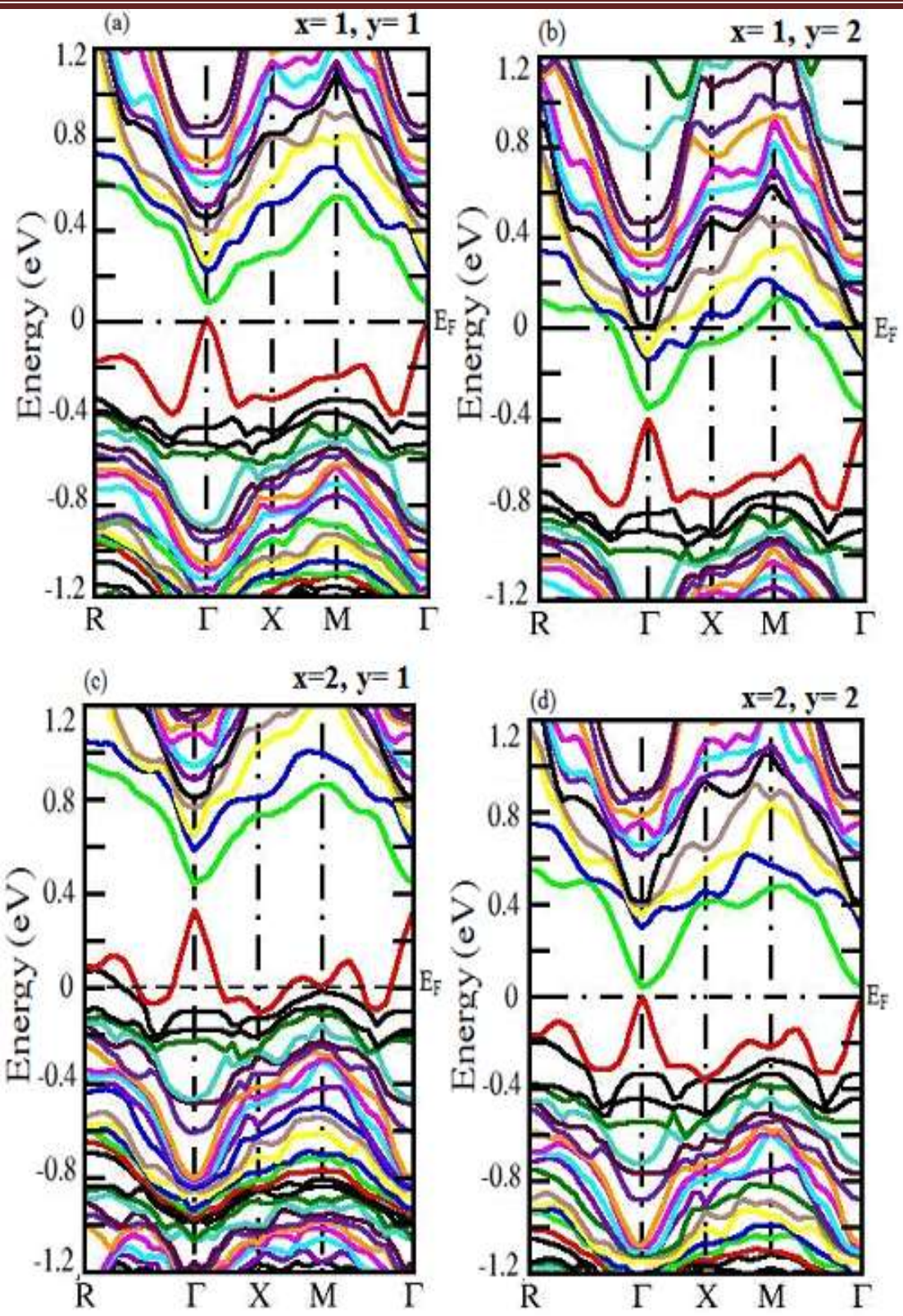

Fig. VI.9: The electronic band structures for $Fe_xCo_{8-x}Sb_{24-y}Te_y$ compounds: (a) x= 1, y= 1, (b) x= 1, y= 2, (c) x= 2, y= 1and (d) x= 2, y= 2.

VI.3.2.b. Electronic density of states (DOS)

In order to achieve a vital understanding of the electronic structure, the total electronic and partial electronic projected densities of states of each atom (TDOSs and PDOSs) in the studied compounds were calculated as shown in Fig. VI.10.

From this figure we can estimate that there are two different regions in the total electronic densities of states (TDOSs), which are divided by energy gap.

As shown in Figs. VI.10(a)–(d), the valence bands near the Fermi level for the $FeCo_7Sb_{23}$ Te and $Fe_2Co_6Sb_{22}Te_2$ compounds mainly come from extremely hybridized contributions between p orbitals of the Sb atoms and their doped Te anions and d orbitals of the both Co and Fe metals mixed with s-orbitals of Sb/Te atoms These results obviously confirm the covalent nature metal-X sites ((Co/Fe)-(Sb/ Te)) bonds in the $FeCo_7Sb_{23}Te$ and $Fe_2Co_6Sb_{22}Te_2$ compounds.

While for the $FeCo_7Sb_{23}Te_2$ and $Fe_2Co_6Sb_{22}Te_1$ compounds the p (d) -orbitals of the both Sb/Te (Co/Fe) atoms create the most important contributions to the valence states above the Fermi level with roughly the same amount (see Figs. VI.10(b) and (c)).

Following Figs. VI.10 (a)–(d), the conduction bands for $Fe_xCo_{8-x}Sb_{24-y}Te_y$ compounds are generally shaped by the d-orbitals of metal atoms (Fe/Co) mixed with the both p- and s-orbitals of Sb/Te anions.

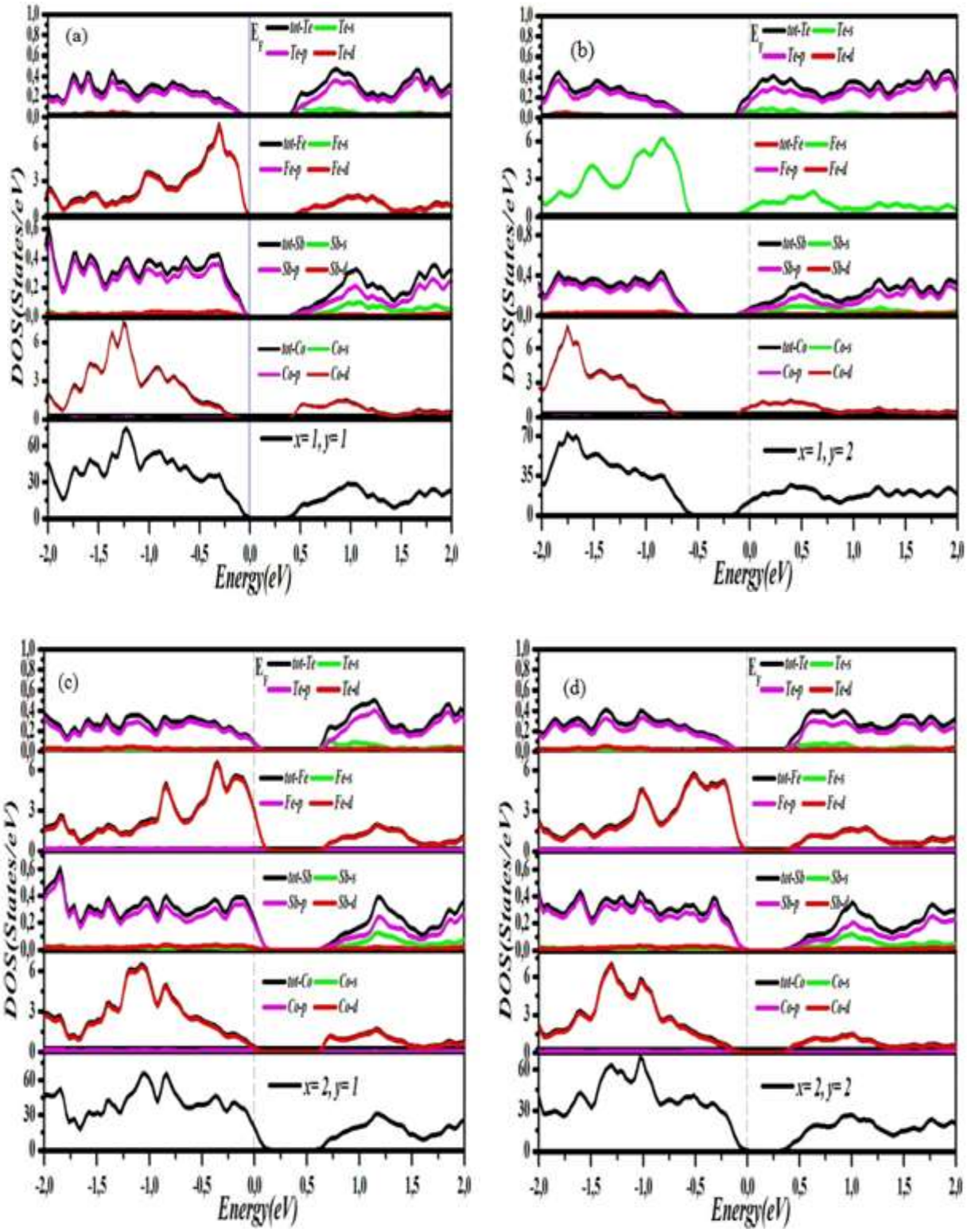

Fig. VI.10: Total and partial electronic densities of states for $Fe_xCo_{8-x}Sb_{24-y}Te_y$ compounds: (a) x= 1, y= 1, (b) x= 1, y= 2, (c) x= 2, y= 1 and (d) x= 2, y= 2.

VI.3.3. Thermoelectric properties

VI.3.3.a. Seebeck coefficient (S)

The seebeck coefficient and temperature dependence of binary skutterudites Co_8Sb_{24}andFe/Te co-doped $CoSb_3$ based skutterudite ($Fe_xCo_{8-x}Sb_{24-y}Te_y$) compounds are shown in Figs. VI.11(a) and (b). As shown Fig. VI.11(a), in The seebeck coefficient of binary skutterudite Co_8Sb_{24} and $FeCo_7Sb_{23}Te$, $Fe_2Co_7Sb_{23}Te$ and $Fe_2Co_7Sb_{23}Te_2$ compounds has a positive sign, suggesting the *p*-type nature carriers. This finding indicates that the main charge carrier is hole and the both dopants Fe and Te atoms have acted as accepters, whereas the seebeck coefficient of $FeCo_7Sb_{23}Te_2$ compound (x= 1, y= 2) shows a negative values (see Fig. VI.11(b)), confirming the *n*-type conduction. This result designates that the major carrier concentrations are electrons and Te atoms in this case have acted as electron donors. Also, it follows from these Figs. that the seebeck coefficient enhanced with the raise of both Fe/Te doping fractions and temperature, which can attributed to the existence of free charge (electron) through the addition of the both types of dopants. Where, the highest absolute seebeck coefficient values for the doped compounds were recorded at $23\ \mu VK^{-1}$, $209\ \mu VK^{-1}$ and $100\ \mu VK^{-1}$ at 900 K for $FeCo_7Sb_{23}Te$, $FeCo_7Sb_{23}Te_2$ and $Fe_2Co_7Sb_{23}Te$ compounds, respectively; and $200\ \mu VK^{-1}$ at 400 K for $Fe_2Co_7Sb_{23}Te_2$ compound.

On the other hand there was a reduction in the absolute seebeck coefficient for $FeCo_7Sb_{23}Te$ compound, in opposition to the increasing tendency of seebeck coefficients and Fe/Te ratio for $FeCo_7Sb_{23}Te_2$, $Fe_2Co_7Sb_{23}Te$ and $Fe_2Co_7Sb_{23}Te_2$ compounds, respectively. We interpret this inconsistency for $FeCo_7Sb_{23}Te$ compound in terms of its reduced density of states in comparison to the others (see Fig. VI.10(a)).

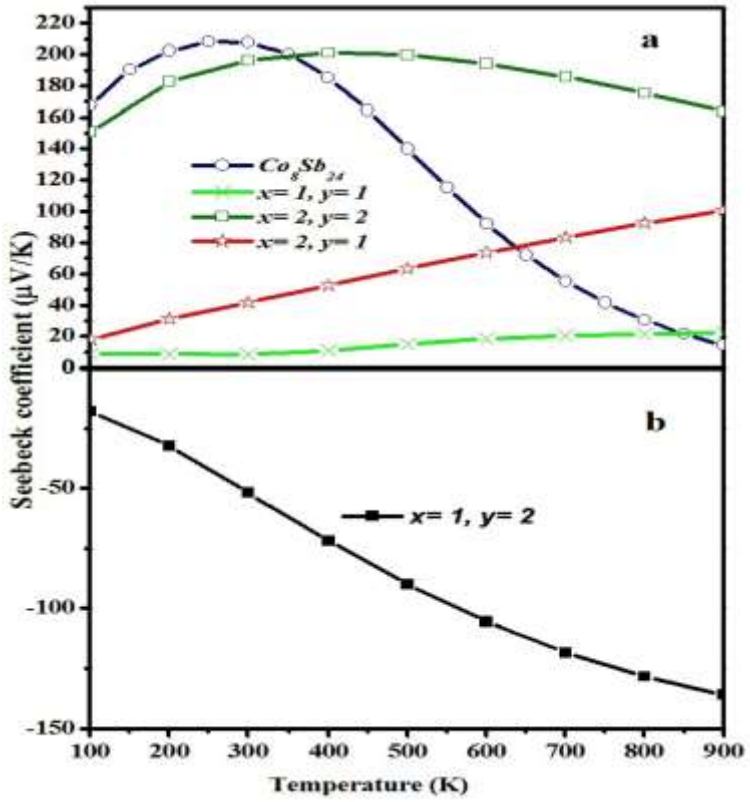

Fig. VI.11: Calculated Seebeck coefficient values as functions of temperature for binary skutterudite Co_8Sb_{24} and $Fe_xCo_{8-x}Sb_{24-y}Te_y$ compounds.

VI.3.3.b. Electrical conductivity (σ)

The temperature dependence of electrical conductivities over relaxation time $\left(\frac{\sigma}{\tau}\right)$ for binary skutterudites and $FeCo_7Sb_{23}Te$, $FeCo_7Sb_{23}Te_2$, $Fe_2Co_7Sb_{23}Te$ and $Fe_2Co_7Sb_{23}Te_2$ systems are presented in Fig.VI.12. The calculated electrical conductivities over relaxation time $\left(\frac{\sigma}{\tau}\right)$ for $FeCo_7Sb_{23}Te$, $FeCo_7Sb_{23}Te_2$ and $Fe_2Co_7Sb_{23}Te_2$ compounds increase with increasing temperature; these are typical trend for degenerated semiconductors. These results agree well with the study of $Co_8Sb_{24-x-y}Te_xSe_y$ samples [17].

Whereas in $Fe_2Co_6Sb_{23}Te$ compound, the electrical conductivity scaled by relaxation time $\left(\frac{\sigma}{\tau}\right)$ values exhibit declining trend with the temperature. It is believed from the electronic densities of states for $Fe_xCo_{8-x}Sb_{24-y}Te_y$ systems that the total electronic density of states for $Fe_2Co_6Sb_{23}Te$ compound has been modified and the electron tenancy has been enhanced at the vicinity of the Fermi level (see Fig. VI.10(c)), thus improve its electrical conductivity. This observation is slightly anticipated as Fe dopant could act as an accepter element.

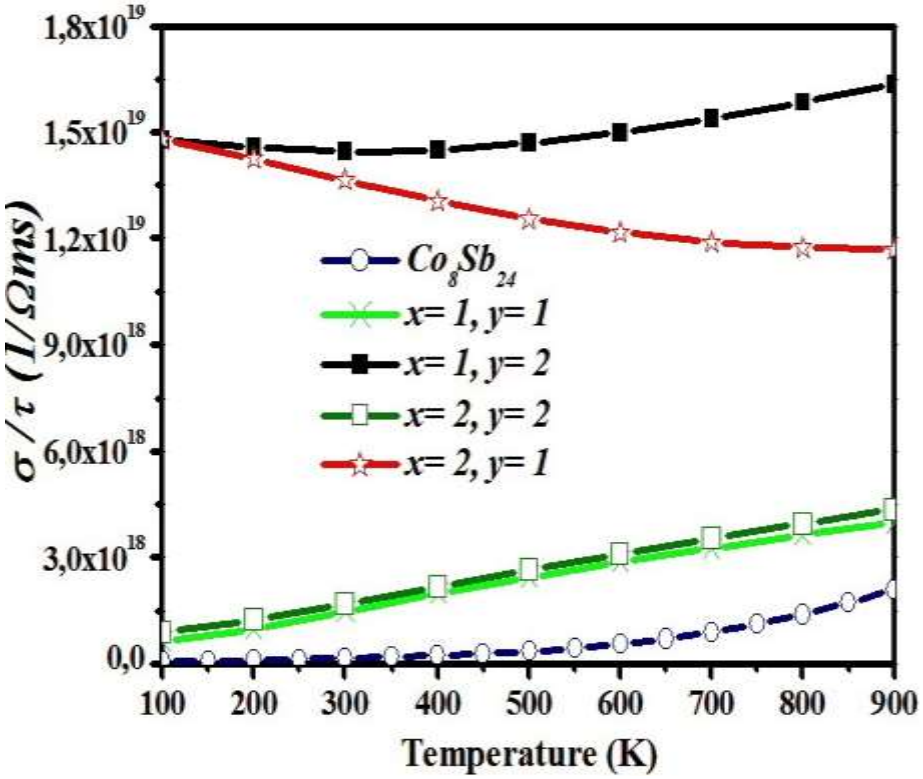

Fig.VI.12: The electrical conductivities over relaxation time $\left(\frac{\sigma}{\tau}\right)$ For binary skutterudite Co_8Sb_{24} and $Fe_xCo_{8-x}Sb_{24-y}Te_y$ compounds.

VI.4.3.c. Electronic thermal conductivity (κ_e)

Fig. VI.13 presents the variation of the electronic thermal conductivity scaled by relaxation time $\left(\frac{\kappa_e}{\tau}\right)$ of Fe and Te co-doped Co_8Sb_{24} based skutterudite compounds ($Fe_xCo_{8-x}Sb_{24-y}Te_y$) as function of temperature. Following this figure, we noticed that the electronic thermal conductivities over relaxation time $\left(\frac{\kappa_e}{\tau}\right)$ increased with increasing the temperature from 100 K to 900 K.

Also it was established to gradually expand with the add of Fe/Te dopants fraction, reaching its higher values for the $FeCo_7Sb_{22}Te_2$ compound. This is attributed to the bipolar conduction by the thermally exited charge carriers. Our results are consistent with the conclusions of Zhoa et *al* for $Ga_xCo_4Sb_{11.7}Te_{0.3}$ systems [18].

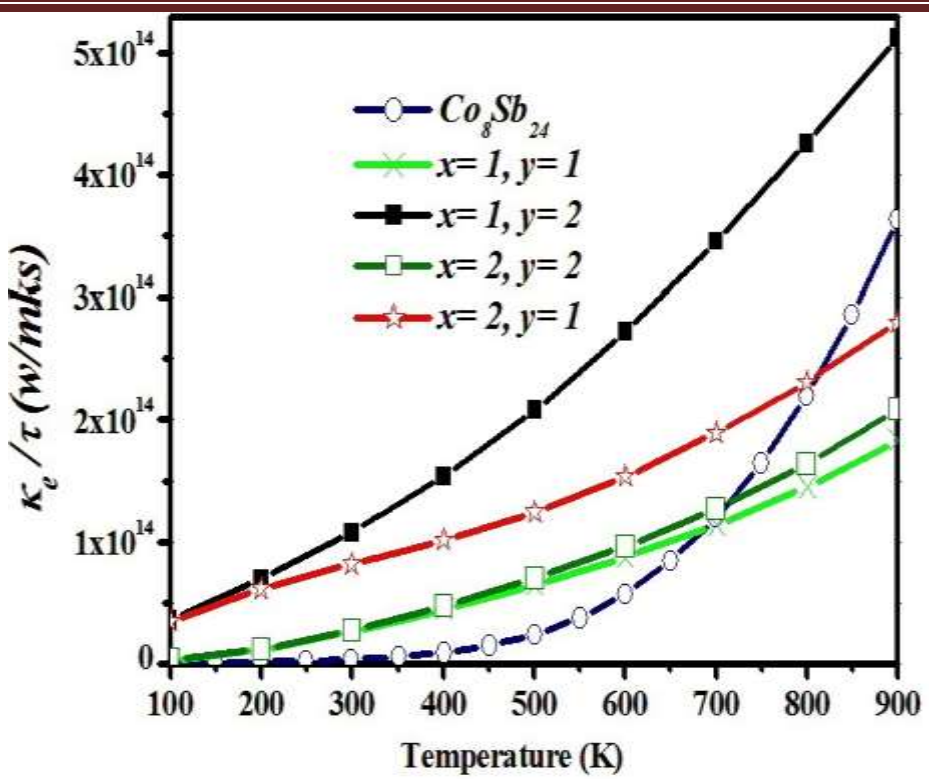

Fig. VI.13: The electrical conductivities over relaxation time $\left(\frac{\kappa_e}{\tau}\right)$ For binary skutterudite Co_8Sb_{24} and$Fe_xCo_{8-x}Sb_{24-y}Te_y$ compounds.

VI.4.2.3.d Dimensionless electronic figure of merit (ZT_e)

Fig. VI.14 displays the electronic dimensionless figures of merit ZT_e for binary skutterudite Co_8Sb_{24}Fe and Te co-doped $CoSb_3$ based skutterudite compounds ($Fe_xCo_{8-x}Sb_{24-y}Te_y$) as function of temperature. The electronic dimensionless figure of merit ZT_e values for $FeCo_7Sb_{23}Te$ and $Fe_2Co_7Sb_{23}Te_2$ compounds are significantly higher than that of the other doped samples, these mainly benefit from the distinct decrease in the electronic thermal conductivity over relaxation time of the both compounds. It can be also explained in terms of their standard semiconductor characteristic. Their seebeck coefficients have enlarged whereas the both electrical and electronic thermal conductivities have reduced due to the balance number of charge carriers introduced by Fe and Te atoms, resulting in a moderate overall ZT_e.

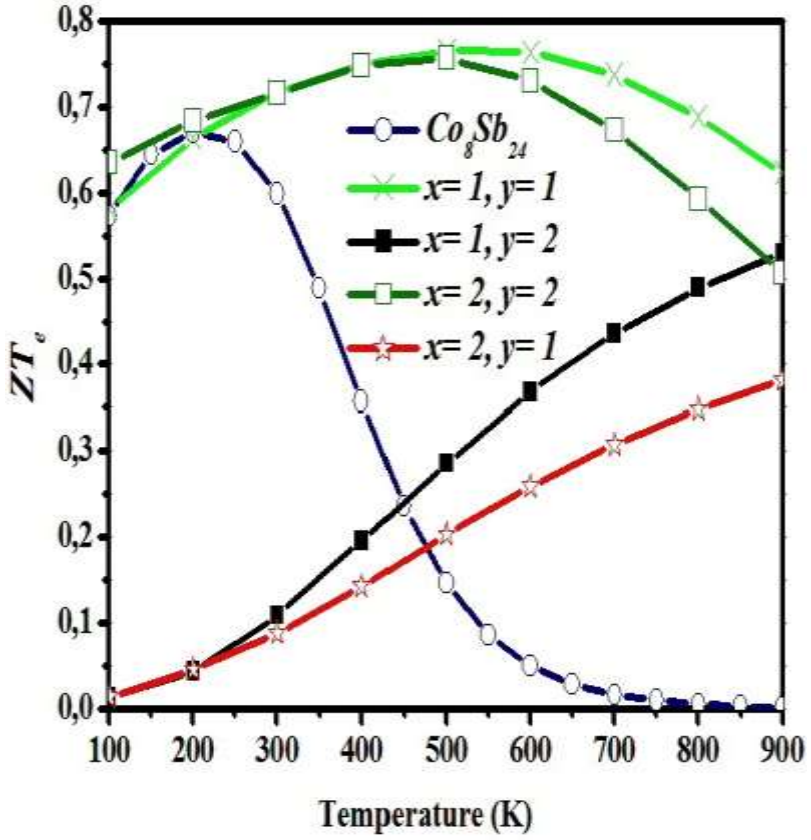

Fig. VI.14: Calculated dimensionless electronic figure of merit values, ZT_e for binary skutterudite Co_8Sb_{24}, $Fe_xCo_{8-x}Sb_{24-y}Te_y$ compounds as functions of temperature.

By examining the Sn/(Fe-Te) substitution effect on the electronic and thermoelectric properties, we point out that the charge balance in the both $Ba_{0.25}Co_8Sb_{24-x}Sn_x$ and $Co_{4-x}Fe_xSb_{24-y}Te_y$ compounds is found to be strongly dependent on the substitution configuration. And the electronic properties are moderate and the TE performance is enhanced with the estimated dimensionless electronic figure of merit (ZT_e) values of about 0.67, 0.72 and 0.78 at T= 500K for $Ba_{0.25}Co_8Sb_{23}Sn$ and $FeCo_7Sb_{23}Te$ and $Fe_2Co_7Sb_{23}Te_2$ compositions, respectively, ranking these compounds as promising candidates for thermoelectric applications.

Bibliography

[1] T. Liang, X. Su, Y. Yan, G. Zheng, X. She, Y. You, C. Uher, M.G. Kanatzidis, and X. Tang, J. NPG. Asia. Mater.**9**, 352 (2017).

[2] R. Guo, X. Wang, and B. Huang, Sci. Rep. **5**, 7806 (2015).

[3] X. Shi, J. Yang, L. Wu, J.R. Salvador, C. Zhang, W.L. Villaire, D. Haddad, J. Yang, Y. Zhu, and Q. Li, J. Sci. Rep, **5**, 14641 (2015).

[4] P.F. Qiu, R.H. Liu, J. Yang, X. Shi, X.Y. Huang, W. Zhang, L.D. Chen, J. Yang, and D.J. Singh, J. App. Phy.111(2012)023705.

[5] D.K. Shin, I.H. Kim, K.H. Park, S. Lee, and W.S. Seo, J. Electron. Mater.44, 1856, (2014).

[6] R. Liu, X. Chen, P. Qiu, J. Liu, J. Yang, X. Huang, and L. Chen, J. Appl. Phys. 109 (2011) 023719.

[7] J. Prado-Gonjal, P. Vaqueiro, C. Nuttall, R. Potter, and A.V. Powell, J. Alloy. Com.**695**, 3598 (2017).

[8] F. Duan, L. Zhang, J. Dong, J. Sakamoto, B. Xu, X. Lia, and Y. Tian, J. Alloy. Com.**639**, 68 (2015).

[9] B.R. Ortiz, C.M. Crawford, R.W. McKinney, P.A. Parillaband E.S. Toberer, J. Mater. Chem. A 10, 1039(2016).

[10] L.D. Chen, T. Kawahara, X.F. Tang, T. Goto, T. Hirai, J. Appl. Phys. 90, 1864, (2001).

[11] X. Shi, J. Yang, L. Wu, J.R. Salvador, C. Zhang, W.L. Villaire, D. Haddad, J. Yang, Y. Zhu, Q. Li, J. Sci. Rep, 5,14641 (2015).

[12] G.K.H. Madsen, D. Singh, Comput. Phys. Commun. 175, 67(2006).

[13] A.F. May, E.S. Toberer, A. Saramat, G.J. Snyder, Phys. Rev. B 80, 125205(2009).

[14] Y.G. Gurevich, O.Y. Titov, G.N. Logvinov, O.I. Lyubimov, Phys. Rev. B 51, 6999(1995).

[15] A.C. Kraemer, M.R. Gallas, J.A.H. Da Jornada, C.A. Perottoni, Phys. Rev. B 75, 024105(2007).

[16] J.O. Sofo, G.D. Mahan, Phys. Rev. B 58, 15620(1998).

[17] B. Duan, P. Zhai, L. Liu, Q. Zhang and X. Ruan, J. Solid. Stat. Chem, 12, 1983 (2012).

[18] D.G. Zhao, H.R. Geng and X.Y. Teng, J. Intermetallics, 35, 2631 (2012).

General conclusion

General conclusion

In recent years, theoretical methods have become one of the most active areas of research in the physics of matter. This involves using ab initio methods to give an interpretation of the experimental spectra and predict the majority of the physical properties of several new materials. In this way, we tried to study the structural, electronic and thermoelectric properties of the MX_3 binary skutterudite compounds (M = Co, Ir, Fe and Rh; X = As, P and Sb) with different theoretical approaches, and to determine the l effect of fillers or / and substitutes for $CoSb_3$-based Skutterudite materials using calculations in the Linearized Full-Potential Augmented Plane Wave Method (FP-LAPW) which is fundamentally based on the functional theory of density (DFT) and in combination with the semi-classical Boltzmann transport theory which are respectively implemented in the wien2k and Boltztrap codes.

- Firstly, we have focused on Binary skutterudites compounds MX_3:

  From the calculation of structural properties of binary skutterudite compounds MX_3 (M= Co, Ir, Fe and Rh; X= As, P and Sb) with various theoretical approaches, i.e. PBE-GGA, PBEsol-GGA, LDA and regular TB-mBJ approximations, we have found that our calculated structural parameters are in excellent agreement with the theoretical and experimental data.

The calculated electronic band structures of the skutterudite compounds show that:

- the $CoSb_3$, $IrSb_3$, $CoAs_3$, $IrAs_3$ and $RhAs_3$ compounds are semiconductors materials with fundamentals narrowing directs band gaps, however, the CoP_3, IrP_3 and $RhSb_3$ compounds exhibit indirects band gaps. Whereas the electronic band structures for the binary skutterudite RhP_3 compound show a metallic behavior.
- In the other hand, the spin up band structures in $FeSb_3$ compound show a direct band gap of semiconductor behavior, while in the opposite case, they show metallic character and thus confirm the half metallicity of this compound.

Since the investigation of their thermoelectric properties, the $CoSb_3$ compound has been found to have a large Seebeck coefficient, combined with high electrical conductivity and consequently resulting in high ZTe value compared to other binary skutterudites compounds, although it has comparatively important thermal conductivity, which apparently makes it less attractive in thermoelectric application.

- Secondly, we have interested by n-type and p-type filled $CoSb_3$ based skutterudites compounds:

From the results of calculations of total energies as a function of the cell volumes for the both n-type and p-type filled $CoSb_3$ based skutterudites compounds skutterudite, we conclude that:

- The lattice parameters obtained at equilibrium (a_0), for the n-type partially filled skutterudite $R_yCo_4Sb_{12}$ (R= Yb, Na and Ba and $x < 0.5$) and alkali metals fully filled $CoSb_3$ based skutterudites compounds, are in good agreement with those reported in literature. They increase simultaneously with the filling fraction (FF) and the size of the filler ions.
- The lattice parameters at equilibrium (a_0), for the p-type $CoSb_3$ based skutterudite fully filled with Bromine ($BrCo_4Sb_{12}$), is in concurrence with the experiment results.

The theoretical study of the electronic properties of the compound, having undergone filling of its structural voids by chemical elements of an electropositive nature such as (AM = Na; EM = Ba and RE = Yb) or by others of an electronegative nature such as Bromine (Br), suggests that:

- The skutterudite Co_4Sb_{12} compound filled in its structural voids with electropositive species (AM = Na; EM = Ba and RE = Yb) appears as a highly degenerate n-type semiconductor. Besides, when these voids are completely filled with bromine, the compound becomes highly degenerate p-type.
- From the electronic band structures, it is observed that the position of the maximum conduction band (CBM) and its flatness are strongly dependent on the nature and the quantity of electropositive species introduced into the voids.
- From the electronic band structures, it is observed that the position of the valence bands at the vicinity of Fermi energy (E_F) and their shape are strongly modified by the introduction of Bromine as electronegative specie into the voids.

From the results of thermoelectric properties, we found that the Seebeck coefficient and the electrical conductivity are improved in the n-type partially filled skutterudite compounds, and consequently, their power factors are extremely enhanced compared to the both n- and p-type fully filled ones. These results are in agreement with those reported in literature.

- Thirdly, we have considered the doping effect of Co/Sb sites separately with Fe/(Ge, Te) atoms in $CoSb_3$ based skutterudites :

General conclusion

The ground state properties were calculated for Fe substituted Co_4Sb_{12} ($Co_{4-x}Fe_xSb_{12}$, x< 0.5) and Ge/Te doped Co_4Sb_{12}, including lattice parameters, bulks modulus and its pressure derivative. Our calculated lattice parameters for $Co_{3.875}Fe_{0.125}Sb_{12}$ and $Co_{3.25}Fe_{0.25}Sb_{12}$ compounds are in good agreement with the available experimental and theoretical data. While for $Co_4Sb_9Ge_3$ and $Co_4Sb_9Te_3$ compounds there is not theoretical or experimental data addressable for comparison.

The calculated electronic properties such as band structures and densities of states (DOSs) for doped Co/Sb sites with Fe/(Ge, Te) atoms in $CoSb_3$ based skutterudites show that:

- Fe substituted Co_4Sb_{12} ($Co_{4-x}Fe_xSb_{12}$, x< 0.5) and Ge doped Co_4Sb_{12} compounds are both p-type degenerate semiconductors. Whereas, Te doped Co_4Sb_{12} is n-type degenerate semiconductor.

From the results of thermoelectric properties, we found that the Seebeck coefficient and the electrical conductivity are improved in Fe substituted Co_4Sb_{12} ($Co_{4-x}Fe_xSb_{12}$, x< 0.5) compared to case of the Ge/Te doped Co_4Sb_{12}.

- Finally, we have analyzed the effect of charge balance on the structural, electronic properties, and thermoelectric performance of partially filled $CoSb_3$ ($Ba_{0.25}Co_8Sb_{24-x}Sn_x$, x= 0, 1, 2, 3 and 4) and Te/Fe co-doped $CoSb_3$, $Co_{4-x}Fe_xSb_{24-y}Te_y$: x =1 and y= 1, x =1 and y= 2, x = 2 and y= 1, x = 2 and y= 2) compounds. We conclude that:
  - The values calculated for the lattice constants of Sn substituted in partially filled skutterudite $Ba_{0.5}Co_8Sb_{24-x}Sn_x$ (x =1, 2, 3 and 4) are slightly larger than the calculated values for those of binary skutterudite (Co_8Sb_{24}) and partially filled $Ba_{0.5}Co_8Sb_{24}$ compounds. They increase with Sn substitution, because the atomic radius of the Sb atoms is smaller than that of the Sn anions.
  - The enthalpy of formation decreases when the number of Sn substitution is reduced from $Ba_{0.5}Co_8Sb_{20}Sn_4$ to $Ba_{0.5}Co_8Sb_{21}Sn_3$, $Ba_{0.5}Co_8Sb_{22}Sn_2$ and $Ba_{0.5}Co_8Sb_{23}Sn$, respectively, indicating that the $Ba_{0.5}Co_8Sb_{23}Sn$ compound is relatively the most stable configuration.
  - The obtained lattice constants values of Fe/Te co-doped $CoSb_3$ are slightly larger than those of binary skutterudite (Co_8Sb_{24}) and of Fe doped $CoSb_3$ based skutterudite compounds with 1% and 2% deviations, respectively. This is mainly due to the fact that the atomic radius of Co (Sb) ions is smaller (larger) than in Fe (Te) ions.
  - The charge balance in the both $Ba_{0.25}Co_8Sb_{24-x}Sn_x$ and $Co_{4-x}Fe_xSb_{24-y}Te_y$ compounds is found to be strongly dependent on the substitution configuration.

- The electronic properties are moderate and the TE performance is enhanced with the estimated dimensionless electronic figure of merit (ZT_e) value of about 0.67, 0.72 and 0.78 at T= 500K for $Ba_{0.25}Co_8Sb_{23}Sn$ and $FeCo_7Sb_{23}Te$ and $Fe_2Co_7Sb_{23}Te_2$ compositions, respectively, ranking these compounds as promising candidates for thermoelectric applications.

Skutterudites remains an area of research and continuous improvement in their effectiveness. Research on skutterudites in recent years has contributed to a better understanding of the physical processes that play an important role in improving their thermoelectric performance, and the discovery of new compounds, one of the ZT values that are in part the most promising for intermediate temperature compounds. Our computational results suggest that the electronic properties are moderate and the TE performance is enhanced in the balance compounds $Ba_{0.25}Co_8Sb_{23}Sn$ and $FeCo_7Sb_{23}Te$ and $Fe_2Co_7Sb_{23}Te_2$ compositions.

Acknowledgements

The work presented in this manuscript was carried out within the Laboratory of Physique Quantique de la Matière et de Modélisation Mathematique (LPQ3M) at the University of Mascara.

The computational resources and services used in this work were provided by the HPC-Emir (High Performance Computing HPC), funded by Mascara University. I would like to acknowledge the Direction Générale de la Recherche Scientifique et du Développement Technologique (DGRSDT) for funding the project.

This thesis is the result of a fourth-year adventure punctuated by collaboration, support, dynamics and enthusiasm of many people that I sincerely wish thank you here.

I would like to express my gratitude to Mr. M. SAHNOUN, Professor at the University of Mascara and thesis Director for the trust he has placed in me by allowing me to carry out this thesis work. I thank him for having directed and supervised this work throughout these fourth years. The availability and the rigor he showed me were a precious help during the writing period. It has been a great pleasure to work with you for all the scientific wealth that you have been able to communicate to me and I am forever grateful. I would like to thank for the trust he has shown in me on a daily basis.

I thank Dr. A. Bekhti-Siad at the University of Mascara, my co-supervisor, for her good mood which has been invaluable during these fourth years. I also thank her for having encouraged me in my work and for her valuables advices and for the opportunity she gave me. She receives here the expression of my deep gratitude.

I am very grateful to Mr. H. Baltach, Professor at the University of Mascara, who gave me the honor of chairing the jury for this thesis.

I thank the examinees who have done me the honor of accepting to read and judge this thesis:

I express my gratitude to S. Fasla, Professor at the University of Oran 1 ENP, to A. Suidini, Professor at the University of Bel abbes and to Dr. O. Sahnoun at the University of Mascara who have agreed to devote their time to the expertise of this thesis. I would like also to express my gratitude to them for their participation in the jury.

I would like to express my sincere thanks to Dr. H. Bouhani-Benziane at the University of Mascara, the first person I met in the laboratory, who gave me a taste of work and who has followed me throughout my career “Student”. Thank you very much for your

patience and understanding. I also thank you for her sense of humor and kindness. Thanks for everything!!

I would also like to express my gratitude to N.H Mokhfi, Phd student at the University of Mascara for becoming much more than just colleague. I have had excellent scientific and social times with you. I would like to thank you for your help and warm welcome to my every request. Thank you very much for your kindness.